NATIONAL AND KAPODISTRIAN UNIVERSITY OF ATHENS
SCHOOL OF SCIENCE – FACULTY OF PHYSICS
DIVISION OF ENVIRONMENTAL PHYSICS

DOCTORAL THESIS

# Statistical Modeling of Extreme Environmental Values

Christos Tsalis M.Sc

Advisory Committee
Emeritus Professor George Kallos
Professor Kostas A. Belibassakis
Research Director Takvor H. Soukissian

Athens, July 2021

**Examination Committee**

| | |
|---|---|
| George Kallos | Emeritus Professor, National & Kapodistrian University of Athens School of Physics Division of Environment Physics - Meteorology |
| Takvor H. Soukissian | Research Director, Hellenic Centre for Marine Research - Institute of Oceanography, Anavissos |
| Kostas A. Belibassakis | Professor, School of Naval Architecture & Marine Eng. NTUA |
| George N. Galanis | Professor, Hellenic Naval Academy |
| Helena Flocas | Professor, National & Kapodistrian University of Athens School of Physics Division of Environment Physics - Meteorology |
| Sofianos Sarantis | Associate Professor, National & Kapodistrian University of Athens School of Physics Division of Environment Physics - Meteorology |
| Nikolaos Themelis | Assistant Professor, School of Naval Architecture & Marine Eng. NTUA |

# Acknowledgments

This doctoral thesis would not have been possible without the guidance and the help of several people who in one way or another contributed in the preparation and completion of this study. First and foremost, I would like to fully express my thanks and gratitude to my supervisor Prof. George Kallos, and Dr. Takvor Soukissian and Prof. Konstantinos Belibassakis for their guidance. Their great thinking, intuition, patient guidance and encouragement has proven a valuable lesson for me. It has been a pleasure and honour to work under their supervision and both contributed many ideas, useful suggestions and constructive comments. I am greatly indebted to them for proof reading the final draft of this thesis.

In addition, I would like to thank all my fellow PhD researchers from the department of Physics at the University of Athens and Naval Architecture & Marine Eng. department of NTUA and my fellow researchers of the Institute of Oceanography of HCMR for their help and moral support. I am greatly indebted for the help of several people who contributed in the preparation and completion of this study, especially Dr Flora Karathanasi for her help and moral support, Mrs Fani Anagnostou and Mr Miltos Stamos for their assistance in computational issues and finally Mr Panagiotis Triantafyllopoulos for his assistance in graphical issues. I would also like to thank Dr Ioannis Papastathopoulos from the department of Mathematics at the University of Edinburgh for his scientific advisory and his advice to extend the present research to other useful scientific areas.

Finally, I would like to thank my family, my father Vasilis, my mother Paraskevi and my sisters Maria and Effie for their constant love and unconditional support over the years. Their encouragement has played a vital role throughout my studies.

Dedicated to all my students

# Declaration

I declare that this thesis entitled Statistical Modeling of Extreme Environmental Values is the result of my own research under the guidance of Prof. George Kallos, Prof. Kostas A. Belibassakis and Dr. Takvor Soukissian except as cited in the references. This thesis has not been submitted in any form for the award of a higher degree elsewhere.

# Abstract (in English)

The accurate estimation of extreme values for metocean parameters (e.g., wind speed) plays a crucial role in the marine renewable energy industry and in coastal and offshore engineering applications. Typical challenges that arise in these fields of interest among others are the limited source of information in samples, commonly associated by the scarcity of long datasets, and the accurate estimation of the underlying dependence structure of the stochastic models that can be used for inference on applied problems with extremes.

The present analysis, aims to assess the effect of the asymptotic distributional behavior of two types of extreme wind speed sampling data that form the basis of all subsequent predictions in the long term time scale. The first type of sampling data considered will be subsets of observations extracted from blocks of annual length and the second type are subset of observations exceeding a high enough threshold. The challenges closely related to the special attributes that form these types of sampling data motivate the present thesis which focuses on constructing and improving extreme value models to assess the risk associated to extreme wind speed episodes. In particular, in this thesis we focus on

- The identification of the combined effects of the samples of wind speed that influence the stability of the parameter estimates as well as the efficiency of the estimators to the modelling of extremes.
- Providing alternative methods of modelling extremes of wind speed that are less known to the relative fields of interest and infer to demonstrate better in comparison to the standard modelling approach.
- Extending the formulation of the stationary model of extremes to the parameterization of a nonstationary model in order to incorporate subject specific knowledge in the presence of trends under the assumption of climate wind changes.
- Extending the classical methods that identify the dependence structure in sample of observations in order to effectively model the extremes that are irregularly spaced in time. Specifically, the reconstruction of a dependent sample of extremes that are irregularly spaced in time is focused on relatively small samples of wind speed where the scarcity of long and complete time series is a common restriction in climatological studies.

In this setting, the statistical analysis of the most used and less known estimators that model the extremes of wind speed is inferred from a twofold approach. A simulation study is performed first to assess the effect of the sample size to the estimators of the asymptotic distribution that model extremes. The evaluation of the simulation results is based on several statistical measures. Afterwards, the optimum methods from the simulation analysis are applied to wind speed datasets of different sample size and different direction step of sampling. The evaluation is based on datasets originated from databases of relatively moderate horizontan resolution to the regional locations at the North Sea, at the Pacific coast of central America and at the eastern Atlantic Ocean where these locations are exposed to a strong wind climate with evidence of extreme wind speeds. Inference of the sample size effect and the directional step of sampling to the demonstration of the model estimators is made on the obtained 50- and 100-year wind speed design values. From this assessment, the combined method of moments is advised as the suitable method when the sample size is limited.

Other challenges that motivated this study is the modelling of extremes when the extremal characteristics are expected not constant over time. To this effect, seasonality and long-term trends are probably the main reasons that influence the stationary hypothesis of the wind speed processes. In this part of this study, an attempt is made to model the possible trends of extremes in the long-term behavior of the process. Since in practice the trend is unknown, various formulations of the trend as a function of time are assessed to represent the extremes of wind speed when the stationary assumption is not valid in order to alleviate the bias effect from

the attempt of de-trending the process before the time series is used. Statistical tests challenged the modeling of the trend of rejection or not in favor of stationarity. For the extremes of non-stationary sequences and the application to wind speed design values, our analysis is based on coarse historical data of long datasets at regional locations at the North Sea where trends are notable to influence the wind speed variability. From this assessment, the simplest form of parameterization in the parameters of the extreme value distribution is advised in modeling extremes when stationarity is violated.

Another common problem of design to assess risk associated to extremes of wind speed in met-ocean fields of interest, is the scarcity of long datasets. To this limitation, many applications utilize as many as possible extremes from the available dataset by re-sampling to a subset of extremes. However, the re-samples are often affected by dependency and the diagnostics related to the independence limitations is usually violated when the observations of these samples are irregularly spaced in time. To alleviate this effect, a resampling strategy is proposed that effectively models extremes irregularly in time when re-sampling of relatively small datasets of wind speed is advised. The proposed DeCA Uncorrelated (DeCAUn) model provides an improvement to the current physical De-Clustering Algorithm (DeCA) modelling the samples of DeCA irregularly in time.

Specifically, the resampling strategy proposed analyzes the correlation effect in samples based on the extension of the standard correlation operator setting weight functions to observations irregularly spaced in time. To infer in terms of precision and variability, design value estimates and confidence bounds of the demonstration of the proposed model are evaluated based on the standard approaches that model extremes. The use of a high resolution database is crucial to derive detailed data to follow-up the requirements of the resampling strategy to short and irregularly samples near the offshore regions of Europe where the demonstration of DeCAUn to wind speed is challenged from the highly dependent regional effects (surface roughness, landmass, etc.). However, to assess the effect of larger sample sizes to the limiting distribution of the excesses that will infer effectively the modelling of DeCAUn, larger samples of wind speed from a fairly coarse resolution database are also required for evaluation. From this assessment, the proposed model demonstrated as an alternative re-sampling strategy for extreme wind speed projections when samples are irregularly spaced in time.

These challenges motivate the present thesis to assess the risk associated to extreme wind speed episodes for direct potential application to the relevant fields of interest. In particular, the most important findings from this assessment in extremes are outlined in the following:

- Based on the evaluation using different sample sizes of wind speed data from both the simulation study and applications, the combined method of moments outperforms, in many respects, compared to the standard likelihood approach. Overall, regarding the design values it is evident that sample sizes greater than 35 years are necessary for a substantial reduction of epistemic uncertainty.
- Under the proviso of nonstationarity at locations where the natural climate variability in extreme wind speeds is challenged, the linear form of parameterization in the parameters of the extreme value distribution will model effectively the trends in extremes.
- For sample periods of wind speed greater than 15 years, the re-samples of DeCAUn demonstrated effective projections in terms of precision and variability.
- The resampling strategy proposed in this setting showed systematically stronger rate of convergence to the asymptotic properties of the extreme value distribution particularly for wind speed datasets of higher spatial resolution and a less stronger rate of convergence for datasets of lower resolution.

# Abstract (in Greek)

Η ανάπτυξη και μελέτη στοχαστικών μοντέλων με σκοπό την επίλυση προβλημάτων που σχετίζονται με την εμφάνιση ακραίων τιμών, αποτελεί, τις τελευταίες τρεις δεκαετίες, σημαντικό πεδίο έρευνας της επιστήμης των εφαρμοσμένων μαθηματικών. Η μοντελοποίηση και μακροπρόθεσμη πρόβλεψη εμφανίσεων ακραίων συμβάντων παίζει σημαντικό ρόλο σε εφαρμοσμένα πεδία όπως η Μετεωρολογία, Υδρολογία αλλά και σε έργα θαλάσσιας μηχανικής όπου η γνώση της κλιματολογίας της περιοχής είναι απαραίτητη για την εκτίμηση της ασφάλειας και την καλή λειτουγία των κατασκευών.

Η εκτίμηση λοιπόν της επικινδυνότητας (ρίσκου) εμφάνισης ακραίων συμβάντων μελετάται μέσω της Θεωρίας των Ακραίων Τιμών. Οι δύο επικρατέστερες ασυμπτωτικές προσεγγίσεις κατανομών από ακραία δεδομένα στην μακροχρόνια κλίμακα του χρόνου είναι οι μέγιστες τιμές διατεταγμένων τυχαίων μεταβλητών και η ακολουθία ανεξάρτητων και ισόνομα κατανεμημένων τυχαίων μεταβλητών οι οποίες υπερβαίνουν μία "αρκετά υψηλή" τιμή κατωφλίου. Στο πλαίσιο της Θεωρίας Ακραίων Τιμών και βασιζόμενοι στις δυο επικρατέστερες ασυμπτωτικές προσεγγίσεις, η παρούσα μελέτη αποσκοπεί στην ανάπτυξη μιας ολοκληρωμένης, κατά το δυνατόν, προσέγγισης για την μοντελοποίηση των μεγίστων τιμών της ταχύτητας του ανέμου, όταν το διαθέσιμο δείγμα είναι περιορισμένο ή εμφανίζει ασυνέχεια καταγραφής δεδομένων. Στο πλαίσιο αυτό, οι βασικοί στόχοι της παρούσας διατριβής είναι οι εξής:

- Μελέτη επίδρασης του διαθέσιμου δείγματος στην μοντελοποίηση των ακραίων ενδεχομένων ταχύτητας ανέμου με χρήση της θεωρίας των ακραίων τιμών,
- Επισήμανση γνωστών αλλά και λιγότερο γνωστών μεθόδων εκτίμησης παραμέτρων της πιθανοθεωρητικής κατανομής των ακραίων τιμών της ταχύτητας του ανέμου και η αξιολόγηση συμπεριφοράς της απόδοσής τους έναντι των καθιερωμένων μεθόδων εκτίμησης,
- μοντελοποίηση των παραμέτρων της τυπικής γενικευμένης κατανομής ακραίων τιμών με συστηματική μελέτη και σύγκριση διαφόρων συνδυασμών χρονικής εξάρτησης των παραμέτρων,
- ανάπτυξη μιας ολοκληρωμένης προσέγγισης για μονοδιάστατες τυχαίες μεταβλητές μέσω ενός προτεινόμενου μοντέλου που λαμβάνει υπόψη την συσχέτιση των ακραίων τιμών όταν αυτές εμφανίζονται ακανόνιστα στην κλίμακα του χρόνου. Ο κύριος στόχος του μοντέλου είναι η δημιουργία νέου υποδείγματος με ασυμπωτική θεώρηση στατιστικά ανεξάρτητων πλέον παρατηρήσεων.

Ειδικότερα, το πρόβλημα που σχετίζεται με την μελέτη της επίδρασης του διαθέσιμου δειγματικού μεγέθους στην εκτίμηση τιμών σχεδιάσεως απο μοντέλα ερμηνείας, εκτιμήσεων και προβλέψεων ακραίων συμβάντων, μελετάται διεξοδικά από δύο δειγματοληπτικές προσεγγίσεις. Απο προσομοιώσεις τύπου Monte-Carlo και από ανεμολογικά δεδομένα χρονοσειρών από βάσεις δεδομένων μέτριας χωρικής ανάλυσης. Η εκτίμηση και η εξάρτηση των παραμέτρων της κατανομής από το διαθέσιμο δείγμα θα γίνεται μέσω βασικών αλλά και λιγότερο γνωστών μεθόδων. Απο την στατιστική ανάλυση των βέλτιστων μεθόδων εκτίμησης με βάση τα κριτήρια καλής απόδοσης σε δεδομένα προσομοίωσης, γίνεται στην συνέχεια εκτίμηση της απόδοσης σε ανεμολογικά δεδομένα  διαφορετικών χρονικών περιόδων και διαφορετικού χρονικού βήματος. Η παρούσα μελέτη εστιάζει σε σημεία της Βορείου Θάλασσας και σε σημεία Ανατολικά και Δυτικά της Κεντρικής Αμερικής όπου ισχυρή μετεωρολογική δραστηριότητα στις περιοχές αυτές οδηγεί αναπόφευκτα σε φαινόμενα που χαρακτηρίζονται από ακραίες τιμές ταχύτητας ανέμων. Η επίδραση του διαθέσιμου δείγματος στην απόδοση των μεθόδων εκτίμησης για τιμές σχεδιάσεως των 50 και 100 ετών περιόδων επαναφοράς θα αξιολογηθεί με στατιστικά κριτήρια. Απο την μελέτη αυτή συμπεραίνεται ότι η συνδυαστική μέθοδος Σταθμισμένων Ροπών προτείνεται ως η ικανοποιητική μέθοδος για την μοντελοποίηση ακραίων τιμών όταν το διαθέσιμο δείγμα είναι περιορισμένο.

Ο επόμενος άξονας μελέτης σχετίζεται με την διερεύνηση της τάσης μεταβολής των πιθανοθεωρητικών χαρακτηριστικών της ασυμπτωτικής κατανομής των ακραίων τιμών της ταχύτητας του ανέμου. Ειδικότερα, για την ευρύτερη περιοχή της Βορείου Θάλασσας, όπου έχουν παρατηρηθεί τα τελευταία χρόνια μεταβολές του ανεμολογικού κλίματος, γίνεται έλεγχος της στασιμότητας των χρονοσειρών ανέμου. Για τις χρονοσειρές στα σημεία που ικανοποιούν τον έλεγχο υπόθεσης στασιμότητας απο κατάλληλα στατιστικά κριτήρια, γίνεται μοντελοποίηση των παραμέτρων της τυπικής Γενικευμένης Κατανομής Ακραίων Τιμών με κατάλληλους συνδυασμούς χρονικής εξάρτησης κυρίως στις κανονικοποιημένες παραμέτρους θέσης και κλίμακας. Στην παραμετροποίηση αυτή, η παράμετρος σχήματος της κατανομής θεωρήθηκε ανεξάρτητη του χρόνου. Η επιλογή του κατάλληλου μοντέλου, παραμετρικού ή μη παραμετρικού, βασίζεται σε στατιστικά κριτήρια καλής προσαρμογής (goodness-of-fit criteria) χρησιμοποιώντας ανεμολογικά δεδομένα χαμηλής χωρικής ανάλυσης σε δείγμα με εύρος πολλών ετών. Στο πλαίσιο αυτής της μελέτης, συμπεραίνεται ότι η απλούστερη παραμετροποίηση της ασυμπτωτικής κατανομής των ακραίων τιμών μοντελοποιεί κατάλληλα τις μεταβολές του ανεμολογικού κλίματος.

Ο τελευταίος άξονας μελέτης εστιάζει στην μελέτη της πιθανής συσχέτισης ακραίων τιμών όταν αυτές εμφανίζονται με ακανόνιστο χρονικό βήμα στην κλίμακα του χρόνου. Στο πλαίσιο αυτό, προτείνεται μια νέα μέθοδος αναδειγματοληψίας με κύριο στόχο την δημιουργία ενός νέου υπο-δείγματος που αποτελείται από ανεξάρτητες παρατηρήσεις έτσι ώστε να πληρούνται τα απαραίτητα στατιστικά κριτήρια για την εκτίμηση των τιμών σχεδιάσεων μέσω της θεωρίας των ακραίων τιμών. Η προτεινόμενη μέθοδος DeCA Uncorrelated (DeCAUn) model βελτιστοποιεί και διορθώνει την υπάρχουσα μέθοδο αναδειγματοληψίας physical De-Clustering Algorithm (DeCA) model, λαμβάνοντας υπόψη την συσχέτιση των παρατηρήσεων όταν αυτές εμφανίζονται με ακανόνιστο χρονικό βήμα στην κλίμακα του χρόνου. Η προτεινόμενη αναδειγματοληπτική μέθοδος θεωρείται ως εναλλακτική από μια σειρά από προτεινόμενα μοντέλα που εκτιμούν τον συντελεστή αυτοσυσχέτισης από παρατηρήσεις με ακανόνιστο χρονικό βήμα στην κλίμακα του χρόνου.

Ειδικότερα, το προτεινόμενο μοντέλο δεν επιχειρεί έλεγχο του φάσματος, αλλά υπολογίζει απευθείας την συσχέτιση των χρονικά ακανόνιστων παρατηρήσεων με κατάλληλες συναρτήσεις βάρους, καθορίζοντας τον βαθμό εξάρτησης μεταξύ των παρατηρήσεων. Συγκριτικά αποτελέσματα των εκτιμώμενων τιμών σχεδιάσεως και διακύμανσης του μοντέλου παρουσιάζονται για περιοχές της Ευρώπης που είναι εκτεθειμένες στα καιρικά συστήματα του Ατλαντικού Ωκεανού, της Βόρειας Θάλασσας και της Μεσογείου. Για την στατιστική ανάλυση του προτεινόμενου μοντέλου χρησιμοποιήθηκε η κλασσική μέθοδος εκτίμησης παραμέτρων μέσω της Μεγίστης Πιθανοφάνειας με χρονοσειρές από βάσεις δεδομένων χαμηλής και υψηλής ανάλυσης. Τα ανεμολογικά δεδομένα απο βάσεις υψηλής ανάλυσης είναι απαραίτητα για την πληρέστερη αναπαράσταση του ακραίου αιολικού δυναμικού ειδικότερα σε κλειστές θαλάσσιες περιοχές. Για τον έλεγχο της ασυμπτωτικής συμπεριφοράς της προτενόμενης μεθόδου αναδειγματοληψίας χρειάστηκαν χρονοσειρές απο δείγμα με εύρος πολλών ετών όπου αναπόφευκτα η μοντελοποίηση σ'αυτή την περίπτωση πραγματοποιήθηκε απο βάσεις δεδομένων χαμηλής ανάλυσης. Στο πλαίσιο αυτής της μελέτης η προτεινόμενη μεθοδολογία αναδειγματοληψίας θεωρείται εναλλακτική προσέγγιση για την μοντελοποίηση ακραίων τιμών απο μικρό δείγμα λαμβάνοντας υπόψη την συσχέτιση των παρατηρήσεων όταν αυτές εμφανίζονται με ακανόνιστο χρονικό βήμα στην κλίμακα του χρόνου.

Τα κυριότερα ευρήματα στο πλαίσιο αυτής της μελέτης για την μοντελοποίηση των μεγίστων τιμών της ταχύτητας του ανέμου παρουσιάζονται συνοπτικά παρακάτω:

- Η συνδυαστική μέθοδος Σταθμισμένων Ροπών προτείνεται ως η κατάλληλη μέθοδος για την μοντελοποίηση ακραίων τιμών σε σχέση με την κλασική προσέγγιση της Μεγίστης Πιθανοφάνειας όταν το διαθέσιμο δείγμα είναι περιορισμένο. Το σφάλμα αβεβαιότητας στην εκτίμηση των επιθυμητών τιμών σχεδιάσεως μειώνεται σημαντικά όταν το διαθέσιμο δείγμα είναι μεγαλύτερο απο 35 έτη.
- Η ανάλυση αυτή ανέξειξε ότι το γραμμικό μοντέλο της χρονικής εξάρτησης στην παράμετρο θέσης μοντελοποιεί κατάλληλα τις ακραίες τιμές της ταχύτητας ανέμου σε

σημεία στην Βόρεια Θάλασσα όπου αποδεδειγμένα παρατηρούνται μεταβολές του ανεμολογικού κλίματος.

- Για χρονοσειρές μεγαλύτερες απο 15 έτη συμπεραίνεται ότι η προτεινόμενη αναδειγματοληπτική μέθοδος θεωρείται ως εναλλακτική για την μοντελοποίηση των ακραίων τιμών της ταχύτητας ανέμου ικανοποιώντας τα κατάλληλα κριτήρια καλής απόδοσης.

- Στα πλαίσια αυτής της μελέτης συμπεραίνεται ότι τα πιθανοθεωρητικά χαρακτηριστικά της ασυμπτωτικής κατανομής των ακραίων τιμών της ταχύτητας του ανέμου ικανοποιούνται σε μεγαλύτερο βαθμό όταν η μοντελοποίηση που πραγματοποιεί η προτεινόμενη μέθοδος DeCAUn με ακανόνιστο χρονικό βήμα στην κλίμακα του χρόνου βασίζεται σε χρονοσειρές δεδομένων υψηλής ανάλυσης και σε μικρότερο βαθμό απο την μοντελοποίηση που πραγματοποιείται απο δεδομένα χαμηλής ανάλυσης.

# Table of Contents

# Contents

# Glossary of terms

The main notation used in this thesis are listed below. All notations are also explained in the text.

| Abbreviation | Definition |
|---|---|
| OM | ordinary moments method |
| MPS | maximum product of spacings |
| EP or EPM | elemental percentile method |
| MLE or ML | Maximum likelihood method |
| QLS | Quantile least squares |
| POME or OEM | Principle of maximum or ordinary entropy method |
| MESE | Maximum entropy parameter space expansion method |
| PWM | probability weighted moments method |
| $LMH_U$ or LMOM | L-moments unbiased method according to Hosking et al.(1985) |
| $LMH_B$ | L-moments biased method according to Hosking et al. (1985) |
| LMW | L-moments method according to Wang |
| POT | Peaks Over Threshold approach |
| GPD | Generalized Pareto Distribution |
| GEV | Generalized Extreme Value Distribution |

| | |
|---|---|
| i.i.d | Independent and Identically Distributed limitations |
| PP | Point Processes |
| WCI | Width of Confidence Interval |
| ACF | Autocorrelation Function |
| PS | Parameter Stability plot |
| NC diagnostics | Threshold model selection proposed from (Northrop and Coleman, 2014) |
| gXCF | Gaussian Kernel smooth function for the Slotting method |
| BM Ref. | Block Maximum Reference method. This BM is counted upon the largest available sample |
| BM | Block Maximum method |
| AM | Annual maxima |
| Runs | Runs method for De-Clustering |
| DeCA | De-Clustering Algorithm (DeCA model) |
| DeCAUn | DeCA Uncorrelated model |

| Variable | Definition |
|---|---|
| $\hat{\xi}$ | shape parameter estimate of the GEV and GP distributions |
| $\hat{\sigma}$ | scale parameter estimate of the GEV distribution |
| $\hat{\mu}$ | location parameter estimate of the GEV distribution |
| SEF | standard error of fit |
| MARD | mean absolute relative deviation |
| $D_{abs}$ | average absolute difference between the true (initial) and the estimated distribution function |
| $D_{max}$ | average of the maximum absolute difference between the true and the estimated distribution function within each sample |
| Ny | The annual sample length of the wind speed time series |
| $h$ | Standard width parameter of the Gaussian weight function |
| $\Delta\tau$ | Effective width of the Gaussian Kernel |
| $C = \text{bdw}(h/\Delta\tau)$ | Normalized bandwidth (bdw) |
| $\hat{\xi}_{Ref}$ | shape parameter estimate with regards to the BM Ref. model |

| | |
|---|---|
| DEP | pre-Defined Energy Percentage level of energy reductions |
| RESID ($\hat{\xi}$) | A visual metric for comparison of the parameter estimates from the models used |
| M-K test | The non-parametric rank-based Mann-Kendall test |
| NAOI | The index of the North Atlantic oscillation |
| $DV$ | Design Values or (Return Levels) |
| $DV(50)$ | $DV$ estimates of the 50 years return period |
| $RP$ | Return period |
| $nrmse$ | The normalized root mean square error |

# Chapter 1
## Introduction

## 1.1 Basic Concepts of Extremes

Extreme value analysis (EVA) of metocean characteristics, such as wind speed, wave height, sea-level, etc., is a field of significant importance for engineers and environmental scientists. One of the main objectives of EVA refers to the estimation of design values and associated return periods with respect to the examined random variable(s). See, for example, (Kharin and Zwiers, 2000), (Ronold and Larsen, 2000), (Engeland et al., 2004), (Chen et al., 2004), (An and Pandey, 2005), (Caires and Sterl, 2005), (Stefanakos et al., 2007), (Larsén and Mann, 2009), (Chen and Huang, 2010), (Vinoth and Young, 2011), (Jonathan and Ewans, 2013), (Panchang et al., 2013), (Gouldby et al., 2014), (Sarkar et al., 2014), (Anastasiades and McSharry, 2014), (Cannon et al., 2015), (Su et al., 2017), (Manis and Bloodworth, 2017), (Pes et al., 2017), (Wang, 2017),(Kunz et al., 2010), (Naveau et al., 2005) where various applications of EVA in ocean, environmental and civil engineering can be found.

Design parameters corresponding to environmental loads implied by wind, waves, etc. are used in practice to evaluate the resistance and/or reliability of an offshore structure in the ultimate limit state. In addition, the accurate estimation of design values greatly facilitates the analysis of different serviceability limit states, (Fujino et al., 2012), (Kasperski, 2013). Applications of EVA in wind energy assessment and wind turbine structural design are provided by (Su et al., 2017) and (Lombardo, 2012), where the effects of wind extremes on the safety of wind turbines have been assessed, by (Ali et al., 2017), where a 50-year extreme wind speed has been used, among others, as a parameter for wind turbine selection, by (Wang et al., 2015), where the current status of extreme wind speeds and wind energy assessment has been reviewed, and by (Pop et al., 2016) where a method for obtaining extreme wind gust speed critical for the safety of wind turbines has been presented. Furthermore, in (Mo et al., 2015), wind hazard maps have been produced for China using reanalysis data, in (Kang et al., 2015), the effects of the surface conditions on the estimation of design values for wind speed have been assessed, and in (Chiodo et al., 2015), a comparison of two different EVA approaches (the block maxima approach and a non-parametric Bayesian approach) has been conducted for the estimation of wind speed extreme values. The effects of wind and wave loads on the reliability of non-axisymmetric support structures have been discussed in (Wei et al., 2016), and in (Viselli et al., 2015), extreme metocean parameters (wave height and wind speed) have been estimated for the design of offshore wind structures.

The most widely used EVA methods are the annual or block maxima (BM) and the peaks over threshold (POT). BM and POT methods utilize different extreme type data, fitting a distribution function based on solid theoretical grounds. Since the derived results from these methods are of asymptotic nature, in practice, limited sample sizes may limit, or even render impossible, their applicability. A discussion and comparison of BM and POT methods has been provided in (Ferreira and de Haan, 2015). For particular applications regarding the estimation of metocean extremes see, e.g. (Caires, 2016), (Orimolade et al., 2016), (Sartini et al., 2015), while more information on EVA methods and various alternatives can be found in (Soukissian and Kalantzi, 2006; Soukissian and Kalantzi, 2009), (Soukissian et al., 2006).

1

For the implementation of the BM method, the grouping of data into blocks of equal length and the selection of the maximum of each block is required. According to the main theoretical result of EVA, these maxima follow asymptotically the Generalized Extreme Value (GEV) distribution and thus, the estimation of the GEV parameters is based on the sample of these maxima; see Chapter 3 of (Coles, 2001) for a discussion on this issue. Though some theoretical restrictions apply (e.g. the maxima should be realizations of independent and identically distributed random variables), an important advantage of the BM method is that it still works when the maxima are not exactly independent and identically distributed (i.i.d), provided that the long range dependence of high level exceedances is weak; (Ferreira and de Haan, 2015). Some important issues of debate as regards the application of the BM method (and other EVA methods as well) to observed data are the following:

**1. The available sample size**: Some of the parameter estimation methods of the GEV distribution perform marginally fair with small sample sizes; for example, it is known, that the performance of the widely used Maximum Likelihood (ML) method can be extremely erratic for small samples, see (Katz et al., 2002), especially with respect to the estimation of extreme quantiles of the GEV distribution, (Soukissian and Tsalis, 2018). Long time series are generally required for the accurate estimation of extremes; however there is not consensus as regards the required length of the time series. For example, in (Cook, 1985), it is suggested that the BM method (with 1-year block size) can produce reliable results, when the available records are at least of 20 years length; see also (Palutikof et al., 1999). In the discussion of (Dukes and Palutikof, 1995), with particular reference to wind speed annual maxima (AM) time series, it has been noted that it is difficult to identify the effects of the time series length on the maximum return period in order to safely consider the obtained estimates as reliable. Using GEOSAT wave measurements, (Panchang et al., 1998) concluded that extreme value estimations from 5 years or 14 years of data are very close. Some authors, (Jeong and Panchang, 2008), also accept that extrapolations to return periods three or four times the data length, are appropriate. In (Devis-Morales et al., 2017) the authors claim that 35 years of data are enough to predict the 100-year wave, while in (Perrin et al., 2006) 30 years of wind speed data have been used for the estimation of 50 and 100-years design winds; see also (Polnikov et al., 2017) for a similar approach as regards wave height. On the other hand, in (Vanem, 2017), it has been suggested that "at-site analyses based on 30 years of data are reasonably accurate for return periods up to about 20 years, but not much more than this". A method introduced by (Cai and Hames, 2011) can be used to determine the minimum sample size required for the estimation of the GEV distribution parameters based on the asymptotic properties of the ML method. Nevertheless, the sample size issue related with the BM approach still remains open.

**2. The choice of the block size**: As already mentioned, the most pronounced problem in EVA, and particularly in the BM approach, refers to the appropriateness of the available sample size for a rational design value estimation. A small block size might lead to bias and a large one to large estimation variance. For wind speed data, there is no natural partition of the year into separate seasons. Fawcett and Walshaw (2006 b, 2007, 2008, 2015) argue that by dividing the year into twelve equal length seasons, a satisfactory balance is achieved between the two conflicting requirements of (i) indicating the continuous nature of seasonal changes in climate appropriately and (ii) retaining a substantial amount of data for analysis in each season withought the loss of valuable information at that seasons. However, for most environmental parameters (wind, waves, sea level, etc.) the block size of one year has been established.

**3. The parameter estimation technique**: For the estimation of GEV parameters, a widely used method is the ML, mainly due to its well-developed asymptotic properties; (see Katz et al., 2002). A detailed review, assessment and evaluation of the performance of nine different estimation methods for the GEV distribution parametrers has been provided by (Soukissian and

Tsalis, 2015); see also Chapter 2. The analysis was based on a simulation study with a constant sample size 30, while an application to real wind speed data has been also presented. In the same work, it was concluded that the ML, Maximum Product of Spacings (MPS) and Elemental Percentile (EP) methods outperform (with respect to bias, variance and mean squared error) ([1]). However, since the simulation study was based on random samples with constant size 30, the potential effects of the available sample size to the estimation of the GEV parameters were not considered.

Regarding the performance of the GEV parameter estimation methods with respect to the available sample size, various works assessed different estimation methods. The ML, and the methods of L-moments (LMOM) and moments (MOM) have been evaluated through a simulation study performed by (Madsen et al., 1997). The evaluation was based on the standardized RMSE with respect to the  year event estimator (for =10, 100 and 1000 years) for sample sizes 10, 30, 50. Although the performance of each method was dependent on the value of shape parameter, the considered return levels and the sample sizes, it was shown that the MOM estimators are preferable. In (Kyselý, 2002), the LMOM and MLE methods have been assessed for EVA of temperature; it was concluded that the individual return values were affected by the choice of the estimation method although there was no sensitivity as regards the estimated parameters by any of the methods. MPS, ML and LMOM methods for small sample sizes (10, 20, 50) have been evaluated through simulation by (Wong and Li, 2006). The evaluation for each parameter estimate was based on the mean absolute error and the authors concluded that the MPS performs better than ML method, while the first is more stable compared to ML and LMOM methods for small sample sizes. (Diebolt et al., 2008) introduced and evaluated the Generalized Probability-Weighted Moments (GPWM) method and compared it with ML and LMOM for small and medium samples (15, 25, 50 and 100). A recent joint evaluation of MPS, ML and EP methods (along with the quantile least squares method) can be found in (Ashoori et al., 2017). The average scaled absolute error criterion has been used for the evaluation of the obtained fits.

**4. The uncertainty in estimations**. Another important issue refers to two types of uncertainty that are associated with extreme value estimation problems, namely: i) the aleatory (inherent) uncertainty, that is due to the randomness of environmental processes and cannot be reduced, and ii) the epistemic uncertainty that can be reduced provided that sufficient data for the examined process are available. According to (Orimolade et al., 2016), the components of epistemic uncertainty are data uncertainty, model (probability) uncertainty, climatic uncertainty, and statistical uncertainty. The latter is mainly raised by the limited statistical information (e.g. limited sample size) and the parameter estimation method. Epistemic uncertainty may be reduced by increasing sample size and/or reducing sample measurement error (Wada et al., 2016), while the uncertainty raised by the sample size can be quantified using bootstrapping. In this framework and taking into consideration that in metocean practical applications EVA is usually based on sample sizes less than 50, (Wada et al., 2016) have taken into account the effects of the epistemic uncertainty in the estimates of return values. After a simulation study, it was concluded that the Likelihood-Weighted method (LW) provides better estimates of epistemic uncertainty from small samples of poor quality. Uncertainties related with wind and wave analysis have been also discussed by (Bitner-Gregersen et al., 2014) while a detailed discussion on wind measurement errors can be found in (Soukissian and Papadopoulos, 2015).

---

[1] According to bias, the MPS method performs better, while according to the mean squared error, the EP, MPS and ML methods seem to outperform.

**5. The presence of non-stationarity in the annual block maxima**. Studying environmental processes, non-stationarity is often necessary, due to seasonal effects or longer-term climate changes behavior. For example, the role of time–dependence in the statistics of extreme weather events has been argued in the context of climate change since the work from Katz and Brown (1992). In particular, the detection of trends in the frequency of intense precipitation has been the objective in Karl et al. (1995); Karl and Knight (1998) for the USA and Brunetti et al. (2004); Panagoulia et al., (2014) for the Mediterranean Sea respectively. The definition of a rigorous approach to the study of extremes is not trivial when the property of stationarity is questioned. One basic reason is that there is lack of a universal theory of extreme values (such as e.g. a generalization of Gnedenko's Theorem, see Chapter 2) for non-stationary stochastic processes. Moreover, in the analysis of observed or generated data from a reanalysis procedure, issues regarding the time scales that define the statistical properties and their changes, become debatable (Serinaldi and Kilsby, 2015). In Young et al. (2012), global altimeter data of a period of more than 20 years is analyzed to determine whether there are measurable trends in extreme value return period estimates of wind speed and wave height.A positive trend in extreme wind speed was supported in their findings. Nevertheless, for a stationary processes the probability characteristics do not change systematically in time, while for non-stationary process the parameters of the GEV distribution are allowed to vary through time. When incorporating non-stationarity into GEV parameters, some major points of concern are (i) what time dependent model to select, (ii) what characteristics must the parametric model satisfy in order to describe adequately the trend of the extreme event, and (iii) if all parameters truly vary in time.

Dixon and Tawn (1998) have studied two major classes of methods for estimating the distribution of the annual maximum sea-level in a non-stationary state condition. When the sea level process is decomposed to the four sources of non-stationarity (mean sea level, tide, surge seasonality and tide-surge interaction) and separately modeled, then these methods belong to the indirect classes. On the contrary, methods that directly estimate the time dependent process using covariate-dependent parameters of the distribution into the likelihood belong to the direct classes.

In addition, a new definition of the return period of a given level value is introduced with respect to a non-stationary continuous-time stochastic process. This definition is general and is based on the consideration of an appropriate crossing problem.This definition has been first used by Middleton, Thompson (1986) (see also Hamon, Middleton (1989)), for the prediction of sea-level extremes. Subsequently, Soukissian (1995) and Athanassoulis et al. (1995) have applied the above definition for the case of the long-term process of sea-states using the MEan Number of Upcrossings (MENU method), in order to estimate return periods and design values for the significant wave height. Finallly, the non-stationary extreme value analysis (NEVA) software package (Cheng et al. 2014) is outlined, as package explicitly designed to facilitate analysis of extremes in the geosciences (see Appendix D).

The benefit on modeling trends in the parameters of the distribution of the extremes is that the original data no longer have to be de-trended as classically modeled (Ferreira, 1997) and can be used directly. In this work (see Chapter 2), an assessment of various parametric models for the detection of the GEV covariate-parameters is made, considering a linear, quadratic and cubic trend through time (for the location and scale parameters) and a time independent model for the shape parameter. Effective return levels for specific values of the covariates is estimated and compared with the stationary case.

However, samples with a limited amount of extremes often fail to provide efficient quantile estimates for large return periods. When only few extremes are available for analysis, augmenting the sample of extremes via data segmentation is often imperative (Ferro and Segers

(2003). The question that often arises is how to successfully enrich a sample of extremes, encompassing as many discrete events as possible avoiding the approximate independent limitations. One classical approach dealing to this dilemma is by including more maxima per year using the annually $r$-largest order statistics concept based on the point process characterization (see Chapter3). Resent applications of this concept in wind speed time series may be found in An and Pandey (2007).

Another sampling approach besides the classical BM is by modeling exceedances over a high enough threshold $u$ at which the Generalized Pareto Distribution (GPD) provides a valid approximation to the excess distribution. The so called POT approach (Simiu and Heckert, 1996; Naess, 1998, Harris, 2005; Caires and Sterl, 2005) is widely accepted as the advance approach for modeling cluster exceedances and the most suitable for short time series. The major disadvantage of POT is related to the selection of the appropriate threshold value in order to satisfy the trade-off between bias and variance. Higher thresholds generally verify the requirements to the independent and identically distributed limitations. The contrary is met with lower thresholds.

Other approaches use the entire time series and consider different ways to extract the values to be processed under the principles of the extreme value theory. In general, in order to obtain a sufficient number of events from the time series, the data must be initially clustered and then de-clustered, selecting the maximum value of each cluster respectively. However, independency criteria between adjacent maxima are essential in EVA though frequently disregarded. The distribution and parameters of limited long-range dependent extremes, are strongly affected by the dependence in the series (Leadbetter, 1983).

In this study (see Chapter 4), a re-sampling procedure is proposed for the irregular samples of observations obtained from physical de-clustering considerations. The proposed model performs re-sampling taking into account the correlation effect in the irregular samples for a range of discrete energy reduction levels in the time series.

## 1.2 Main Objectives of this Dissertation

The present study focuses on the characterization of univariate extreme values. In particular, we aim on estimating the probability of extreme events occurred in a given period of time based on the modelling and extrapolation of these events using EVA on historical data. Clearly, these issues of risk analysis are of major importance in ocean and coastal engineering, meteorology and offshore wind energy section where this study anticipates to contribute in practical applications.

The specific objectives of this Thesis are outlined in three parts as shown below:

I.      Study the factors (sample size effect and parameter estimation methods) that influence the modelling of extremes of wind speed in the univariate case.

II.      Modelling extremes when the stationarity assumption of the process of wind speed is violated.

III.      Identify the effect of dependency in extremes when samples of wind speed are irregularly spaced in time and find ways to re-sample accordingly to the i.i.d limitations.

## 1.3 Outline

This rest of this Thesis is organized as follows:

In Chapter 2, models and methods along with the main mathematical framework for modelling univariate extremes are presented as the theoretical background of this study.

In Chapter 3 the modeling procedure of dependent sequences is in short discussed with emphasis on the demonstration of the well-known models that effectively re-sample the dependent events.

In Chapter 4 a suitable resampling strategy is analytically presented regarding the modelling of extremes that are irregularly spaced in time. The proposed methodology and the re-sampling schemes of reconstruction are presented in detail.

In Chapter 5 the datasets of wind speed at the study areas that will be used for this assessment are described in short with a preliminary statistical analysis of the samples originated from each data product.

Inference of the model fit obtained from the simulation process and applications is thoroughly discussed in Chapter 6 (sub-Section 6.1 and 6.2). The main findings from the proposed methodology is presented in 6.3, 6.4, and 6.5 .

Finally, the conclusions from this assessment are summarized and future work and improvements is also proposed.

# Chapter 2
## Standard modelling of Univariate Extremes

In this Chapter, a short introduction to the basic theory of univariate extremes is presented, along with the main mathematical aspects of the underlying distribution, i.e., the Generalized Extreme Value (GEV). In this context an analytical discussion of the theoretical background of the examined parameter estimation methods is made, along with the standard statistical tools that are used for the modelling of the i.i.d random variables. For a complete review of this material see Leadbetter et al. (1983) and de Haan and Ferreira (2006) for mathematical accounts and Beirlant et al. (2004) for more statistical treatments.

## 2.1 Asymptotic Model Formulation

The classical extreme value theory (EVT) studies the asymptotic derivations of the distributions of the maxima from a sequence of random variables, focusing on the inferences from the tail estimation where extreme events can be extrapolated with small probability. Let $\{X_1, \ldots, X_n\}$ denote a sequence of independent random variables, with a common cumulative distribution function (cdf) $H(x)$. The distribution function for the maxima of the sequence $M_n = \max(X_1, X_2, \ldots, X_n)$ is easily derived as follows,

$$\Pr\{M_n \leq x\} = \Pr\{X_1 \leq x\} \cdot \Pr\{X_2 \leq x\} \cdots \Pr\{X_n \leq x\} = H(x)^n, \text{ as } n \rightarrow \infty. \tag{2.1}$$

Since extremes occur in the upper or lower tails of a distribution, it is important to characterize the tail behavior of the distribution $H(x)$. For this, one needs to consider the asymptotic behavior of $M_n$ and how this is related to the distribution function $H(x)$ near the end points of the tails as $\rightarrow \infty$.

As pointed out by Coles (2001) and Embrechts et al. (1997), the disadvantage of $M_n$ in its current form (relation 2.1) is that its distribution function will degenerate to a point mass on the right end point $x_+ = \sup\{x \in R : H(x) < 1\}$, or $M_n \overset{P}{\rightarrow} x_+$ as $n \rightarrow \infty$. This provides no further information regarding the asymptotic distribution of $M_n$. The solution to this problem is to normalize the maximum. By choosing an appropriate sequence of normalizing constants $\{a_n > 0\}$ and $\{b_n \in R\}$, a linear transformation of $M_n$ can be found which stabilizes the location $b_n$ and scale $a_n$ of $M_n$ as $n$ increases, such that

$$\Pr\left\{\frac{M_n - b_n}{a_n} \leq x\right\} = H^n(a_n x + b_n) \rightarrow F(x) \tag{2.2}$$

where $F(x)$ is a non-degenerate distribution function. One of the key results in classical extreme value theory is that there are only three possible limiting distributions $F(x)$ for the normalized maximum. This result originally derived by Fisher and Tippett (1928) and later by Gnedenko (1943), is presented in the Fisher-Tippett Theorem, also referred to as the Extremal Types Theorem.

**Theorem 2.1** (Fisher-Tippett Theorem)

*Having an i.i.d sequence $\{X_n\} = X_1, X_2, \ldots, X_n$ of a random sample from a population with cdf $H(x)$, then, for appropriately defined normalizing sequences of constants $\{a_n > 0\}$ and $\{b_n\}$ such that as $n \rightarrow \infty$*

$$Pr[(M_n - b_n)/a_n \leq x] \rightarrow F(x), \tag{2.3}$$

*where $F(x)$ is a non-degenerate cdf, then $F(x)$ belongs to one of the following three families of distributions:*

$$F_I(x) = \exp\left[-\exp\left(-\left(\frac{x-b}{a}\right)\right)\right], \quad -\infty < x < \infty, \; a > 0, \tag{2.4}$$

$$F_{II}(x) = \begin{cases} \exp\left[-\left(\frac{x-b}{a}\right)^{-c}\right], & x > b, \; a > 0, \; c > 0 \\ 0, & x \leq b, \; a > 0, \; c > 0, \end{cases} \tag{2.5}$$

*and*

$$F_{III}(x) = \begin{cases} \exp\left\{-\left[-\left(\frac{x-b}{a}\right)^{c}\right]\right\}, & x < b, a > 0, c > 0 \\ 1, & x \geq b, a > 0, c > 0. \end{cases} \tag{2.6}$$

In other words, the above result states that the normalized maximum $M_n$ converges in distribution to a random variable following one of three possible cdf's shown in the above relations. The distribution functions $F(x)$ as presented in the Fisher-Tippett Theorem are called the extreme value (EV) distributions and are also commonly referred to as the Fisher-Tippet type I (FT-I or Gumbel class of distributions), type II (FT-II or Fréchet class of distributions) and type III (FT-III or reverse Weibull class of distributions) respectively. The Fisher-Tippett Theorem has one major implication, i.e., regardless of the distribution function $H(x)$, the extreme value distributions are the only possible limit distributions for a maximum for which the scale and the location have been stabilized. Analytical proof of the Fisher-Tippett Theorem is provided in Embrechtset al. (1997) and Leadbetter et al. (1983).

## 2.2 The Generalized Extreme Value Distribution

The three EV distributions can be combined into a single class of distribution known as the Generalized Extreme Value (GEV) distribution which is attributed to Von Mises (1954) and Jenkinson (1955). Specifically, the following theorem holds:

**Theorem 2.2** (Generalised Extreme Value Distribution GEV). *Let $X_1, X_2, \ldots, X_n$ be a sequence of i.i.d random variables arising from a non-degenerate distribution function $H(x)$. Then, if there exist sequences of constants $a_n > 0$ and $b_n$, such that, as $n \rightarrow \infty$, Theorem 2.1 holds for some non-degenerate distribution function $F(x)$, then $F$ is a member of the GEV $(\mu, \sigma, \xi)$ class of distributions given by*

$$F(x) = \exp\left\{-\left[1 + \xi\left(\frac{x-\mu}{\sigma}\right)\right]^{-1/\xi}\right\}, -\infty < x < \infty \tag{2.7}$$

*where the support is defined by $1 + \xi(x - \mu)/\sigma > 0$ and the parameters satisfy $-\infty < \mu < \infty$, $\sigma > 0$ and $-\infty < \xi < \infty$.*

The quantities $\mu$, $\sigma$ and $\xi$ represent the location, scale and shape parameters for the GEV distribution. The Fréchet class of distributions is derived when $\xi > 0$ and setting $\xi = 1/a$, $\sigma = b/a$ and $\mu = a + b$. The reverse Weibull class of distributions is derived when $\xi < 0$, and setting $\xi = -1/a$, $\sigma = b/a$ and $\mu = a - b$. Finally, the Gumbel class of distributions is derived when $\xi = 0$ and is interpreted as the limit $\xi \rightarrow 0$ with $\sigma = b$ and $\mu = a$, which results in the following expression

$$F(x) = \exp\left[-\exp\left(\frac{\mu - x}{\sigma}\right)\right], \quad -\infty < x < \infty \tag{2.8}$$

## 2.2.1 GEV properties for $\xi \neq 0$

The shape parameter $\xi$ affects the tail behavior of the GEV distribution. Considering $\xi > 0$, the distribution is skewed to the right and the support $1 + \xi \left(\frac{x-\mu}{\sigma}\right)^{-1/\xi} > 0$ is bounded to the left with $x > \mu - \frac{\sigma}{\xi}$. When $\xi < 0$, the distribution is skewed to the left and the support of GEV is bounded to the right with $x < \mu - \frac{\sigma}{\xi}$. Differentiating the GEV distribution, yields the probability density function (pdf)

$$f(x) = \frac{1}{\sigma} \exp\left(-\left[1 + \xi\left(\frac{x-\mu}{\sigma}\right)^{-1/\xi}\right]\right)\left[1 + \xi\left(\frac{x-\mu}{\sigma}\right)\right]^{-\left(\frac{1}{\xi}+1\right)}, \tag{2.9}$$

where $1 + \xi\left(\frac{x-\mu}{\sigma}\right)^{-1/\xi} > 0, -\infty < \mu < \infty, \sigma > 0, -\infty < \xi < \infty$.

The characteristic function, see (Appendix A), determines the behavior and properties of the probability distribution of a random variable $X$. Considering the GEV pdf, it is derived, Muraleedharanet all. (2007):

$$\varphi_X(t) = E[\exp(itX)] = \int_{\infty}^{\mu - \sigma/\xi} \exp(itx) f(x; \mu, \sigma, \xi) dx \tag{2.10}$$

and substituting correspondingly, yields

$$\varphi_X(t) = \exp(it\mu)\left[\exp(-it\sigma/\xi) - \sum_{r=0}^{\infty}\frac{-(it\sigma)^{r+1}}{r!\xi^r}\sum_{n=0}^{r}(-1)^n C_n^r \frac{\Gamma(1-(n+1)\xi)}{(n+1)\xi}\right], \tag{2.11}$$

for $= 0,1,2,\dots$, where $C_n^r = \frac{r!}{n!(r-n)!}$ and $\Gamma(u) = \int_0^{\infty} y^{u-1}\exp(-y)dy$, (see Appendix B for the Gamma function and derivatives).

The first three moments of the GEV distribution result from the moment generating function (MGF),

$$M_X^{(n)}(0) = E(X^n) = \left[\frac{d^n \varphi_X(t)}{dt^n}\right]_{t=0}, \tag{2.12}$$

where from differentiating correspondingly the characteristic function it is easily obtained:

$$M_X^{(1)}(0) = E(X) = \mu - \frac{\sigma}{\xi} + \frac{\sigma}{\xi}\Gamma(1-\xi) \tag{2.13}$$

$$M_X^{(2)}(0) = E(X^2) = \frac{\sigma^2}{\xi^2}\left(1 - 2\Gamma(1-\xi) + \Gamma(1-2\xi)\right) - \frac{2\mu\sigma}{\xi}\left(1 - \Gamma(1-\xi)\right) + \mu^2 \tag{2.14}$$

$$M_X^{(3)}(0) = E(X^3) = -\frac{\sigma^3}{\xi^3}\left(1 - 3\Gamma(1-\xi) + 3\Gamma(1-2\xi) - \Gamma(1-3\xi)\right) +$$

$$+ \frac{3\mu\sigma^2}{\xi^2}\left(1 - 2\Gamma(1-\xi) + \Gamma(1-2\xi)\right) - \frac{3\mu^2\sigma}{\xi}\left(1 - \Gamma(1-\xi)\right) + \mu^3 \tag{2.15}$$

The first moment only exists when $\xi < 1$, the second moment only when $\xi < 1/2$ and the third moment only when $\xi < 1/3$. Therefore, if $\xi < 0$ the GEV distribution consists of finite moments and if $\xi > 0$ the GEV distribution has finite moments of order less than $1/\xi$.

Considering $g_k = \Gamma(1 - k\xi), k = 1,2,3$, the theoretical mean, variance and skewness for the GEV distribution yields respectively:

$$\text{mean}(X) = \begin{cases} M_X^{(1)}(0) = E(X) = \mu - \frac{\sigma}{\xi} + \frac{\sigma}{\xi} g_1 & \xi \neq 0, \xi < 1 \\ \infty & \xi \geq 1 \end{cases}, \quad (2.16)$$

$$\text{Var}(X) = \begin{cases} E[X^2] - (E[X])^2 = \frac{\sigma^2}{\xi^2}[g_2 - g_1^2] & \xi \neq 0, \xi < 1/2 \\ \infty & \xi \geq 1/2 \end{cases}, \quad (2.17)$$

and

$$\text{Skewness}(X) = \frac{E[(X - E[X])^3]}{(E[(X - E[X])^2])^{3/2}} = \frac{E[X^3] - 3E[X] \cdot Var(X) - (E[X])^3}{(Var(X))^{3/2}} =$$

$$= \text{sign}(\xi)\left[\frac{g_3 - 3g_1 g_2 + 2g_1^3}{(g_2 - g_1^2)^{3/2}}\right] = \begin{cases} \text{sign}(\xi)\left[\frac{g_3 - 3g_1 g_2 + 2g_1^3}{(g_2 - g_1^2)^{3/2}}\right] & \xi \neq 0, \xi < 1/3 \\ \infty & \xi \geq 1/3 \end{cases}. \quad (2.18)$$

The median and the mode of the GEV distribution yield respectively

$$\text{median}(X) = \left\{ \mu + \frac{\sigma}{\xi}\left[(\ln 2)^{-\xi} - 1\right], \quad \xi \neq 0, \text{ and} \right. \quad (2.19)$$

$$\text{mode}(X) = \left\{ \mu + \frac{\sigma}{\xi}\left[(1 + \xi)^{-\xi} - 1\right], \quad \xi \neq 0. \right. \quad (2.20)$$

## 2.2.2 GEV Properties for $\xi \to 0$

The distribution function for the Gumbel is obtained by considering the limit of GEV as $\xi \to 0$, $\lim_{\xi \to 0} F(x; \mu, \sigma, \xi)$, leading to $F(x; \mu, \sigma)$ as shown previously. Differentiating with respect to $x$, yields the pdf

$$f(x) = \frac{1}{\sigma}\exp\left[-\exp\left[-\left(\frac{x - \mu}{\sigma}\right)\right]\right]\exp\left[-\left(\frac{x - \mu}{\sigma}\right)\right]. \quad (2.21)$$

In order to find the characteristic function, the Gumbel random variable $X$ is first transformed into a standard Gumbel random variable using $Z = \frac{X - \mu}{\sigma}$. The density of $Z$ is then given by

$$f(z) = \exp(-\exp(-z))\exp(-z), \text{ for} -\infty < z < \infty. \quad (2.22)$$

The characteristic function of $Z$ yields:

$$\varphi_Z(t) = E[e^{itZ}] = \int_{-\infty}^{\infty} e^{itz} e^{-e^{-z}} e^{-z} dz = \int_0^{\infty} u^{-it} e^{-u} du = \Gamma(1 - it), i = \sqrt{-1}.$$

Consequently, the characteristic function of variable $X = \mu + Z\sigma$ is provided as follows:

$$\varphi_X(t) = E[e^{itX}] = e^{it\mu}\Gamma(1 - it\sigma).$$

The first three moments of the variable $X$ of the Gumbell type I distribution, result from the moment generating function (MGF),

$$M_X^{(n)}(0) = E(X^n) = \left[\frac{d^n \varphi_X(t)}{dt^n}\right]_{t=0}, \tag{2.23}$$

differentiating correspondingly the characteristic function $\varphi_X(t)$ in (2.23) as follow:

$$\begin{cases} M_X^{(1)}(0) = E(X) = \mu\Gamma(1) - \sigma\Gamma'(1) = \mu + \sigma\gamma, \\ M_X^{(2)}(0) = E(X^2) = \mu^2\Gamma(1) - 2\mu\sigma\Gamma'(1) + \sigma^2\Gamma''(1) = (\mu + \sigma\gamma)^2 + \sigma^2\frac{\pi^2}{6}, \\ M_X^{(3)}(0) = E(X^3) = \mu^3\Gamma(1) - 3\sigma\mu^2\Gamma'(1) + 3\mu\sigma^2\Gamma''(1) - \sigma^3\Gamma'''(1), \end{cases} \tag{2.24}$$

where $\gamma = -\Gamma'(1) = -\int_0^\infty e^{-x}\ln(x)dx \simeq 0.5772156649...$ is Euler's constant, and approximations $\Gamma(1) = 1, \zeta(2) = \frac{\pi^2}{6}, \Gamma''(1) = \gamma^2 + \zeta(2)$, and $\Gamma'''(1) = -2\zeta(3) - 3\gamma\zeta(2) - \gamma^3$.

The theoretical mean, variance and skewness for the Gumbel distribution yields respectively:

$$\begin{cases} \text{mean}(X) = M_X^{(1)}(0) = E(X) = \mu + \sigma\gamma, \\ \\ \text{Var}(X) = E[X^2] - (E[X])^2 = \sigma^2\frac{\pi^2}{6}, \\ \text{Skewness}(X) = \frac{E[(X-E[X])^3]}{(E[(X-E[X])^2])^{3/2}} = \frac{E[X^3] - 3E[X]\cdot Var(X) - (E[X])^3}{(Var(X))^{3/2}} = \frac{12\sqrt{6}\zeta(3)}{\pi^3}. \end{cases} \tag{2.25}$$

Moreover, the median and the mode of the Gumbel distribution yield respectively

$$\begin{cases} \text{median}(X) = \mu - \sigma(\ln(\ln 2)), \\ \text{mode}(X) = \mu. \end{cases} \tag{2.26}$$

## 2.2.3 Return Levels of the Block Maxima

The limiting distribution form of the normalized maxima as presented in Theorem 2.2, points out a probability model for the distribution of (BM). The maxima are considered as a sequence of single maxima values corresponding each to a specific block of time. Blocks are generally considered of equal size, e.g. annual maxima, monthly maxima etc., satisfying the asymptotic properties of Theorem 2.2, through the trade-off between bias and variance, i.e. small blocks increase the bias, whereas large blocks result in large estimation variance. The BM approach presumes that the observed sequence of $n$ independent and identically distributed maxima $x_1, x_2, \ldots, x_n$ is modelled by the GEV distribution. Estimates of extreme quantiles of the BM distribution are commonly used in EVA for inference, providing the henceforth definition.

**Definition 2.1**. *Assuming $p \in (0,1)$ and $F(x)$ a distribution function, then the level $x_p$, for which $F(x_p) = 1 - p$, is defined as the return level with the associated return period of $1/p$. If $F(x)$ belongs within the class of $GEV(\mu, \sigma, \xi)$, then estimates of the extreme quantiles (design values) for the GEV distribution are provided through the following relation:*

$$x_p(\mu, \sigma, \xi) = \begin{cases} \mu - \frac{\sigma}{\xi}\{1 - [-\log(1-p)]^{-\xi}\}, & \xi \neq 0, \\ \mu - \sigma\log[-\log(1-p)], & \xi = 0. \end{cases} \tag{2.27}$$

The level $x_p$ is expected to be exceeded on average once in $1/p$ blocks. From the property of a parameter estimator (see subsequent Section), it follows that the parameter estimates of the return levels are given by $\hat{x}_p = x_p(\hat{\mu}, \hat{\sigma}, \hat{\xi})$.

## 2.3 Parameter estimation methods

In this section, the following methods for the estimation of the parameters of the GEV distribution are presented: the ordinary moments method, the probability weighted moments method, the L-moments methods according to Hosking and according to Wang, the maximum likelihood method, the maximum product spacings method, the quantile least squares method, the elemental percentile method, the method based on the principle of maximum entropy and the maximum entropy parameter space expansion method. All methods are also analytically studied in (Soukissian and Tsalis, 2015). For reasons of simplicity, we will frequently denote by $f(x; \boldsymbol{\theta})$ any distribution function with parameter(s) $\boldsymbol{\theta}$, while, specifically for the GEV distribution function, $\boldsymbol{\theta} = (\xi, \sigma, \mu)$. Descriptions for some of the above mentioned estimation methods for the GEV case can be found in Castillo et al. (2005), Kotz and Nadarajah (2000) and a variety of graphical methods for model selection can be also found therein.

For the most well-known under-examination estimation methods (maximum likelihood, ordinary moments, L-moments and least-squares methods) a short description will be provided. On the other hand, for the rather unknown or complicated estimation methods (principle of maximum entropy, maximum product of spacings method and elemental percentile methods) a more detailed presentation of the corresponding mathematical background will be given. Additionally, the most popular framework vastly reported in the relative literature for stationary POT exceedances, is the maximum likelihood method. Therefore, in this study it will be considered as the only parameter estimation method modelling exceedances under the POT approach. Specifically, only the maximum likelihood method is theoretically efficient and provides approximate normal distributions and approximate sample variances that can be used to generate confidence bounds for estimations.

### 2.3.1 The maximum likelihood method

The likelihood function $L(x_1, x_2, \ldots, x_n; \boldsymbol{\theta})$ is the joint density pdf evaluated at $x_1, x_2, \ldots x_n$. For the GEV distribution the logarithm of the likelihood function is given as:

$$l(\mu, \sigma, \xi) = -n\log\sigma - (1 + \xi)\sum_{i=1}^{n} z_i - \sum_{i=1}^{n} \exp(-z_i), \quad \xi \neq 0, \qquad (2.28)$$

where $z_i = \frac{1}{\xi}\log\left(1 + \xi\frac{(x_i - \mu)}{\sigma}\right),$ $\qquad\qquad(2.29)$

and $1 + \xi\left(\frac{x_i - \mu}{\sigma}\right) > 0$ for $i = 1, 2, \ldots, n.$ $\qquad\qquad(2.30)$

For $\xi = 0$, GEV distribution simplifies to the Gumbel distribution and the corresponding log-likelihood function is

$$l(\mu, \sigma) = -n\log\sigma - \sum_{i=1}^{n} \exp\left[-\left(\frac{x_i - \mu}{\sigma}\right)\right] - \sum_{i=1}^{n}\left[-\left(\frac{x_i - \mu}{\sigma}\right)\right]. \qquad (2.31)$$

Assuming that the log-likelihood function is differentiable, parameters $\hat{\xi}$, $\hat{\sigma}$, $\hat{\mu}$, can be estimated by maximizing the log-likelihood function respectively. No closed-form solution to

the maximization problem is available; thus, it has to be solved numerically using nonlinear optimization methods. It is noted in Hosking, (1985) and Coles and Dixon (1999) that for $\xi > -0.5$ the MLE estimates have usual asymptotic properties, for $-1 < \xi < -0.5$ MLE estimates are obtainable but do not have standard asymptotic properties, for $\xi < -1$ MLE estimates do not exist and when $\xi > 0.5$ second and higher moments do not exist. The case where $\xi \leq -0.5$ is rarely encountered in practical applications in extremes leading to distributions with very short bounded upper tail. It is also noted that the MLE method introduces negligible bias for sample sizes from 30 up to 100. Furthermore, MLE and relation $l(\mu, \sigma, \xi)$ in the neighborhood of $\xi = 0$ should be avoided. In general, for the modeling of random variables like wind speed it is likely to obtain more often zero and negative shape parameter estimates rather than positive (Jonathan and Ewans, 2013; Brabson and Palutikof, 2000; and Cheng E, Yeung C, 2002).

## 2.3.2 The Ordinary Moments method

The method of ordinary moments (will be referenced as OM from now on), was developed to estimate parameters of linear hydrological models and was initially presented by Pearson in 1894, see Pearson (1894) and Nash (1959). The basic assumption of the OM method is that sample moments are good estimators of the corresponding population moments. Sample moments are equated to corresponding population moments and the obtained equations are solved for the unknown parameters of the distribution. Regarding the GEV distribution and taking into account Equations (2.16), (2.17) and (2.18) we result to a system with three unknowns ($\hat{\xi}$, $\hat{\sigma}$, and $\hat{\mu}$), that is not susceptible to a closed form solution and should therefore be solved numerically. Accounts for the OM method can be found in Wallis et al. (1974), Madsen et al. (1997) and references cited therein.

## 2.3.3 The probability weighted moments method

Greenwood et al. (1979), introduced the method of Probability Weighted Moments (called hereafter PWM) in hydrological applications; see also Hosking et al. (1985). For a continuous random variable $X$ with pdf $f(x; \boldsymbol{\theta})$ and cdf $F(x; \boldsymbol{\theta})$, the PWM estimators are obtained by matching the population $k^{th}$ weighted-moments with the corresponding weighted sample moments. The PWM method for the GEV distribution was implemented in Hosking et al. (1985) ([2]).

The general expression for the weighted moments of order $r, s, t$ of a random variable $X$, is given as follows, see Greenwood et al. (1979):

$$M(r, s, t) = E\{X^r [F(X; \boldsymbol{\theta})]^s [1 - F(X; \boldsymbol{\theta})]^t\}. \tag{2.32}$$

For the special case $r = 1$, $t = 0$ the above relation is written as

$$\beta_s = M(1, s, 0) = E[X\{F(X; \boldsymbol{\theta})\}^s] = \int_0^1 x(F) F^s dF, s = 0,1,2, .... \tag{2.33}$$

Considering the GEV distribution, we obtain the following expression for $\beta_s$:

$$\beta_s = (1 + s)^{-1} \left[ \mu - \frac{\sigma}{\xi} \left( 1 - (1 + s)^{\xi} \Gamma(1 - \xi) \right) \right], \xi < 1, \text{ and } \xi \neq 0. \tag{2.34}$$

Furthermore, for $s = 0,1,2$, after rearrangement, we yield respectively the following equations:

---

([2]) The expressions for the parameters of the GEV distribution according to the PWM method, are the same as those obtained by the method of L-moments. For the sake of completeness though, we will present the theoretical background of both methods.

$$\beta_0 = \mu - \frac{\sigma}{\xi}\{1 - \Gamma(1 - \xi)\}, \tag{2.35}$$

$$\frac{3\beta_2 - \beta_0}{2\beta_1 - \beta_0} = \frac{(3^\xi - 1)}{(2^\xi - 1)}, \tag{2.36}$$

$$2\beta_1 - \beta_0 = \frac{\sigma}{\xi}\Gamma(1 - \xi)(2^\xi - 1). \tag{2.37}$$

For an ordered sample $x_{1:n} \leq x_{2:n} \leq \ldots \leq x_{n:n}$, of size $n$, the general unbiased sample estimator $\hat{\beta}_{s,U}$ of $\beta_s$ is given as follows:

$$\hat{\beta}_{s,U} = \frac{1}{n}\sum_{j=1}^{n}\frac{(j-1)(j-2)\ldots(j-s)}{(n-1)(n-2)\ldots(n-s)}x_{j:n}. \tag{2.38}$$

The asymptotic normality of the above estimator for $\xi < 0.5$ is proved in Hosking et al. (1985), where it is also stated that the PWM estimators are superior to the maximum likelihood estimators for small samples, see also Martins and Stedinger (2000).

Another simpler, but biased, sample estimator $\hat{\beta}_{s,B}$ for $\beta_s$ is suggested in Hosking et al. (1985) as follows:

$$\hat{\beta}_{s,B} = \frac{1}{n}\sum_{j=1}^{n}p_{j:n}^s x_j, \tag{2.39}$$

where $p_{j:n}$, $j = 1,2,\ldots,n$, is the sample (empirical) estimate of $F(x)$, see Equation (D1) in Appendix. For reasonable choices of $p_{j:n}$, the above estimator is a consistent estimator for $\beta_s$.

Combining relation (2.38) or (2.39) for $s = 0,1,2$ with relations (2.35), (2.36), (2.37), respectively, we result to a system which can be solved with respect to $\hat{\xi}$, $\hat{\sigma}$ and $\hat{\mu}$. Accordingly, equation (2.36) is written

$$\frac{3\hat{\beta}_2 - \hat{\beta}_0}{2\hat{\beta}_1 - \hat{\beta}_0} = \frac{(3^\xi - 1)}{(2^\xi - 1)}. \tag{2.40}$$

This equation may be solved both numerically and by following the approximation estimate:

$$\hat{\xi} = 7.8590C + 2.9554C^2, \tag{2.41}$$

where

$$C = \frac{2\hat{\beta}_1 - \hat{\beta}_0}{3\hat{\beta}_2 - \hat{\beta}_0} - \frac{\log 2}{\log 3}. \tag{2.42}$$

Having estimated $\xi$, parameters $\hat{\sigma}$ and $\hat{\mu}$ can be then easily obtained from equations (2.35) and (2.37). Accounts of the PWM method can be found in Hosking (1986).

### 2.3.4 The L-moments method according to Hosking

The method of L-moments, (LMH) was developed by Hosking (1986, 1990), and is based on the order statistics theory. Since then, this method has become very popular for characterization of probability distributions and parameter estimation. L-moments are linear combinations of order statistics and can be expressed through probability weighted moments. Analogously to the conventional moments, the L-moments of order one to three characterize the location, scale, and skewness parameter,respectively.

For the GEV cdf, the first three L-moments are expressed as follows:

$$L_1 = \int_0^1 x(F)dF = \mu - \frac{\sigma}{\xi}\big(1 - \Gamma(1 - \xi)\big) = \beta_0, \tag{2.43}$$

$$L_2 = \int_0^1 x(F)(2F - 1)dF = -\frac{\sigma}{\xi}\big(1 - 2^\xi\big)\Gamma(1 - \xi) = 2\beta_1 - \beta_0, \tag{2.44}$$

$$L_3 = -\left(\frac{2(1-3^\xi)}{(1-2^\xi)} - 3\right)\frac{\sigma}{\xi}\big(1 - 2^\xi\big)\Gamma(1 - \xi) = 6\beta_2 - 6\beta_1 + \beta_0. \tag{2.45}$$

The right-hand side equalities of equations (2.43), (2.44) and (2.45) have been obtained taking into account relations (2.35), (2.36) and (2.37). Therefore, the results of the L-moments method are the same as those of the PWM method. Furthermore, by using either the sample unbiased estimators for the probability weighted moments $\hat{\beta}_{s,U}$ (referred to as the L-Hosking unbiased estimation method LMH$_U$) or the corresponding sample biased estimators $\hat{\beta}_{s,B}$ (referred to as the L-Hosking biased estimation method LMH$_B$), the above system can be solved numerically with respect to the parameters $\xi, \sigma$ and $\beta$. Recently accounts of this method is found in Hosking and Wallis, (1997).

### 2.3.5 The L-moments method according to Wang

The method of L-moments according to Wang (LMW), see Wang (1996), provides direct estimations of the sample L-moments, using expressions without involving PWM and considering all possible combinations. In this case, the first three sample L-moments are given respectively as follows:

$$\hat{L}_1 = \binom{n}{1}^{-1}\sum_{i=1}^n x_{i:n}, \tag{2.46}$$

$$\hat{L}_2 = \frac{1}{2}\binom{n}{2}^{-1}\sum_{i=1}^n \left[\binom{i-1}{1} - \binom{n-i}{1}\right]x_{i:n}, \tag{2.47}$$

$$\hat{L}_3 = \frac{1}{3}\binom{n}{3}^{-1}\sum_{i=1}^n \left[\binom{i-1}{2} - 2\binom{i-1}{1}\binom{n-i}{1} + \binom{n-i}{2}\right]x_{i:n}. \tag{2.48}$$

Equating the above sample L-moments from equations (2.46), (2.47) and (2.48), with the corresponding GEV L-moments of equations (2.43), (2.44), and (2.45), we result in a system with unknowns the parameters of interest $\hat{\xi}, \hat{\sigma}, \hat{\mu}$.

## 2.3.6 The maximum product of spacings method

The method of maximum product of spacings (MPS) was first introduced for estimating parameters in continuous distribution families in Cheng and Amin (1983), Ranneby (1984). Since the ML estimators may fail to converge due to the restraints implied from the second derivative of the log-likelihood, the MPS method can be considered instead. It is noted in Wong and Li (2006) that although there are problems quite often arising with the use of ML, the MPS method has been neglected in the extreme value analysis.

The general set-up of the MPS method is as follows: Let $x_{1:n} \leq x_{2:n} \leq \cdots \leq x_{n:n}$ be a sequence of ordered points. Define the spacing between the values of the distribution at two consecutive ordered points, i.e.:

$$D_i(\boldsymbol{\theta}) = F(x_{i:n}; \boldsymbol{\theta}) - F(x_{i-1:n}; \boldsymbol{\theta}) = \int_{x_{i-1:n}}^{x_{i:n}} f(x; \boldsymbol{\theta}) dx, i = 1, 2, \dots, n+1, \qquad (2.49)$$

where $x_{0:n} = -\infty$ and $x_{n+1:n} = \infty$. It then follows immediately that the spacing's sum to unity, i.e.,

$$\sum_{i=1}^{n} D_i(\boldsymbol{\theta}) = 1, \qquad (2.50)$$

and that

$$D_1(\boldsymbol{\theta}) = F(x_{1:n}; \boldsymbol{\theta}), \qquad D_{n+1}(\boldsymbol{\theta}) = 1 - F(x_{n:n}; \boldsymbol{\theta}). \qquad (2.51)$$

The MPS method estimates the appropriate value of $\boldsymbol{\theta}$, so that the product of probabilities of a new observation is maximized between each two neighboring sample points. $D_i$'s are as close to each other as possible. We choose the parameter $\boldsymbol{\theta}$ so as to maximize the logarithm of the geometric mean $GM$ of the spacing's, i.e.,

$$H(\boldsymbol{\theta}) = \log(GM) = \log\left\{\prod_{i=1}^{n+1} D_i(\boldsymbol{\theta})\right\}^{1/(n+1)} = \frac{1}{n+1} \sum_{i=1}^{n+1} \log[D_i(\boldsymbol{\theta})], \qquad (2.52)$$

under the constraints for the parameters $\boldsymbol{\theta}$ of the distribution. The optimum MPS log-estimator is given as:

$$H_{opt}(\boldsymbol{\theta}) = \log\frac{1}{n+1}, \qquad (2.53)$$

see also Ranneby (1984). From the above relation, it can be concluded that the basic advantage of MPS method over the ML is that the log-likelihood function can go to positive infinity, whereas the MPS log-estimator is always bounded above by $\log(1/(n+1))$. It may easily be proved that the optimum maximum of $GM$ is obtained only when all $D_i$'s are equal to $D_i = i/(n+1)$. Taking into account relation (2.49) and the specific expression for the GEV pdf, we obtain the following expression

$$H_{opt}(\xi, \sigma, \mu) = \frac{1}{n+1} \sum_{i=1}^{n+1} \log \int_{x_{i-1}}^{x_i} \left[\exp\left(-(1 + U_i)^{-1/\xi}\right)(1 + U_i)^{-1/(\xi+1)} \frac{1}{\sigma}\right] dx, \qquad (2.54)$$

where,

$$U_i = \xi\left(\frac{x_i - \mu}{\sigma}\right), i = 1,2,\cdots,n+1. \tag{2.55}$$

The parameters $\xi$, $\sigma$ and $\mu$ are estimated by maximizing the above MPS log-estimator. Similarly as before, there are not available closed-form solutions; therefore MPS estimators have to be found numerically using nonlinear optimization methods.

## 2.3.7 The quantile least squares method

The method of quantile least squares (QLS) has been introduced in Castillo et al. (1997). The basic principle of QLS method is to estimate the parameters of interest by minimizing the sum of squares of the differences between the theoretical and the empirical quantiles.

The sample quantile of the GEV distribution, see relation (2.27), may be estimated, by using any appropriate plotting position (see Appendix C), as follows:

$$x_{i:n} = \mu - \frac{\sigma}{\xi}\left[1 - \left(-\log(p_{i:n})\right)^{-\xi}\right], \tag{2.56}$$

where $p_{i:n}$, $i = 1,2,\ldots,n$ is the empirical estimate of the unknown cumulative distribution function. The quantity which is to be minimized is the following:

$$Q = \sum_{i=1}^{n}\left[x_{i:n} - x_p\right]^2. \tag{2.57}$$

This is achieved by partially differentiating (2.57) with respect to each parameter. Since no closed-form solutions are available, the QLS estimators have to be estimated numerically using nonlinear optimization methods. It is evident that for various plotting positions different results will be obtained.

## 2.3.8 The elemental percentile method

The Elemental Percentile (EP) method has been introduced in Castillo and Hadi (1994) and its estimators are based on order statistics. Specifically, the method consists in two steps:

1. The estimators are obtained by first equating the cdf evaluated at the observed order statistics, to the corresponding percentile values, and then by using the resulting equations to obtain initial estimates of the parameters.
2. These estimates are then combined in such a way to be statistically more efficient estimates of the parameters.

Let $x_{1:n} < x_{2:n} <\ldots< x_{n:n}$ be an ordered random sample drawn from the GEV distribution, with corresponding quantile function $x(F) = F^{-1}(x;\xi,\sigma,\mu)$. In the first step, let $I = \{i,j,r\}$ be a set of three ordered indices $i < j < r \in (1,2,\ldots,n)$. By considering an appropriate plotting position for $p_{i:n}$, as e.g., the one of equations (C1) or (C2) in the Appendix, and equating the ordered sample values with the theoretical GEV quantiles for the three indices, we obtain the following relations:

$$x_{i:n} = \mu - \frac{\sigma}{\xi}\left[1 - (-\log p_{i:n})^{-\xi}\right], \tag{2.58}$$

$$x_{j:n} = \mu - \frac{\sigma}{\xi}\left[1 - (-\log p_{j:n})^{-\xi}\right], \tag{2.59}$$

$$x_{r:n} = \mu - \frac{\sigma}{\xi}\left[1 - (-\log p_{r:n})^{-\xi}\right]. \tag{2.60}$$

By eliminating $\mu$ and $\sigma$ from the above equations, we obtain the ratio

$$\frac{x_{j:n} - x_{r:n}}{x_{i:n} - x_{r:n}} = \frac{C_r^{-\xi} - C_j^{-\xi}}{C_r^{-\xi} - C_i^{-\xi}} = \frac{1 - A_{jr}^{-\xi}}{1 - A_{ir}^{-\xi}}, \tag{2.61}$$

where $C_i = -\log(p_{i:n})$ and $A_{ir} = \frac{C_i}{C_r}$. Equation (2.61) may be solved using the bisection method and $\hat{\xi}_{ijr}$ is estimated as a function of the three observations $x_{i:n}, x_{j:n}, x_{r:n}$. Substituting $\hat{\xi}_{ijr}$ into equations (2.59) and (2.60) we obtain:

$$\hat{\sigma}_{ijr} = \frac{\hat{\xi}_{ijr}(-x_{i:n} + x_{r:n})}{C_r^{-\hat{\xi}} - C_i^{-\hat{\xi}}}, \tag{2.62}$$

and

$$\hat{\mu}_{ijr} = x_{i:n} + \frac{\hat{\sigma}_{ijr}\left(1 - C_i^{-\hat{\xi}_{ijr}}\right)}{\hat{\xi}_{ijr}}. \tag{2.63}$$

If the estimated parameters do not satisfy the appropriate conditions provided in Theorem 2.2 they are rejected. An analogous procedure can be followed for $\xi = 0$.

At the second step, the above procedure is repeated by choosing all the possible combinations $I = \{i, j, r\}$. As before, inconsistent estimates are rejected. The final estimates of $\hat{\xi}, \hat{\sigma}, \hat{\mu}$ are considered to be the corresponding medians of the estimated parameter samples, i.e.:

$$\hat{\xi}_{MED} = \text{median}(\hat{\xi}_1, \hat{\xi}_2, \ldots, \hat{\xi}_N), \tag{2.64}$$

$$\hat{\sigma}_{MED} = \text{median}(\hat{\sigma}_1, \hat{\sigma}_2, \ldots, \hat{\sigma}_N), \tag{2.65}$$

$$\hat{\mu}_{MED} = \text{median}(\hat{\mu}_1, \hat{\mu}_2, \ldots, \hat{\mu}_N). \tag{2.66}$$

Instead of the median the least median of squares can be also used.

## 2.3.9 The concept of maximum entropy method

The parameter estimation method that is based on the concept of maximum entropy is probably the most complicated and rather unknown method for the ocean and coastal engineering communities. An analytic introduction to this method and the resulting relevant parameter estimation methods is provided in the monograph of Singh (1998), which is considered as the basic reference for this subsection.

The concept of entropy quantifies the uncertainty associated with a distribution function which is employed for the description of a random variable. Shannon first, see Shannon (1948), provided a measure of uncertainty connected with the pdf $f(x; \boldsymbol{\theta})$ of a random variable $X$, defined as follows:

$$H(f(x; \boldsymbol{\theta})) = -\int_a^b f(x; \boldsymbol{\theta})\ln f(x; \boldsymbol{\theta})dx, \tag{2.67}$$

with

$$\int_a^b f(x; \boldsymbol{\theta})dx = 1. \tag{2.68}$$

$H(f(x; \boldsymbol{\theta}))$ is called Shannon entropy functional and can be thought of as the mean value of $-\ln(f(x; \boldsymbol{\theta}))$.

The principle of maximum entropy (POME), closely related to the concept of entropy, was formulated by Jaynes (1982), who stated that "the minimally prejudiced assignment of probabilities is that which maximizes the entropy subject to the given information".

The principle of maximum entropy (POME) method

According to Jaynes (1982), the mathematical translation of the above statement is the following, see also Singh (1998):

By defining $N$ linearly independent constraints $C_i$:

$$C_i = \int_a^b y_i(x)f(x)dx, \quad i = 1,2,\dots,N, \tag{2.69}$$

where $y_i(x)$ are functions whose averages over $f(x)$ are specified, the maximum of the Shannon entropy functional (2.68) subject to the conditions implied from equation (2.69) is given by the following distribution:

$$f(x) = \exp\left[-a_0 - \sum_{i=1}^N a_i y_i(x)\right], \tag{2.70}$$

where $a_i$, $i = 0,1,\dots N$, are Lagrange multipliers determined from equations (2.69) and (2.70) taking also into account the normalizing condition that $f(x)$ must satisfy; see equation (2.68). In this case, the value of the Shannon entropy functional is given as follows:

$$H(f(x; \boldsymbol{\theta})) = a_0 + \sum_{i=1}^N a_i C_i, i = 1,2,\dots,N. \tag{2.71}$$

In order to estimate the parameters of the distribution, the following steps should be made:

 I. The "given information" should be defined through constraints, which are related to the data sample,
 II. The entropy, which is subject to the given information, should be maximized and finally,
 III. The sought-for parameters should be related to the given information.

The available information from the sample is given by equation (2.69). Combining equations (2.70) and the normalizing condition for $f(x)$ in equation (2.68), we obtain the following zero-th order Lagrange multiplier:

$$a_0 = \log \int_a^b \exp\left[-\sum_{i=1}^N a_i y_i\right]dx, \tag{2.72}$$

It can be also shown that Lagrange multipliers are expressed by means of the constraints as follows:

$$-\frac{\partial a_0}{\partial a_i} = C_i, \tag{2.73}$$

and that

$$\frac{\partial^2 a_0}{\partial a_i^2} = Var[y_i(x)] \text{ and } \frac{\partial^2 a_0}{\partial a_i \partial a_j} = Cov[y_i(x), y_j(x)], \, i \neq j, \tag{2.74}$$

where $Var(\cdot)$ and $Cov(\cdot)$ denote variance and covariance respectively. In this way, $f(x)$ in equation (2.70) is uniquely defined.

If, now, a certain form of the pdf $f(x)$ is available and the estimation of the parameters is the task in hand, then (2.71) has to be maximized. For this, we differentiate partially with respect to $(N-1)$ number of Lagrange multipliers, and to $N$ numbered specified parameters directly, i.e.,

$$\frac{\partial H(f(x;\boldsymbol{\theta}))}{\partial a_i} = 0 \, , \, i = 1, 2, \ldots, N-1, \tag{2.75}$$

$$\frac{\partial H(f(x;\boldsymbol{\theta}))}{\partial \theta_i} = 0 \, , i = 1, 2, \ldots, N. \tag{2.76}$$

Then, the parameter estimates are provided as the solutions of the $(2N-1)$ equations (2.75) and (2.76).

Following the above discussion, let us consider the GEV distribution case and denote $U = \frac{\xi}{\sigma}(x - \mu)$. According to Singh (1998), the GEV constraints in this case are the following:

$$\int f(x)dx = 1, \tag{2.77}$$

$$-\int \ln[1+U]f(x)dx = -E[\ln(1+U)], \tag{2.78}$$

$$\int [1+U]^{-1/\xi} f(x)dx = E[1+U]^{-1/\xi}. \tag{2.79}$$

The least-biased pdf based on the POME method will then take the following form:

$$f(x) = \exp\left\{-a_0 - a_1 \ln[1+U] - a_2[1+U]^{-1/\xi}\right\}. \tag{2.80}$$

Substituting equation (2.80) into (2.77) we obtain the zeroth Lagrange multiplier as follows:

$$a_0 = \ln \int \exp\left\{-a_1 \ln[1+U] - a_2[1+U]^{-1/\xi}\right\}dx. \tag{2.81}$$

Taking under consideration the relations between Lagrange multipliers and constraints, we obtain three (since the sought-for parameters are three) partial differentiate equations for the zero Lagrange multiplier as follows:

$$\frac{\partial a_0}{\partial a_1} = E[\ln\{1+U\}] = -\xi \ln a_2 - \xi \Psi(-\xi(a_1+1)), \tag{2.82}$$

$$\frac{\partial a_0}{\partial a_2} = E\left[\{1+U\}^{-\frac{1}{\xi}}\right] = -\xi \frac{(a_1+1)}{a_2}, \tag{2.83}$$

$$\frac{\partial^2 a_0}{\partial a_2^2} = Var\left[\{1+U\}^{-\frac{1}{\xi}}\right] = \frac{\xi(a_1+1)}{a_2^2}, \tag{2.84}$$

where $\Psi(\cdot)$ is the digamma function, defined as follows:

$$\Psi(u) = \frac{d\log[\Gamma(u)]}{du}. \tag{2.85}$$

Comparing equation (2.80) with the GEV pdf we obtain the following expressions for the Lagrange multipliers:

$$a_1 = -\frac{1+\xi}{\xi}, \quad \text{and} \quad a_2 = 1. \tag{2.86}$$

Using equation (2.86), the relations (2.82), (2.83) and (2.84) reduce to the following:

$$E\left[(1+U)^{-1/\xi}\right] = 1, \tag{2.87}$$

$$E[\ln\{1+U\}] = -\xi\Psi(1), \tag{2.88}$$

$$Var\left[\{1+U\}^{-1/\xi}\right] = 1. \tag{2.89}$$

As before, no closed-form solutions for the above equations are available and therefore nonlinear optimization methods should be used. An application of the POME method in extreme wind speed analysis can be found in Deng et al. (2011).

A variant of the POME method is also analytically discussed. The method is called (maximum entropy) parameter space expansion (MESE) method and its application for the GEV distribution case is presented below.

The maximum entropy parameter-space expansion method

The GEV constraints for this case are the following:

$$\int f(x)dx = 1, \tag{2.90}$$

$$\int \frac{\xi+1}{\xi}\ln[1+U]f(x)dx = E\left[\frac{\xi+1}{\xi}\ln(1+U)\right], \tag{2.91}$$

$$\int [1+U]^{-1/\xi}f(x)dx = E[1+U]^{-1/\xi}. \tag{2.92}$$

The least-biased pdf based on parameter space expansion method takes the following form:

$$f(x) = \exp\left\{-a_0 - a_1\ln[1+U]^{\frac{\xi+1}{\xi}} - a_2[1+U]^{-1/\xi}\right\}. \tag{2.93}$$

Following the same steps as before, using equation (2.93), equation (2.90) gives:

$$a_0 = \ln\sigma - [1 + (-\xi - 1)(1 - a_1)]\ln a_2 + \ln\Gamma([1 + (-\xi - 1)(1 - a_1)]). \tag{2.94}$$

where $\Gamma(\cdot)$ is the Gamma function. Substituting the above expression for $a_0$ into equation (2.93), we obtain

$$f(x) = \exp\{-\ln\sigma + K\ln a_2 - \ln\Gamma[1 + (-\xi - 1)(1 - a_1)]$$
$$-a_1\ln(1+U)^{(1+\xi)/\xi} - a_2[1+U]^{-1/\xi}\}. \tag{2.95}$$

The relation between Lagrange multipliers and parameters is obtained by comparing equation (2.95) with the GEV pdf, from where we have

$$a_1 = 1 \text{ and } a_2 = 1. \tag{2.96}$$

The final GEV entropy function is obtained by taking the logarithm of equation (2.95) and substituting into (2.68), i.e.:

$$H(f) = \ln\sigma - K\ln a_2 + \ln\Gamma\left[\left(1 + (-\xi - 1)(1 - a_1)\right)\right] +$$
$$+ a_1 E\left[\frac{\xi+1}{\xi}\ln(1 + U)\right] + a_2 E[1 + U]^{-1/\xi}. \tag{2.97}$$

The relation between parameters and constraints is obtained by taking partial derivatives of equation (2.97) with respect to $\xi, \sigma, \mu, a_1, a_2$ and equate to zero, as we search for the maximum GEV entropy function. Since no closed-form solutions are available, nonlinear optimization methods should be used.

## 2.4 Confidence Intervals of the parameter estimates

Quantifying the precision of an estimator is usually made more explicit by calculating the confidence interval. In this section, the following methods for the confidence bound estimation of the parameters of the GEV and the GPD distribution (latter introduced in sub-Section 3.2) are presented in short: the normal approximation to the likelihood, the bootstrap method (parametric and non-parametric) and the pointwise approach.

## 2.4.1 The normal approximation of the maximum likelihood estimator

The maximum likelihood principle for parameter estimation is considered the standard approach for approximations in terms of standard errors and confidence intervals. We restrict the discussion to continuous random variables generated from an existing probability density function. The framework is set for data $\{x_n\} = x_1, x_2, \ldots, x_n$ originated as independent realizations of a random variable $\{X_n\}$ whose probability density function belongs to the asymptotic forms of probability distributions of parameter $\theta$ with density functions $f(x; \theta)$.

**Definition 2.2** (multivariate normal distribution)

*Based on the validity of the regularity conditions for a large dataset of size $n$, the standard result using the maximum likelihood parameter estimation method derives that for the $d$-dimensional model parameter $\theta$, the maximum likelihood estimator $\hat{\theta}$ has a limiting multivariate normal distribution with mean $\theta_0$ and variance-covariance matrix $V_{\theta_0}$ denoted*

$\hat{\theta} \rightarrow MVN_d(\theta_0, V_{\theta_0})$, *if its joint density function has the form*

$$f(\theta) = \frac{1}{(2\pi)^{d/2}|V_{\theta_0}|^{1/2}} exp\left\{-\frac{1}{2}(\theta - \theta_0)^T V_\theta^{-1}(\theta - \theta_0)\right\}, \ \theta \in R^d \tag{2.98}$$

*where $|V_{\theta_0}|$ is the determinant of $V_{\theta_0} = I_E(\theta_0)^{-1}$. The "expected information matrix" which measures the expected curvature of the log-likelihood surface is defined by*

$$I_E(\theta) = \begin{bmatrix} e_{1,1}(\theta) & \cdots & \cdots & e_{1,d}(\theta) \\ \vdots & \ddots & e_{i,j}(\theta) & \cdots \\ \vdots & e_{j,i}(\theta) & \ddots & \cdots \\ e_{d,1}(\theta) & \cdots & \cdots & e_{d,d}(\theta) \end{bmatrix},$$ (2.99)

with $e_{i,j}(\theta) = E\left\{-\frac{\partial^2}{\partial e_i \partial e_j} l(\theta)\right\}$ and $l(\theta) = \sum_{i=1}^{n} \log f(x_i; \theta)$ is the log-likelihood function evaluated at $\theta = \theta_0$.

This definition infers that each of the marginal distributions is normal and that the complete joint distribution is determined when the marginal distribution of the mean $\theta_0$ and the variance-covariance matrix at $\theta_0$ are identified.

Since the true value of $\theta_0$ is generally unknown, it is usual to approximate the terms of $I_E$ with those of the "observed information matrix", defined by

$$I_O(\theta) = \begin{bmatrix} -\frac{\partial^2}{\partial \theta_1^2} l(\theta) & \cdots & \cdots & -\frac{\partial^2}{\partial \theta_1 \partial \theta_d} l(\theta) \\ \vdots & \ddots & -\frac{\partial^2}{\partial \theta_i \partial \theta_j} l(\theta) & \cdots \\ \vdots & -\frac{\partial^2}{\partial \theta_j \partial \theta_i} l(\theta) & \ddots & \cdots \\ -\frac{\partial^2}{\partial \theta_d \partial \theta_1} l(\theta) & \cdots & \cdots & -\frac{\partial^2}{\partial \theta_d^2} l(\theta) \end{bmatrix},$$ (2.100)

and evaluated at $\theta = \hat{\theta}$. For a general d-dimensional vector model of parameter $\theta$ the inverse of the information matrix is equivalent to the variance-covariance matrix. Hence, confidence intervals for the parameters of the model, using the asymptotic normality of the MLEs, are provided as follows:

$$\hat{\theta}_j \pm Z_{a/2} \sqrt{I_O(\hat{\theta})_{jj}^{-1}},$$ (2.101)

where $\hat{\theta}_j$ is the mle of the $j - th$ estimated parameter, $Z_{a/2}$ is the percentile point of the standard normal distribution for constructing $(1 - a)100\%$ confidence interval and $I_O(\hat{\theta})_{jj}^{-1}$ is the $j - th$ diagonal component of the variance-covariance matrix of the maximum likelihood estimator.

A generalization of the latter stated Definition 2.2 for a scalar function $\phi = g(\theta)$ is considered as the delta method for obtaining confidence intervals for $\phi$ using the approximate normality of $\hat{\phi}$. Specifically, if the maximum likelihood estimator of $\phi$ is $\hat{\phi} = g(\hat{\theta})$, then $\hat{\phi} \to N(\phi_0, V_\phi)$ is the limiting multivariate normal distribution with mean $\phi_0$ and variance covariance matrix $V_\phi$, where $V_\phi = \nabla \phi^T V_\theta \nabla \phi$ and $\nabla \phi = \left[\frac{\partial \phi}{\partial \theta_1}, \cdots, \frac{\partial \phi}{\partial \theta_d}\right]^T$ with $T$ the transpose operator evaluated at $\theta = \hat{\theta}$. For more details see, Casella and Berger (2002). Therefore, the approximate normality of $\hat{\theta}$ to estimate confidence intervals for the components of the d-dimensional vector parameter $\theta$ is extendend to the approximate normality of $\hat{\phi}$ to obtain confidence intervals for the scalar functional of $\phi$.

Using the delta method for the confidence intervals of the return levels from the GEV distribution, the variance of the estimated $\hat{x}_p$ (see sub-Section 2.2.3) is approximated $Var(\hat{x}_p) \approx \nabla x_p^T V_\theta \nabla x_p$, where $V_\theta$ is the variance-covariane matrix of the parameters $(\hat{\mu}, \hat{\sigma}, \hat{\xi})$ and

$$\nabla x_p{}^T = \left[\frac{\partial x_p}{\partial \mu}, \frac{\partial x_p}{\partial \sigma}, \frac{\partial x_p}{\partial \xi}\right]^T$$

$$= \left[1, -\xi^{-1}\left(1 - \left(-\log(1-p)\right)^{-\xi}\right), \sigma\xi^{-2}\left(1 - \left(-\log(1-p)\right)^{-\xi}\right) - \sigma\xi^{-1}\left(-\log(1-p)\right)^{-\xi}\log\left(-\log(1-p)\right)\right]$$

$$(2.102)$$

is evaluated at $\hat{\theta} = \left(\hat{\mu}, \hat{\sigma}, \hat{\xi}\right)$ with $p$ the ploting position formula (see Appendix C).

Finally, if $\hat{\xi} = 0$ then $\nabla x_p{}^T = \left[\frac{\partial x_p}{\partial \mu}, \frac{\partial x_p}{\partial \sigma}\right]^T = \left[1, -\log\left(-\log(1-p)\right)\right]$ evaluated at $(\hat{\mu}, \hat{\sigma})$.

## 2.4.2 The bootstrap method

The bootstrap method introduced by Efron (1979) is a resampling process of the $N$ data points $(x_1, \cdots, x_N)$. The method uses boot data sets each containing $N$ points obtained by random (Monte Carlo) sampling of the original set of $N$ points. During the Monte Carlo sampling, the probability that a data point is picked is $1/N$ irrespective of whether it has been picked before. (In the statistics literature this is called picking from a set "with replacement"). Hence a given data point $x_i$ will, on average, appear once in each Monte Carlo-generated data set, but may appear not at all, or twice, and so on. The probability that $x_i$ appears $n_i$ times is close to a Poisson distribution with mean unity. The term "bootstrap" data sets denotes the Monte Carlo-generated data sets. Various bootstrap methods have been reviewed by Tajvidi (2003) for the construction of confidence intervals for the GEV and GPD distribution parameters and quantiles. The procedure on resampling with replacement from the given sample and calculating the required statistic from a large number of repeated samples from which standard errors and CIs of the examined statistic can be determined, is defined as non-parametric. The parametric version of the bootstrap is based on randomly generated samples from a parametric model (distribution) fitted to the data. The latter version of the bootstrap is preferred if a suitable model for the examined sample is known and if the data samples are relatively short and the tail behavior is particularly important (Davison and Hinkley 1997). Both cases are used in this analysis.

The results from Kyselý (2008) pointed out that for small to moderate sample sizes the nonparametric bootstrap should be interpreted with caution because it leads to confidence intervals that are too narrow and underestimate the real uncertainties. It is admitted in general that the parametric bootstrap should be preferred with caution whenever inferences are based on small to moderate sample sizes (less or equal to 60) and a suitable bootstrap model for the data is known, for applications to confidence intervals related to extremes in global and regional climate model projections.

Parametric bootstrap

The parametric bootstrap method is summarized in the following steps for estimating the confidence intervals of the extreme value parameters.

**Step 1**: Estimate the parameters $\left(\hat{\mu}, \hat{\sigma}, \hat{\xi}\right)$ of the GEV (see sub-Section 2.2.3) or the $\left(\hat{\hat{\sigma}}, \hat{\xi}, \hat{\zeta}_u\right)$ of the GPD (see sub-Section 3.2.3) from the available dataset using one of the estimation methods as described previously (e.g. MLE, LMOM).

**Step 2**: Draw a random sample of the same size as the dataset from the estimated parameters in Step 1 and fit the Extreme Value Distribution (GEV or GPD) of interest to the random sample and record the parameter estimates and/or return level(s). This is based on the assumption that the original dataset is realization of a random sample from a distribution of a specific parametric type.

**Step 3**: Repeat step 2 for a large number of repetitions (999 or more).

**Step 4**: The (1-a)% level of confidence intervals of the parameters/return level(s) is estimated by finding the $(1 - a)$ quantiles from the large number of repeated samples. The *alpha-level* is selected to $a = 0.05$ in general providing the apparent proportion of samples for which the 95% confidence intervals would fail to cover the examined parameters/return level(s) from the replicate samples.

## Non-Parametric bootstrap

The non-parametric or standard resampling bootstrap approach performs sample replications without any prior knowledge of the distribution of the sampling data. In general, bootstraping for deriving confidence bounds in the percentile concept (percentile bootstrap) is arguably the simplest and most intuitive bootstrap interval approach. This approach is found in various environmental applications (Davison and Hinkley, 1997; Ferro et al., 2005; Kharin and Zwiers, 2005). The 95% confidence intervals of the examined statistics are estimated from the large number of repeated samples.

This bootstrap procedure formulates random samples with replacement from the dataset and analyzes each sample the same way. For the Step 1 now, each observation is selected separately at random from the original dataset without excluding the possibility that a particular data point from the original data set could appear multiple times in a given bootstrap sample. The number of elements in each bootstrap sample equals the number of elements in the original data set. In addition, the previous Steps 2,3 and 4 are identical.

In the present bootstrap application, 999 bootstrap replicates were produced from resampling with replacements from the given sample. Furthermore, the so called *alpha-level* was selected to $a = 0.05$ for which the 95% confidence intervals would fail to cover the examined statistics from the generated samples.Moreover, Coles and Simiu (2003) proposed an empirical correction of the bootstrap estimates, based on a bias correction to the bootstrap parameter estimates, since there is a tendency of the bootstrap procedure to provide generally shorter tails than the one from the original time series.Application of this bootstrap approach in extreme wind speed prediction can be also found in (Naess and Clausen, 2001).

## 2.4.3 Pointwise confidence interval approach

This method returns confidence interval estimates of the underlining distribution or related quantiles based on one or two order statistics from the Kolmogorov-Smirnov statistic (Doksum and Sievers, 1976) of a given sample at given probabilities. Specifically, for the sample quantile estimates confidence interval are defined as weighted averages of consecutive order statistics. In general, the quantile of a distribution is defined as

$$q(p) = F^{-1}(p) = \inf\{x: F(x) \geq p\}, \ 0 < p < 1, \tag{2.103}$$

where $F(x)$ is the distribution function. Sample quantiles provide nonparametric estimators of their population counterparts based on a set of independent observations $\{x_1, \dots x_n\}$ from the distribution $F$.

**Definition 2.3** (sample quantiles)

*Denoting $\{x_{(1)}, \ldots, x_{(n)}\}$ the order statistics of $\{x_1, \ldots x_n\}$ and $\hat{q}_i(p)$ the sample quantiles of specific type (see the quantile algorithms discussed in Hyndman and Fan (1996), then it is defined*

$$\hat{q}_i(p) = (1 - \gamma)x_{(j)} + \gamma x_{(j+1)}, \tag{2.104}$$

*where $\frac{j-m}{n} \leq p \leq \frac{j-m+1}{n}$, $x_j$ is the $j$-th order statistic, $n$ the sample size, $\gamma$ is a function defined at $0 \leq \gamma \leq 1$ with $\gamma = np + m - j$ and $m \in R$ is a constant determined by the sample quantile type. The function $\hat{q}_i(p)$ is defined as a continuous function of $p$ and the sample quantiles are obtained equivalently by linear interpolation between the points $\left(G^{-1}(p_k), x_{(k)}\right)$ where $x_{(k)}$ is the $k$-th order statistic and $G$ the empirical distribution function.*

Various rules have been suggested for the plotting position formulae $p_k$ (see Appendix C). In practice, each plotting rule corresponds to a sample quantile definition by defining $\hat{q}_i(p_k) = x_{(k)}$ and using linear interpolation for $p \neq p_k$. The specific expression for $p_k$ used is $p_k = \frac{k-1}{n-1}$ with $m = 1 - p$. The lower and upper confidence bands are about the sorted and interpolated $x_{(k)}$ values using $\left(G^{-1}(p_k - K/\sqrt{M}), x_{(k)}^{lower}\right)$ for the lower and $\left(G^{-1}(p_k + K/\sqrt{M}), x_{(k)}^{upper}\right)$ for the upper respectively where $K = 1.36$ and $M = m_k n / m_k + n$ with $m_k$ the length of $x_{(k)}$.

## 2.5 Non stationary sequences

The majority of studies in extreme winds are analyzed under the assumption of stationarity. As a remark, Lins and Cohn (2011) and Koutsoyiannis and Montanari (2007) supported the stationarity of climate despite the detection of non-stationarity of climate change. However, recent studies have pointed out that extremes of weather and climate variables have been changing in time and that change is considered to obtain in the future (Zwiers and Kharin 1998; Houghton et al. 2001; Solomon et al. 2007; Yan and Jones 2008). Therefore, it is necessary to examine if trends or any type of non-stationarity are present in data and to adapt if possible an analytical unified method in such a way that justifies non-stationarities. This approach in extreme studies, considers estimations in design values in a more realistic way under the assumption of a time changing climate (Chavez-Demoulin and Davison, 2012; Jonathan et al., 2014).

If the underlying process is non-stationary, then the parameters of the extreme value distribution function can be considered as time-dependent functions, Renard et al. (2013), Gilleland and Katz (2011), Katz (2010), Cooley (2009), which in turn implies that all the properties of the distribution vary with time (Meehl et al. (2000); Butler et al., (2007); Kyselý et al., (2010); Northrop and Jonathan, (2011)). In the literature, studies have been made introducing covariates in the parameters of the extreme value distribution (Wang et al. 2004; Kharin and Zwiers 2005). Coles (2001) investigated annual maximum sea level data at Fremantle, where only the location parameter was set as time-dependent with a linear model. In addition, the location parameter was linearly related to the Southern Oscillation Index (SOI). Katz et al. (2002) introduced a non-stationary GEV model, and suggested a linear model for the location and a log-transformed model for the scale parameter, whereas the shape parameter was kept constant. Mendez et al. (2007) published a wide application of a time-dependent GEV model to monthly extreme sea levels. They used nonlinear time-dependent models for all three parameters containing seasonal and long-term effects. Hundecha et al. (2008) analyzed changes in extreme annual wind speeds in Canada with a non-stationary GEV, where location and scale parameters are considered time-dependent.

The modeling of the time variation of the parameters have found various applications also in hydrology, where the linear or log-linear models are usually preferred (Beguería et al.,

2011; Villarini et al., 2010; Villarini et al., 2009; Cunderlik and Burn, 2003; Towler et al., 2010; Lima et al., 2015). It is most common to assume the location parameter $\mu$ as a linear function of time, holding constant values on scale $\sigma$ and shape parameter $\xi$. The main reason is that reliable estimates of scale and shape parameter require long-term observations which are not always available. The main scope of the above studies was to model one or more of the parameters as linear or nonlinear functions of the covariates on which the data show dependence. Comparing different methods of detecting trends in extreme values, Zhang et al. (2004 b) came to a conclusion that methods that are based on modeling trends in the parameters of the distribution of the extremes are evident methods of detecting significant trends in the extremes. The benefit of this approach is that the original data no longer have to be de-trended and can be used directly.

## 2.5.1 Likelihood

If the time series is assumed to be non-stationary, then the limiting distribution function is not considered as GEV distributed or any other family. No strong theories of extreme values exist in this area. However we can use GEV distribution as a template and inserting time dependent parameters of the form:

$$G\big(x; \mu(t), \sigma(t), \xi(t)\big). \tag{2.105}$$

For a non-stationary process, the associated GEV parameters $\theta = (\mu, \sigma, \xi)$ are considered time-dependent and the properties of the distribution would vary with time. Each of the GEV distribution parameters are expressed as a function of time $t$ (for the annual maxima approach, $t$ is the index $\mu(t), \sigma(t), \xi(t)$ of the year). In this way, time is included as a covariate. The likelihood function takes now the following form:

$$L\big(x_1, x_2, \ldots, x_n; \mu(t), \sigma(t), \xi(t)\big) = \prod_{t=1}^{n} g\big(x_t; \mu(t), \sigma(t), \xi(t)\big), \tag{2.106}$$

where $g\big(x_t; \mu(t), \sigma(t), \xi(t)\big)$ is the GEV time dependent probability density function evaluated at $x_t$. Usually, the shape parameter $\xi$ is considered time independent in order to avoid numerical conflicts, due to its importance concerning the distribution.

Consequently, for a time dependent model the log-likelihood function for $\xi \neq 0$ has the following form:

$$l(x_1, x_2, \ldots, x_n; \theta) = -\sum_{t=1}^{n} \left( \ln\sigma(t) + \left(\frac{1+\xi(t)}{\xi(t)}\right) \ln[1 + \xi(t)z(t)] + [1 + \xi(t)z(t)]^{-\frac{1}{\xi(t)}} \right), \tag{2.107}$$

where $1 + \xi(t)z(t) > 0$ and $z(t) = \frac{\xi(t)(x_t - \mu(t))}{\sigma(t)}$ with index $t = 1, 2, \ldots, n$ denoting the number of the BM $(x_1, x_2, \ldots, x_n)$.

In addition, the confidence intervals for the parameters of the model are estimated using the asymptotic normality of the MLE (see sub-Section 2.4.1).

## 2.5.2 Testing for non-stationarity

To test whether the common assumption of stationarity is violated two classes of tests are considered, the trend and unit root tests. The main idea of the non-stationarity tests (see Appendix F) is to analyze the statistical differences of different data group of the entire time

series (e.g. Chen and Rao, 2002). Specifically, trend tests such as Mann-Kendall (MK) non-parametric trend test (Kendall 1976; Mann 1945) and the Cox Stuart (CS) trend test (Cox and Stuart 1955), are applied to examine whether the values of a series have a general increase or decrease with the time increase. The choice of the significance level is the default value ($a$=0.05) in this setting.

Unit root tests are implemented to determine whether the mean values and variances of a series vary with time (e.g., see Razmi et al., 2017). If the observed variations in a certain parameter of different data group are found to be significant, the time series is regarded as nonstationary. The unit root tests in this setting are referred as the augmented Dickey-Fuller (ADF) unit root test modified by Said and Dickey (1984) and the Kwiatkowski-Phillips-Schmidt-Shin (KPSS) stationarity test by Kwiatkowski et al. (1992). The first test seeks for the presence of a unit root in the series (difference stationarity[3]), while the second tests for the stationarity around a fixed level (level stationarity) or the stationarity around a deterministic trend (trend stationarity) as a complement unit root test such as the ADF test. In this assessment, we considered the level stationarity KPSS test whether the data show stationarity around a fixed level or not and the ADF test whether there is a unit root present or not. The choice of the significance level in this setting is the default value a=0.05 for each examined station and test respectively.

## 2.5.4 Model selection criteria

There are various combinations modelling the parameters as a function of time and the question is which model represents effectively the extremes in wind speed when the stationarity of the process is violated. Simple tests of choosing one model against another is the likelihood ratio test (Deviance Statistic).

Deviance Statistic

The test is based on a comparison of maximized likelihoods for nested models. We consider two models, $M_0$ and $M_1$, such that $M_0 \subset M_1$. The maximized likelihood under the smaller model (stationary model) $M_0$ is $\max_{\theta \in M_0} L(x; \theta) = L(x; \hat{\theta}_{M_0})$, where $\hat{\theta}_{M_0}$ refers to the MLE of $\theta$ under model $M_0$. The maximized likelihood under the larger model (non-stationary model) $M_1$, is $\max_{\theta \in M_1} L(x; \theta) = L(x; \hat{\theta}_{M_1})$, where $\hat{\theta}_{M_1}$ refers to the MLE of $\theta$ under model $M_1$. The ratio of these two quantities, namely

$$\lambda = \frac{L(x; \hat{\theta}_{M_0})}{L(x; \hat{\theta}_{M_1})}, \tag{2.108}$$

is considered to vary between $0 < \lambda < 1$. Likelihoods are non-negative and the likelihood of the smaller model can't exceed that of the larger model because it is nested on it. Values close to 0 indicate that the smaller model is not acceptable, compared to the larger model, because it would correspond to unlikely observed data. Values close to 1 indicate that the smaller model is acceptable over the large model. The likelihood ratio test statistic (LRT) is defined as

$$-2\ln(\lambda) = 2\left(\ln L(x; \hat{\theta}_{M_1}) - \ln L(x; \hat{\theta}_{M_0})\right) = 2\left(l(x; \hat{\theta}_{M_1}) - l(x; \hat{\theta}_{M_0})\right), \tag{2.109}$$

where $l(x; \hat{\theta}_{M_1})$ and $l(x; \hat{\theta}_{M_0})$ are the maximized log likelihood functions of the non-stationary and stationary model respectively.

---

[3] Difference stationarity of a process is equivalent to a presence of a unit root. Differencing the reconstructed higher-order autoregressive process of a mixture of deterministic and stochastic trend yields a stationary process when a unit root is present.

Asymptotically, for large samples sizes, $n \to \infty$, Wilks theorem (Wilks 1938) imposes that the test statistic (LRT) or deviance statistic, is distributed as a chi-squared random variable $x_k^2$, with degrees of freedom $k$ equal to the difference in the number of parameters to be estimated between the two models yielding

$$-2\ln(\lambda) = 2\left(l\left(x; \hat{\theta}_{M_1}\right) - l\left(x; \hat{\theta}_{M_0}\right)\right) \sim x_k^2. \tag{2.110}$$

In conclusion, model $M_0$ is to be rejected over model $M_1$ when the deviance statistic is large enough by a test at the $a - level$ of significance as follows:

$$2\left(l\left(x; \hat{\theta}_{M_1}\right) - l\left(x; \hat{\theta}_{M_0}\right)\right) > c_a, \tag{2.111}$$

where $c_a$ is considered the $(1 - a)$ quantile of the chi-squared $x_k^2$ distribution.

## Akaike Information Criterion (AIC)

AIC is not a hypothesis test, does not imply a test at the $a - level$ of significance. Instead, the AIC focuses on the strength of evidence and gives a measure of uncertainty for each model. Akaike (1973) cited by Burnham and Anderson (2002) proposed using Kullback-Leibler information for model selection. He established a relationship between the maximum log likelihood and the Kullback-Leibler information. In particularly, he developed an information criterion to estimate the Kullback-Leibler information. Akaike's information criterion (AIC) is defined as follows:

$$\text{AIC}_{\text{model}} = -2l\left(x; \hat{\theta}_{\text{model}}\right) + 2p_{\text{model}}, \tag{2.112}$$

where $p_{\text{model}}$ is the number of estimated parameters included in the model and $l\left(x; \hat{\theta}_{\text{model}}\right)$ is the maximized log likelihood for each model. The model that explains the data variability sufficiently well, is the one among all examined models having the lowest AIC. In this way, we consider the model which minimizes the loss of information.

For small samples we use the corrected AIC (denoted AICc), which includes a small-sample correction. If $n$ is the sample size, the corrected AIC criteria is defined as follows:

$$\text{AIC}_{\text{model}}^{cor} = -2l\left(x; \hat{\theta}_{\text{model}}\right) + 2p_{\text{model}} + \frac{2p_{\text{model}}(p_{\text{model}}+1)}{n-p_{\text{model}}-1}, \tag{2.113}$$

where the third term is the correction term. Further discussion of the formula with examples is given by Konishi and Kitagawa (2008).

## Bayesian Information Criterion (BIC)

In statistics, the Bayesian information criterion (BIC) or Schwarz criterion (Schwarz, 1978) (also SBC, SBIC) is a criterion for model selection among an examined set of models; the model with the lowest BIC is preferred. BIC is closely related to the Akaike information criterion (AIC) and is given as follows:

$$\text{BIC}_{\text{model}} = -2l\left(x; \hat{\theta}_{\text{model}}\right) + p_{\text{model}}\ln(n), \tag{2.114}$$

where $p_{\text{model}}$ denotes the number of estimated parameters included in the model, $n$ is the number of data observations and $l\left(x; \hat{\theta}_{\text{model}}\right)$ is the maximized log likelihood for each model. Bayesian information criterion generally penalizes more complex models more strongly than does the AIC, but care must be given in models with values close to the minimum.

# Chapter 3
## Threshold Excesses

A crucial problem often arising in climatological and hydrological extreme assessments is the scarcity of long and complete time series. Regarding wind speed time records, many authors have outlined a minimum annual length of 10 years to be regarded as the absolute minimum for a comprehensive Extreme Value Analysis (EVA) based on the Annual-Block Maximum (BM) sampling approach (Cook, 1985; Abildet al., 1992; Coles and Walshaw, 1994). Additional studies on BM outlineda minimum annual length of 13 years for a successfully fit to the Generalized Extreme Value (GEV) distribution as proposed by Brabson and Palutikof (2000). However, samples with a limited amount of extremes often fail to provide efficient quantile estimates for large return periods. When only few extremes are available for analysis re-sampling procedures of the dataset is introduced. The drawback from the use of these procedures that often arise is the possible effect to the approximate independent limitations of the re-sample. In this Section, a short review of the annually *r*-largest order statistics concept is introduced as the classical approach for re-sampling more maxima within a year block. In addition, the well proposed threshold models from the relevant literarure is also reviewed as the basic structure for re-sampling. Inevitable, all re-samples will be penalized by a sort of dependency, where further examination of the excesses is mandatory for the i.i.d limitations.

Other models are also examined and discussed in this Section where they aim to initially cluster the events from the time series and then de-cluster selecting the maximum value of each cluster respectively. However, the issue of strong debate is if the de-cluster models consider the independency limitations that are mandatory between adjacent clusters. From a review of the most considerable de-clustering models found and standout in the relevant literature that sample approximately independent events, are the Block and Runs (Smith and Weissman, 1994), the improved Method of Independent Storms (MIS) (Harris, 1999), the filtering de-clustering approach (Fawcett and Walshaw, 2007), the Standard Storm length (SSL) (Tawn, 1988), the Separation time approach by (Walshaw, 1994; Morton et al., 1997), and the physical De-Clustering Algorithm (DeCA model) (Soukissian et al., 2006; Soukissian and Kalantzi, 2009; Bernardara et al., 2014; Arns et al., 2013; Vanem, 2011; Oikonomou et al., 2020).

## 3.1 Model Generalization from r-largest Order Statistics

The inference from Point Processes (PP) will generalize the BM approach, providing the likelihood of an inhomogeneous PP for the r largest extremes in each block. The likelihood of a non-homogeneous PP is proportional to the likelihood for the $r^{th}$ largest order maxima. The general form of the non-homogeneous Poisson Process likelihood is defined as follows:

$$L_{\{[t_1,t_2] \times [u_n,\infty)\}}(x; \xi, \sigma, \mu) = \exp[-\Lambda(u_n; \xi, \sigma, \mu)] \cdot \prod_{i=1}^{r} \left( \lambda(x^{(i)}; \xi, \sigma, \mu) \right), \qquad (3.1)$$

and proportional to the likelihood for the $r^{th}$ largest ordered maxima that exceed over a high threshold level $u_n$,

$$\propto \exp\left[-(t_2 - t_1)\left[1 + \xi\left(\frac{u_n - \mu}{\sigma}\right)\right]^{-1/\xi}\right]\prod_{i=1}^{r}\left(\frac{1}{\sigma}\left[1 + \xi\left(\frac{x^{(i)} - \mu}{\sigma}\right)\right]^{-1/\xi - 1}\right), \tag{3.2}$$

where $-\infty < \mu < \infty$, $\sigma > 0$, $-\infty < \xi < \infty$ and $x^{(1)} \geq x^{(2)} \geq \ldots \geq x^{(i)} \geq \ldots \geq x^{(r)} = u_n$

with $1 + \xi(x^{(i)} - \mu)/\sigma > 0$ for $i = 1,2,3,\ldots,r$. In addition, $\Lambda(u_n; \xi, \sigma, \mu)$ and $\lambda(x^{(r)}; \xi, \sigma, \mu)$ are defined as the intensity measure and the occurrence rate of points per unit region or intensity density function respectively for the $r^{th}$ largest ordered maxima in the region $\{[t_1, t_2] \times [u_n, \infty)\}$, where $[t_1, t_2] = [0,1]$, (Smith, 1986). The Theorem H.1 (stated in Appendix H), unifies the PP representation for Extremes due to Pickands (1971). The statistical modeling of the $r^{th}$ largest ordered maxima and the corresponding log likelihood over all available $m$ blocks is analytically presented in Appendix H. The $r^{th}$ largest order statistic model gives a likelihood whose parameters correspond to those of the GEV of BM, but utilizes more information from the available dataset.

At this point it is important to highlight the unique relation between the point process characterization of extremes and the threshold excess model. Inference is made in both model approaches, since the likelihood expression stated in Equation (3.2) for the $r$-th largest ordered maxima that exceed over a high threshold level $u_n$ is proportional equal to the likelihood of the limiting joint distribution function for the $r$ largest order statistics stated in Equation H.8 (Appendix H). Working directly with the full joint distribution of the $M_n^{(r)}$ exceedances stated in Equation (3.2) guarantees a more robust expression for the exceedances.

## 3.2 Peak Over Threshold (POT) approach

Pickands (1975) and Balkema & de Haan (1974) showed that if there is a non-degenerate limiting distribution for appropriately linearly rescaled excesses of a sequence of i.i.d distributed observations above a high enough threshold, then the limiting distribution of the excesses, will be assigned as the Generalized Pareto Distribution (GPD).

**Theorem 3.1** (Pickands-Balkema-de Haan Theorem). *Assuming $Y = X - u$ for $X > u$ and that for $n$ random variables $X_1, X_2, \ldots, X_n$ the conditions of the Fisher-Tippett-Gnedenko Theorem hold* (Theorem 2.1), *the distribution function $P(X \leq y)$ of the exceedances $y = (x - u)|_{x>u}$, considering $u$ is high enough, can be approximated by the GPD i.e.,*

$$G(y) = 1 - \left[1 + \frac{\xi y}{\tilde{\sigma}}\right]^{-1/\xi}, \text{ for } y > 0, \tag{3.3}$$

*where the support is defined by $1 + \xi y/\tilde{\sigma} > 0$.*

The scale parameter is defined as $\tilde{\sigma} = \xi(u - \mu)$ and supported for $\tilde{\sigma} > 0$, while the shape parameter $\xi$ is supported for $-\infty \leq \xi \leq \infty$. The GPD distribution is generalized because it assumes different distributions in the same sense as the GEV when $\xi$ undertakes the following values: if $\xi < 0$ and $0 \leq y \leq -\tilde{\sigma}/\xi$, the GPD distribution has a finite right end point and is considered (bounded), following the Uniform or the Beta class of distributions. If $\xi > 0$ and $y \geq 0$ the distribution has an infinite right end point and is considered (unbounded) or heavy-tailed, following the Pareto class of distributions. Finally, the case where $\xi \to 0$, is interpreted as the limiting case for GPD converging to the exponential class of distributions

$$G(y) = 1 - \exp\left(-\frac{y}{\tilde{\sigma}}\right), y > 0. \tag{3.4}$$

EVA establishes a link between the GEV and GPD distributions. If $X$ is a random variable arising from $F$ and the limit of Theorem 2.1 holds, then for a large threshold the threshold excess of the random variable $X - u | X > u$, converges in distribution within the GPD family and vice versa. GEV parameterization can be obtained from the GPD under suitable conditions. In particular, the shape parameter $\xi$ of the limiting GPD is equal to that of the corresponding GEV distribution. Additionally, differentiating the GPD, yields the associated pdf

$$g(y) = \begin{cases} \frac{1}{\tilde{\sigma}}\left(1 + \xi \frac{y}{\tilde{\sigma}}\right)^{-1-\frac{1}{\xi}}, & \xi \neq 0 \\ \frac{1}{\tilde{\sigma}} \exp\left(-\frac{y}{\tilde{\sigma}}\right), & \xi = 0 \end{cases}, \tag{3.5}$$

considering $y \geq 0$ if $\xi \geq 0$, and $0 \leq y \leq -\frac{\tilde{\sigma}}{\xi}$ when $\xi < 0$.

## 3.2.1 Formulation of Pickands-Balkema-de Haan Theorem

Noting $\{X_1, \ldots, X_n\}$ as a sequence of i.i.d random variables with a common cumulative distribution function $H(x)$, the distribution function of $M_n$ for appropriately defined normalizing sequences of constants $\{a_n > 0\}$ and $\{b_n\}$ is obtained from Eq. (2.2) as follows:

$$\Pr\left\{\frac{M_n - b_n}{a_n} \leq x\right\} = H^n(a_n x + b_n).$$

Furthermore, using the classical asymptotic formulation in Theorem 2.1 such that as $n \to \infty$,

$$\Pr\left\{\frac{M_n - b_n}{a_n} \leq x\right\} \to F(x) = \exp\left\{-\left[1 + \xi\left(\frac{x-\mu}{\sigma}\right)\right]^{-1/\xi}\right\}.$$

Equating the latter statements and using the Taylor expansion [4],

$$H(a_n x + b_n)^n \approx \exp\left\{-\left[1 + \xi\left(\frac{x-\mu}{\sigma}\right)\right]^{-1/\xi}\right\}, \tag{3.6}$$

where for large enough $n$, the derivation in (3.6) yields:

$$1 - H(a_n u + b_n) \approx \frac{1}{n}\left[1 + \xi\left(\frac{u-\mu}{\sigma}\right)\right]^{-1/\xi}. \tag{3.7}$$

Similarly for $y > 0$,

$$1 - H(a_n(u + y) + b_n) \approx \frac{1}{n}\left[1 + \xi\left(\frac{u+y-\mu}{\sigma}\right)\right]^{-1/\xi}. \tag{3.8}$$

Using the formulation from the conditional distribution, an extreme event is defined for $y > 0$ as follows:

$$\Pr(X > u + y | X > u) = \frac{1 - \Pr(X \leq u+y)}{1 - \Pr(X \leq u)} = \frac{1 - H(a_n(u+y)+b_n)}{1 - H(a_n u + b_n)}. \tag{3.9}$$

Moreover, using the conditional probability law, yields:

---

[4] The Taylor expansion: $\log H(a_n x + b_n) \approx -[1 - H(a_n x + b_n)]$.

$$\Pr(X > u + y | X > u) = \Pr(X > y) = 1 - \Pr(X \le y). \tag{3.10}$$

Substituting respectively all formulas stated from Equations (3.7) and (3.8) into the latter (3.9), it is derived:

$$\Pr(X > u + y | X > u) = \frac{\frac{1}{n}\left[1+\xi\left(\frac{u+y-\mu}{\sigma}\right)\right]^{-1/\xi}}{\frac{1}{n}\left[1+\xi\left(\frac{u-\mu}{\sigma}\right)\right]^{-1/\xi}} = \left[\frac{\sigma+\xi(u+y-\mu)}{\sigma+\xi(u-\mu)}\right]^{-1/\xi} = \left[1+\frac{\xi y}{\tilde{\sigma}}\right]^{-1/\xi}.$$

The GPD is written in the following form using the conditional distribution stated in (3.10):

$$\Pr(X \le y) = G(y) = 1 - \left[1 + \frac{\xi y}{\tilde{\sigma}}\right]^{-1/\xi}, \tag{3.11}$$

where $y > 0$, $(1 + \xi y / \tilde{\sigma}) > 0$ and $\tilde{\sigma} = \sigma + \xi(u - \mu)$.

## 3.2.2 Likelihood of the Threshold Exceedances

Assuming $y_1, y_2, \ldots, y_{n_u}$ and $y_i = (x_i - u)\big|_{x_i > u}$ a sequence of $n_u$ exceedances of a high enough threshold $u$, the joint density pdf will be assigned as $L(y_1, y_2, \ldots, y_n; \tilde{\sigma}, \xi)$. The corresponding log-likelihood function is derived as follows:

$$l(\tilde{\sigma}, \xi) = \begin{cases} -n_u \log\tilde{\sigma} - \left(1 + \frac{1}{\xi}\right)\sum_{i=1}^{n_u} \log\left(1 + \xi\frac{y_i}{\tilde{\sigma}}\right), & \xi \ne 0 \\ -n_u \log\tilde{\sigma} - \frac{1}{\tilde{\sigma}}\sum_{i=1}^{n_u} y_i, & \xi = 0, \end{cases} \tag{3.12}$$

where $\left(1 + \xi\frac{y_i}{\tilde{\sigma}}\right) > 0$ for $i = 1, 2, \ldots, n_u$, contrariwise $l(\tilde{\sigma}, \xi) = \infty$. However, under the provision that the $\xi$ parameter characterizes the upper tail behavior of both the GEV and GPD, the MLE estimator of the GPD follows the exact asymptotically normal properties as the GEV. As a consequence, regularity conditions do not always exist similarly as in the GEV, e.g., see Grimshaw (1993) and Tajvidi (2003). The MLE's are denoted as $\hat{\tilde{\sigma}}$ and $\hat{\xi}$, providing local maximum of the $l(\tilde{\sigma}, \xi)$. Similarly, no closed-form solution to the maximization problem is available; thus, it has to be transcend numerically using nonlinear optimization methods.

## 3.2.3 Return Levels of the Threshold exceedances

The advantage of considering the Peak-Over-Threshold (POT) approach against the classical BM, is that different but still large block size would affect the GEV parameters but not those of the corresponding GPD distribution of threshold excesses. In addition, quantile estimates for large return periods will be significant improved by the augmentation of the available sample size. Parameter $\xi$ is invariant to block size, while calculations of $\tilde{\sigma}$ is unperturbed by changes in $\mu$ and $\sigma$. The major disadvantage of considering the POT approach, consists in the selection of the appropriate threshold value in order to safely provide a trade-off between bias and variance. The suitable threshold will successfully verify that peaks of all exceedances, meet the requirements of the i.i.d limitations.

Similarly to the BM approach, evaluating return levels for the model of exceedances described by the GPD with parameters $(\tilde{\sigma}, \xi)$, the return level $x_p$ that is exceeded on average once every $1/p$ observations for the model of the POT exceedances assuming that $x_p > u$ over a suitable high threshold $u$, is given by

$$x_p(\tilde{\sigma}, \xi, \zeta_u) = \begin{cases} u + \frac{\tilde{\sigma}}{\xi}\left[(\zeta_u/p)^\xi - 1\right], & \xi \neq 0, \\ u + \tilde{\sigma}\log(\zeta_u/p), & \xi = 0. \end{cases} \quad (3.13)$$

Moreover, (Coles, 2001) suggested that the probability of an exceedance of $u$ denoted as $\zeta_u = \Pr(X > u)$ follows the binomial distribution $\text{Bin}(n, \zeta_u)$, where $n$ is the total number of observations from the time series. Hence, a natural estimator of $\zeta_u$ is $\hat{\zeta}_u = \frac{n_u}{n}$ where $n_u$ denotes the number of exceedances. Estimates of the return levels are obtained by $\hat{x}_p = x_p(\hat{\tilde{\sigma}}, \hat{\xi}, \hat{\zeta}_u)$.

## 3.2.4 Bound estimates of GPD based on the delta method

Standard errors and confidence intervals for the return levels $x_p(\tilde{\sigma}, \xi, \zeta_u)$ of the GPD distribution are obtained similar from the delta method based on the normal approximation of the maximum likelihood estimator (see also sub-Section 2.4.1). Specifically, considering the variance in the estimation of the $\zeta_u$ approximated by $Var(\hat{\zeta}_u) \approx \hat{\zeta}_u(1 - \hat{\zeta}_u)/n$, the variance of the return level estimate is approximated in the form

$$Var(\hat{x}_p) \approx \nabla x_p^T V_\theta \nabla x_p.$$

The variance-covariance matrix for $(\hat{\tilde{\sigma}}, \hat{\xi}, \hat{\zeta}_u)$ is identified as $V_\theta$ and the transpose of the differential operator of the return level is approximated

$$\begin{aligned} \nabla x_p^T &= \left[\frac{\partial x_p}{\partial \zeta_u}, \frac{\partial x_p}{\partial \tilde{\sigma}}, \frac{\partial x_p}{\partial \xi}\right]^T \\ &= \left[\tilde{\sigma} p^\xi \zeta_u^{\xi-1}, \xi^{-1}\{(p\zeta_u)^\xi - 1\}, -\tilde{\sigma}\xi^{-2}\{(p\zeta_u)^\xi - 1\} + \tilde{\sigma}\xi^{-1}(p\zeta_u)^\xi \log(p\zeta_u)\right] \end{aligned}$$

$$(3.14)$$

and evaluated at $\hat{\theta} = (\hat{\tilde{\sigma}}, \hat{\xi}, \hat{\zeta}_u)$.

As a note, the delta method is arguable the most applied method of inference for return levels in extremes.

## 3.3 Extremal Index

The discussion below is based partly on Leadbetter et al. (1983), a standard reference to the literature on extremes of time series and random processes, and on Beirlant et al., (2004, Ch. 10), which provides a more recent summary.

**Definition 3.1** (the condition of $D(u_n)$)

*A strictly stationary sequence $\{X_1, X_2, \ldots, X_n\}$ with marginal distribution $H(x)$, satisfies the $D(u_n)$ condition if for all $i_1 < \cdots < i_p < j_1 < \cdots < j_q$ with $j_1 - i_p > l$, $\left|Pr\left\{X_{i_1} \leq u_n, \ldots, X_{i_p} \leq u_n, X_{j_1} \leq u_n, \ldots, X_{j_p} \leq u_n\right\} - Pr\left\{X_{i_1} \leq u_n, \ldots, X_{i_p} \leq u_n\right\}Pr\left\{X_{j_1} \leq \right.\right.$*

$u_n, \dots, X_{j_p} \le u_n\big\}\Big| \le a(n, l)$, where $a(n, l) \to 0$ for some sequence $l_n$ such that $l_n/n \to 0$ as $n \to \infty$.

The $D(u_n)$ condition in Definition 3.1 guarantees that rare events sufficiently separated apart are approximately independent. More generally, for a sequence of thresholds $u_n$ that increase with the increase of $n$, the condition ensures that the maxima of dependent data to limit to the GEV distribution. Thereby, maxima of stationary time series in the long range dependence at extreme levels, follow the same distributional limit law as those of the independent series.

**Theorem 3.2** (maxima in the long range dependence)

*Let $\{X_i\}$ be a stationary sequence with $M_n = max(X_1, X_2, \dots, X_n)$ for which there exist sequences of normalizing constants $\{a_n > 0\}$ and $\{b_n \in R\}$ with a non-degenerate distribution $F(x)$ such that*

$$Pr\left\{\frac{M_n - b_n}{a_n} \le x\right\} \to F(x),$$

*then for $n \to \infty$ and the $D(u_n)$ condition holds with $u_n = a_n x + b_n$ for every real $x$, $F(x)$ follows the GEV distribution.*

Related to the above conditions, it is important to understand the quantitative impact of non-independent extremes on the estimations of extreme quantiles. The most common measure of the effect of the short range dependence exhibited by the extremes of a process is the extremal index $\theta$, defined in the range $0 < \theta \le 1$. If the sequence $\{X_i\}$ is independent then $\theta = 1$. Moreover, the extremal index indicates the tendency of the extremes to occur in clusters. The relation between the maxima of a dependent and of an independent sequence respectively is summarized in the following theorem:

**Theorem 3.3** (limit distribution in the long range dependence)

*We denote two sequence of variables $\{X_i\}$ (stationary) and $\{\tilde{X}_i\}$ (independent) with the same marginal distribution, setting their corresponding maxima as $M_n = max(X_1, X_2, \dots, X_n)$ and $\tilde{M}_n = max(\tilde{X}_1, \tilde{X}_2, \dots, \tilde{X}_n)$ respectively. If there exist sequences of normalizing constants $\{a_n > 0\}$ and $\{b_n \in R\}$ for the independent process such that*

$$Pr\left\{\frac{\tilde{M}_n - b_n}{a_n} \le x\right\} \to \tilde{F}(x), \text{ for } n \to \infty, \text{ then under suitable regularity conditions the stationary}$$

*sequence follow a non-degenerate distribution function $F(x)$ subsequently,*

$$Pr\left\{\frac{M_n - b_n}{a_n} \le x\right\} \to F(x) \text{ . For some constant (extremal index) } \theta \in (0,1], \text{ the effect of the}$$

*dependence in the stationary series is considered with the replacement by the limit distribution followed $F(x) = \tilde{F}(x)^\theta$.*

The parameters of the limit distribution are also strongly affected by the dependence in the series, influencing only the location and scale parameters. Accordingly, if distribution of the maxima $\tilde{M}_n$ is GEV with parameters $(\mu, \sigma, \xi)$, then the distribution of $M_n$ is also GEV but with parameters $(\mu_\theta, \sigma_\theta, \xi_\theta)$ in the form $\mu_\theta = \mu + \frac{\sigma}{\xi}\left(\theta^\xi - 1\right)$, $\sigma_\theta = \theta^\xi \sigma$ and $\xi_\theta = \xi$.

Leadbetter (1983) notes the following connection between the cluster-size distribution and the extremal index $\theta$. Assuming the sample of size $n$ is divided into blocks of length $m_n$, then a cluster of high level exceedances is obtained as a set of observations above a given

threshold $u_n$ within a block given that there is at least one exceedance in that block. The cluster size distributionis defined as (see Ancona-Navarrete & Tawn, 2000)

$$\pi_n(j; u_n, m_n) = \Pr\{\sum_{i=1}^{m_n} I(X_i > u_n) = j | \sum_{i=1}^{m_n} I(X_i > u_n) > 0\}, \text{ for } j = 1, \ldots, m_n, \quad (3.15)$$

where $I(.)$ is the indicator function. Therefore, the extremal index $\theta$ is expressed as the reciprocal of the limiting mean cluster size,

$$\theta^{-1} = \lim_{n \to \infty} \sum_{j=1}^{m_n} j \pi_n(j; u_n, m_n). \quad (3.16)$$

Another characterization of $\theta$ in terms of down-crossings in clusters of extremes is given by O'Brien (1987) yielding

$$\theta = \lim_{n \to \infty} \Pr\{X_i \le u_n, 2 \le i \le l_n | X_1 > u_n\}, \text{ where } l_n = o(n). \quad (3.17)$$

Summarizing, the exceedances from a stationary sequence occur in clusters. The expected number of exceedances within each cluster is asymptotically unaffected by the strength of the dependence. Therefore, an average of $1/\theta$ exceedances must occur in each cluster. The aforementioned characterizations define the extremal index setting the index $\theta$ as the key parameter when extending the limiting behavior of extremes from independent to stationary sequences of some dependency.

## 3.3.1 Intervals Estimate

Investigating the point process of the exceedance times, Hsing et al. (1988) resulted that the asymptotic distribution of the inter-exceedance times belongs to a one-dimensional parametric family of distributions indexed by the extremal index. Recent studies from Ferro and Segers (2003), yield estimation of the extremal index by equating theoretical moments of the limiting distribution to their empirical counterparts. The observed inter-exceedance times is denoted as $T_i$, where $i = 1, 2, .., n_u - 1$, yielding limiting argument of the estimated extremal index $\hat{\theta}(u)$,

$$\hat{\theta}(u) = \begin{cases} \dfrac{2\left(\sum_{i=1}^{n_u-1}(T_i-1)\right)^2}{(n_u-1)\sum_{i=1}^{n_u-1}(T_i-1)(T_i-2)} & \text{if } \max\{T_i: 1 \le i \le n_u - 1\} > 2 \\ \dfrac{2\left(\sum_{i=1}^{n_u-1}T_i\right)^2}{(n_u-1)\sum_{i=1}^{n_u-1}T_i^2} & \text{if } \max\{T_i: 1 \le i \le n_u - 1\} \le 2 \end{cases} \quad (3.18)$$

The method is referred as 'Intervals Estimate' and in addition supports a bootstrap procedure for obtaining confidence intervals on estimates of the cluster characteristics.

## 3.3.2 Return Levels based on the Extremal Index

Taking into account the dependency of extremes, evaluating return levels is also interpreted as the $x_p$ return level that is exceeded on average at least once every $1/p$ observations in the same context as previously defined Eq. (3.13). Considering that the GPD

with parameters $(\tilde{\sigma}, \xi)$ is a suitable model for exceedances provided that $x_p > u$ and $\xi \neq 0$ over a suitable high threshold $u$, then

$$x_p(\tilde{\sigma}, \xi, \zeta_u) = \begin{cases} u + \frac{\tilde{\sigma}}{\xi}\left[(\zeta_u \theta/p)^{\xi} - 1\right], & \xi \neq 0, \\ u + \tilde{\sigma}\log(\zeta_u \theta/p), & \xi = 0. \end{cases} \tag{3.19}$$

A natural estimator of $\theta$ is obtained $\hat{\theta} = \frac{n_c}{n_u}$ (Hsing et al., 1988), where $n_u$ denotes the number of exceedances and $n_c$ denotes the number of clusters obtained over the selected high enough threshold. Other estimators of $\theta$ and their model performance is found in (Smith and Weissman, 1994; and Gomes, 1993). A latest approach of the generalization of the extremal index estimator of Ferro and Segers (2003) for the extension to non-stationary random sequences with periodic dependence structure is found in Auld and Papastathopoulos (2021).

In our analysis we considered the Extremal Index estimator from the Intervals Estimate method by Ferro and Segers, (2003) for the identification of clusters.

## 3.4 Threshold selection

How should someone choose the threshold $u$? The choice of an appropriate threshold requires a compromise between precision and bias. There are several technics of choosing an appropriate value for threshold. High threshold reduces the bias in the extrapolation of the extreme value but penalizes the variance for the estimators of the GPD parameters from the reduction of the available sample size. On the contrary, a lower threshold produces a higher bias along with a moderate variance for the estimators.

The most prominent threshold model-value acceptable used in literature are: (i) Mean Residual Life Plot (MRL) introduced by Davison & Smith (1990) and examples given by Beirlant et al. (2004) (ii) Parameter Stability Plot by Coles (2001) and references given in, Scarrott and Mac Donald (2012), (iii) Rules of Thumb considering one of the sample points as the optimum threshold with references in Du Mouchel (1983), Reiss and Thomas (2007) and Ferreira et al. (2003), and finally (iv) Multiple-Threshold Model by Wadsworth & Tawn (2012) and references given in Bommier (2014). The threshold choosing methods are presented briefly as followed particularly for the POT model, but can also be used to extract the extreme-type sample required for clustering.

### 3.4.1 Mean Residual Life Plot (Graphical diagnostics)

The mean residual life (MRL) plot introduced by Davison & Smith (1990) is the common graphical diagnostics for threshold choice. This diagnosticsuses the expectation of the GPD excesses,

$$E\left(X - u_p | X > u_p\right) = \frac{\sigma_{u_p}}{1-\xi} \text{ defined for } \xi < 1, \tag{3.20}$$

where $\sigma_{u_p}$ denotes the scale parameter corresponding to excesses of the physical threshold $u_p$. Similarly for threshold choice $u > u_p$, yields the following expression

$$E(X - u | X > u) = \frac{\sigma_u}{1-\xi} = \frac{\sigma_{u_p} + \xi u}{1-\xi} \tag{3.21}$$

which is linear in $u$ with gradient $\frac{u}{1-\xi}$ and intercept $\frac{\sigma_{u_p}}{1-\xi}$. Empirical estimates of the sample mean excesses are typically plotted against a range of thresholds, and the appropriate threshold

is chosen to be the lowest level where all the higher threshold satisfy linearity in the mean excess above the selected threshold.

The mean residual life plot is considered as a graph which points are as follows:

$$\left\{ \left( u, \frac{1}{n_u} \sum_{i=1}^{n_u} \left( x_{(i)} - u \right) \right) : u < x_{\max} \right\}, \tag{3.22}$$

where $n_u$ is the maximum number of observations that exceed $u$, $\left( x_{(1)}, x_{(2)}, \ldots, x_{(n_u)} \right)$ are the number of observations that exceed $u$, and $x_{\max}$ is considered as the largest observation that exceeds $u$.

Due to practical difficulties in interpreting the (MRL) plots they are acknowledged as threshold diagnostics of a major disadvantage. Considering such a plot, a subjective selection in threshold is inevitable as the graph is approximately linear from a very small threshold.

Figure 3.1 provides an example of a MRL plot for the Fort Collins total daily precipitation data from the extRemes package (Ver. 1.62) in R (Gilleland et al., 2010). The threshold of $u = 0.4$ inches suggested by Katz et al. (2002) is justified by the empirical MRL, considering close to linear above this level, and below this level a curved MRL is observed indicating a bias due to the GPD asymptotic breaking down.
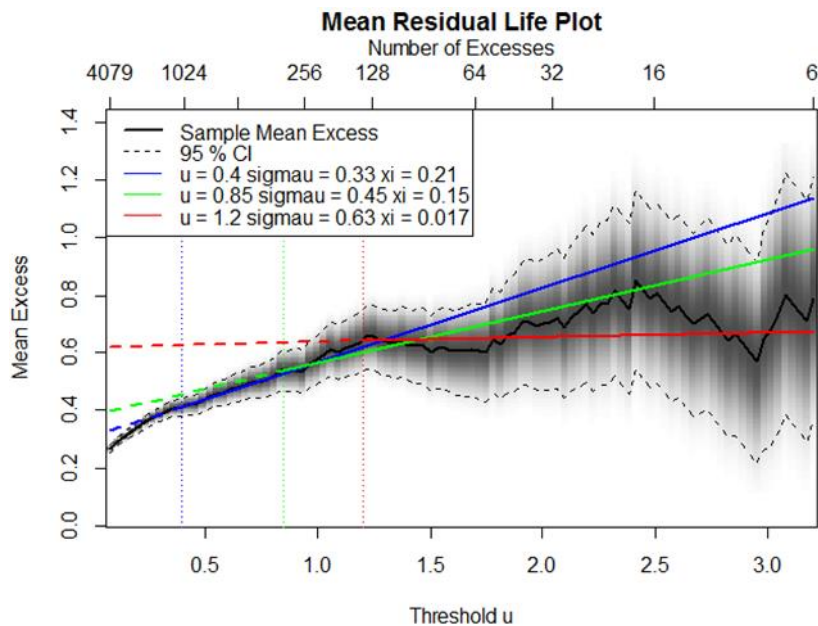


Figure 3.1: Mean residual life plot for the Fort Collins daily precipitation data. Solid jagged line is empirical MRL with approximate pointwise Wald 95% confidence intervals as dashed lines. The MRL implied by maximum likelihood (ML) parameter estimates for thresholds u = 0.395, 0.85 and 1.2 inches are the upper, middle and lower straight lines respectively. Vertical dashed lines mark these thresholds. Example of the MRL plot from Gilleland et al. (2010) using the extRemes package in R

## 3.4.2 Parameter Stability (PS) Plot

The Parameter Stability plot (PS), (Coles, 2001) is one of the most used methods for threshold selection. The method involves plotting the parameter estimates from the GPD or

point process models against $u$, for a range of values of $u$. The parameter estimates should be stable (i.e. constant) above the threshold at which the GPD model becomes valid.

If the exceedances of a high threshold $u_p$ follows a GPD distribution with parameters $\xi$ and $\sigma_{u_p}$, then for any other threshold $u$ such that $u > u_p$, the exceedances will follow a GPD distribution, with shape parameter $\xi_u = \xi$ and scale parameter $\sigma_u = \sigma_{u_p} + \xi(u - u_p)$. Parameterizing the scale parameter as $\sigma^* = \sigma_u - \xi u$, concludes that for a large enough physical threshold $u_p$, $\sigma^*$ is invariant of the increase in threshold $u$.

As a result, if a GPD distribution describes exceedances in extremes above a threshold $u_p$, then exceedances in extremes will also follow the same distribution for a higher threshold $u$, and parameters $\sigma^*, \xi$ will remain invariant of the threshold choice $u$ where $u > u_p$. The idea is to find the lowest possible threshold whereby a higher threshold would give the same results within uncertainty bounds.

The considerable disadvantage of Parameter stability plot method, is that the accepted threshold values often require a great deal of subjective judgement, and are not relied to analytical unified selection method.

Figure 3.2 provides an example of a Parameter Stability plot for a location in the North sea (54.00N 2.25E) using daily wind speed data from the ERA-Interim database (sub-Section 5.4.1) of 20 years (1979 to 1998). The threshold value selections of $u$=(13, 14.8 and 16.59 m/s) in vertical dashed lines are justified by the empirical PS plot, considering closely unperturbed estimations above this level.

**(a)**                                                    **(b)**
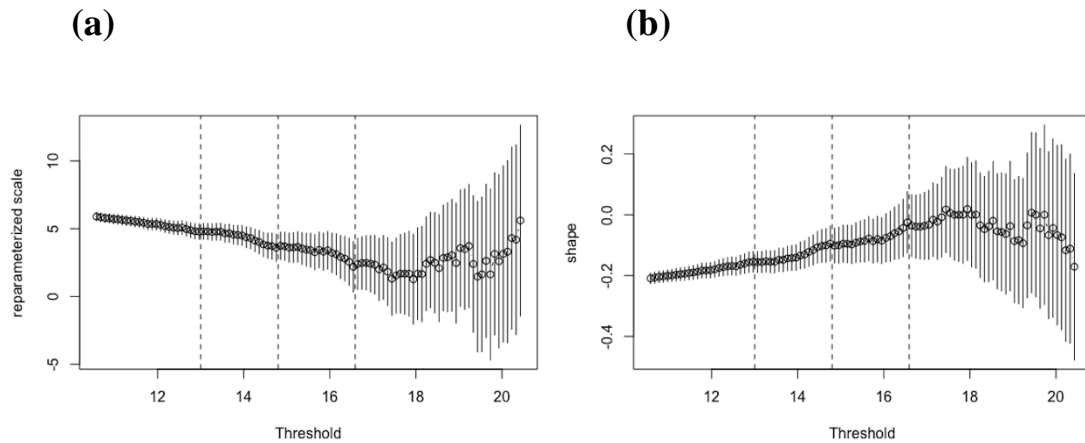


Figure 3.2: Parameter Stability plot for the location in the North Sea of 20 years of wind speed data from the ERA-Interim database. Solid dot line is empirical PS plot for the parameters scale (a) and shape (b), with approximate pointwise Wald 95% confidence intervals as vertical solid lines. The PS plot used maximum likelihood (ML) parameter estimates for a range of thresholds (60% quantile $\leq u \leq$ 99.5% quantile). Vertical dashed black lines mark the empirical threshold selection. Example of the PS plot (Tsalis et al., 2019) using the extRemes package in R of Gilleland and Katz (2016).

## 3.4.3 Rules of thumb

This procedure known as rules of thumb, consists in choosing one of the sample points as the appropriate threshold. The method is equivalent of setting the $k^{th}$ order upper statistic $X_{n-k+1}$ from the ordered sample $X_{(1)}, X_{(2)}, \ldots, X_{(n)}$, of size $n$. (Scarrott and Mac Donald, 2012) in their review, pointed out the predominant widely used threshold values. As shown, the 90% quantile or rule of Du Mouchel (1983), although widely used, this threshold value is not relied to strong theoretical background. Other threshold choices are to be used such as $k = \sqrt{n}$ as

pointed out by Ferreira et al. (2003), and $k = \dfrac{n^{2/3}}{\log(\log(n))}$ proposed by Loretan & Philips (1994). Reiss & Thomas (2007) proposed as threshold selection the lowest upper order statistic value $k$, in order to minimize the expression:

$$\min = \frac{1}{k}\sum_{i=1}^{k} i^{\beta} \left| \hat{\xi}_i - median(\hat{\xi}_1, \hat{\xi}_2, \dots, \hat{\xi}_k) \right|, \ 0 \leq \beta \leq 0.5. \tag{3.23}$$

Where $\hat{\xi}_i$ is denoted as the estimated shape parameter of the GPD distribution.

Another selection approach proposed by Ruggiero et al. (2010), was the 99.5th percentile of the data. Rosbjerg et al. (1992) suggest calculating the physical threshold as the mean value of the observed series plus three standard deviations. The considerable disadvantage of The Rules of thumb method, is that the accepted threshold values rely on a hieratical approach and not derived analytically.

## 3.4.4 Multiple Threshold Model

Improved threshold diagnostic plots for extreme value analyses is suggested from Wadsworth & Tawn (2012) and Northrop & Coleman (2014). Score and likelihood ratio tests fit of equality of the shape parameter over multiple thresholds, considering null hypothesis $H_0: \xi(u) = \xi(u_o)$, for all $u \geq u_o$. Rejection of $H_0$ suggests that a threshold higher than $u_o$ is required.

Wadsworth and Tawn (2012) proposed a two-threshold penultimate extreme value model in which the shape parameter is modelled as a partially constant function of threshold. For a pair of thresholds $(u, v)$, where $v < u$ the shape parameter has a change-point at the threshold $u$:

$$\xi(x) = \begin{cases} \xi_{vu}, & v < x < u \\ \xi_u, & x > u \end{cases}. \tag{3.24}$$

Later on, Northrop & Coleman (2014) proposed a better approximation for $\xi(x)$, extending the partially constant representation to an arbitrary number $m$ of thresholds $(u_1, u_2, \dots, u_m)$ as follows:

$$\xi(x) = \begin{cases} \xi_i, & u_i < x < u_{i+1} \\ \xi_m, & x > u_m \end{cases}, \text{ for } i = 1, 2, \dots, m-1. \tag{3.25}$$

The latter model is commonly referred to as the NC diagnostics. Provided that $\xi_m > -0.5$ (Smith, 1985), p-values of the tests are estimated in a range of thresholds $(u_i, \dots, u_m)$ for $i = 1, 2, \dots, m-1$, whether a threshold higher than $u_i$ is required. The asymptotic null distribution of each test statistic is approximated by the chi-squared $x^2_{m-i}$ distribution. The optimum threshold value is considered as the lowest value $u_o$ with the property that the null hypothesis is not rejected at it and at all the higher thresholds considered $u_{o+1}, \dots, u_m$. The idealized scenario is that the p-values increase with threshold until approximate stabilization at a point where one could set the threshold. An informal approach is by looking for the sharpest increase in the p-value, referring to threshold that segregates no fewer than 50 events totally, Jonathan and Ewans (2013) and non-exceeding 5 to 10 events/year, Palutikof et al. (1999). The considerable advantage of the threshold from the NC diagnostics is that this selection requires less subjective judgment.

Example of the threshold selection is presented in Figure 3.3 for the 20 year time series extending from 1979 to 1998 corresponding to location L18 (54.00 N 2.25 E in the North Sea) from the ERA-Interim database, with standard Parameter Stability (PS) plot (see sub-Section 2.7.2) as a comparative measure. For the diagnostics, score test is performed for the shape parameter over multiple thresholds.The threshold range for the test was limited between the 60% and 99.5% sample quantile of the daily wind speed maxima with a step of 0.01. The empirical threshold selection is depicted as the value associated to the sharpest p-value increase at the significance level of 0.05. For easier representation, peak p-values and threshold are located on the vertical dashed line on the diagram of the NC diagnostics. Furthermore, threshold exceedances are also denoted on the top scale of the same diagram.

**(a)** **(b)**
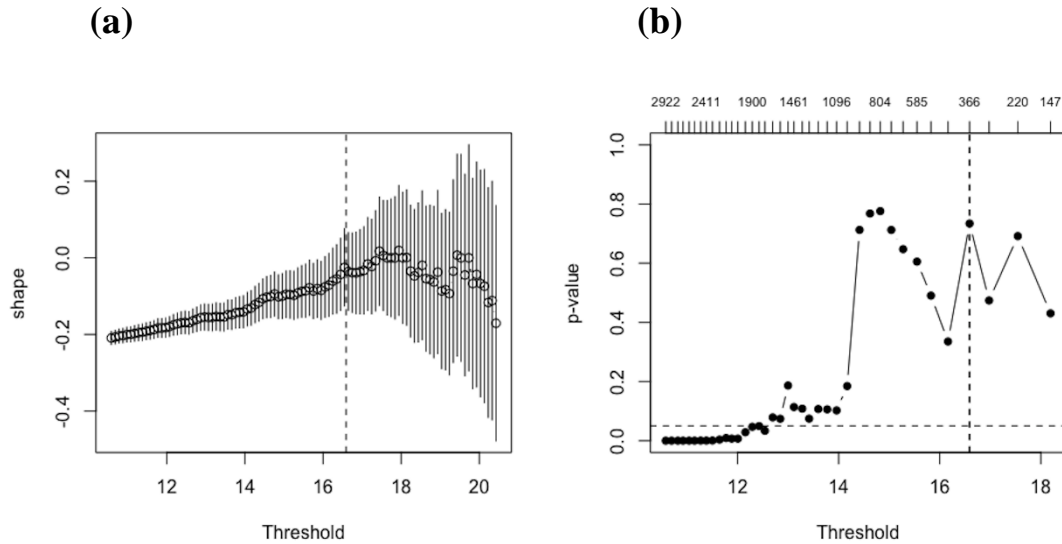


Figure 3.3: Left Panel (a): PS plot. Solid dot line is empirical estimation for shape parameter, with approximate point wise Wald 95% confidence intervals as vertical solid lines. Vertical dashed line marks the threshold imported from the NC diagram. Right panel (b): NC diagram. Score test for shape parameter over multiple thresholds. Vertical dashed line marks the empirical threshold selection of the p-values at the significance level of 0.05. The threshold is selected at 16.590 m/s where the peak p-value is at 0.734. Example of the threshold diagnostics (Tsalis et al., 2019) using the extRemes and mev package in R of Gilleland and Katz (2016) and Northrop & Coleman (2014) respectively.

## 3.5 De-Clustering models

In order to obtain approximately independent Threshold excesses, some kind of filtering of the dependent observations is considered removing the dependence by De-clustering the excesses. In this way De-Clustering approaches of extremes are introduced.

### 3.5.1 Standard Storm Length (SSL) method

The standard storm length (SSL), is estimated through the autocorrelation function of an equal distant process and represents the required minimum time distance between successive maxima in order for them to be statistically independent. The method is based on filtering observations, in order to extract the $r^{th}$ largest independent values. The extraction was performed as follows:

a)  Identifying and picking out the largest value of the time series which is extracted;

b) Discarding values with a lag of $\Delta t = \frac{(SSL)}{2}$ and less, from both side of the value chosen in (a);

c) Selecting the following largest value of the remaining data;

d) Repeating steps (b) and (c) until the $r$-largest is finally extracted.

The $r$-largest of such values for each block size year, could be considered as the required $r$-largest independent annual events. The optimum lag time is referred as the SSL Tawn (1988), satisfying the independence criteria (min. correlation) between events. Extremes are more likely to be independent if $r$ is kept small (Smith, 1986). Finally, as an application to wind speed data, Coles & Walshaw (1994) resulted that a possible choice for the standard storm length is $60h$, advocating a reasonable number of maxima within each year to be equal to 10.

## 3.5.2 Method of Independent Storms (MIS)

The Cook (1982) model of independent storms (MIS) increases the number of extremes available for analysis, whilst ensuring their independence by separating the parent time series into independent storms and then selecting the highest value from each storm.

First of all the continuous records are first subjected to a simple block-averaging low-pass filter technique with a period of ten hours.

Secondly, downward crossings will define the start of the so called lull in the record and by definition between each pair of lulls, there exist an independent storm. Between lulls the peak value is selected, the maxima of the event. The selected arbitrary threshold is set at $u$=5 (m/s) illustrated in Figure 3.4.
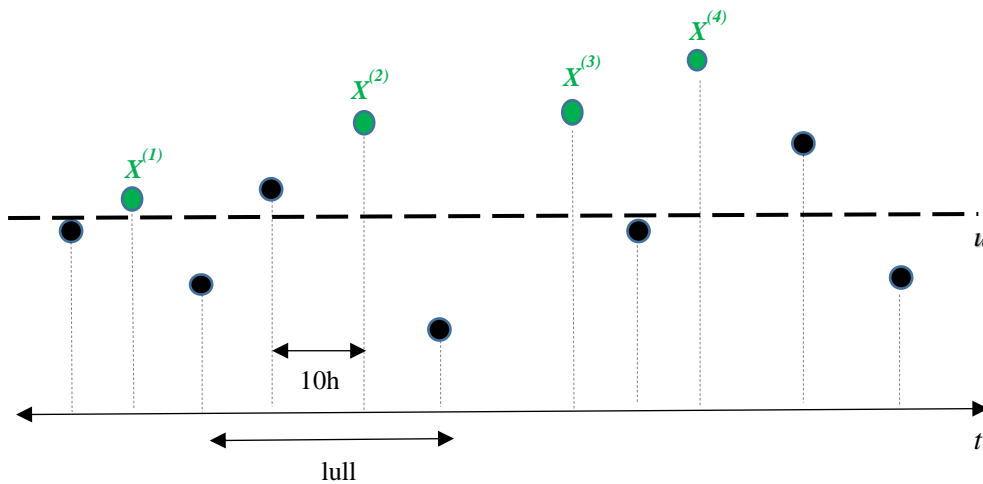


Figure 3.4: De-clustering the time series to the sample of ($X^{(1)}$, $X^{(2)}$,…, $X^{(n)}$) using the MIS model. The selected threshold is u = 5 (m/s) (Supplamentary material of Tsalis et al., 2019).

Defining $N$ the independent maxima events and $R$ the wind years of the record, the MISmethod set a typical storm frequency rate to be around $r$=100 (events/year), where $r = N/R$ .

Third, the extracted maxima are squared in order to transform the parent distribution closer to an exponential, and converge to the Fisher-Tippett Type 1 extreme value distribution. Since the event maxima are all independent, it follows that the distribution of the largest annual maximum out of $r$ independent maxima per year, has a probability distribution for which an empirical estimate is the set of values $(p_m)^r$ associated with the ordered squared data. The ascending ranked order follows

$$p_m = \frac{m}{N+1}, \, m = 1,2,\ldots,N. \tag{3.26}$$

The squared data values against the return value $y$ is illustrated in Figure 3.5, where

$$y = -\ln(-\ln(p_m)^r) = -\ln(-r\ln(p_m)), \tag{3.27}$$

and obtain the straight line for $y = a \cdot (squared\ data) + \beta$.
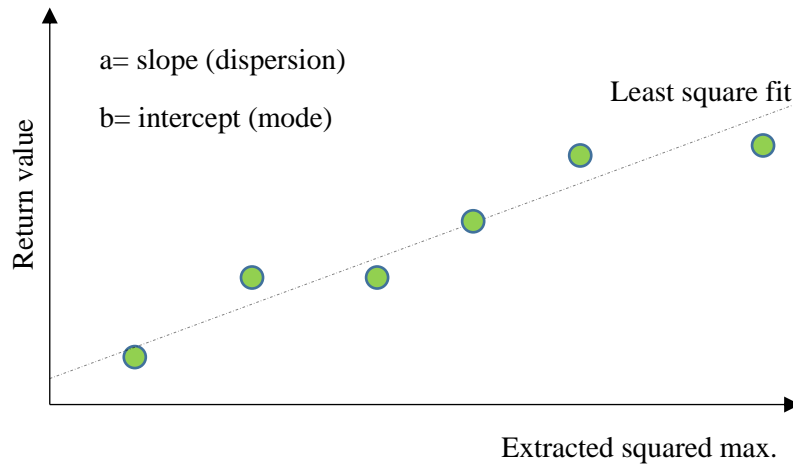


Figure 3.5: Least square fit to the squared of the extremes for the estimation of the parameters of the Gumbel distribution. (Supplamentary material of Tsalis et al., 2019).

Although taking the square of the extremes makes no difference to their rank order, it does affect the fitting of the straight line in the above figure and hence the parameters of the Gumbel model. Using a least-squares method to find the best-fit line gives equal weight to each of the plotted points. However, this approach is often considered unsuitable for extreme value data, since the error associated with each point varies systematically, being greatest for the largest extremes.

Various alternative fitting strategies have therefore been developed. One method widely used for wind extremes has been the Lieblein BLUE (best linear unbiased estimators) method (Lieblein, 1974, and described in detail by Cook, 1985). The modified BLUE (10) method follows that the rank of the lowest storm maximum used, is given by the integer which is the nearest solution to $\left(\frac{m}{N+1}\right)^r = \frac{1}{11}$. The maximum events to be used are $N - m$ and not $N$, setting the threshold at a point where an annual rate of $r=10$ events/year gives a reliable estimate of the 50-year extreme. Simulations reported by Gross et al. (1994), suggest that in samples taken from normal or extreme value populations, optimal results are obtained if threshold is chosen so that the number of exceedances is of order of 10 events/year. Thus, the threshold must be chosen in order to improve linearity in the Gumbel plot, conducting the appropriate annual rate of events.

Finally, Harris (1999) introduces two improvements to the MIS. First, to avoid systematic errors, he modifies the plotting position used by Cook (1982). Second, he substitutes his own method to find the best-fit line (Harris, 1996) for the BLUE method. This avoids the need for data reduction, which Cook (1985) found necessary.

### 3.5.3 Smith's de-clustering model (1991)

Smith (1991) pointed out that there is no universally accepted method for identifying clusters. To his model approach, he consists of specifying a threshold and a time interval. Two exceedances of the threshold which are closer together than the cluster interval are deemed part of the same cluster. But when the time interval between successive exceedances is longer than the cluster interval it is considered that the old cluster has finished and a new one is to begin. In this way clusters are defined and clusters maxima are pointed out. Threshold and cluster interval are to be considered arbitrary and different values are used for comparison.

## 3.5.4 Separation time model

In the literature, a well-known model identifying independency between events, is the separation time between the end of one event and the beginning of another. It is stated as the time-lag, for which the autocorrelation between the observations becomes weak and two consecutive events can be safely considered independent. The value of the time lag is considered greater than the typical duration of the physical event itself, but not too long in order to avoid discarding independent events and excluding valuable data information.

Some examples concerning time lag between events are proposed by Egozcue et al. (2005) who studied wave heights along the Mediterranean coast of Spain and set the time lag to be 4 days. Haigh et al. (2010) studied the extreme wave height along the English Channel and required the surge peaks to be separated by 30 h at least. USWRC (1976), Cunnane (1979) and Lang et al. (1999) concluded that successive river flood events are to be separated by at least as many days as five plus the natural logarithm of square miles of the basin area. Willems (2000) required that two rainfall events are separated by at least a 12 h lag. In the study of the extreme behavior of daily maximum wind gusts over Belgium , Van de Vyver and Delcloo (2011) set a minimum time separation equal to 3 days.

Zachary et al. (1998) proposed three choices of minimum storm separation interval, namely 24, 48 or 72 h, Alves, Young (2003) have chosen 72 h, while Morton et al. (1997) and Morton, Bowers (1997) have proposed 30 hand Mathiesen et al. (1994) 5 to 7 days. Van Vledder et al. (1993) mention that the optimum minimum time between successive independent events can be assessed by means of correlation analysis and Soares, Scotto (2004) proposed a time separation interval of the order of 480 h (20 days).

Using correlation analysis, the time lag can also be defined using the autocorrelation function of the primary time series. For extreme wave heights, Mathiesen et al. (1994), proposed that the appropriate time lag between successive events cannot be longer than the time interval for which the autocorrelation function of the primary series drops under 0.3-0.5.

It is clear reviewing the relevant literature, that the proposed from authors time separation intervals (time-lag), vary dramatically. There is still no robust theory in order to justify the selection of the optimum separation time interval ensuring the independency between the events.

## 3.5.5 Standard Runs model

A method for estimating the extremal index of a stationary sequence (and consequently a procedure for identifying clusters) regarded as the Runs Estimator was initially proposed from Smith and Weissman (1994), introducing the idea of runs of observations below a high enough threshold $u$. More precisely, the idea was that any sequence of consecutive observations from a time series exceeding the threshold belongs to the same cluster. Obtaining observations that fall below the threshold, the previous cluster is defined and once appearing the next exceedance, a new cluster is initiated. The number of the consecutive observations below the threshold is defined as the runs length and denoted as $r_n$ separating the clusters. Two excesses of the

threshold belong to the same storm (cluster) if they are separated by less than $r_n$ consecutive non-exceeding values. The de-clustering procedure of a sample $\{X_i\}$ of size $n$ is stated as follows:

First, an indicator function is defined as $W_{n,i} \to 1$ if the $i^{th}$ observation is above the threshold (i.e., $X_i > u_n$) and $W_{n,i} \to 0$ otherwise. The total number of observations above the threshold will be then $n_u = \sum_{i=1}^{n} W_{n,i}$.

Second, the number of clusters containing at least one observation above threshold will be denoted as $Z_n^*$. Ensuring that an exceedance of threshold in position $i$ is counted in the cluster if and only if the following $r_n$ observations are all below the threshold. In this sense then,

$$Z_n^* = \sum_{i=1}^{n} W_{n,i}\left(1 - W_{n,i+1}\right)\left(1 - W_{n,i+2}\right) \cdots \left(1 - W_{n,i+r_n}\right). \tag{3.28}$$

The mean size of the clusters using the runs model is estimated by the ratio $n_u/Z_n^*$. The $r_n$ is closely related with the extremal index $\theta$, where the latter index is defined as the reciprocal of the limiting mean cluster size (Nandagopalan, 1990),

$$n_u/Z_n^* = \theta^{-1}. \tag{3.29}$$

Finally, the maximum value of each of the defined clusters is extracted.

The choice of $r_n$ is very important for bias and variance considerations. Small values will arise problems of non-independence for nearby clusters, while large values will lead to unnecessary concatenation of clusters and so loss of data information. There is no formal consideration to the choice of $r_n$. Nandagopalan (1990) and Leadbetter et al. (1989) have used a version of the runs length with $r_n = 1$. The advantage of this method, as described in Walshaw (1994), is that it allows both the duration (persistence) of storms and the duration of intervals between them to vary according to the data. This procedure was developed for POT and GPD models, extracting from any given time series the optimum extreme-type sample approximating the independence limitations, (Fawcett and Walshaw, 2006 b; and Caires and Sterl, 2005). From these studies, the clusters length varied from 24 to 60 hours.

Before applying the Runs model in this setting for the identification of clusters, the extremal index should be estimated in order to specify the optimal runs length parameter of the given time series. Summarizing the implementation of the Runs model, the essential parameters for identifying clusters and ensuring independent events are optimum values of $u$ and $r_n$. The Runs model used, relies in the Intervals Estimate for the associated $\theta(u)$, providing an optimum threshold $u$ from the Multiple-Threshold Model by the NC diagnostics. The threshold range for the Score test of the NC diagnostics was limited between the 60% and 99.5% sample quantile of the daily wind speed maxima with a step of 0.01. Example of the Runs de-clustering model is illustrated in Figure 3.6.
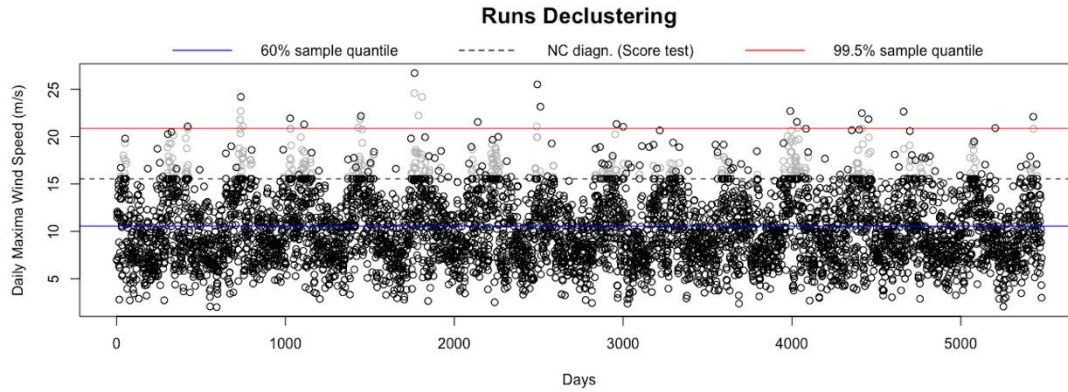
Figure 3.6: De-cluster daily wind speed data by the Runs model. The extremal index and consequently the runs length separating the approximately independent clusters is obtained from the Intervals Estimate and the threshold selection is made from the NC diagnostics. The dataset used is from the MARINA Platform database (sub-Section 5.4) regarding sample period of 15 years (from 1996 to 2010) for location (52.05N 2.15E) in the North Sea. Example of the Runs de-clustering model (supplementary image of Tsalis et al., 2021) using the extRemes package in R of Gilleland and Katz (2016).

## 3.5.6 DeCA model

The physical de-clustering model originaly proposed from Soukissian et al., (2006) aims at creating approximately independent events assuming physical considerations. The events are defined as a continuous physical phenomenon of the environmental variable. The model separates all events by looking at energy reductions between consecutive time steps.

Initially, the available time series are filtered twice using a simple monotonicity criterion obtaining the series of local maxima. Successive points with the exact same value are removed thereupon the monotonicity criterion. From the latter series the local maxima and minima are identified and the cubic power of their corresponding values is estimated. Therefore, numerical differences of cubic local maxima to the next consecutive cubic local minima are considered. Selecting a pre-Defined Energy Percentage (DEP) with respect to the third power of the local max values, the method introduces wind energy percentage reductions. Wind climatology studies have established that the wind power potential available in a flow of air per unit cross-sectioned area, normal to the flow, is proportional to the third power of wind speed (Reed, 1974)

$$P_{wind} = \frac{1}{2}\rho v^3 \ , \tag{3.30}$$

where $\rho$ is denoted as the air density and $v$ is the wind speed.

The time indexes of local minima that correspond to the identified energy reductions are referred to as *transition points*. As a result, the series of *transition points* clarified the initial time series into successive and approximately independent wind-state clusters of generally unequal length. Then, by selecting the maximum value of each previous defined cluster, a sample of approximately irregular maxima randomly spaced in the time axis is derived. Even if each event can be associated with a particular instant of occurrence on the time axis, the derived sample does not depend on time any more. The optimum DEP level should generally be high enough in order to safely separate independent events. But it should not be extremely high in order to avoid unnecessary concatenation of clusters and thus loss of data information. Profound knowledge of the examined phenomenon guarantees that the DeCA model will include all events in the process.

At this point, it should be mentioned that the initial de-clustering approach by Soukissian et al. (2006) avoided assumptions regarding the important regularity restrictions of sampling at

any DEP level. Furthermore, DeCA presumed that the statistical threshold of the de-clustered sample for the GPD fit should be provided hierarchically and set to the modal value without further investigation. The rank of dependence of the DeCA samples is analytically presented in Chapter 4, where a suitable re-sample model is proposed addressing the dependence limitations when sampling from DeCA.

Taking into account the re-scaled series of local wind energy, for this analysis we considered eight levels clarifying the series of *transition points*. The supported DEP reduction levels are set constant at % values (60, 65, 70, 75, 80, 85, 90 and 95) with the time indexes of local minima that correspond to these levels, initiating the successive irregular clusters. Example of the DeCA model is illustrated in Figure 3.7.
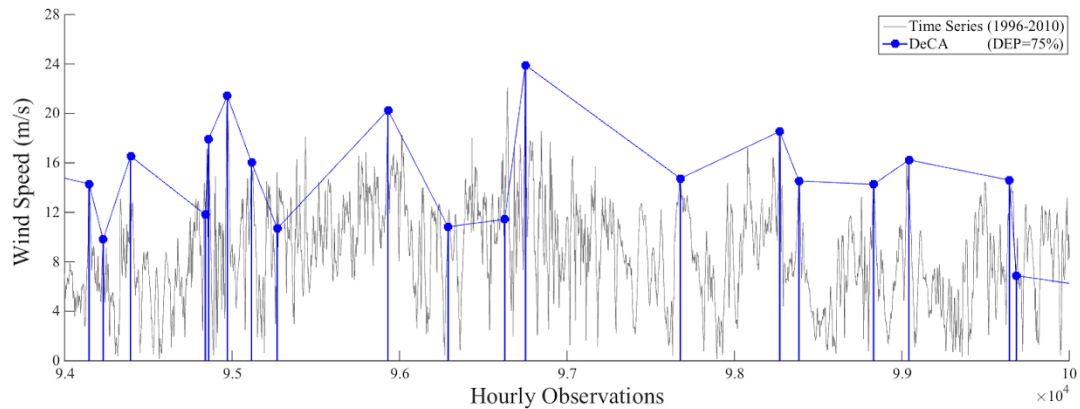


Figure 3.7: Example of the DeCA model with optima DEP level at 75% in order to safely separate approximately independent events avoiding unnecessary concatenation of clusters. The dataset used is from the MARINA Platform database (sub-Section 5.4) regarding sample period of 15 years (from 1996 to 2010) for location L6 (58.4N 10.3E) in the North Sea. Demonstration of the DeCA model of Soukissian et al., (2006) as supplementary image of Tsalis et al., (2021)

# Chapter 4
## Reconstruction of regularly and irregularly spaced samples in time

The attempt for developing approaches to enlarge the sample extreme values beyond the annual maxima often provides de-clustered samples that are subjected to irregular sampling effect. In the irregularly spaced in time samples, the successive differences $\Delta t = t_{i+1} - t_i$ at the corresponding observation times $t_1 < t_2 < \cdots < t_i < \cdots < t_N$ in the sample of $N$ observations, are not necessarily equal. Unevenly spaced time samples result to an additional bias and a propagated error, both of which are latter imported in the data processing when applying standard statistical analysis (Vio et al., 2000; Broersen, 2009; Mondal and Percival, 2010). However, a question arises of how to measure the rate of dependency in a sample of observations when they are located irregularly in time.

Much research arround this field of interest has been undertaken and in Chapter 4 an attempt is made in order to transcend the important regularity restrictions of a resample. Specifically, a proposed methodology is analytically presented as an alternative resampling procedure considering the irregularly sampling scheme effect in time and deriving asymptotically independent observations.

Traditionally, the Pearson correlation estimator is the standard approach detecting the related dependency from de-clustered observations. However, is the standard correlation estimator the correct approach when the de-clustered samples are irregularly spaced in time? One of the most classical approaches modelling irregular observations spaced in time is the Autoregressive Conditional Duration (ACD) model introduced by Engle and Russell (1998). The model treats the time intervals between events as a stochastic process and proposes a new class of point processes with dependent arrival rates. Specifically, the arrival times are treated as random variables of a point process. The basic formulation of the model parameterizes the conditional intensity as a function of the time between past events, and numerous natural extensions include other effects such as characteristics associated with past outcomes. The ACD model has been partly assessed in financial studies such as Bauwens and Giot (2001), Engle and Russell (2002), Tsay (2002), and Hautsch (2004), that model the behavior of irregularly time-spaced financial data.

In general, the Pearson estimator is condemned when the sampling is irregular (Scargle, 1989; Zhang et al., 2008). The accepted methods processing irregular observations in terms of correlation analysis are sorted into three major classes:

(i)   Direct transform methods (Spectral Analysis) that estimate the spectrum of the irregular sample by generalization of the Fourier transform (Lomp-Scargle Periodogram) (Stoica et al., 2009; Babu and Stoica, 2010),

(ii)  Interpolation methods that suggest re-sampling at uniform intervals (Schulz & Stattegger, 1997; Kreindler & Lumsden, 2006) and finally

(iii) Slotting methods that compute the correlation of irregularly spaced samples in order to generalize the Pearson correlation operator (Mayo, 1993). This is achieved by calculating the products of observations according to their sampling time differences using the Gaussian Kernel as a weight function over the observations. The technique was developed in fluid mechanics and relevant applications can be found in (Tummers and Passchier, 1996; Benedict et al., 2000; and Rehfeld et al., 2011).

The classical methods for analyzing the correlation effect in samples irregularly spaced in time, often yield poor performance in comparison to the non-rectangular (Gaussian) Slotting

method. Examples of other Slotting approaches such as slot boundaries, local normalization, fuzzy slotting and variable windowing, can be found in Nobach (2002) or in Damaschke et al. (2018) and references therein.

Resamples are often affected by dependency and the independence limitations is usually disregarded. To this effect, a suitable model denoted as (DeCAUn) is proposed in sub-Section 4.4. This model provides an improvement to the current physical De-Clustering model Algorithm (DeCA; see Chapter 3), re-sampling effectively the irregularly in time DeCA samples. The re-sampling strategy is processed using the Slotting Autocorrelation approach, which is also analytically presented in this Section.

At the following sub-sections, the standard Direct transform methods (Spectral Analysis) and Interpolation methods will be briefly discussed. However, our analysis will be based on the Slotting method. In addition, the Standard Correlation estimator and Standard Periodogram which disregards the irregular sampling scheme effect is briefly presented before introducing the Slotting method.

## 4.1 Analysis of equally spaced samples in time

### 4.1.1 Standard Correlation estimator

Autocorrelation or lagged correlation refers to the correlation among members of a series of numbers arranged in time. A random process is considered statistically steady if the first and second moments are time invariant (covariance stationary) and if the sample moments converge in probability to the population moments (ergodic). Under this assumption, from a sample of $N$ number of observations regularly spaced at times $t_1 < t_2 < \cdots < t_i < \cdots < t_N$, the correlation between observations that are separated by a lag number of $k$ equally distant time steps $\Delta t$ ($\Delta t = t_{i+1} - t_i$) is defined as the sample Autocorrelation Function (ACF) at each time lag ($k$):

$$\rho_x(k) = \frac{Cov(k)}{\sigma_x^2} = \frac{\frac{1}{N-k}\sum_{t=1}^{N-k}(x_t-\bar{x})(x_{t+k}-\bar{x})}{\frac{1}{N}\sum_{t=1}^{N}(x_t-\bar{x})^2}, \tag{4.1}$$

for any positive integer $k < N$. $Cov(k)$ is the sample autocovariance at time lag ($k$), and $\bar{x}$ and $\sigma_x^2$ are the sample mean and variance respectively. The sample ACF takes both positive and negative values $-1 \leq \rho_x(k) \leq 1$, while the associated plot is referred to as correlogram. The Generalized Bartlett's formula for ACF (Bartlett, 1946), yields the following standard error

$$SE_{\rho_x} = \sqrt{\frac{1+2\sum_{i=1}^{k-1}\left(\rho_x(i)\right)^2}{N}} \tag{4.2}$$

for the associated 95% confidence interval. The confidence bounds of the correlogram, effectively test the null hypothesis of convergence to an uncorrelated approximation by that particular lag number of $k$ time steps. If $\rho_x(k)$ is located outside the bounds, this means that the preceding autocorrelations have not been successfully reduced to close to zero. The desired lag number of $k$ or lag ($k$) is set as the first time lag entering the confidence bounds.

For samples irregularly spaced in time the inter-sampling times vary and the standard ACF described in Equation (4.1) cannot be directly applied (Chatfield, 1996).

### 4.1.2 Standard Periodogram

We consider a random process as a continuous function of time and observed data $x(t_n)$, where $N$ data points are considered at time $t_n$, $\{t_n, n = 1, 2, \ldots, N\}$. Ordering the times

as $t_1 < t_2 < \ldots < t_N$ and considering evenly spaced intervals $\Delta t = t_{n+1} - t_n$, the Discrete Fourier Transform (DFT) is defined as follows:

$$DFT[x(\omega_k)] = \sum_{n=1}^{N}\left(x(t_n)\exp(-i\omega_k t_n)\right) \tag{4.3}$$

The Fourier series theory shows that $\hat{x}(t_n)$ can be reproduced from a finite Fourier series of $N$ terms by inverting (4.3) as follows:

$$\hat{x}(t_n) = \Re\left(F^{-1}[DFT[x(\omega_k)]]\right) = \sum_{k=-N/2}^{+N/2}\left(DFT[x(\omega_k)]\exp(it_n\omega_k)\right), \tag{4.4}$$

where the sum is defined on evenly spaced frequencies $\omega_k = \frac{2\pi k}{T}$, $k = \left\{-\frac{N}{2},..0,..,+\frac{N}{2}\right\}$, and the sampling interval is defined as $T = t_n - t_1 = (N-1)\Delta t$.

For discrete, equally spaced data and frequencies, the Rayleigh theorem is known as Percival theorem (see Appendix E.1) and is described as follows:

**Corollary 4.1** (Parcival equality)

$$\frac{1}{N}\sum_{n=1}^{N}\left(x(t_n)\right)^2 = \sum_{k=-N/2}^{+N/2}|DFT[x(\omega_k)]|^2, \tag{4.5}$$

*where the contribution of $|DFT[x(\omega_k)]|^2$ to the power at frequency $\omega_k$ is called the intensity at this frequency.*

The plot of intensity versus frequency, is the Fourier line spectrum $P_x(\omega_k)$ (Deeming, 1975):

$$P_x(\omega_k) = \frac{1}{N}|DFT[x(\omega_k)]|^2$$

$$= \frac{1}{N}\left(\sum_{n=1}^{N}\left(x(t_n)\exp(-i\omega_k t_n)\right)\right)^2$$

$$= \frac{1}{N}\left[\left(\sum_{n=1}^{N}\left(x(t_n)\cos(\omega_k t_n)\right)\right)^2 + \left(\sum_{n=1}^{N}\left(x(t_n)\sin(\omega_k t_n)\right)\right)^2\right]. \tag{4.6}$$

By plotting $P_x(\omega_k)$ (Equation (4.6)) against frequency, one will obtain a large narrow peak, meaning that around that specific frequency range, $x(t_n)$ and $\exp(-i\omega_k t_n)$ will be in phase.

As described in Scargle (1989), the fundamental frequency is defined as

$$\omega_{fund} = \omega_{\min} = \frac{\pi(N-1)}{T \cdot N}, \tag{4.7}$$

and corresponds to a frequency with the minimum information in the observed data. The number of frequencies determining the spacing of the frequency vector is given as $ofac \cdot N$. According to Hocke and Kämpfer (2008) there is no principal limit for the oversampling factor ($ofac$), where in general $ofac > 1$ and is regarded as a smoothing factor. In most cases the oversampling factor is set to $ofac = 2$.

The Nyquist frequency is defined as

$$\omega_{Nyq} = \frac{1}{2}\left(\frac{2\pi}{\Delta t}\right) = \frac{\pi N}{T}, \text{ or } f_{Nyq} = \frac{1}{2\Delta t}, \tag{4.8}$$

where $\Delta t = \frac{T}{N}$ corresponds to a value in frequency with the maximum information in the observed data. In the case of equally spaced data, $\hat{x}(t_n)$ in Equation (4.4) is in line with the properties of the Sampling Theorem stated as follows (Bracewell, 2000):

**Theorem 4.1** (Sampling Theorem)

*Any function whose Fourier transform is zero for $f_k \geq f_{Nyq}$, $\omega_\kappa = 2\pi f_k$, is fully specified by values spaced at equal intervals not exceeding $\frac{1}{2f_{Nyq}}$. The highest frequency which may be recovered from samples at intervals $\Delta t$ is one-half the sampling rate or the Nyquist frequency.*

## 4.1.3 Autocorrelation Function & Power Spectrum

The energy spectrum or power spectrum in the frequency domain is defined by Parseval's identity for Fourier transforms or Rayleigh's theorem (Jenkins and Watts 1969, Priestley 1981, Press et al., 1992), as the square of the complex absolute value of the Discrete Fourier Transform, i.e.:

$$P_x(\omega_k) = |DFT[x(\omega_k)]|^2. \tag{4.9}$$

Considering the Wiener-Khinchin Theorem (Khintchine 1934, Papoulis 1991; Bracewell 2000), the normalized expression of the power spectrum of a stationary random process is related with the (ACF) as a Fourier transform pair. The corresponding ACF in the time domain is obtained as follows (see E.1 and E.3 in Appendix):

$$\rho_x(k) = \Re(F^{-1}[P_x(\omega_k)]). \tag{4.10}$$

## 4.1.4 Example of the inverse Fast Fourier Transform (iFFT) for samples regularly spaced in time

An example of the Standard Periodogram and the iFFT to the Standard Correlation estimator is given in Figures 4.1-4.3, illustrating the hourly time series from the MARINA Platform database of sample period of 15 years (from 1996 to 2010) for location L2 (52.05N 2.15E) in the North Sea.
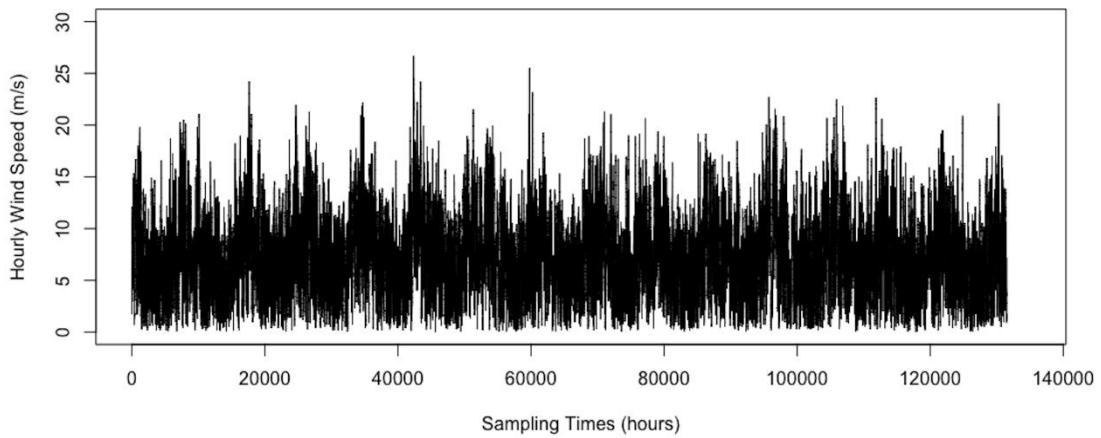


Figure 4.1: The time series from the MARINA Platform database (sub-Section 5.4) of sample period of 15 years for location L2 (52.05N 2.15E) in the North Sea. (Tsalis et al., 2021)
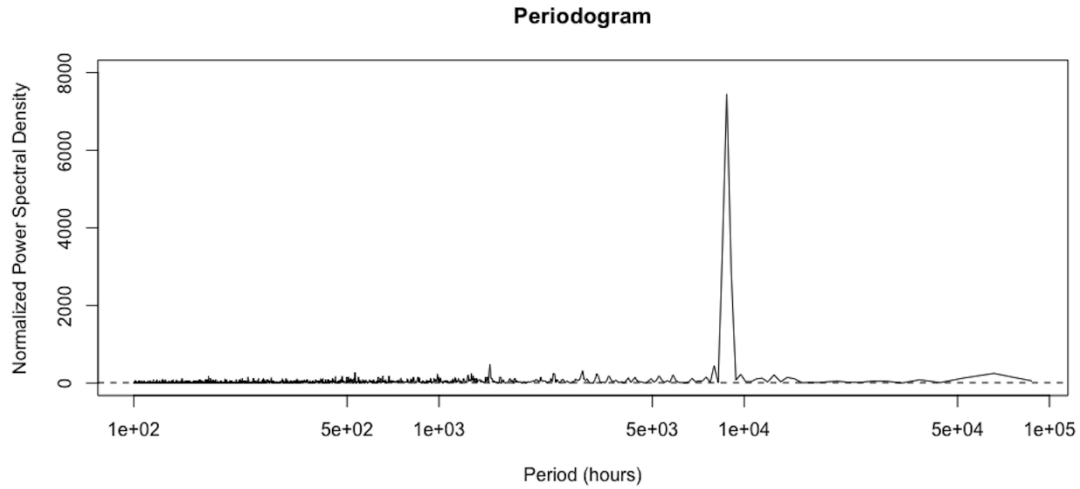
Figure 4.2: The Standard Periodogram of the equally spaced in time sample of 15 years for location L2 (52.05N 2.15E of the MARINA Platform database) in the North Sea. The choice of the periods is described in Scargle (1989) and set at 1 (hours) for the fundamental period $T_0 = T_{min} = 2\pi/\omega_{max}$. The maximum period is set at 262990 (hours) from $T_{max} = 2\pi/\omega_{min} = 2(t_{max} - t_{min})N/(N-1)$, where $(t_{max}, t_{min}, N)$ is the max, min observation times and the length of the hourly sample respectively. The peak is obtained at period 8766.3 (hours) and the number of frequencies-periods used is $ofac \cdot N$=2627 controlled by the oversampling factor (ofac=2). In addition, the significance level denoted from the dashed line is at 10.8438 (dB5) corresponding to false-alarm probabilities of alpha level=5%. Example of the Standard periodorgam (supplementary image of Tsalis et al., 2021) using the lsp package in R of Ruf, (1999).
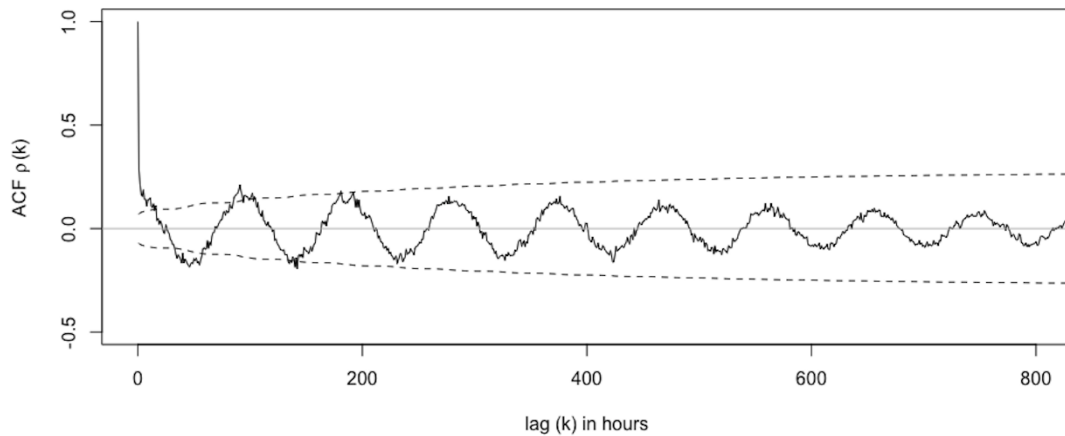


Figure 4.3: Example of the Correlogram of IFFT from the Periodogram of the regularly spaced in time sample of observations as a function of the lag time in hours for location L2 (52.05N 2.15E of the MARINA Platform database in the North Sea). The 95% confidence intervals in dashed line are obtained from the Generalized Bartlett's formula for ACF (see sub-Section 4.1.1). The Correlogram of the regularly sample is supplementary image of Tsalis et al., (2021) using the stats package in R of Venables and Ripley, (2002).

---

[5]dB=10log$_{10}$(measured PSD), PSD= Power Spectral Density

In the following section, we briefly present the principle of the Lomb-Scargle periodogram as the standard direct transorm method modeling irregular samples in time and the equivalence of the periodogram to harmonic least square fit.

## 4.2 Analysis of unequally spaced samples in time

A reasonable approximation of unequally spaced samples in time to the spectrum was presented initially in the work of (Lomb, 1976; Press et al., 1992) by fitting sine and cosine waves in a least-squares sense to the observed data and plotting the reduction in the sum of the residuals against a range of frequencies. This approximation is also known in the relevant literature as the equivalence to a harmonic least square fit (Lomb, 1976; Scargle, 1981). A Periodogram analysis equivalent to the Lomb method for handling unequally spaced data by similar techniques, was introduced by (Barning, 1963).

The least squares fit can be regarded as the natural extension of Fourier methods to non-uniform data. In the limit of equal spacing, the method reduces to the Fourier power spectrum. As a result, a maximum in the Periodogram is obtained at the same frequency where it minimizes the sum of squares of the residuals of the fit of sin and cosine signals to the data.

Specifically, denoting a signal model $x_{f_k}(t_n)$ as a discrete second-order stationary time series with zero mean at observation times $t_n$ and $n = 1,2,3,\ldots,N$, the signal model yields:

$$x_{f_k}(t_n) = A_k \sin[2\pi f_k(t_n - \tau)] + B_k \cos[2\pi f_k(t_n - \tau)]. \tag{4.11}$$

The amplitudes $A_k, B_k$ of the cos and sin signals are unknown but constant functions of $f_k$. The choice of the number $k$ of frequencies to be used is quite arbitrary but in general a finite-length time series will have meaning in a finite amount of statistically independent Fourier components.

A time delay $\tau$ is obtained in order to ensure time translation invariance. The latter invariance statement ensures that a constant shift of the sampling times $(t_n \rightarrow t_n + T)$, will not affect the approximation because such a shift will produce an identical shift in $(\tau \rightarrow \tau + T)$ and therefore $T$ will cancel out in the argument of equation $x_{f_k}(t_n)$, (Scargle, 1982).

From Lomb (1976) a useful formula is obtained for all values of $\tau$ as follows:

$$\sum_{n=1}^{N} \cos\big(2\pi f_k(t_n - \tau)\big) \cdot \sin\big(2\pi f_k(t_n - \tau)\big) = 0, \tag{4.12}$$

where the derivation of (4.12) provides the explicit formula of $\tau$,

$$\tau(\omega_k) = \frac{1}{2\omega_k} \tan^{-1}\left[\frac{\sum_{n=1}^{N} \sin(2\omega_k t_n)}{\sum_{n=1}^{N} \cos(2\omega_k t_n)}\right], \ \omega_\kappa = 2\pi f_k. \tag{4.13}$$

The least squares approach can be considered as a minimization of the sum of squares of the differences between the signal model $x_{f_k}(t_n)$ and the observed data $x(t_n)$, as follows:

$$E(f_k) = \sum_{n=1}^{N}\big[x(t_n) - x_{f_k}(t_n)\big]^2, \text{ with frequency} f_k, \ k = 1,2,3,\ldots,K. \tag{4.14}$$

From Horne and Baliunas (1986) it was proven that in the situation of an evenly spaced time series of length $N$, the number of independent frequencies in the range $\left[-f_{Nyq}, +f_{Nyq}\right]$ is $N$, where $f_{Nyq} = \frac{1}{2 \cdot \Delta t}$ denotes the Nyquist frequency according to the sampling Theorem 4.1 (e.g. see Bendat and Piersol, 1993) and is thus identical to a standard Fourier transformation.

For unevenly spaced time series, the Nyquist frequency cannot be defined, because the sampling theorem applies only to evenly spaced time series. In this situation, an average

Nyquist frequency, $average(f_{Nyq}) = \frac{1}{2 \cdot average(\Delta t)}$ , with $average(\Delta t)$ being the average sampling interval, can be used as an alternative. A conservative choice of the frequency range (Schulz and Stattegger 1997) is by setting $k$ as $f_k = average(f_{Nyq})$.

The minimum value of $E(f_k)$ as a function of frequency $f_k$ or $(E_{min}(f_k))$, is estimated using numerical or graphical technics. Defining the residual in the sum of squares as $\Delta E(f_k)$, the problem is stated as of estimating a frequency that maximizes $\Delta E(f_k)$, i.e.,

$$\Delta E(f_k) = \sum_{n=1}^{N} [x(t_n)]^2 - E_{min}(f_k). \tag{4.15}$$

The useful formula maximizing the residuals in the sum of squares is presented as follows:

$$\Delta E(f_k) = \frac{\left[\sum_{n=1}^{N} x(t_n) \cdot \cos(2\pi f_k(t_n - \tau))\right]^2}{\sum_{n=1}^{N} \cos^2(2\pi f_k(t_n - \tau))} + \frac{\left[\sum_{n=1}^{N} x(t_n) \cdot \sin(2\pi f_k(t_n - \tau))\right]^2}{\sum_{n=1}^{N} \sin^2(2\pi f_k(t_n - \tau))}, \tag{4.16}$$

where for evenly space sampling the time delay $\tau$ is considered to be zero $\tau = 0$.

## 4.2.1 Power Spectrum estimation (Lomb-Scargle Periodogram)

The Lomb-Scargle method proposed by Scargle (1982, 1989) focuses on the construction of a Fourier spectrum which is used for the inverse Fourier transform from the frequency domain back to the time domain. The flow chart of the data analysis for reconstruction of the irregular sample is illustrated in Figure 4.4.
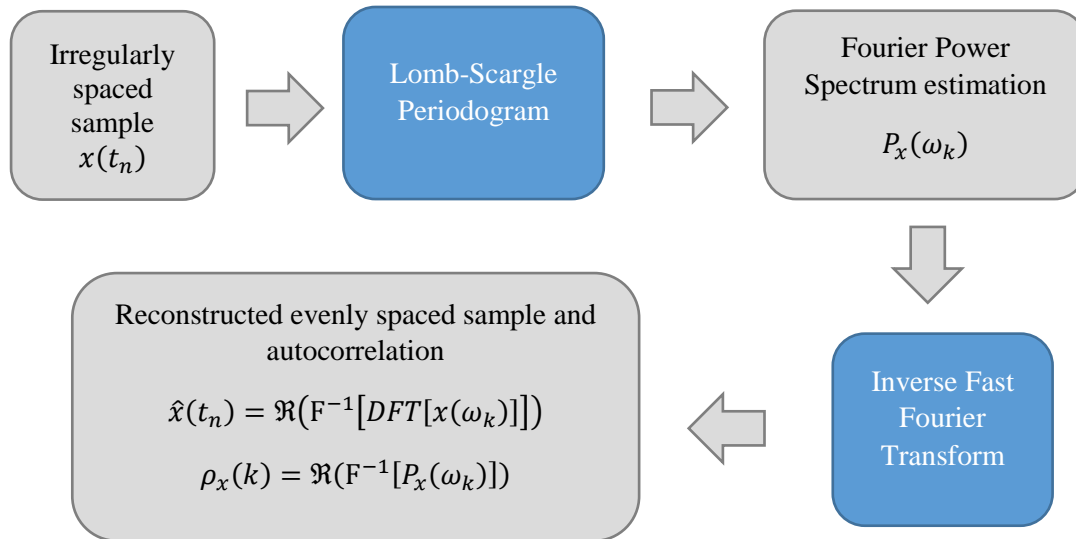
Figure 4.4. Flow chart of the reconstruction method: The Lomb-Scargle periodogram is used to estimate the Fourier Power Spectrum of an irregular sample from the time to the frequency domain. The real part of the inverse fast Fourier transform of the Power Spectrum back to the time domain provides the autocorrelation function for the equally spaced in time reconstructed sample. (Supplementary chart of Tsalis et al., (2019))

Specifically, this method introduced a discrete Fourier transformation (DFT) that can be applied to evenly and unevenly spaced time series. The generalization of the Discrete Fourier

Transform for the observed data $x(t_n)$ as a discrete, second-order stationary time series, with zero mean, obtained at observation times $t_n$, $n = 1,2,3,\ldots,N$ is formed as follows:

$$DFT[x(\omega_k)] =$$
$$= F_0(\omega_k) \cdot \sum_{n=1}^{N}\left(A(\omega_k)x(t_n)\cos[\omega_k(t_n - \tau(\omega_\kappa))] + iB(\omega_k)x(t_n)\sin[\omega_k(t_n - \tau(\omega_\kappa))]\right)$$

(4.17)

Coefficients $A(\omega_k), B(\omega_k)$ in (4.17) depend on frequency $\omega_k$ and not on the data $t_n$ in the same context as previously stated in (4.11). It is analytically proven that $A(\omega_k), B(\omega_k)$ yield as follows:

$$A(\omega_k) = \left[\sum_{n=1}^{N}\cos^2[\omega_k(t_n - \tau(\omega_\kappa))]\right]^{-1/2} \text{ and}$$

$$B(\omega_k) = \left[\sum_{n=1}^{N}\sin^2[\omega_k(t_n - \tau(\omega_\kappa))]\right]^{-1/2}.$$

The choice of the $k$ number of frequencies to be used $\omega_k = 2\pi f_k$, $k = 1,2,3,\ldots,K$ is quite arbitrary but in general $K > N$ (Scargle, 1982; Schulz and Stattegger, 1997). Specifically, the choice of $K$ depends on the number of independent frequencies $N_0$ (Press et al., 2007). Horne and Baliunas (1986) proved a relationship between $K$ and $N_0$ performing extensive Monte Carlo simulations. In their study, they provided a simple formula to estimate the number of independent frequencies $N_0$ from the number of observations $N$ in a time series, as $N_0 \approx 6.362 + 1.193N + 0.00098N^2$. This empirical deterministic formula is suitable for most problems, considering henceforth $K = N_0$.

$F_0(\omega_k)$ in (4.17) is defined as follows:

$$F_0(\omega_k) = \sqrt{\frac{N}{2}}\exp(-i\omega_k t^*),$$

(4.18)

where $t^*$ functional is $t^* = -\tau(\omega_k)$ and

$$\tau(\omega_k) = \frac{1}{2\omega_k}\tan^{-1}\left[\frac{\sum_{n=1}^{N}\sin(2\omega_k t_n)}{\sum_{n=1}^{N}\cos(2\omega_k t_n)}\right],$$

(4.19)

is considered as the time delay. The expression stated in the tangent in (4.19) ensures time translation invariance in the same context as stated for the explicit formula of $\tau$ obtained in (4.13). For evenly space sampling, $\tau(\omega_k)$ is considered to be zero (i.e., $\tau(\omega_k) = 0$).

For univariate spectral analysis, the generalized formula for the Lomb–Scargle periodogram of the Discrete Fourier Transform yields as a normalized expression (Press and Rybicki 1989),

$$P_x(\omega_k) = \frac{1}{N}|DFT[x(\omega_k)]|^2$$
$$= \frac{[A(\omega_k)]^2}{2}\left[\sum_{n=1}^{N}(x(t_n) - \bar{x})\cos[\omega_k(t_n - \tau(\omega_\kappa))]\right]^2 + \frac{[B(\omega_k)]^2}{2}\left[\sum_{n=1}^{N}(x(t_n) - \bar{x})\sin[\omega_k(t_n - \tau(\omega_\kappa))]\right]^2,$$

or,

$$P_x(\omega_k) = \frac{1}{2\sigma^2}\left(\frac{\left[\sum_{n=1}^{N}(x(t_n)-\bar{x})\cos[\omega_k(t_n-\tau(\omega_\kappa))]\right]^2}{\sum_{n=1}^{N}\cos^2[\omega_k(t_n-\tau(\omega_\kappa))]} + \frac{\left[\sum_{n=1}^{N}(x(t_n)-\bar{x})\sin[\omega_k(t_n-\tau(\omega_\kappa))]\right]^2}{\sum_{n=1}^{N}\sin^2[\omega_k(t_n-\tau(\omega_\kappa))]}\right),$$

(4.20)

where $\bar{x}$ and $\sigma^2$ refer correspondingly to the sample mean and sample variance.

Suumarizing the Lomb-Scargle Periodogram approximation to the equivalence of a harmonic least square fit, a maximum in the periodogram of (4.20) is obtained at the same

frequency where it maximizes the sum of squares of the residuals in (4.15) or (4.16) of the fit of sine and cosine signals to the data.

At this point it is important to outline that various authors have proposed modifications in the sums of the Lomp-Scargle Periodogram, (Reegen, 2007), (Cumming et al., 1999) resulting inability to account for statistical fluctuations in the mean of the sampled sinusoids. In addition, there is no theoreticaly procedure for testing the significance of the Periodogram peaks, Schwarzenberg-Czerny (1998), Vio et al. (2000), Koen (2006), Stoica et al. (2009). Furthermore, the significant bias in the spectrum does not diminish with the sample size Broersen et al. (2004 a, b). Summarizing, the LS periodogram as an estimator of the spectrum is characterized as

(i)     statistically inconsistent (i.e., its variance does not go to zero as infinite data are collected),
(ii)    biased for finite samples, and
(iii)   suffers from spectral leakage.

These issues from a statistical standpoint will bias the aucorrelation estimate when standard inverse Fourier Transform is applied. While the standard LS periodogram in geoscience studies remains the common approach for characterizing the properties of unevenly samples in time (e.g., to compute periodicity of unequally spaced data), many authors question this approach e.g. (Springford et al. 2020; VanderPlas, 2018; and Hocke and Kämpfer, 2008). Due to the significant drawbacks regarding Periodogram analysis, we therefore do not employ this approach in the case of uneven sampling. However, an example of the Lomb-Scargle Periodogram of the irregularly DeCA sample is illustrated in the following section for inference. Finally, there are a number of alternative methods available for spectral analysis of unevenly spaced data, where references are found from the work of Roberts et al. (1987) with the CLEAN method and Schulz and Stattegger (1997) with the SPECTRUM method.

## 4.2.2 Example of the inverse Fast Fourier Transform for samples irregularly spaced in time

As an example of the Lomp-Scargle periodogram, the hourly time series from the MARINA Platform database of sample period of 15 years for location L2 in the North Sea given in Figure 4.1, is first de-clustered from the DeCA model to the irregularly sample illustrated in Figure 4.5.
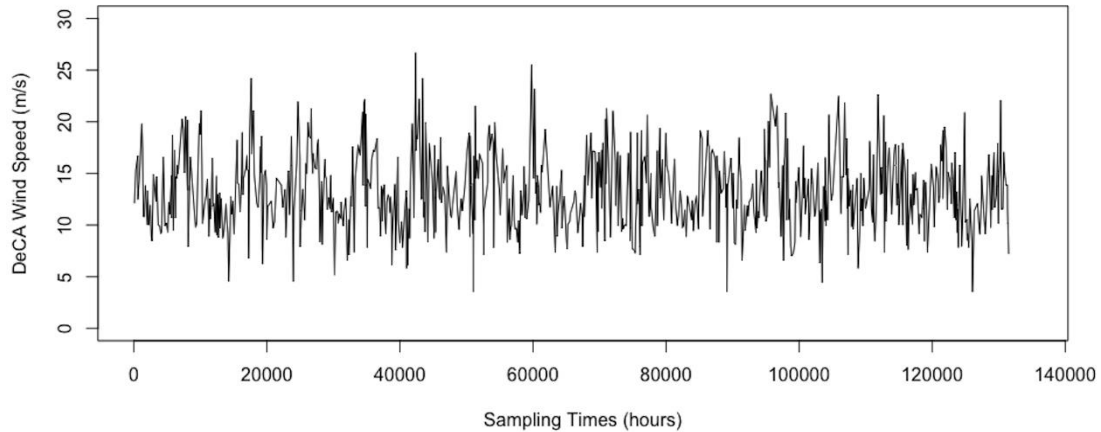
Figure 4.5: The sample of observations irregularly spaced in time considering the sample period of 15 years at location L2 (52.05N 2.15E of the MARINA Platform database). The de-clustering procedure is performed from the DeCA model setting the optima DEP level at 65% in order to safely separate approximately independent events. (Tsalis et al., 2021)

In the following Figure 4.6 the Lomb-Scargle Periodogram is illustrated in the frequency domain, considering the irregularly DeCA sample of Figure 4.5. In addition, Figure 4.7 illustrates the ACF of the reconstructed evenly sample in the time domain as the inverse FFT of the spectrum from the Lomb-Scargle Periodogram.
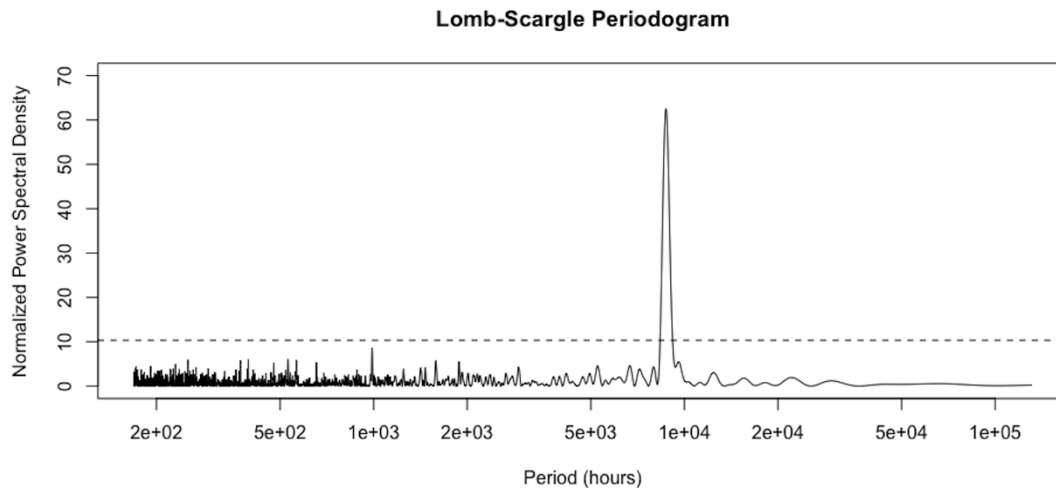


Figure 4.6: The Lomb-Scargle Periodogram considering the DeCA sample of Figure 4.5. The choice of the periods is described in Scargle (1989) and set at 169.12 (hours) for the fundamental period $T_0 = T_{min} = 2\pi/\omega_{max} = \overline{\Delta t}$, where $\overline{\Delta t} = \frac{1}{N}\sum_{i=1}^{N-1}(t_{i+1} - t_i)$ is the mean sampling time interval of the DeCA sample used. The maximum period is set at 131401 (hours) from $T_{max} = 2\pi/\omega_{min} = 2(t_{max} - t_{min})N/(N-1)$, where $(t_{max}, t_{min}, N)$ is the max, min observation times and the length of the DeCA sample respectively. The peak is obtained at period 8731 (hours) and the number of frequencies-periods used is $ofac \cdot N$=15520 controlled by the oversampling factor (ofac=20). In addition, the significance level denoted from the dashed line is at 10.31751 (dB) corresponding to false-alarm probabilities of alpha level=5%. Example of the Lomp-Scargle Periodorgam (supplementary image of Tsalis et al., 2021) using the lsp package in R of Ruf, (1999).

57
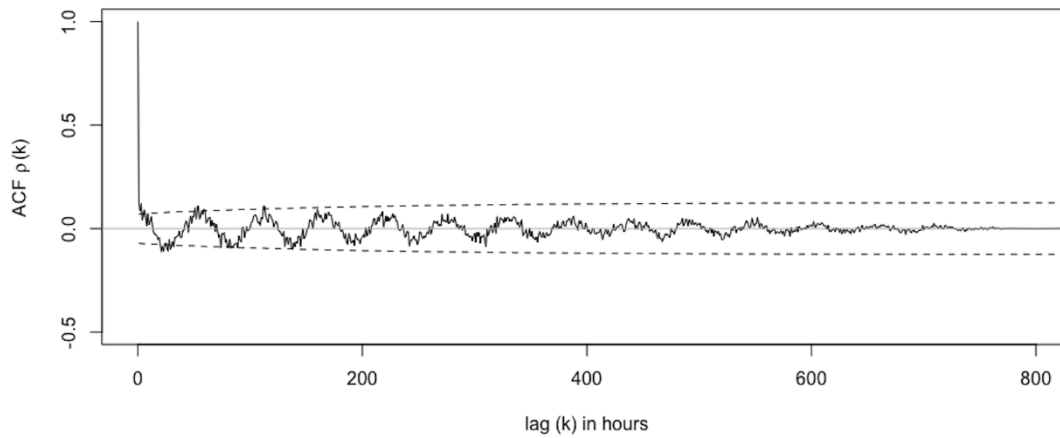
Figure 4.7: Example of the Correlogram of the irregular DeCA sample obtained from the inverted FFT of the Spectrum from the Lomp-Scargle Periodogram as a function of the lag time in hours for location L2 (52.05N 2.15E of the MARINA Platform database). The 95% confidence intervals are obtained from Generalized Bartlett's formula for ACF. The Correlogram of the irreregularly sample is supplementary image of Tsalis et al., (2021) using the stats package in R of Venables and Ripley, (2002).

## 4.2.3 Interpolation methods

The Interpolation methods consider that the irregularly sampled time series is to be resampled onto a common regular time grid with constant time increments. The grid spacing is defined as the mean sampling time intervals of the total time series. One of the most popular resampling methods considered as interpolation techniques, is the *nearest neighbor technique*, where the (ACF) is approximated at the desired grid points by the value of the observation closest in time. After resampling, standard (ACF) can be employed. This approach revealed important results such as to a significant shifting bias Broersen (2009), we therefore do not employ in the case of uneven sampling.

## 4.3 Slotting method

For irregular time series the inter-sampling times vary, and the standard ACF cannot be directly applied (Chatfield, 1996). Generalizing the regular correlation operator through a rectangular or Non-rectangular Kernel function, is commonly called Slotting or Slotting Autocorrelation approach.

In order to analyze the irregular samples spaced in time, Edelson and Krolik (1988) and Mayo (1993) considered estimating the pair products of all available observations and discretizing them into bins according to their sampling time differences. In this study, the estimator of ACF for irregular samples of $N$ number of observations is derived as the weighted mean over all available products according to their sampling time differences and desired time lag for which the correlation is estimated (replacing the sample autocovariance), divided by the sample variance of the irregular process for zero time lag and is presented as:

$$\rho_x(k) = \frac{Cov(k)}{\sigma_x^2} = \frac{\sum_{i=1}^{N}\sum_{j=1}^{N} x_i x_j \, b_h(k; t_j - t_i, h)}{\sum_{i=1}^{N}\sum_{j=1}^{N} b_h(k; t_j - t_i, h)} \Big/ \frac{\sum_{i=1}^{N}\sum_{j=1}^{N} x_i x_j b_h(0; t_j - t_i, h)}{\sum_{i=1}^{N}\sum_{j=1}^{N} b_h(0; t_j - t_i, h)}. \quad (4.21)$$

The observations $x$ with indexes $i,j$ in Equation (4.21) hereafter are considered as centralized and standardized values. In addition, the associated discrete time variables for these observations are re-scaled as a transformation from the observed $t^{obs}$ to the $t = t^{obs}/\overline{\Delta t}$ for each $i,j$ respectively, where $\overline{\Delta t} = \frac{1}{N}\sum_{i=1}^{N-1}(t_{i+1} - t_i)$ is the mean sampling time interval. Accordingly, the lag number of $k$ is also dimensionless considering the re-scaled $k$=lag$(k)/\overline{\Delta t}$ for which the ACF is estimated.

The weighting function $b_h$ used in Equation (4.21) is generally referred to as the Kernel estimator for the inter-sampling time intervals $t_j - t_i$. The estimator $b_h$ was introduced by de Oliveira (1963) and Nadaraya (1964) and is provided as follows:

$$b_h(k; t_j - t_i, h) = \frac{1}{h} K\left(\frac{k - (t_j - t_i)}{h}\right), \quad (4.22)$$

where $K$ is the Kernel that determines the shape of the weighting function (rectangular, triangle, Gaussian, etc.) which is symmetrical placed around $t_j - t_i$, and positive on the interval $[t_j - t_i - h, t_j - t_i + h]$. The parameter $h$ is defined as the bandwidth or smoothing parameter, which determines the width of the weighting function and adjusts the amount of smoothing applied over the inter-sampling time intervals. Hence, the Kernel estimate of the unknown density $f(k)$ is approximated by

$$\hat{f}_h(k) = \frac{1}{N^2} \sum_{i=1}^{N} \sum_{j=1}^{N} b_h(k; t_j - t_i, h), \quad (4.23)$$

where $N^2$ in (4.23) is the number of the weights used for the inter-sampling time intervals. Moreover, isolated peak estimates are derived for $h \to 0$, where $h \in (0, \infty)$. The Kronecker Delta function denoted as $\delta$ is the approximation to the asymptotic limit $\lim_{h\to 0} K(k; t_j - t_i, h) = \delta(k - (t_j - t_i))$. In general, any function having the following properties can be used as a Kernel estimator:

(i)  $K$ is considered as a pdf with $K(u) \geq 0$ and $\int_{-\infty}^{+\infty} K(u)du = 1$,
(ii)  $K$ is symmetric around zero $K(u) = K(-u)$,
(iii)  $K(u) = 0$ considering $|u| > 1$,
(iv)  $\int_{-\infty}^{+\infty} uK(u)du = 0$,
(v)  finite second moment $\int_{-\infty}^{+\infty} u^2 K(u)du < \infty$.

The disadvantage of the kernel estimators arises when suggesting the required valuable shape function $K$ and bandwidth $h$ parameter in order to optimize the properties of the estimator; see e.g.(Bean and Tsokos, 1980),(Silverman, 1986),(Marron, 1988), (Wand and Jones, 1994), (Simonoff, 1996), and (Scott, 1992). The most popular kernel in practice is the Gaussian kernel due to its analytic properties. In addition, the optimum bandwidth $h_{opt}$ is not guided by mathematical considerations e.g., (Babu and Feigelson, 1996) and Hall et al. (2004). There is a vast amount of literature suggesting practical optimal bandwidth methods for Kernel estimation, derived by the minimization of the distance between the unknown density function

$f(k)$ and the estimator $\hat{f}_h(k)$. The measure of distance is guided by the Asymptotic Mean Integrated Squared Error (AMISE) type criteria:

$$AMISE(\hat{f}_h) = E\left\{\int \left(\hat{f}_h(u) - f(u)\right)^2 du\right\} \tag{4.24}$$

suggesting an integrability assumption on the unknown function $f(u)$, and by the Integrated Squared Error (ISE) type criteria

$$ISE(\hat{f}_h) = \int \left(\hat{f}_h(u) - f(u)\right)^2 du. \tag{4.25}$$

The most well known methods of bandwidth selection using the above measures are summarized:

**1**. Rule-based methods. These methods are commonly referred as *Rule of thumb* and *Maximal Smoothing Principal,* based by means of the (AMISE) type criteria. They replace the unknown density function $f(u)$ by a reference distribution function, rescaling to variance equal to sample variance $\hat{\sigma}^2$, pointing out $h_{opt}$ bandwidth formula. Considering the usual Gaussian distribution as reference function, it is determined for The *Rule of thumb* (Silverman, 1986):

$$h(aMISE)_{opt} = 1.06\hat{\sigma}n^{-1/5}, \tag{4.26}$$

and accordingly for The *Maximal Smoothing Principal* by (Terrell, 1990)

$$h(AMISE)_{opt} = 1.144\hat{\sigma}n^{-1/5} \tag{4.27}$$

under the requirements $h(n) \to 0$ asymptotically at a very slow rate with the increase of observations $n \to \infty$, and $nh(n) \to \infty$. The major drawback of both approaches is that they provide over-smooth density estimates, (Park and Turlach, 1992).

**2**. A data-driven approach. Other most common numerical approaches dealing with bandwidth selection, are referred as *Least Square Cross-Validation* (*LSCV*) developed by (Rudemo, 1982) and later from (Bowman, 1984),following the *Biased Cross Validation* (*BCV*) in (Scott and Terrell, 1987). Estimates based by means of the (ISE) type criteria are derived by the(*LSCV*), while (*BCV*) employs the (AMISE) criteria. The major drawback of these approaches is a slow relative rate of convergence to the optimal bandwidth of order$n^{-1/10}$, obtaining estimates of high variability. In addition, both approaches may provide multiple minima, less often observed in (*BCV*) rather than for (*LSCV*) e.g.,(Hall and Marron, 1991) and (Jones et al., 1996). As a result, *Cross Validation* (*CV*) approaches lead to bandwidth selection that provide under-smooth density estimates (Simonoff, 1996).

**3.** Plug-in methods. These approaches mitigate the problem of (*CV*) methods regarding slow convergence to the optimal bandwidth. The Plug-in consideration, replaces the unknown functional of second derivative continuous and square integrable in the (AMISE) type criteria, with a suitable estimate, resulting faster convergence (Woodroofe, 1970). Suitable estimates of this approach may be found in *Park-Marron Plug-in*, (Park and Marron, 1990), resulting to a rate of order $n^{-4/13}$ and in *Sheather-Jones Plug-in* (Sheatherand Jones, 1991), with a rate of order $n^{-5/14}$.

The major drawback of this measure of distance is over and under smooth density estimates (Jones et al., 1996; Simonoff, 1996). Therefore, in our study for the weighting

function as defined in Eq. (4.22), we considered the usual Gaussian distribution as the Kernel function and for the bandwidth selection we did not restrict our analysis to a single optima. On the contrary, we examined the performance of the irregular ACF estimator as stated previously in Eq. (4.21) against a range of possible bandwidths recommended by Sheather (2004).

## 4.3.1 Statistical properties of Kernel estimators

A Java applet that allows a practitioner to obtain the effects of changing the bandwidth and the shape of the kernel function on the resulting density estimate can be found at *http://www-users.york.ac.uk/~jb35/mygr2.htm*. It is well known that the value of the bandwidth is of critical importance, while the shape of the kernel function has little practical impact. Assuming that the underlying density is sufficiently smooth and that the Kernel has finite fourth moment, the expected value, bias and variance of the $\hat{f}(x)$ is shown respectively using Taylor series from Wand and Jones (1994, Ch. 2).

1. Expected value of $\hat{f}(x)$

$$E\big[\hat{f}(x)\big] = f(x) + \frac{1}{2}h^2 f''(x)\int_{-\infty}^{+\infty} z^2 K(z)dz + 0(h^2), \tag{4.28}$$

2. Bias of $\hat{f}(x)$

$$Bias\left(\hat{f}(x)\right) = E\big[\hat{f}(x)\big] - f(x) = \frac{1}{2}h^2 f''(x)\int_{-\infty}^{+\infty} z^2 K(z)dz + 0(h^2), \text{ and} \tag{4.29}$$

3. Variance of $\hat{f}(x)$

$$Var\big[\hat{f}(x)\big] \simeq f(x)\frac{1}{nh}\int_{-\infty}^{+\infty}(K(z))^2 dz + 0\left(\frac{1}{nh}\right). \tag{4.30}$$

The Mean Squared Error (MSE) and Mean Integrated Squared Error (MISE) are the standard measures serving as criteria for bandwidth selection and efficiency of estimation performance. Specifically, using the combinations of the latter expressions stated in Equations (4.28), (4.29) and (4.30) (see proof in Appendix G), it is defined:

$$\begin{aligned}MSE\left(\hat{f}(x)\right) &= Var\left(\hat{f}(x)\right) + \left(Bias\left(\hat{f}(x)\right)\right)^2 \\ &= \frac{1}{nh}f(x)\int_{-\infty}^{+\infty}(K(z))^2 dz + \frac{1}{4}h^4(f''(x))^2\left(\int_{-\infty}^{+\infty} z^2 K(z)dz\right)^2,\end{aligned} \tag{4.31}$$

and

$$MISE\left(\hat{f}(x)\right) = E\left[\int_{-\infty}^{+\infty}\left(\hat{f}(x) - f(x)\right)^2 dx\right] = \int_{-\infty}^{+\infty} E\left[\left(\hat{f}(x) - f(x)\right)^2\right] dx,$$

or,

$$MISE\left(\hat{f}(x)\right) = \int_{-\infty}^{+\infty} MSE\left(\hat{f}(x)\right) dx. [6] \tag{4.32}$$

Substituting (4.31) in (4.32), yields

$$MISE\left(\hat{f}(x)\right) = \frac{1}{nh}\int_{-\infty}^{+\infty}(K(z))^2 dz + \frac{1}{4}h^4\left(\int_{-\infty}^{+\infty} z^2 K(z)dz\right)^2 \cdot \int_{-\infty}^{+\infty}(f''(x))^2 dx.$$

$$\tag{4.33}$$

---

[6] $MISE\left(\hat{f}(x)\right) = \int_{-\infty}^{+\infty} Var\left(\hat{f}(x)\right) dx + \int_{-\infty}^{+\infty}\left(Bias\left(\hat{f}(x)\right)\right)^2 dx.$

The true density $f(x)$ must have its second derivative $f''(x)$ continuous and square integrable. Selecting small bandwidth $h$ reduces the $Bias\left(\hat{f}(x)\right)$ in (4.29) but increases the $Var\left(\hat{f}(x)\right)$ in (4.30). The standard selection for optimum bandwidth is derived by minimizing the $MISE$ measure in (4.33) as follow:

$\frac{\partial MISE\left(\hat{f}(x)\right)}{\partial h} = 0$, deriving

$$h^3\left(\int_{-\infty}^{+\infty} z^2 K(z)dz\right)^2 \cdot \int_{-\infty}^{+\infty}\left(f''(x)\right)^2 dx - \frac{1}{nh^2}\int_{-\infty}^{+\infty}\left(K(z)\right)^2 dz = 0, \text{ and}$$

$$h_{opt} = \frac{\left(\int_{-\infty}^{+\infty}\left(K(z)\right)^2 dz\right)^{1/5} \cdot n^{-1/5}}{\left(\int_{-\infty}^{+\infty} z^2 K(z)dz\right)^{2/5} \cdot \left(\int_{-\infty}^{+\infty}\left(f''(x)\right)^2 dx\right)^{1/5}}. \tag{4.34}$$

Substituting the optimum bandwidth in (4.34) into (4.33) for the $MISE$ of $\hat{f}(x)$, yields the minimum value expression,

$$MISE\left(\hat{f}(x)\right)_{opt} = \frac{5n^{-4/5}}{4}\left(\int_{-\infty}^{+\infty} z^2 K(z)dz\right)^{2/5}\left(\int_{-\infty}^{+\infty}\left(K(z)\right)^2 dz\right)^{4/5}\left(\int_{-\infty}^{+\infty}\left(f''(x)\right)^2 dx\right)^{1/5}. \tag{4.35}$$

The expression found in (4.35) is intractable and not applicable in practice. It has been found that Kernel function that minimizes $MISE$, as initially presented by Epanechnikov in (1969), has the following form

$$K(z) = \begin{cases} \frac{3}{4\sqrt{5}}\left(1 - \frac{1}{5}z^2\right) & \text{for } |z| < \sqrt{5} \\ 0 & otherwise \end{cases} \tag{4.36}$$

Efficiency of any Kernel function is considered by comparing it with the Epanechnikov Kernel as follow:

$$efficiency(K) = \left(\frac{MISE\left(\hat{f}(x)\right)_{opt}^{Epanechnicov}}{MISE\left(\hat{f}(x)\right)_{opt}^{other\ Kernel}}\right)^{5/4} = \frac{3}{5\sqrt{5}\sqrt{\left(\int_{-\infty}^{+\infty} z^2 K(z)dz\right)\cdot\left(\int_{-\infty}^{+\infty}\left(K(z)\right)^2 dz\right)}}, |z| < 5. \tag{4.37}$$

Efficiency measure as expressed in relation (4.37) provides a measure to compare different symmetric Kernels with the Epanechnikov Kernel. For any other symmetric Kernel the closer the efficiency to one, the smaller is the $MISE$ type criteria.

Table 4.1: Kernel estimators and their efficiencies.

| Kernels | $K(z)$ | Efficiency |
|---|---|---|
| Epanechnikov | $\begin{cases} \frac{3}{4\sqrt{5}}\left(1 - \frac{1}{5}z^2\right) & \text{for } |z| \leq \sqrt{5} \\ 0 & otherwise \end{cases}$ | 1 |
| Biweight | $\begin{cases} \frac{15}{16}(1 - z^2)^2 & \text{for } |z| \leq 1 \\ 0 & otherwise \end{cases}$ | 0.9939 |

| | | |
|---|---|---|
| Triangular | $\begin{cases} 1 - \lvert z \rvert & \text{for } \lvert z \rvert \leq 1 \\ 0 & otherwise \end{cases}$ | 0.9859 |
| Gaussian | $\dfrac{1}{\sqrt{2\pi}} \cdot e^{-z^2/2}$ | 0.9512 |
| Rectangular | $\begin{cases} 1/2 & \text{for } \lvert z \rvert \leq 1 \\ 0 & otherwise \end{cases}$ | 0.9295 |

The choice of Kernel type is not so significant. The latter Table 4.1 shows that there is a very little difference between the various Kernels on being used from (4.35) at $MISE\left(\hat{f}(x)\right)_{opt}$ calculations. The most frequently used Kernel is the Gaussian Kernel and has efficiency approximately 95%. Therefore the choice of Kernel type is based on other considerations, such as computational expense.
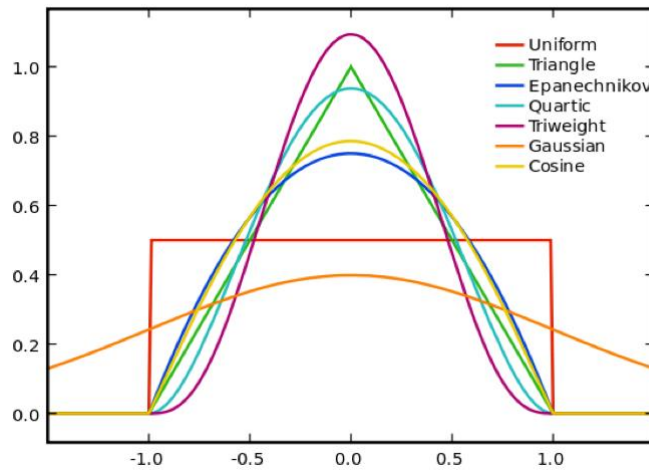


Figure 4.8: The most commonly used Kernel based estimators (Amberg, 2008)

## 4.3.2 Rectangular Kernel slotting

The Slotting method from Edelson and Krolik (1988) applied rectangular Kernel function in order to bin the observations into discrete sets, considering discontinuousness in time. In this case the weighting function selects the products whose time lag is not further than half the bin width from the given time lag $(k)$, taking the following form:

$$b_h\big(k; t_j - t_i, h\big) = \begin{cases} 1 & \text{for } \big\lvert \lvert (t_j - t_i) \rvert - k \big\rvert < 1/2, \\ 0 & \text{otherwise}, \end{cases} \tag{4.38}$$

where the lag bin width in their study is set equal to the mean sampling time interval.

The disadvantage of this technique is that it yields a high variance of the ACF estimator, excluding a significant number of products accounting to a particular time lag, (Benedict et al., 2000; Babu and Stoica, 2010). In order to increase the valuable pairs to be averaged into the sample autocovariance in ACF in Equation (4.21), the Non Rectangular slotting approach is introduced, considering a certain approximation of the distribution of the inter-sampling times.

Examples of other slotting approaches such as *slot boundaries*, *local normalization*, *fuzzy slotting* and *variable windowing*, can be found in (Nobach, 2002), (van Mannen et al., 1999), and (Damaschke et al., 2018).

### 4.3.3 Non-rectangular Kernel

In the Slotting method used for this study, the inter-sampling time intervals will not be binned into discrete sets by a rectangular Kernel. Instead, weighting the products by applying a non-rectangular Gaussian Kernel weight function will increase the valuable pairs to be averaged into the irregular ACF in Equation (4.21). In this way, a sudden cutoff in the time domain is prevented, weighting the products smoothly according to the difference between the inter-sampling time interval $t_j - t_i$ and the considered time lag ($k$). The Gaussian Kernel density function tends to zero for time differences much larger or smaller than the considered time lag ($k$) (Hall et al.,1994; Bjornstad and Falck, 2001), and is defined as follows:

$$b_h\left(k; t_j - t_i, h\right) = \left\{ \frac{1}{h\sqrt{2\pi}} \exp\left( -\frac{\left|k - (t_j - t_i)\right|^2}{2h^2} \right), \quad h = C\Delta\tau. \right. \tag{4.39}$$

However, there is no theoretical definition of the effective width of the weight functions. The Gaussian Kernel used in this study considers the standard width parameter $h$ to be scaled to the mean sampling time intervals, i.e. $\Delta\tau = \overline{\Delta t} = \frac{1}{N}\sum_{i=1}^{N-1}(t_{i+1} - t_i)$ in order to adjust the effective width of the weight function satisfactorily to the mean width of the time intervals. In this way, it is ensured that observations appearing at an almost constant frequency are rated higher than infrequent observations. In addition, parameter $C$ is defined as the normalized bandwidth. For accurate estimations the degree of smoothing is of great importance. Selection of a large bandwidth will result in an over-smoothed performance of the density function while a small value will under-smooth the estimation. Examinations on Asian monsoon records from Rehfeld et al. (2011), revealed empirical normalized bandwidth at $C = 0.25$. In our analysis we considered the range $C \in [0.125, 1]$ with a 0.125 step, in order to optimize the irregular ACF estimator in Equation (4.21) as defined in the Slotting method. In the following sub-Sections the DeCAUn model will be described in detail.

## 4.4 DeCAUn model

In this section, a re-sampling strategy is analytically presented to alleviate the effect of dependency in samples of irregularly observations (demonstrated at the 11th international conference on Extreme Value Analysis, Zagreb 2019). The proposed DeCA Uncorrelated (DeCAUn) model performs re-sampling taking into account the correlation effect in the irregular samples of DeCA for a range of discrete energy reduction levels in the samples. In addition, the proposed model analyzes the correlation effect obtained in the irregular samples using the Gaussian Kernel weight function for the computation of the generalize Pearson correlation operator from the Slotting method.

The DeCAUn model also examines the response of the Kernel function used over a range of smoothing parameters or bandwidth, enhancing the performance of the Gaussian function as a weight function over the irregular samples of observations. At this point it is outlined that the DeCAUn model used the Slotting method and not the Lomb-Scargle periodogram for the analysis of the correlation effect of the irregular samples as previously discussed.

The proposed model requires two subjective admissions for its successful statistical application. These admissions that consist the main objectives of the evaluation of the DeCAUn model are:

1. The favorably bound estimation of the energy-reduction level, and
2. the optimal bandwidth smoothing response of the weight function to the irregularly spaced observations in time.

The response of the DeCAUn model in applications considering a limited availability in data is the key factor in this work. Therefore, the assessment is carried out for relatively small datasets of annual wind speed time series, corresponding to four sample periods of 10, 15, 20 and 25 years long. In the following sub-Section, the irregular samples to be fit are defined. In addition, the Irregular modeling procedure of DeCAUn is presented in steps, considering all DEP and bandwidth values.

## 4.4.1 Proposed Methodology for re-sampling

The samples of DeCA at the associated DEP levels required further investigation in terms of correlation. Re-sampling is advised when the condition of independence is violated (Miquel, 1984; Lang et al., 1999). In this assessment, two re-sampling scheme strategies for the samples of DeCA are proposed and denoted as DeCAUn.1 and DeCAUn.2 respectively. The re-sampling scheme DeCAUn.1 is formed as follows:

(i)     Selecting the maximum value of the corresponding DeCA sample,
(ii)    identifying and selecting the following lag($k$)-apart values of the remaining data from both sides of the value chosen in (i) until all available values are considered.

The re-sampled DeCAUn.2 is closely related to the concept of the SSL, (Soares and Scotto, 2004). The DeCAUn.2 scheme consists of the following steps:

(i)     Identifying and selecting the largest value of the correspondent DeCA sample,
(ii)    Discarding values with a lag($k$)-apart from both sides of the value chosen in (i),
(iii)   Selecting the next largest value of the remaining data and finally,
(iv)    Repeat steps (ii) and (iii) until all data are used.

At this point, the lag (k)-apart value for re-sampling is difficult to estimate. It is the required minimum value between successive irregular maxima of DeCA clusters, which renders the maxima statistically independent. The desired lag(k) is obtained from the estimator algorithm of ACF for different time lags. The latter algorithm is defined as SIMILARITY (Rehfeld and Kurths, 2014) providing estimates for the irregular ACF in Eq. (4.21) using the non-rectangular Gaussian Kernel (gXCF) in Equation (4.39). In this way, the products $x_i x_j$ of the irregular ACF estimator are weighted according to their difference between the product inter-sampling time interval $t_j - t_i$ and the associated time lag ($k$) for the samples of DeCA.

The desired lag($k$)-apart value is derived as a time lag transformation from the correlogram. It is set as the value of $k$ observations obtained from the transformation of the first time lag entering the confidence bounds (i.e., roughly 1 in 20 of the successive $\rho_x(k)$ to have absolute value greater than 95% CI of zero autocorrelation) described by the Generalized Bartlett's formula in sub-Section 4.1.1. Example of the autocorrelation from the SIMILARITY algorithm is illustrated in Figure 4.9.
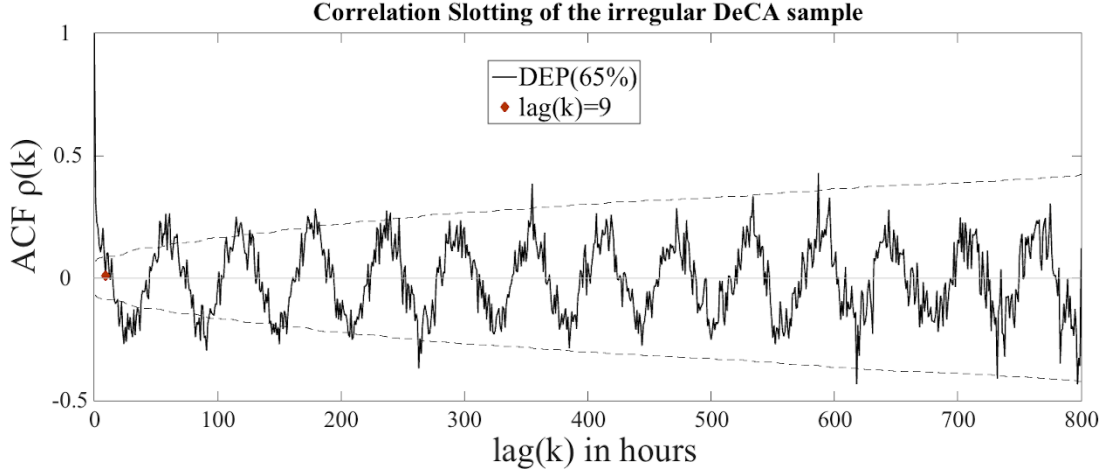
Figure 4.9: Example of the autocorrelation from SIMILARITY as a function of the time lag ($k$) for the irregularly DeCA sample. The correlation Slotting method uses the Gaussian Kernel and the 95% confidence intervals of the ACF are derived from the Generalized Bartlett's formula. The sample period of the Correlogram is at 15 years considering the dataset from the MARINA Platform database at location L2 (52.05N 2.15E in the North Sea). The Correlogram of the irregularly DeCA sample is supplementary image of Tsalis et al., (2021) using the ACF estimator algorithm SIMILARITY in Matlab (Rehfeld and Kurths, 2014)

The ACF estimator algorithm SIMILARITY is utilized in sample periods of (10, 15, 20 and 25 years) at the locations described in Chapter 5. The available software analyzing irregular samples in time and the correlogram at given time lags can be found in the NESToolbox (https://tocsy.pik-potsdam.de/nest.php) cited in Rehfeld and Kurths, (2014).

## 4.4.2 Modeling DeCAUn irregularly in time

The irregularly modeling process was carried out for eight DEP reduction level values (60, 65, 70, 75, 80, 85, 90 and 95 percent), deriving equal number of DeCA samples. Furthermore, each DeCA sample was modeled at eight $C$ normalized bandwidths $C \in [0.125, 1]$ with a 0.125 step, deriving equal number of SIMILARITY results. In this way, all DeCA samples are re-sampled to DeCAUn.1 and DeCAUn.2 respectively as described above. The associated lag ($k$)-apart value for re-sampling will be estimated by the SIMILARITY function for all bandwidth considerations.

At this point it is noted that for the evaluation of the statistical model fit of the DeCAUn re-samples to the GPD analytically presented in the following three steps, the concept of design values and return periods is used. In relevant wind and coastal engineering applications where the proposed model focuses, the concept of return period and design value is widely used. The formal definition of the return period implies that the design value is expected to be exceeded on average once during the next $N$ years of observations. The period of $N$ years is called return period $RP$, associated with the design value. Specifically, the distribution function $\Pr(X \leq y)$ of the exceedances $y = (x - u)|_{x > u}$, considering $u$ is high enough, can be approximated by the GPD i.e. $G(y) = \Pr(X \leq y)$. The return period is associated with the exceedance event $X > x_p$, that has probability of occurrence $\Pr(X > u + x_p | X > u) = \Pr(X > x_p) = 1 - \Pr(X \leq x_p) = 1 - G(x_p)$. Therefore, the return period is defined as follows:

$$RP(x_p) = \frac{1}{1 - G(x_p)}, \tag{4.40}$$

where $x_p$ is the design value associated with the return period $RP$, or else the $RP$-year design value. Some authors use instead of $G(x_p)$, the expression $1 - p$, where $p = \Pr[X > x_p] = 1/N$. In this case, $x_p$ is the level expected to be exceeded on average once in any particular $N$ year with probability $p$ (see also sub-Section 3.2.3).

**Step 1**: The re-samples of DeCAUn.1 and DeCAUn.2 are effective only if the common assumption of stationarity is not violated. For this reason, the non-parametric rank-based Mann-Kendall (M-K) test at a significance level of $a = 0.05$ was implemented; see also (sub-Section 2.5.2). The aim of the test was to ensure the absence of a monotonic upward or downward trend of the examined re-samples. The null hypothesis of the test is $H_0$: *No monotonic trend is present*, against the alternative $H$: *There is a monotonic trend present*. The test is used and discussed in the context of EVA in Cheng et al. (2014). It should be noted that the application of the M-K tests to the re-samples is a fundamental step as the presence of possible temporal dependence and monotonic trends can affect and bias the GPD model fit, which relies on the hypothesis of independent observations.

**Step 2**: The re-samples of DeCAUn at each DEP level are subjected to a statistical GPD model fit. However, the statistical threshold considerations for the model fit will be set within a range of values $u = (0,$ first quartile, mean, mode, and median) obtained from the re-samples respectively. The optimum re-samples are assigned in terms of the lowest AIC and the lowest statistic MSE under the statistical threshold considerations.

**Step 3**: The DeCAUn re-samples derived from Step 2 are considered optimum for the statistical GPD model fit. All previous Steps 1 and 2 are repeated over all normalized bandwidth considerations. At this point, we note that the quantitative comparison of the DeCAUn re-sampled model fit was not based on the standard AIC and MSE criteria. Thus, neither common criteria for model selection nor goodness-of-fit tests are appropriate for evaluating the quality of the model fit. Therefore, we considered a metric guide rule in the least-square sense to measure the goodness of fit. Each optimum model fit will be counted upon a relative measure of performance based on the estimated design values ($DV$) per sample period (Ny) denoted as $DV_{opt}(\text{DEP}, u, C, \text{Ny})$. The relativity of the metric is gauged by the associated estimates from the BM approach within the largest annual available time series $DV(\max)$. The quantitative measure is defined as a normalized root mean square error ($nrmse$), based on the modal position of Hyndman and Fan (1996)

$$nrmse(\text{Ny}) = \sqrt{\frac{1}{N_T} \sum_{RP \in T} \left( \frac{DV(RP; \max) - DV_{opt}(RP; \text{DEP}, u, C, \text{Ny})}{DV(RP; \max)} \right)^2}, \tag{4.41}$$

where $T = (2, 10, 20, \ldots, 90$ and $100)$ indicating the return periods ($RP$) of length $N_T = 11$ and Ny $= 10, 15, 20$ and $25$ years denoting the four sample periods of examination. The precision of the $nrmse$ measure will be counted upon the $DV(\max)$ estimates of the reference model (BM Ref.) using the largest available sample of 20 years for the MARINA Platform dataset, 50 years for the ERA-20C and 38 years for the ERA-Interim dataset respectively (see Chapter 5). Moreover, the parameter estimation method used is the standard MLE for the GEV and GPD model fit of DeCAUn and BM Ref. respectively to all datasets.

In this implementation, the optimum normalized bandwidth of $C \in [0.125, 1]$ with a 0.125 step is the value that minimizes the $nrmse$ estimates from the re-samples in Step 2. At this optimum bandwidth selection the optimum DEP level is also derived and the optimum re-sampling scheme of DeCAUn. This empirical procedure applied for the selection of the optimum normalized bandwidth to the weighting function is a result of no theoretical rule of

the effective bandwidth. The aforementioned Steps 1,2, and 3 are respectively applied to the four sample periods of examination (10,15,20 and 25 years). For clarity, the empirical optimum bandwidth selection with the associated *nrmse* at the two sample periods of examination is presented for only one location (L21; see Table 5.6) in the following Figure 4.10.
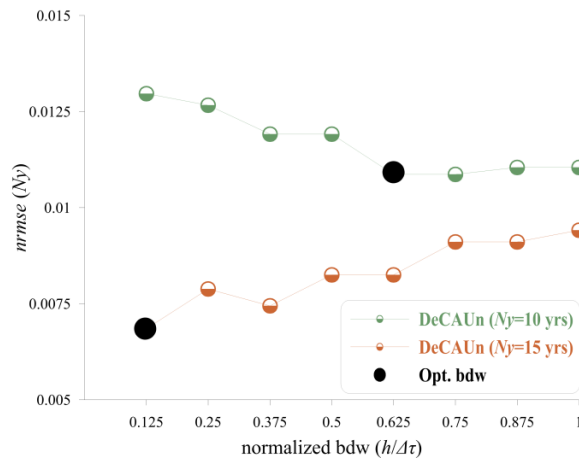


Figure 4.10: Optimum normalized bandwidth (bdw) selection for L21 from the MARINA Platform database. The empirical procedure applied for the selection of the optimum normalized bandwidth is supplementary image of Tsalis et al., (2021)

From the empirical procedure described in Step 3, the DeCAUn model set optimum normalized bandwidth values at 0.625 for the 10 years and 0.125 for the 15 years as illustrated in Figure 4.10. For a comprehensive overview of the irregularly modeling procedure, a flow diagram is illustrated in Figure 4.11 summarizing in brief the key-steps in this setting from the time series to the re-sampling scheme.
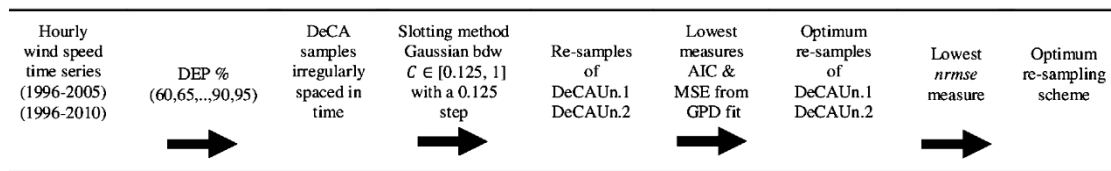


Figure 4.11: Example of the re-sampling strategy illustrating the procedure from the time series to the selected re-sampling scheme of DeCAUn. The flow chart diagram describes in brief the irregularly modeling process considering eight DEP % reduction levels and eight normalized bandwidth values. The minimum nrmse measure derived the optimum scheme for re-sampling. The flow chart is found in Tsalis et al., 2021.

In addition, an example of the declustering process under the DeCA and DeCAUn model is illustrated for inference in Figure 4.12.

**(a)**
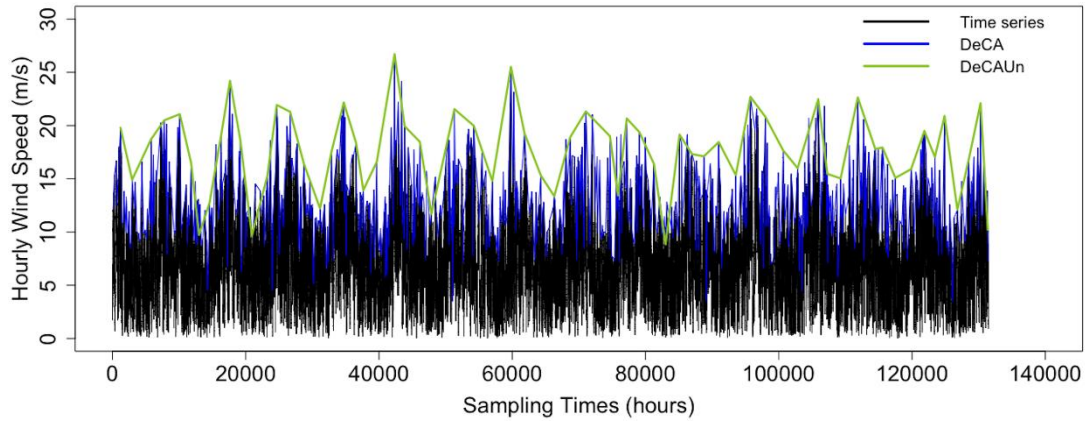


**(b)**
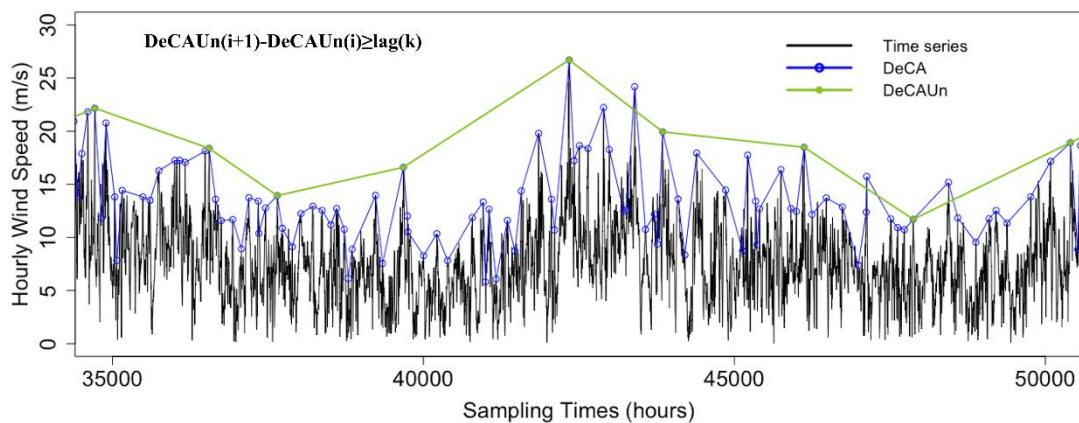


Figure 4.12: Example of the DeCAUn model in (a) with optimum DEP reduction level at 65% in order to safely separate approximately independent events avoiding unnecessary concatenation of clusters. The desired $\lag(k)$-apart value for re-sampling from DeCAUn.2 the irregular observations from DeCA in (b) is estimated at $\lag(k)$=9 as a time lag transformation from the correlogram. In addition, the No. of DeCA clusters is 778 and the DeCAUn clusters is 66, withoptimum normalized bandwidth set at 0.25. The dataset used is from the MARINA Platform database (sub-Section 5.4) regarding sample period of 15 years (from 1996 to 2010) for location L2 in the North Sea. The demonstration of the re-sampling strategy of DeCAUn is illustrated also in Tsalis et al., (2021)

Summarizing the implementation of DeCAUn, we recall that the main idea is to re-sample the irregular samples from DeCA to re-samples approximating to the i.i.d limitations. The re-sampling procedure was processed by the Slotting method, employing a Gaussian Kernel weight function into the irregular ACF estimator. Moreover, the re-sampling process accounted a range of DEP reduction levels and a range of bandwidths. In this way, the foregoing ranges encompassed as many discrete events as possible and avoided over or under smooth effects on the weight function respectively.

# Chapter 5
## Study area and wind speed dataset used

In this Section the time series with their statistical properties are provided for the wind speed data that are used for the response of the proposed models with regards to the return levels (design values) and return periods presented in Chapter 6. The datasets are obtained from four available databases, namely (i) from the National Oceanic and Atmospheric Administration (NOAA) for buoys located in the Pacific coast of central America and eastern Atlantic Ocean, (ii) the ERA-20C, (iii) ERA-Interim and (iv) MARINA Platform for locations selected at the North Sea, the Atlantic Ocean and the Mediterranean Sea.

Our assessment is focused on different offshore regions in Europe, with special focus in the North Sea, the European coastline that is exposed to the Atlantic Ocean and finally the Mediterranean. The considered locations in these regions are of high interest in terms of wind energy and offshore activities. Their characteristics vary and are highly affected by the different climatological patterns for each region. The wind conditions in the North Sea are driven by the passage of cyclonic systems such as extra-tropical cyclones influenced by the inflow of oceanic water from the Atlantic Ocean. This, combined with North Sea's shallow water basins, result to a remarkable offshore wind profile (Sušelj et al., 2010). The West European offshore locations exposed to the Atlantic Ocean are affected by the extra or post-tropical cyclones that are generated along the Polar and the Arctic front respectively (Dodet et al., 2010). Finally, the Mediterranean Sea is a semi-enclosed basin surrounded by complex mountainous terrain and is divided in several sub-basins with contradistinctive characteristics. In addition, the Mid-Latitude cyclone passage results to complicated wind patterns with extreme winds. A detailed description of the main Mediterranean winds is provided by Zecchetto and Cappa (2001) and Soukissian et al., (2018) with references therein, where wind climate and wind power potential characteristics of the Greek Seas found in (Soukissian et al., 2017; Katopodis et al., 2019).

All models are assessed against the BM from these datasets (see Chapter 6). The maximum available time series is extending from 1976-2012 (37 years long) from the NOAA product, the ERA-20C is extending from 1961-2010 (50 years long) and the ERA-Interim product from 1979-2016 (38 years long). The maximum wind speed time series used from the MARINA Platform database is from 1996 to 2015 (20 years), referred also as the reference series of the BM model (BM Ref.). A short description of the above mentioned datasets is presented in the following sub-Sections.

## 5.1 NOAA database

The National Oceanic and Atmospheric Administration (NOAA) National Data Buoy Center (NDBC), a part of the National Weather Service (NWS), designs, develops, operates, and maintains a network of moored buoys and coastal stations throughout the world's oceans, seas, and lakes for the purpose of providing civil earth marine observations. NDBC has provided real-time, oceanographic, and meteorological observations since 1967 to a wide variety of stakeholders and users. NDBC provides high quality ocean and coastal observations for public safety use in direct support of short range and extended range NWS forecasts, Warnings, and Watches.

Wind measurements are made at all NDBC weather stations. NDBC uses 4-blade, impeller-driven, wind-vane sensors. The final measurements are statistical estimates of the wind from time series of instantaneous wind samples taken at a minimum rate of 1 Hertz (Hz) over a particular length of time. The sampling rate is a function of the payload. CMAN stations

use a 2-minute data acquisition period, and moored buoys use an 8-minute acquisition period. The following standard wind measurements are produced each hour.

Continuous-wind data are accumulated in segments of 10 minutes, yielding 600 samples per segment, and six 10-minute segments each hour. After each segment period, the mean of the segment is calculated and stored in a temporary buffer. The accumulations are also stored for later hourly statistical processing. The payload saves the most recent six accumulations. At the end of each 10-minute segment, the oldest data, now more than an hour old are removed from memory and replaced with the most recent.

At the end of an acquisition period, statistical processing is performed, and the output message is updated with the new statistics and six 10-minute segments. Statistical processing includes the calculation of the mean for both direction and speed and the standard deviation of the speed. The hour's data do not represent data from minute 0 to minute 59. Rather, it represents the latest, complete six 10-minute segments before the end of the last acquisition. The 10-minute segments are, however, bounded by minutes 0, 10, 20, etc.

Wind measurements undergo range, consistency, standard deviation, and gust-to-speed ratio checks. Wind speed at 10 m above site elevation (WSPD11, WSPD21) and 20 m above site elevation (WSPD12, WSPD22) are derived from an algorithm (Liu et al., 1979) that uses the height of the anemometer, the wind speed (WSPD1 or WSPD2), a constant relative humidity of 85%, a constant sea-level pressure of 1013.25, and the air (ATMP1 or ATMP2) and water temperature (WTMP1). If either the air or water temperature are unavailable, then the neutral stability is assumed. Assuming neutral stability can introduce an error of up to 5 percent. If both are missing then neither 10 nor 20-m wind speeds are made. Finally many buoys that are climatologically in the path of hurricanes or intense low pressure systems have the capability of measuring supplemental one-minute average wind data. A comprehensive documentation of the NDBC can be downloaded from http://www.ndbc.noaa.gov/NDBCHandbookofAutomatedDataQualityControl2009.pdf and available data sets from http://www.ndbc.noaa.gov/ .

## Dataset

In this setting, wind speed datasets from the NOAA database is used to address effectively the intractable problems of inference of the most used and less known parameter estimation methods of the GEV distribution. Inference of the demonstration of the parameter methods is made to the regional locations in the Pacific coast of central America and locations in the North West Atlantic Ocean which are exposed to a strong wind climate with evidence of extreme wind speed (Lavin et al., 2006). Specifically, locations (41001 and 44004) in the Tropical North Atlantic ocean (see Figure 5.1), are related to hurricane activity and locations (46006 and 51003) are highly exposed to the Eastern North Pacific tropical cyclones (Landsea et al., 2004). The code numbers of the buoys selected along with the corresponding geographical locations and the measurement periods are the following:

- 41001 (34°33'40" N 72°37'50" W, 1976-2012),
- 44004 (38°29'2" N 70°25'57" W, 1977-2008),
- 46006 (40°45'16" N 137°27'51" W, 1977-2012),
- 51003 (19°1'6" N 160°34'54" W, 1984-2012).
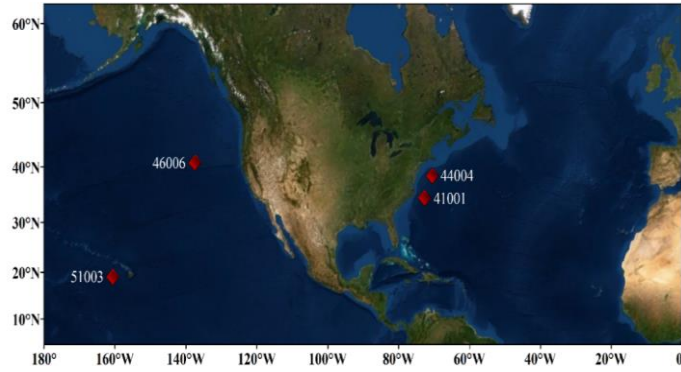
Figure 5.1: Code numbers of the buoys used for the wind speed dataset from the NOAA database illustrated at the corresponding geographical locations. These locations are also used in the work from Soukissian and Tsalis, (2015).

The basic statistics of the wind data for the entire measurement period is provided in Table 5.1. Specifically, the following remarks are outlined: On a mean annual basis, the most intense wind climate corresponds to the location of the buoy 46006 (mean annual value of wind speed 7.54 m/s). The overall maximum wind speed was recorded at buoys 41001 and 46006 (equal to 31.2 m/s), while the highest 0.99 percentile point (17.1 m/s) corresponds to the location of buoy 44004. The greatest variability corresponds to buoy 44004 (coefficient of variation 50.67 %), which is also characterized by the largest variance. The values of the kurtosis are of comparable order of magnitude for all locations, and apart from buoy 51003, the same holds true for skewness.

Table 5.1: Basic statistical parameters for wind speed at the examined buoy locations.

| Buoy no. | 41001 | 44004 | 46006 | 51003 |
|---|---|---|---|---|
| Annual Sample | 1976-2012 | 1977-2008 | 1977-2012 | 1984-2012 |
| | 37 (yrs) | 32 (yrs) | 36 (yrs) | 29 (yrs) |
| Number of records | 209942 | 200854 | 195315 | 209176 |
| Max | 31.2 | 30.7 | 31.2 | 19.4 |
| Min | 0 | 0 | 0 | 0 |
| Mean | 7.193 | 7.323 | 7.541 | 6.122 |
| Variance | 12.585 | 13.768 | 12.871 | 4.526 |
| Skewness | 0.505 | 0.546 | 0.494 | -0.017 |
| Kurtosis | 3.221 | 3.128 | 3.152 | 3.245 |
| 0.99 percentile | 16.6 | 17.1 | 16.9 | 11.3 |
| Coefficient of variation | 49.32 | 50.67 | 47.57 | 34.75 |

In addition, the annual wind speed maxima from the time series are illustrated in Figure 5.2 for the four examined locations to assess the effect of the parameter estimation methods to the GEV distribution where inference is made in Chapter 6 (sub-Section 6.1).
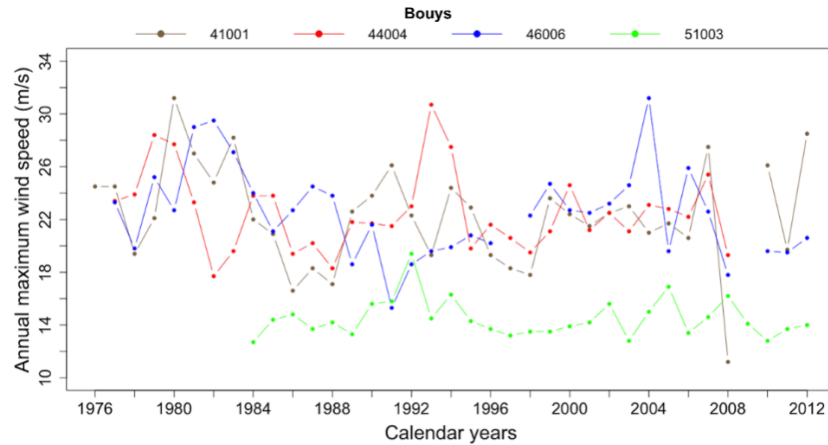
Figure 5.2: Time series of the annual maxima for buoys 41001, 44004, 46006 and 51003. The wind speed datasets at these locations are also found in Soukissian and Tsalis, (2015).

## 5.2 ERA-20C database

In this section, the statistical features of the ERA-20C wind speed dataset used are outlined to assess the effects of the sample size and the parameter estimation methods to the $n$-year design values of wind speed ($n = 10,20,...,100$). In order to effectively assess these effects, long-term wind speed time series are required. In this respect, reanalysis wind data have several advantages compared to in-situ measurements: the acquired time series are continuous, the spatial coverage is appropriate, the sampling intervals are constant and they are usually of long duration (in contrast to in-situ measurements or satellite data that are usually temporally limited). Reanalysis data has been used in several EVA related applications, see e.g. (Caires and Sterl, 2005), (Fang et al., 2008), (de Oliveira et al., 2011), (Agarwal et al., 2013), (Panchang et al., 2013), (Mo et al., 2015), (Bitner-Gregersen, 2015), (Nicolae Lerma et al., 2015), (Patlakas et al., 2016). Since reanalysis data offer the convenience to generate long-term datasets on a defined homogeneous grid for climate research at different historical periods, a detailed assessment of the effects of the sample size of BM to the wind speed design values is effectively made.

Based on the above discussion, wind data from the recently released ERA-20C climatology are utilized. Let it be noted though that numerical model data are subjected to different limitations, such as model uncertainties and lack of high-frequency information. However, the temporal resolution (3h) of ERA-20C data is considered satisfactory for the representation of the high-frequency fluctuations; see also (Reguero, 2011). Moreover, in (Bitner-Gregersen et al., 2014; Bitner-Gregersen, 2015) it is emphasized that since the reanalysis data cover long time periods (more than 30 years as in our case), it is anticipated that the GEV distribution fits are not affected by the model sampling variability.

ERA-20C is the first atmospheric reanalysis of the 20th century (covering the period 1900–2010) provided by the European Centre for Medium Range Weather Forecasting (ECMWF), developed within the context of the ERA-CLIM project. The weather reanalysis is based on a coupled Atmosphere/Land-surface/Ocean-waves model by assimilating surface observations (surface pressures from ISPD v3.2.6 and ICOADS v2.5.1, and surface marine winds from ICOADS v2.5.1). The horizontal model resolution is approximately 125 km. A description of the ERA-20C product can be found in (Poli et al., 2016). See also http://www.ecmwf.int/en/research/climate-reanalysis/era-20c.

In order to identify the effects of BM on the wind speed design values and assess the sensitivity of the latter estimates, the wind speed data time series are split into series of different lengths, namely 20, 25, 30, 35, 40, 45 and 50 years. Although the primary times series lengths

are of the order of 110 years, wind data have been restricted to the last 50 years, i.e. 1961–2010, based on the following grounds: 1) the examined time series and subseries should be stationary in order to secure the validity of EVA and the assessment of the obtained numerical results; and 2) 1960 is a key-year as regards the number of assimilated observations for the northern hemisphere with respect to surface pressure and wind zonal and meridional components. This number is rather stabilized after 1960, while during the 2nd World War took its minimum values. Therefore, in order to avoid potential inhomogeneities of the examined time series, the analyzed data are limited in 1960-2010. See also (Poli et al., 2013).

Moreover, a new type of comparative assessment is also introduced in the work of (Soukissian and Tsalis, 2019). Taking into consideration that the available time series extends from 1961 to 2010, the assessment of the sample size effects can be made in two directions: i) by allowing the sample size to increase from 1961 forward or ii) by allowing the sample size to increase from 2010 backwards. For the sake of brevity, the samples obtained by the forward direction of their size increase are called *F–samples* (e.g. the sample of 30 annual maxima obtained during the period 1961–1990, or of 40 annual maxima obtained during the period 1961–2000) and the samples obtained by the backward direction of their size increase are called *B–samples* (e.g. the sample of 30 annual maxima obtained during the period 1981-2010, or of 40 annual maxima obtained during the period 1971–2010). See also Figure 5.3 for the schematic illustration of the different sampling step.

The former case (F–samples) is usually of interest in classical assessment of sample size effects. This is the case encountered in wind speed measurements, as the corresponding sample size continuously increases in the time domain. The latter one (B–samples) may also refer to the estimation of design values based on hindcast model results, a case that is often encountered in offshore wind energy applications. As hindcast model results extend over the past, the corresponding sample size of the annual maxima also increases. As far as the authors are aware of, this case has not been studied. From an alternative point of view, B–samples can be regarded as F–samples with a different starting and ending point in time.
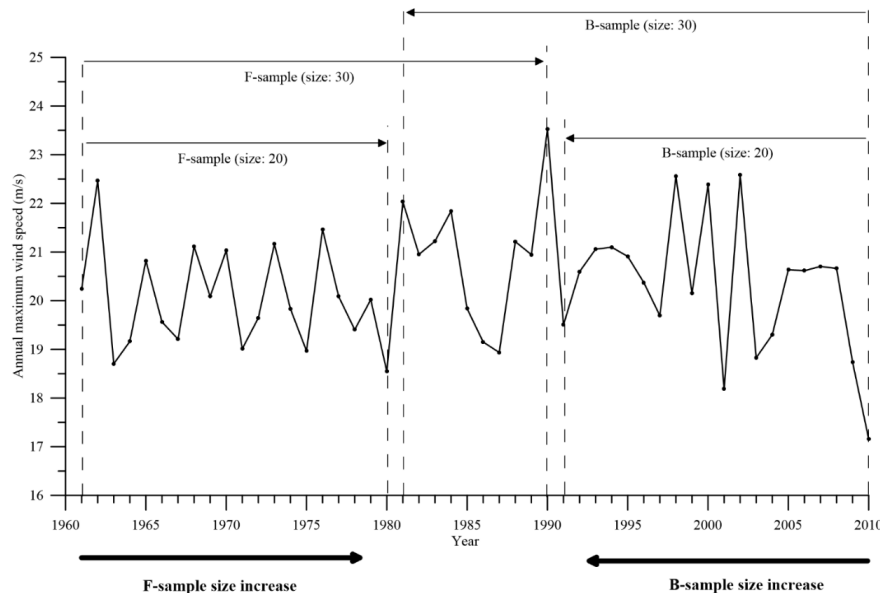


Figure 5.3: The illustration of the F– and B–samples definition on a time series of annual maxima. The different starting and ending point in time is inferred in sub-Section (6.1.2). Supplementary material of Soukissian and Tsalis, (2019)

## 5.2.1 Dataset (Stationary analysis)

Based on the stationary analysis for extremes and the combined effects of the sample size to the estimators, the extreme wind profile in this setting is represented using a suitable reanalysis dataproduct such as ERA-20C in the offshore region of the North Sea focused at locations away from the land-sea boundaries. The specific locations are shown in Figure 5.4.
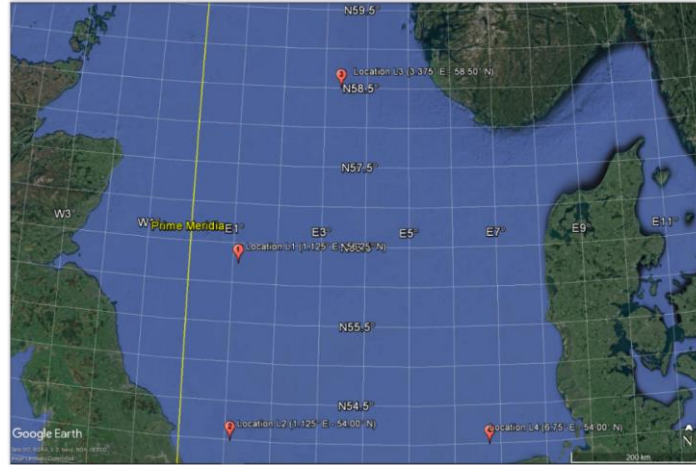


Figure 5.4: Geographical locations of grid points of the ERA-20C data set (from Google maps) illustrated also in Soukissian and Tsalis, (2018).

The low-resolution dataset used is less vulnerable to systematic errors which may lead to artificial trends (e.g., see Alexandersson et al. 2000; Matulla et al. 2007). Nevertheless, the effective representation of the surface wind conditions over the North Sea using a low-resolution wind speed dataset is challenged and unclear (Sušelj et al., 2010). It is evident in their study that the low-resolution datasets effectively secure and capture the large-scale forcing on the wind field but rather fail capturing the local effects. To alleviate any inconsistencies of the model in the nearshore areas the locations in this setting are at distance from the land-sea topography.

Specifically, for locations L(1,2 and 3) de Winter et al., (2013) resulted that high wind speeds are compared suitable with those of ERA-20C or the later ERA-Interim. Zappa et al., (2013) show that the characteristics of extra tropical cyclones obtained at L(1,2, and 3) are very close to the representations made from several reanalysis products. The latter reproductions also discussed in Sterl et al., (2015) is somehow explained by the good representation of the predominant force pressure pattern over the North Atlantic i.e., the North Atlantic Oscillation. The extreme wind profile in the German Bight where L4 is located, is well represented by the relatively low reanalysis resolution of ERA-20C (Sušelj et al., 2010). As a remark from the work of Befort et al., (2014) it is pointed out that the rarest events in the region where L4 is selected, will potentially show reduced intensity. However, inference of the low reanalysis product is challenged at the coastal areas where in this part of the study locations are carefully selected avoiding inconsistencies near the coast.

Further on, the effects of the available time series length on the time series statistics are assessed. In Table 5.2, the main statistical parameters of wind speed for locations L1, L2, L3 and L4 for different time series lengths are shown. The particular parameters estimated are the mean value $m$ and standard deviation ($s$), minimum (min), and maximum (max), the 99th percentile point, coefficient of variation ($CV$), excess kurtosis ($k$) and skewness($sk$). $N$ denotes the specific time series length in years (i.e. 20, 25, 30, 35, 40, 45, and 50) where the statistical parameters are estimated.

Table 5.2: Descriptive statistics of wind speed at locations L1 (1.125° E - 56.25° N), L2 (1.125° E - 54.00° N), L3 (3.375° E - 58.50° N) and L4 (6.75° E - 54.00° N) for different time series lengths. The case encountered in wind speed measurements is the F-sample size increase in the time domain, e.g. 20,25,30,35,40,45 and 50 yrs length corresponded from 1961 to 1980,1985,1990,1995,2000,2005 and 2010 respectively.

| Time series length (years) | Location | Sample size | mean (m/s) | min (m/s) | max (m/s) | 99% (m/s) | $s$ (m/s) | $CV$ | $sk$ | $k$ |
|---|---|---|---|---|---|---|---|---|---|---|
| 20 | L1 | 58440 | 8.165 | | 22.469 | 17.162 | 3.580 | 43.845 | 0.451 | -0.334 |
| | L2 | | 7.536 | 2.000 | 21.703 | 16.088 | 3.436 | 45.599 | 0.416 | -0.328 |
| | L3 | | 8.176 | | 22.245 | 17.755 | 3.808 | 46.580 | 0.455 | -0.333 |
| | L4 | | 7.045 | | 21.419 | 15.088 | 3.160 | 44.857 | 0.463 | -0.216 |
| 25 | L1 | 73048 | 8.176 | | 22.469 | 17.233 | 3.606 | 44.110 | 0.458 | -0.325 |
| | L2 | | 7.554 | 2.000 | 21.703 | 16.155 | 3.455 | 45.742 | 0.421 | -0.331 |
| | L3 | | 8.218 | | 24.662 | 17.805 | 3.817 | 46.448 | 0.450 | -0.337 |
| | L4 | | 7.065 | | 21.419 | 15.153 | 3.180 | 45.005 | 0.463 | -0.212 |
| 30 | L1 | 87656 | 8.244 | | 23.525 | 17.221 | 3.619 | 43.895 | 0.438 | -0.356 |
| | L2 | | 7.617 | | 21.703 | 16.212 | 3.473 | 45.601 | 0.414 | -0.338 |
| | L3 | | 8.275 | 2.000 | 24.662 | 17.751 | 3.817 | 46.127 | 0.423 | -0.370 |
| | L4 | | 7.118 | | 21.419 | 15.178 | 3.201 | 44.963 | 0.451 | -0.244 |
| 35 | L1 | 102264 | 8.292 | | 23.525 | 17.305 | 3.631 | 43.793 | 0.432 | -0.361 |
| | L2 | | 7.644 | 2.000 | 22.070 | 16.248 | 3.484 | 45.581 | 0.410 | -0.344 |
| | L3 | | 8.324 | | 24.662 | 17.806 | 3.830 | 46.016 | 0.415 | -0.383 |
| | L4 | | 7.136 | | 21.419 | 15.189 | 3.209 | 44.968 | 0.452 | -0.250 |
| 40 | L1 | 116880 | 8.283 | | 23.525 | 17.276 | 3.633 | 43.854 | 0.437 | -0.366 |
| | L2 | | 7.646 | 2.000 | 22.070 | 16.244 | 3.490 | 45.643 | 0.407 | -0.364 |
| | L3 | | 8.331 | | 24.662 | 17.813 | 3.830 | 45.977 | 0.413 | -0.383 |
| | L4 | | 7.152 | | 21.419 | 15.207 | 3.214 | 44.945 | 0.448 | -0.265 |
| 45 | L1 | 131488 | 8.260 | | 23.525 | 17.220 | 3.611 | 43.713 | 0.437 | -0.356 |
| | L2 | | 7.629 | 2.000 | 22.070 | 16.212 | 3.482 | 45.642 | 0.406 | -0.365 |
| | L3 | | 8.303 | | 24.662 | 17.755 | 3.813 | 45.927 | 0.415 | -0.375 |
| | L4 | | 7.129 | | 21.419 | 15.171 | 3.203 | 44.931 | 0.449 | -0.266 |
| 50 | L1 | 146096 | 8.232 | | 23.525 | 17.204 | 3.608 | 43.833 | 0.440 | -0.355 |
| | L2 | | 7.623 | 2.000 | 22.070 | 16.183 | 3.477 | 45.612 | 0.404 | -0.372 |
| | L3 | | 8.281 | | 24.662 | 17.742 | 3.814 | 46.061 | 0.420 | -0.370 |
| | L4 | | 7.137 | | 21.419 | 15.160 | 3.196 | 44.777 | 0.446 | -0.266 |

Some conclusions that can be drawn from the above results are the following:

1. The largest 99th percentile values are observed for the time series with 35 years length (for L1 and L2), and 40 years length (for L3 and L4).
2. New ("fresh") annual maxima (outside the annual maxima range of the previous time period), enter into the analysis for the 30 years long time series (for L1), 35 years long time series (for L2) and 25 years long time series (for L3).
3. Excess kurtosis parameter is systematically negative suggesting light-tailed distributions for wind speed.

4.  Excess kurtosis and skewness parameters remain rather constant for the examined time series lengths.

In Figure 5.5, the time series of BM of wind speed for locations L1, L2, L3 and L4 are shown for the period 1961–2010. Notice the presence of an abrupt shift for L3 that occurred in 1981. The presence of this maximum affects the extreme value analysis and in particular, the design values of wind speed (see sub-Section 6.1.2).
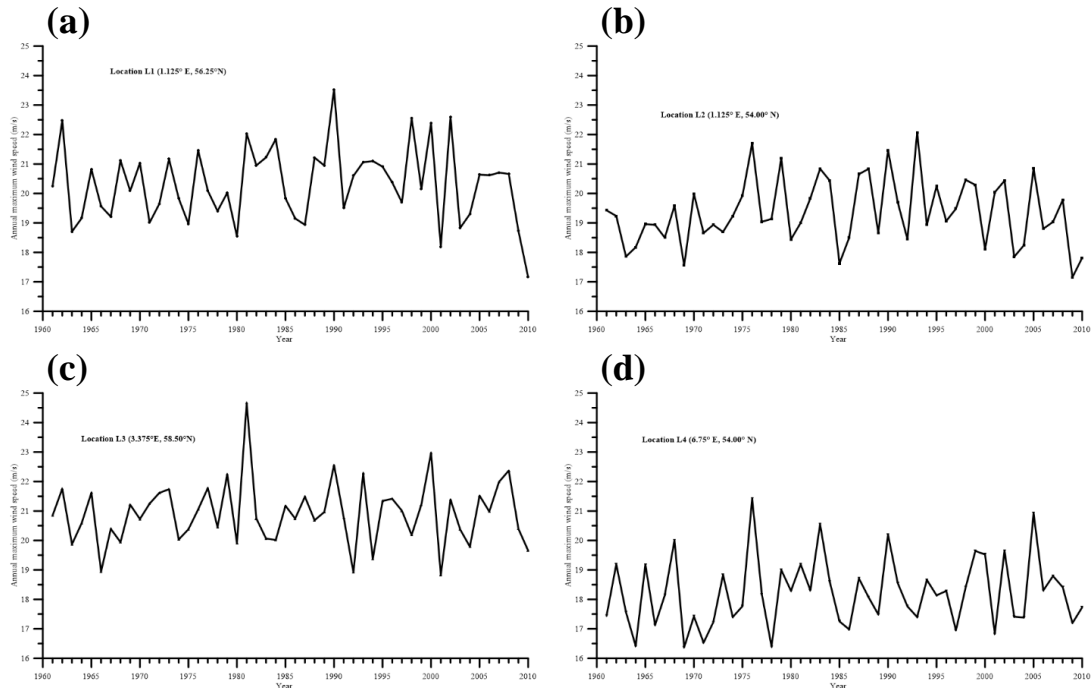


Figure 5.5: Time series of annual maxima of wind speed (1961-2010) for locations L1 illustrated in (a), L2 in (b), L3 in (c), and L4 in (d). These locations are used to assess the effect of the parameter estimation methods to the GEV distribution and the sample size in Chapter 6 (sub-Section 6.1). Illustrated also in Soukissian and Tsalis, (2018).

## 5.2.2 Dataset (Non-Stationary analysis)

The complex dynamics of large-scale atmospheric circulation in a few recurrent and quasi-stationary patterns is characterized in Synoptic climatology as weather regimes (Cortesi et al., 2019). The impact of these weather regimes influences near-surface wind speed variability particularly at mid-latitudes in the Euro-Atlantic region. For a comparison of the uncertainty affecting near-surface wind speed trends from different reanalyses, see Torralba et al. (2017a).

In this setting, for the extremes of non-stationary sequences and the application to wind speed design values, our analysis is based on coarse historical data of annual length 40 years. The samples of annual maxima wind speed are extracted from the atmospheric weather reanalysis product ERA-20C, covering the period (1961-2000). Specifically, the samples of annual maxima will be considered for 5 different locations at the North Sea denoted as L(1,2,3,4, and 5) in Figure 5.6.
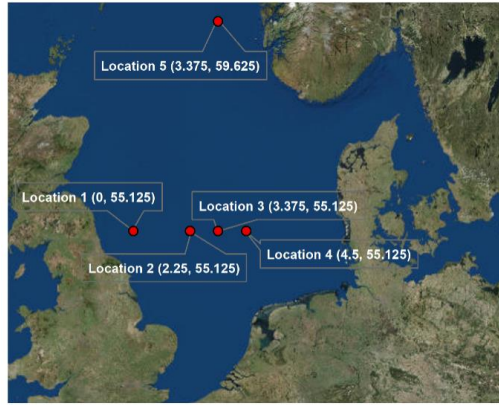
Figure 5.6: Geographical locations of the ERA 20 dataset for the non-stationary analysis. Wind speed datasets from these locations are used to assess the effect of trends in the parametric modelling of the likelihood of the GEV distribution when stationarity is violated. Illustrated also in Tsalis and Kallos, (2017).

The basic statistics of the samples of annual maxima of wind speed extending from 1961 to 2000 are given in Table 5.3. Specifically, the following statistical remarks of the dataset used for the nonstationary approach are outlined as follows:

- On a mean annual basis, the most intense wind climate corresponds to L5 (mean annual value of wind speed 20.418 m/s). The maximum wind speed of all locations ranges from 23.2 to 23.7 (m/s), while the greatest variability is shown in L4 (coefficient of variation 6.8 %), which also shows the largest variance.
- The skewness parameter is systematically positive indicating longer right tail for all locations. This is inline to regions of positive skewness located at midlatitudes in the Northern Hemisphere, characterized by intermediate mean wind speeds and strong variability (Monahan, 2006; Part I). Particularly, L1 and L5 show the largest skewness (0.94 and 0.457) respectively, indicating that at these locations the forcing has larger mean and considerable larger flunctuations away from the mean. In addition, the kurtosis parameter is negative (lighter-tail) for L (2,3, and 4) and positive (heavier-tail) for L1 and L5. Wind speed datasets at Locations L1 and L5 are characterized of having heavier tails (tail extremity) suggesting more intense extremes than at L (2,3, and 4).

Table 5.3: Basic statistics for samples of annual maxima wind speed at the locations used in the nonstationary approach.

| Location/ Statistics | nbr.val | min | max | median | mean | SE. mean | CI. mean. 0.95 | var | std. dev | cef. var | skewness | kurt- osis |
|---|---|---|---|---|---|---|---|---|---|---|---|---|
| L1 | 40 | 17.5 | 23.6 | 19.5 | 19.465 | 0.181 | 0.365 | 1.303 | 1.142 | 0.059 | 0.94 | 2.25 |
| L2 | 40 | 18.2 | 23.2 | 20.15 | 20.168 | 0.194 | 0.393 | 1.508 | 1.228 | 0.061 | 0.53 | -0.311 |
| L3 | 40 | 18.1 | 23.7 | 20.25 | 20.270 | 0.215 | 0.436 | 1.857 | 1.363 | 0.067 | 0.367 | -0.515 |
| L4 | 40 | 18.1 | 23.3 | 20.15 | 20.345 | 0.218 | 0.44 | 1.896 | 1.377 | 0.068 | 0.386 | -0.84 |
| L5 | 40 | 17.5 | 23.4 | 20.25 | 20.418 | 0.162 | 0.328 | 1.05 | 1.025 | 0.05 | 0.457 | 1.844 |

In Figure 5.7, the annual wind speed maxima is illustrated for the five examined locations used in the nonstationary approach. The apparent trend illustrated at these locations meet the requirements of the MK, CS and KPSS test discussed in sub-Section (2.5.2) and analytically formulated in Appendix F. The statistical analysis made to the series at these locations pointed out that the Trend and Stationarity test hypothesis cannot be rejected at the significance level of 0.05, regarding the absence of a monotonic upward trend over time and the presence of stationarity around a fixed level. The statistical tests applied in this part of our analysis to extremes of wind speed strengthens the parameteric modelling in the nonstationary approach. The test results of this analysis are presented in Chapter 6 (sub-Section 6.2).
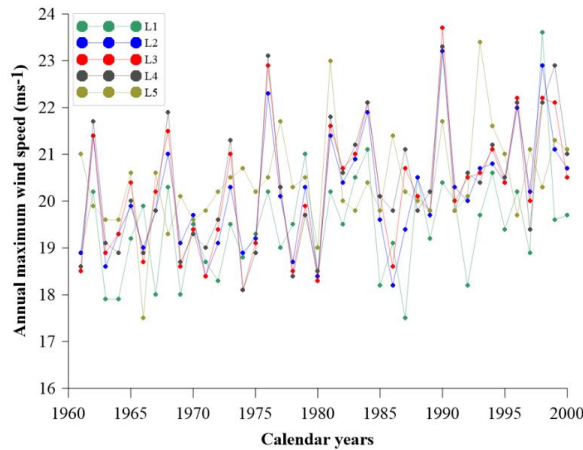


Figure 5.7: Time series of annual maxima of wind speed (1961-2000) per location. Datasets from these locations are used to assess the effect of the various parametric models used to the parameter estimation of the time dependant likelihood of the GEV distribution shown in Chapter 6 (sub-Section 6.2). Illustrated also in Tsalis and Kallos, (2017).

## 5.3 ERA-Interim database

In this sub-section, we describe in short the ERA-Interim data product and the wind speed time series originated from this database. The relatively small resolution of ERA-Interim and the previous ERA-20C reanalysis database within the context of the ERA-CLIM project will challenge the demonstration of the proposed DeCAUn model for the extrapolation of extreme wind speed estimates.

ERA-Interim is a global atmospheric reanalysis from 1979, continuously updated in real time. The dynamical core of the atmospheric model is based on a spectral representation for the basic dynamical variables, a hybrid sigma-pressure vertical coordinate, and a semi-Lagrangean semi-implicit time stepping scheme. The ERA-Interim configuration uses a 30 min time step and has a spectral T255 horizontal resolution, which corresponds to approximately 79 km spacing on a reduced Gaussian grid. The vertical resolution uses 60 model layers with the top of the atmosphere located at 0.1 hPa.

The weather reanalysis is based on a coupled Atmosphere/Land-surface/Ocean-waves model by assimilating surface observations, producing ERA-Interim assimilation data consisting on four analyses per day, at 00:00 the first, 06:00 the second, 12:00 the third, and 18:00 UTC the fourth. Archived ERA-Interim data and current data availability can be downloaded from the ECMWF Data Server at http://data.ecmwf.int/data, or on ECMWF website at http://www.ecmwf.int/research/era. The data are available at full resolution with options for regional selection and gridding. A comprehensive documentation of the ERA-Interim reanalysis system http://onlinelibrary.wiley.com/doi/10.1002/qj.828/abstract has been published as an open-access article in the Quarterly Journal of the Royal Meteorological Society, (Dee et al., 2011).

## Dataset

The examined locations are 32 in total, denoted as L1, L2,…,L31 and L32 respectively as shown in Table 5.4.

Table 5.4: Locations of daily wind speed records using the ERA-20 and ERA-Interim products.

| | ERA-20C | | | ERA-Interim | |
|---|---|---|---|---|---|
| Location | Latitude | Longtitude | Location | Latitude | Longtitude |
| L1 | 38.250N | 24.750E | L17 | 56.250N | 4.500E |
| L2 | 41.625N | 16.875E | L18 | 54.000N | 2.250E |
| L3 | 33.750N | 33.750E | L19 | 60.000N | 2.250E |
| L4 | 34.875N | 24.750E | L20 | 58.500N | 0.000E |
| L5 | 40.500N | 5.625E | L21 | 56.250N | 17.250E |
| L6 | 42.750N | 4.500E | L22 | 57.000N | 19.500E |
| L7 | 42.750N | 6.750E | L23 | 37.500N | 11.250W |
| L8 | 42.750N | 31.500E | L24 | 51.000N | 6.750W |
| L9 | 42.750N | 34.875E | L25 | 58.500N | 10.500W |
| L10 | 58.500N | 4.500E | L26 | 33.000N | 31.500E |
| L11 | 46.125N | 4.500W | L27 | 41.250N | 18.000E |
| L12 | 47.250N | 3.375W | L28 | 34.500N | 12.000E |
| L13 | 47.250N | 10.125W | L29 | 36.000N | 2.250W |
| L14 | 34.875N | 10.125W | L30 | 37.500N | 17.250E |
| L15 | 36.000N | 11.250W | L31 | 42.000N | 3.750E |
| L16 | 38.250N | 10.125W | L32 | 45.000N | 32.250E |
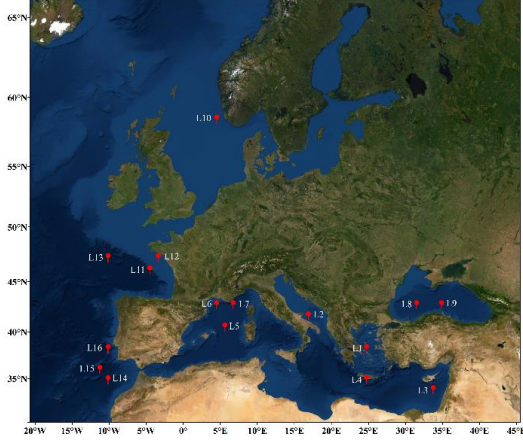
**(a)**                                      **(b)**
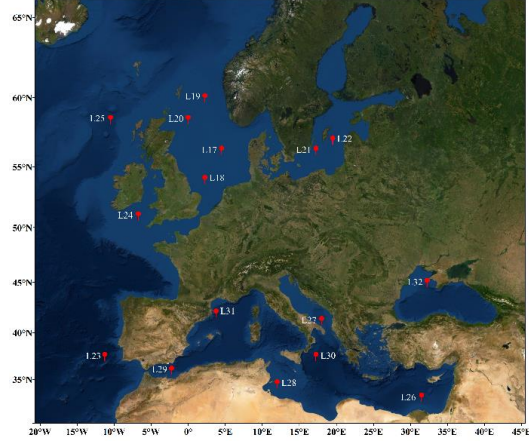


Figure 5.8: Geographical locations of the ERA-20C (a) and ERA-Interim (b) data set for the DeCA and DeCAUn model analysis. Supplementary image of Tsalis et al., (2019).

The descriptive statistics of the wind speed dataset of the 32 locations from the ERA-20C and ERA-Interim database is presented analyticaly in Table 5.5. The interesting feature from the statistics associated to the relatively small resolution database is that the skewness parameter is systematically positive. This finding indicates that the probability density estimate of the wind speed time series at 10 (m) height at the 32 locations selected from the ERA-20C and ERA-Inrerim database is characterized by a longer right tail suggesting that the mean value is larger than the most likely observed values in the series (Marcos et al., 2019).

Another interesting feature is that the excess kurtosis parameter depicts slightly negative and positive values and varies between -1 and 1 throughout most of the midlatitudes except L3 depicted at 1.932 and L26 at 1.165. This indicates that the distribution of wind speed

originated from a fairly coarse resolution database such as the ERA-Interim, in general suggests light-tails for the majority of the midlatitude regional locations used in this study which is also in agreement based on the study of Monahan, (2006; Part II) and Marcos et al., (2019).

Given the sparsity of global wind observations, the relatively small reanalysis data products such as ERA-Interim have demonstrated their potential usefulness for large-scale wind energy applications (Torralba, et al., 2017b). It is emphasized that since the reanalysis dataset of low resolution covers long time periods (38 and 50 years in this part of the study) it is anticipated that the asymptotic model formulation of GEV and GPD will be unaffected from the climate uncertainty when modelling BM Ref. at the larger available length and will challenge the modelling of DeCAUn at sample periods of shorter length. The modelling of extreme wind parameters is usually manifested using statistical methods based on long datasets (Kunz et al., 2010; Bonazzi et al., 2012; Jonathan and Ewans, 2013).

The forcing mechanism deriving wind speed observations particularly near the coast is subjected to many complex, small-scale phenomena which produce large differences over small distances. The use of database of larger resolution for the demonstration of DeCAUn will challenge the resampling strategy by incorporating inevitably more extremes. It is rather expected at that case positive and larger excess kurtosis suggesting distributions of heavy right-tails as an approximation to the probability density function of the wind speed (see Figure 5.11). However, the analysis based on the realively small resolution enables us to make the best possible reconstraction of the irregularly samples given the limitations in the length of records and their spatial density.

Table 5.5: Descriptive statistics for the 32 locations of the datasets used from the ERA-20C database extending from 1961 to 2010 (50 years) and the ERA-Interim database extending from 1979 to 2016 (38 years).

| Location | min | max | median | mean | SE. mean | CI.mean 0.95 | var | std. dev | coef. var | skewness | kurtosis |
|---|---|---|---|---|---|---|---|---|---|---|---|
| L1 | 0.003 | 21.736 | 6.537 | 6.914 | 0.010 | 0.019 | 13.674 | 3.698 | 0.535 | 0.470 | -0.317 |
| L2 | 0.004 | 21.050 | 4.666 | 5.228 | 0.008 | 0.016 | 9.210 | 3.035 | 0.581 | 0.888 | 0.630 |
| L3 | 0.005 | 21.321 | 4.363 | 4.794 | 0.007 | 0.013 | 6.745 | 2.597 | 0.542 | 1.144 | 1.932 |
| L4 | 0.030 | 21.562 | 6.636 | 6.713 | 0.007 | 0.015 | 8.026 | 2.833 | 0.422 | 0.313 | 0.084 |
| L5 | 0.022 | 21.243 | 5.492 | 5.980 | 0.009 | 0.017 | 10.909 | 3.303 | 0.552 | 0.703 | 0.191 |
| L6 | 0.025 | 20.608 | 5.390 | 6.046 | 0.009 | 0.018 | 12.267 | 3.502 | 0.579 | 0.714 | -0.029 |
| L7 | 0.019 | 21.287 | 4.987 | 5.561 | 0.009 | 0.017 | 10.995 | 3.316 | 0.596 | 0.687 | -0.078 |
| L8 | 0.015 | 18.836 | 5.035 | 5.358 | 0.007 | 0.014 | 7.255 | 2.694 | 0.503 | 0.611 | 0.187 |
| L9 | 0.013 | 19.562 | 4.708 | 5.033 | 0.007 | 0.013 | 6.915 | 2.630 | 0.522 | 0.700 | 0.434 |
| L10 | 0.026 | 25.095 | 7.586 | 7.895 | 0.010 | 0.020 | 15.087 | 3.884 | 0.492 | 0.420 | -0.250 |
| L11 | 0.031 | 29.785 | 6.706 | 7.159 | 0.009 | 0.019 | 13.054 | 3.613 | 0.505 | 0.689 | 0.427 |
| L12 | 0.023 | 21.461 | 5.030 | 5.407 | 0.007 | 0.014 | 7.425 | 2.725 | 0.504 | 0.785 | 0.707 |
| L13 | 0.027 | 29.122 | 7.434 | 7.812 | 0.010 | 0.019 | 13.985 | 3.740 | 0.479 | 0.551 | 0.155 |
| L14 | 0.030 | 22.119 | 6.395 | 6.427 | 0.007 | 0.014 | 7.338 | 2.709 | 0.421 | 0.290 | 0.155 |
| L15 | 0.017 | 24.504 | 6.689 | 6.777 | 0.008 | 0.015 | 8.492 | 2.914 | 0.430 | 0.265 | -0.139 |
| L16 | 0.013 | 23.919 | 6.355 | 6.482 | 0.007 | 0.014 | 7.746 | 2.783 | 0.429 | 0.334 | 0.060 |
| L17 | 0.026 | 27.667 | 8.128 | 8.414 | 0.016 | 0.032 | 14.592 | 3.820 | 0.454 | 0.420 | -0.054 |
| L18 | 0.040 | 27.058 | 7.697 | 8.026 | 0.016 | 0.031 | 13.994 | 3.741 | 0.466 | 0.437 | -0.100 |
| L19 | 0.062 | 34.147 | 7.896 | 8.261 | 0.018 | 0.034 | 17.037 | 4.128 | 0.500 | 0.510 | 0.047 |
| L20 | 0.049 | 28.471 | 8.108 | 8.440 | 0.017 | 0.033 | 16.074 | 4.009 | 0.475 | 0.439 | -0.079 |

| | | | | | | | | | | |
|------|-------|--------|-------|-------|-------|-------|--------|-------|-------|-------|--------|
| L21 | 0.006 | 24.266 | 6.783 | 7.063 | 0.014 | 0.027 | 10.799 | 3.286 | 0.465 | 0.457 | -0.014 |
| L22 | 0.037 | 26.062 | 7.091 | 7.386 | 0.015 | 0.029 | 11.898 | 3.449 | 0.467 | 0.444 | -0.052 |
| L23 | 0.042 | 21.805 | 6.651 | 6.801 | 0.012 | 0.024 | 8.588 | 2.930 | 0.431 | 0.328 | -0.055 |
| L24 | 0.025 | 26.707 | 7.849 | 8.170 | 0.016 | 0.032 | 14.546 | 3.814 | 0.467 | 0.458 | -0.049 |
| L25 | 0.065 | 28.907 | 8.969 | 9.296 | 0.018 | 0.036 | 18.242 | 4.271 | 0.459 | 0.418 | -0.076 |
| L26 | 0.035 | 19.039 | 5.012 | 5.259 | 0.010 | 0.020 | 6.051 | 2.460 | 0.468 | 0.804 | 1.165 |
| L27 | 0.013 | 19.307 | 4.449 | 4.894 | 0.012 | 0.024 | 8.091 | 2.844 | 0.581 | 0.825 | 0.581 |
| L28 | 0.016 | 20.789 | 5.507 | 5.839 | 0.012 | 0.024 | 8.061 | 2.839 | 0.486 | 0.627 | 0.315 |
| L29 | 0.013 | 20.456 | 5.787 | 5.928 | 0.014 | 0.027 | 10.503 | 3.241 | 0.547 | 0.380 | -0.333 |
| L30 | 0.020 | 21.295 | 4.847 | 5.347 | 0.012 | 0.024 | 8.579 | 2.929 | 0.548 | 0.892 | 0.824 |
| L31 | 0.023 | 21.825 | 5.053 | 5.798 | 0.014 | 0.028 | 11.627 | 3.410 | 0.588 | 0.926 | 0.599 |
| L32 | 0.014 | 19.561 | 5.659 | 5.949 | 0.012 | 0.024 | 8.350 | 2.890 | 0.486 | 0.506 | -0.004 |

The wind speed datasets originated from the relatively small resolution database will challenge the assessment of the resamples irregularly spaced in time derived from the DeCAUn model for sample periods of (10,15,20 and 25 years). Specifically, sample periods are set from 1961 to 1985 with a 5 years step considering the ERA-20C dataset and from 1979 to 2003 with a 5 years step using the ERA-Interim dataset that will challenge the asymptotic properties of GPD modelling DeCAUn to these sample periods. For inference, two representative locations from the ERA-20C (L5 and L10) and the ERA-Interim (L18 and L30) database are selected for the demonstration of DeCAUn in terms of the return level estimates and variability of the proposed model to each sample period; (see the demonstration of DeCAUn to these locations in sub-Section 6.4).

In the following Figure 5.9 the wind speed time series originated from the ERA-20C and ERA-Interim database is illustrated for the four selected locations L(5, 10, 18, and 30). A smoothing line (red line) was fitted to the annual maxima wind speed values for better visualisation of the long-term variability of BM. It is important to point out that the assessment of DeCAUn is based to stationary wind speed time series, as the presence of possible temporal dependence and monotonic trends can affect and bias the GPD model fit, which relies on the hypothesis of independent observations. The illustration of BM shows not any increase or decrease over time, i.e., there is no trend present. There is also no obvious anomalies or jumps in BM. The results are similar for the 32 locations of the ERA-20 and ERA-Interim database.

**(a)**                                              **(b)**



82

**(c)**                                                        **(d)**
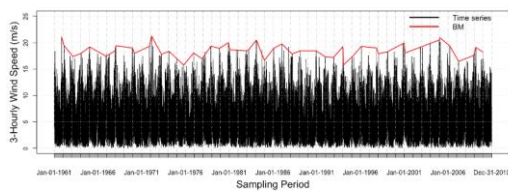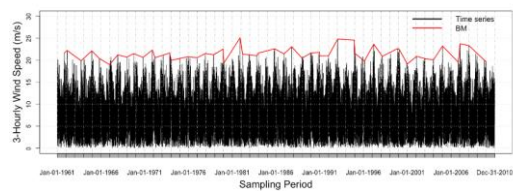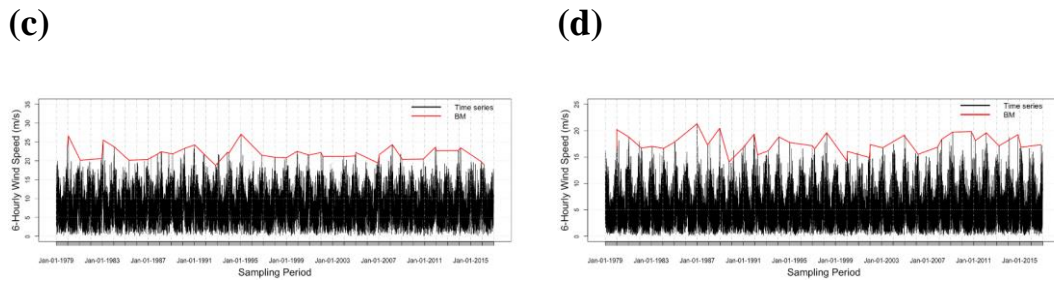


Figure 5.9: The time series and the annual or block maxima (BM) of wind speed as the reference dataset for locations L5 (a) and L10 (b) from ERA-20C are illustrated for the period 1961–2010 (50 years). Locations L18 (c) and L30 (d) from ERA-Interim correspond to sample period from 1979 to 2016 (38 years). The four locations are selected considered the intense wind profile that is present at these locations (Tsalis et al., 2019).

## 5.4 MARINA Platform database

For this statistical analysis of the proposed DeCAUn model, a high resolution database was employed providing wind speed series on different offshore regions in Europe, with special focus in the North Sea, the European coastline that is exposed to the Atlantic Ocean and finally the Mediterranean Sea.

### Dataset

The demonstration of DeCAUn in this assessment is also challenged considered a high resolution data product for the statistical analysis of the proposed resampling model. Specifically, the time series of wind speed used in this part of the analysis cover a period of 20 years (from 1996 to 2015) extracted from the MARINA Platform database (2014) created within the framework of the homonymous project. The dataset was produced as an outcome of atmospheric modeling hindcast simulations providing information for the entire European coastline with an hourly time frequency and a spatial resolution of 5 km. The atmospheric model used is SKIRON (Kallos et al., 1997). The outcome has been evaluated within the framework of MARINA Platform project (see http://forecast.uoa.gr/oldproj.php). In the present study, the wind components of the model are obtained at 10m above sea level for the 30 in total selected locations denoted as L1, L2,…, L29 and L30 in Table 5.6 with their descriptive statistics in Table 5.7.

Table 5.6: Locations of daily wind speed records from the MARINA Platform database used for this analysis.

| North Sea | | | Atlantic Ocean | | | Mediterranean Sea | | |
|---|---|---|---|---|---|---|---|---|
| Location | Lat | Lon | Location | Lat | Lon | Location | Lat | Lon |
| L1 | 55.7 N | 7.4 E | L11 | 50.45 N | 1.55 W | L21 | 40.8 N | 5.5 E |
| L2 | 52.05 N | 2.15 E | L12 | 50.05 N | 4.25 W | L22 | 35.5 N | 26.4 E |
| L3 | 51.65 N | 3.45 E | L13 | 42.85 N | 9.95 W | L23 | 33.9 N | 29.9 E |
| L4 | 54.8 N | 1.35 E | L14 | 53.25 N | 10.25 W | L24 | 43.4 N | 15.4 E |
| L5 | 57.15 N | 3.1 E | L15 | 49.65 N | 6.55 W | L25 | 36.5 N | 3.5 W |
| L6 | 58.4 N | 10.3 E | L16 | 57.25 N | 7.65 W | L26 | 37.9 N | 3.1 E |
| L7 | 51.65 N | 1.35 E | L17 | 52.75 N | 9.75 W | L27 | 43.3 N | 7.5 E |
| L8 | 57.95 N | 3.1 E | L18 | 50.65 N | 0.95 E | L28 | 42.2 N | 11.4 E |
| L9 | 56.2 N | 4.15 E | L19 | 54.85 N | 8.95 W | L29 | 40.5 N | 12.2 E |
| L10 | 55.75 N | 2.25 E | L20 | 53.35 N | 4.85 W | L30 | 42.2 N | 17.9 E |

The re-sampling assessment of DeCAUn to samples of wind speed observations irregularly spaced in time is challenged from the model demonstration of BM, Runs and DeCA

analyticaly discussed in previous sub-Sections. All models however are applied to the wind speed datasets of the MARINA Platform at locations respectively shown in Figure 5.10.
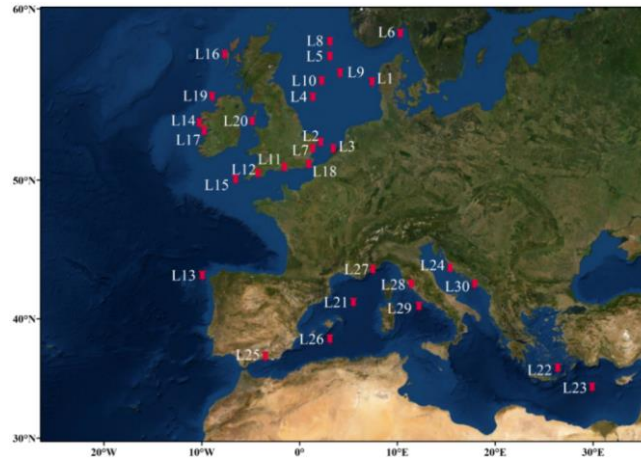


Figure 5.10: Wind speed datasets at locations used for the irregular extreme value analysis based on the MARINA Platform database. Illustrated also in Tsalis et al., (2021)

At this point it is important to highlight the use of a high horizontal resolution dataproduct such as the MARINA Platform database especially near the offshore regions of Europe where the demonstration of DeCAUn to wind speed is challenged from the highly dependent regional effects (surface roughness, landmass, etc.). The use of a high resolution database is crucial to derive detailed data to follow-up the requirements of the resampling strategy of DeCAUn to short and irregularly samples at regional locations where the meteorological model of lower resolution is not able to reproduce the underlying terrain and capture the wind speed variations sufficiently (Kaiser et al., 2015).

The descriptive statistics of Table 5.7 infer the extremity of wind speed reproduced from the MARINA Platform database. Specifically, skewness is systematically positive indicating an elongated right tail distribution as a reasonable approximation to the probability density function of wind speed at 10 (m) height of the 30 locations, suggesting intermediate mean and strong variability as in the ERA-20C and ERA-Interim dataproducts. Another interesting characteristic of the high resolution database is the systematically positive excess kurtosis parameter to all locations indicating heavy-tailed distributions for the wind speed. Positive excess kurtosis evidently inferences the ability of high resolution databases to reproduce more intense extremes particularly at the European offshore regions and strengthens the re-sampling strategy of DeCAUn to short samples at these locations; (see the discussion from Kalogeri et al., (2017) and Weber et al., (2019) for the positive excess kurtosis of wind speed at closely arranged regional locations to the present study). We highlight the extremity of wind speed data characterized of being heavy right-tailed and extremes are typically modeled from short-tailed distributions with finite right endpoint (Pinheiro and Ferrari, 2015).

To infer the extremity of the datasets (i.e., suggesting heavy tail distributions of elongated right tails as approximations to the probability density function of wind speed) at regional locations closely arranged from the relatively small resolution database (ERA-20C), the moderate resolution (ERA-Interim), and the high resolution database (MARINA Platform), the following three Kernel Density plot diagrams are illustrated in Figure 5.11. The density estimates illustrated in Figure 5.11 (a) and to a lower extent in Figure 5.11 (b) are characterized of having a light-right hand tail, where on the contrary density in Figure 5.11 (c) is characterized of having a heavy-right hand tail.
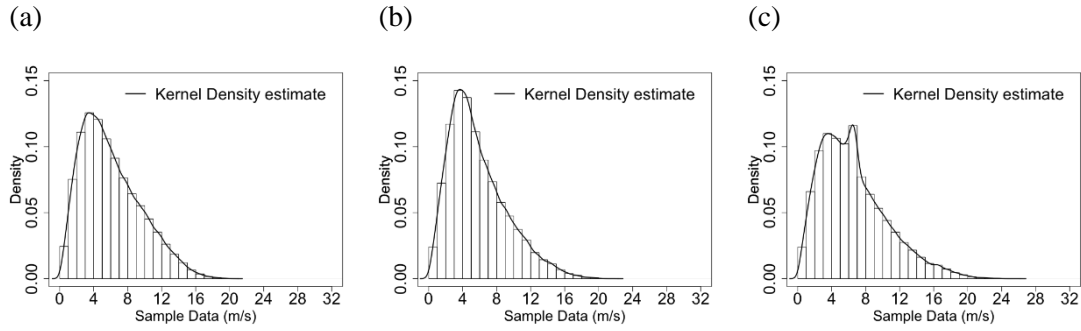
Figure 5.11: The Kernel Density estimates as an approximation to the probability density function of wind speed to the maximum available time series extending from 1961-2010 (50 years long) originated from the ERA-20C data product of relatively small resolution in (a), the moderate resolution of ERA-Interim extending from 1979-2016 (38 years long), and the high resolution database of the MARINA Platform for the period 1996–2015 (20 years). The regional locations closely arranged in the Western Mediterranean Sea are set at (42.750N 4.500E) for ERA-20C, at (42.000N 3.750E) for ERA-Interim, and at (40.800N 5.500E) for the MARINA Platform. The bandwidth of the Gaussian Kernel estimator is set at (0.2922, 0.3375, and 0.3129) for the Kernel density estimate in (a), (b), and (c) respectively based on the Silverman's 'rule of thumb', Silverman (1986, page 48, Eq. (3.31))[7]. The statistical software package (extRemes) in R (Gilleland and Katz, 2016) is used for the histogram and Kernel Density diagram illustration. (Supplementary material of Tsalis et al., 2021)

Table 5.7: Descriptive statistics for the 30 locations of the datasets used from the MARINA Platform database extending from 1996 to 2015 (20 years).

| Location | min | max | median | mean | SE mean | CI.mean 0.95 | var | std. dev | coef. var | skewness | kurtosis |
|---|---|---|---|---|---|---|---|---|---|---|---|
| L1 | 0 | 25.965 | 7.691 | 8.058 | 0.009 | 0.017 | 12.992 | 3.604 | 0.447 | 0.454 | 3.113 |
| L2 | 0 | 26.704 | 7.236 | 7.627 | 0.008 | 0.017 | 12.446 | 3.528 | 0.463 | 0.487 | 3.129 |
| L3 | 0 | 26.436 | 6.925 | 7.327 | 0.008 | 0.017 | 12.579 | 3.547 | 0.484 | 0.570 | 3.210 |
| L4 | 0 | 25.840 | 7.417 | 7.904 | 0.009 | 0.017 | 13.750 | 3.708 | 0.469 | 0.497 | 3.050 |
| L5 | 0 | 28.389 | 7.831 | 8.300 | 0.009 | 0.018 | 14.535 | 3.812 | 0.459 | 0.499 | 3.110 |
| L6 | 0 | 23.912 | 7.170 | 7.572 | 0.009 | 0.018 | 14.169 | 3.764 | 0.497 | 0.372 | 2.661 |
| L7 | 0 | 24.480 | 6.810 | 7.173 | 0.008 | 0.016 | 11.068 | 3.327 | 0.464 | 0.527 | 3.119 |
| L8 | 0 | 28.801 | 7.968 | 8.455 | 0.009 | 0.019 | 15.738 | 3.967 | 0.469 | 0.525 | 3.131 |
| L9 | 0 | 26.495 | 7.714 | 8.153 | 0.009 | 0.017 | 13.583 | 3.685 | 0.452 | 0.489 | 3.111 |
| L10 | 0 | 28.029 | 7.623 | 8.098 | 0.009 | 0.018 | 14.139 | 3.760 | 0.464 | 0.494 | 3.077 |
| L11 | 0 | 24.330 | 6.912 | 7.303 | 0.009 | 0.017 | 13.128 | 3.623 | 0.496 | 0.546 | 3.162 |
| L12 | 0 | 24.877 | 6.946 | 7.378 | 0.009 | 0.017 | 13.297 | 3.646 | 0.494 | 0.551 | 3.154 |
| L13 | 0 | 25.098 | 7.556 | 7.903 | 0.009 | 0.018 | 14.682 | 3.832 | 0.485 | 0.304 | 2.513 |
| L14 | 0 | 28.752 | 7.777 | 8.200 | 0.009 | 0.018 | 15.351 | 3.918 | 0.478 | 0.523 | 3.125 |
| L15 | 0 | 27.063 | 7.544 | 8.015 | 0.009 | 0.017 | 13.568 | 3.684 | 0.460 | 0.539 | 3.183 |
| L16 | 0 | 28.671 | 7.653 | 8.111 | 0.010 | 0.019 | 16.469 | 4.058 | 0.500 | 0.554 | 3.081 |
| L17 | 0 | 26.142 | 6.508 | 7.025 | 0.009 | 0.017 | 13.602 | 3.688 | 0.525 | 0.706 | 3.400 |
| L18 | 0 | 25.769 | 7.032 | 7.396 | 0.009 | 0.017 | 13.036 | 3.611 | 0.488 | 0.493 | 3.131 |
| L19 | 0 | 28.851 | 7.427 | 7.898 | 0.010 | 0.019 | 15.906 | 3.988 | 0.505 | 0.543 | 3.041 |

---

([7]) Silverman's 'rule of thumb': Bandwidth set at 0.9 times the minimum of the standard deviation and the interquartile range divided by 1.34 times the sample size to the negative one-fifth power.

| | | | | | | | | | | |
|---|---|---|---|---|---|---|---|---|---|---|
| L20 | 0 | 24.816 | 7.175 | 7.639 | 0.009 | 0.018 | 15.415 | 3.926 | 0.514 | 0.548 | 3.042 |
| L21 | 0 | 25.901 | 5.950 | 6.582 | 0.009 | 0.019 | 15.637 | 3.954 | 0.601 | 0.911 | 3.642 |
| L22 | 0 | 20.863 | 7.225 | 7.121 | 0.008 | 0.016 | 11.392 | 3.375 | 0.474 | 0.072 | 2.499 |
| L23 | 0 | 20.874 | 5.758 | 5.822 | 0.006 | 0.012 | 7.112 | 2.667 | 0.458 | 0.584 | 3.733 |
| L24 | 0 | 23.377 | 4.941 | 5.487 | 0.008 | 0.016 | 11.976 | 3.461 | 0.631 | 0.847 | 3.478 |
| L25 | 0 | 20.752 | 4.191 | 5.194 | 0.009 | 0.018 | 15.145 | 3.892 | 0.749 | 0.855 | 2.951 |
| L26 | 0 | 21.371 | 5.866 | 6.021 | 0.007 | 0.015 | 9.625 | 3.102 | 0.515 | 0.637 | 3.453 |
| L27 | 0 | 23.511 | 4.054 | 5.323 | 0.010 | 0.019 | 16.441 | 4.055 | 0.762 | 1.131 | 3.665 |
| L28 | 0 | 19.200 | 3.865 | 4.460 | 0.007 | 0.013 | 8.101 | 2.846 | 0.638 | 1.008 | 3.927 |
| L29 | 0 | 21.085 | 4.382 | 5.040 | 0.008 | 0.015 | 9.881 | 3.143 | 0.624 | 0.976 | 3.800 |
| L30 | 0 | 21.555 | 4.601 | 5.047 | 0.007 | 0.015 | 9.725 | 3.118 | 0.618 | 0.769 | 3.406 |

The wind speed datasets originated from the high resolution MARINA Platform database will challenge the assessment of DeCAUn for sample periods of 10 and 15 years. Notably, for this database sample periods are set from 1996 to 2010 with a 5 years forward step. For inference of the demonstration of DeCAUn in terms of the return level estimates and variability of the proposed model to sample periods of 10 and 15 years, three locations (L2, L16, and L21) are selected as a good representation of the extreme wind profile observed at the North Sea, Atlantic Ocean, and Mediterranean Sea respectively; (see the demonstration of DeCAUn to these locations in sub-Section 6.3).

In the following Figure 5.12, the wind speed time series originated from the high resolution database at locations L2, L16 and L21 is illustrated for the period 1996–2015 (20 years) as the reference dataset for the demonstration of DeCAUn. In order to ensure stationarity of the series in the same context as in the relatively small resolution database, a smoothing line (red line) was fitted to the annual maxima wind speed for better visualisation of the absence of possible temporal dependence and monotonic trends of BM. The stationarity of the time series is ensured for the 30 locations of the MARINA Platform database.

**(a)** **(b)**



**(c)**
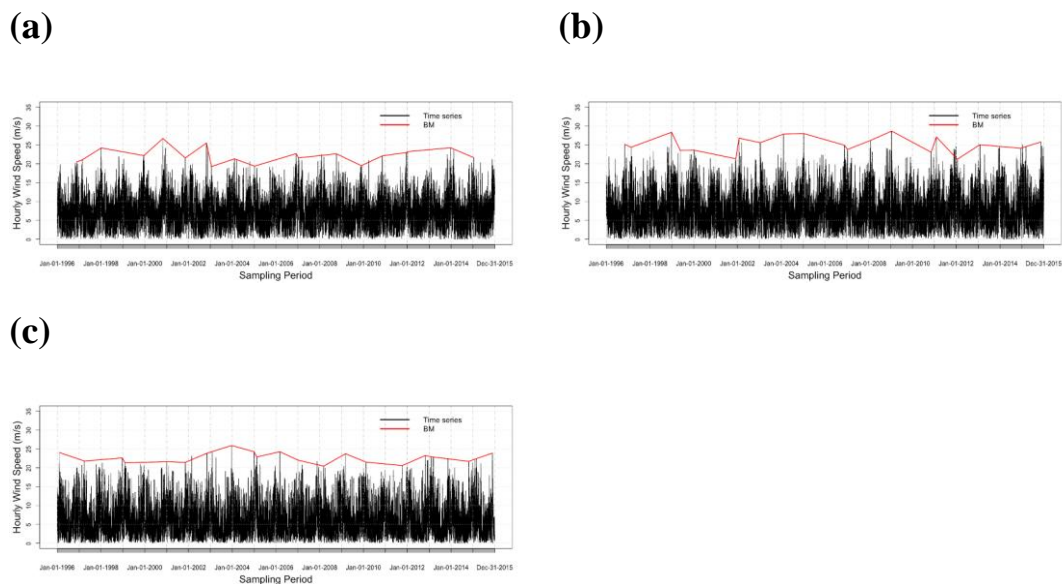


Figure 5.12: Time series and BM of wind speed for locations L2 in (a), L16 in (b) and L21 in (c) from the MARINA Platform database. The three locations are selected considering the intense wind profile that is present at these regional locations. Supplementary image of Tsalis et al., (2021)

# Chapter 6
## Results and discussion

In this Chapter, results of the demonstrastion from all models is presented and inference is made. Specifically, in sub-Section 6.1 under the proviso that the BM method is selected and the GEV distribution model is adopted, the primary aim is the identification of the combined effects of i) the sample size and the direction step of sampling of the annual maxima and ii) the comparison of the GEV parameter estimation methods to the EVA of wind speed time series. To this objective, several very common as well some less known distribution parameter estimation methods are firstly assessed through a simulation analysis. The results of the analysis showed that the maximum product of spacings (MPS), the elemental percentile (EP), the principle of ordinary entropy method (POME) or (OEM) or and, in a lesser degree, the Maximum Likelihood method (ML) or (MLE) and L-moments method (LMOM) or (LMH$_U$) unbiased method according to Hosking et al., (1985) seem to be, in general, superior to the other examined methods with respect to bias, mean squared error and variance of the estimated parameters. The effects of the estimation methods have been also assessed with respect to the n-year design values of real wind speed measurements. The obtained results suggest that the MPS and EP methods, which are rather unknown to the engineering community, describe adequately well the extreme quantiles of the wind speed fixed data samples.

Considering a variable sample period, the performance of the GEV parameter estimation methods on both the method and the available sample size is analytically performed. Firstly, a simulation study is implemented based on the ML, the L–moments (LMOM), the EP and the MPS methods for different sample sizes. It is concluded that the ML should not be taken for granted since LMOM method performs better in many respects. Afterwards, both methods are applied for the estimation of the GEV parameters of wind speed annual maxima series. LMOM method provided the best fits for the overwhelming majority of cases considered. All results illustrated in sub-Section 6.1 is a part of the work from (Soukissian and Tsalis, 2015; Soukissian and Tsalis, 2018 and Soukissian and Tsalis, 2019).

In Sub-Section 6.2, a nonstationary EVA that incorporates time as a covariate is implemented to model the distribution of the extremes in the presence of a significant trend. An attempt is made under the assumption of climate change to model one or more of the parameters of the GEV as linear or nonlinear functions of the covariates on which the wind speed data show dependence. Specifically, an assessment of various parametric models for the estimation of the GEV parameters is made, considering a linear, quadratic and sinusoidal trend through time (for the location and scale parameters) and a time independent model for the shape parameter. The common method used for the estimation of the time dependent GEV parameters is maximum likelihood (ML) method. The approximate tests of significance in the comparison between nested models are conducted by Akaike Information Criterion (AIC) and the Bayesian Information Criterion (BIC). The optimum models are penalized by the likelihood-ratio test (LR), and effective return levels for specific values of the covariates is estimated and compared with the stationary case. All results illustrated in sub-Section 6.2 is a part of the work from (Tsalis and Kallos, 2017).

Further on, in sub-Sections 6.3 and 6.4 an assessment and comparison of the classical methods analyzing the correlation (dependence) effect in samples that are irregularly spaced in time is demonstrated. In this part of the study, a re-sampling procedure is proposed for the irregularly spaced in time wind speed observations obtained from physical de-clustering considerations. The de-clustering procedure of a dependent sample of extremes from the proposed model is focused and evaluated on relatively small samples where the scarcity of long and complete time series is a common restriction in climatological studies. Finally, inference can be made of the effective sample size and the influence of the data product to the resampling strategy of DeCAUn in sub-Section 6.5. From this evaluation, the proposed model

demonstrated as an alternative model for extreme wind speed projections considering samples irregularly spaced in time, reconstructing successfully a dependent sample of extremes to an efficient independent sample converging to the i.i.d limitations

Specifically, inference is made from the challenges obtained in assessing the effect of the asymptotic distributional behavior of two types of extreme wind speed sampling data. The first type of sampling data used will be the classical BM and modeled by the GEV family of distributions. The second type used is the peaks obtained in wind speed samples exceeding a high enough threshold by the approximation to the GPD within the POT concept. The latter two distributions is proven to be the limiting distribution of the annual maxima and peak exceedances for the modeling of extremes in environmental samples, (see Nikulin et al., 2011; Papalexiou and Koutsoyiannis, 2013). For extreme value analysis, the asymptotic forms of the GEV and GPD are the most widely used statistical distributions for describing extremes of wind speed (Beirlant et al., 2004) and (Holmes, 2015). However, when the analysis is restricted to a set of cluster peak exceedances, the use of a GPD distribution with an upper bound to the modeling of extremes of wind speed requires caution in applications (Fawcett and Walshaw, 2007). It is shown that the parameter inconsistency of the MLE estimator to small samples affects the return level estimates of extremes. However, when wind speed is characterized of being heavy right-tailed and extremes are typically modeled from short-tailed distributions with finite right endpoint, the asymptotic forms of GEV and GPD can be a reasonable assumption for modeling recognizing the possible bias effect to the estimates (Fawcett and Walshaw, 2006a, 2006b; Ashkar and Tatsambon, 2007; Pinheiro and Ferrari, 2015).

The performance of the proposed DeCAUn model for relatively small wind speed samples is evaluated systematically alongside the existing DeCA, the BM and the standard Runs estimator which is assigned as the standard comparable model in this assessment. For this evaluation the standard MLE method was implemented although the MLE estimation performance is questioned in comparison to the LMOM method for environmental extreme distributions (e.g. Mazas et al., 2014). The MLE estimation approach is selected setting the discussion within the most popular framework for stationary BM and POT samples, where all results are easily comparable with those reported in the relative literature. The model results is illustrated and discussed for wind speed time series from three datasets, the MARINA Platform database, the ERA-Interim and ERA-20C respectively. All results illustrated in sub-Sections 6.3, 6.4, and 6.5 is a part of the work from (Tsalis et al., 2019) and (Tsalis et al., 2021).

## 6.1 Parameter estimation methods

In this Section results for the assessment of the most used GEV distribution parameter methods are presented for the fixed and variable sample period of examination. At each sample period considered, results in terms of the simulation study and applications is illustrated.

### 6.1.1 Fixed sample size (simulation study and applications)

Main scope of a fixed sample period study, is the assessment of the effect of the aforementioned GEV parameter estimation methods on the design values and return periods of wind speed. In order to do that, a two-stage procedure will be implemented. Firstly, a detailed simulation study will be performed for the evaluation of all examined estimation methods. Moreover, three main statistical criteria of the performance of each method will be adopted and will be assessed. Secondly, the entire group of GEV parameter estimation methods will be applied to real wind data sets, to identify the deviations in the obtained design values and associated return periods of wind speed. It should be noted that since the methods presented here are quite generic, they can be applied equally well to any other environmental parameter potentially affecting the safety of an offshore or coastal structure (sea level, wave height, etc.).

Simulation study

In this section, a simulation study has been performed based on 1000 random samples drawn from the GEV distribution with sample size 30. The sample size of 30 has been chosen as being appropriate for wind speed extreme value analysis. Most of the measured offshore wind data in the world cover a period of around up to 30 years while some established wind and wave climatologies refer, more or less, to the same time period (such as the ERA-Interim data obtained from the European Centre for Medium-Range Weather Forecasts - ECMWF). In this sub-Section, the examined estimation methods will be applied to the measured wind speed data from the Atlantic Ocean in order to quantify the uncertainties in the $n-$year wind speed design values, which are raised by the parameter estimation method of the GEV probability model. The GEV distribution parameters estimation methods that have been tested in the simulation study are the following:

1)  Ordinary moments method (OM);
2)  L-moments method according to Hosking: i) unbiased (LMH$_U$) ([8]) and ii) biased (LMH$_B$). It should be noted that LMH$_U$ estimators exist if $\xi < 1$, since the quantity $1 - \xi$ appearing in the Gamma function in relations (2.53), (2.54) and (2.55) should be positive. Hence the LMH$_U$ estimator is well defined even when the MOM estimator is not defined, i.e., for $\xi < 1/3$. In addition, the LMH$_U$ estimator is known to be better than the ML estimator for small sample cases;
3)  L-moments method according to Wang (LMW);
4)  Maximum likelihood method (ML);
5)  Maximum product of spacings method (MPS);
6)  Quantile least squares (QLS) method with different plotting positions as suggested in (Cunnane, 1978), see also relation (C.2). In this context, various values of $0 < a < 1$ are tested and the one providing the best results is finally selected;
7)  Elemental percentile method (EP);
8)  Maximum entropy parameter space expansion method (MESE).
9)  Principle of maximum or ordinary entropy method (POME) or (OEM);

The steps used for the numerical simulation analysis were the following:

**Step 1:** Generate 1000 random samples with sample size 30, choosing values for shape parameter in the range $-0.5 \leq \xi \leq +0.5$ with step 0.1, and keeping constant the values of the scale and location parameters, namely $\sigma = 1$ and $\mu = 0$, respectively.

**Step 2:** Evaluate $(\hat{\xi}_1, \hat{\xi}_2, ..., \hat{\xi}_{1000})$, $(\hat{\sigma}_1, \hat{\sigma}_2, ..., \hat{\sigma}_{1000})$, $(\hat{\mu}_1, \hat{\mu}_2, ..., \hat{\mu}_{1000})$, for the shape, scale and location parameters respectively for each of the 1000 samples and by each estimation method. If some of the estimated parameter values are not consistent with the conditions of Theorem 2.2, then these values are discarded.

**Step 3:** From the obtained parameter samples, estimate the corresponding sample means and variances, i.e.,

$$\bar{\bar{\theta}} = \frac{\sum_{i=1}^{N} \hat{\theta}_i}{N} \tag{6.1}$$

and

---

([10]) As mentioned above, the method of probability weighted moments provides the same results as the L-moments method; therefore, PWM method will not be further assessed.

$$s_{\hat{\theta}}^2 = \frac{\sum_{i=1}^{N}(\hat{\theta}_i - \bar{\hat{\theta}})^2}{N-1},\tag{6.2}$$

where $\hat{\theta}_i$, $i = 1,2,3,\ldots,N$ denotes the parameter estimates obtained from each of the $N$ samples, $\bar{\hat{\theta}}$ denotes the sample mean obtained from all samples, and $s_{\hat{\theta}}^2$ the corresponding sample variance ($\theta$ can be any of the (population) parameters $\xi$, $\sigma$ or $\mu$).

**Step 4:** Evaluate the bias, the mean squared error and the variance for the shape, scale, and location parameter for each estimation method as follows:

$$Bias = \hat{\theta} - \theta,\tag{6.3}$$

$$MSE = s_{\hat{\theta}}^2 + \left(Bias[\hat{\theta}]\right)^2,\tag{6.4}$$

Let us note that the bias measures the systematic error while the variance measures the random error.

In Figure 6.1, the bias, the mean squared error and the variance of the $\xi$ parameter for various values of $\xi$ are shown. In Figure 6.2, the same quantities are shown for the $\sigma$ parameter and in Figure 6.3 for the $\mu$ parameter.

**(a)**   **(b)**

**(c)**
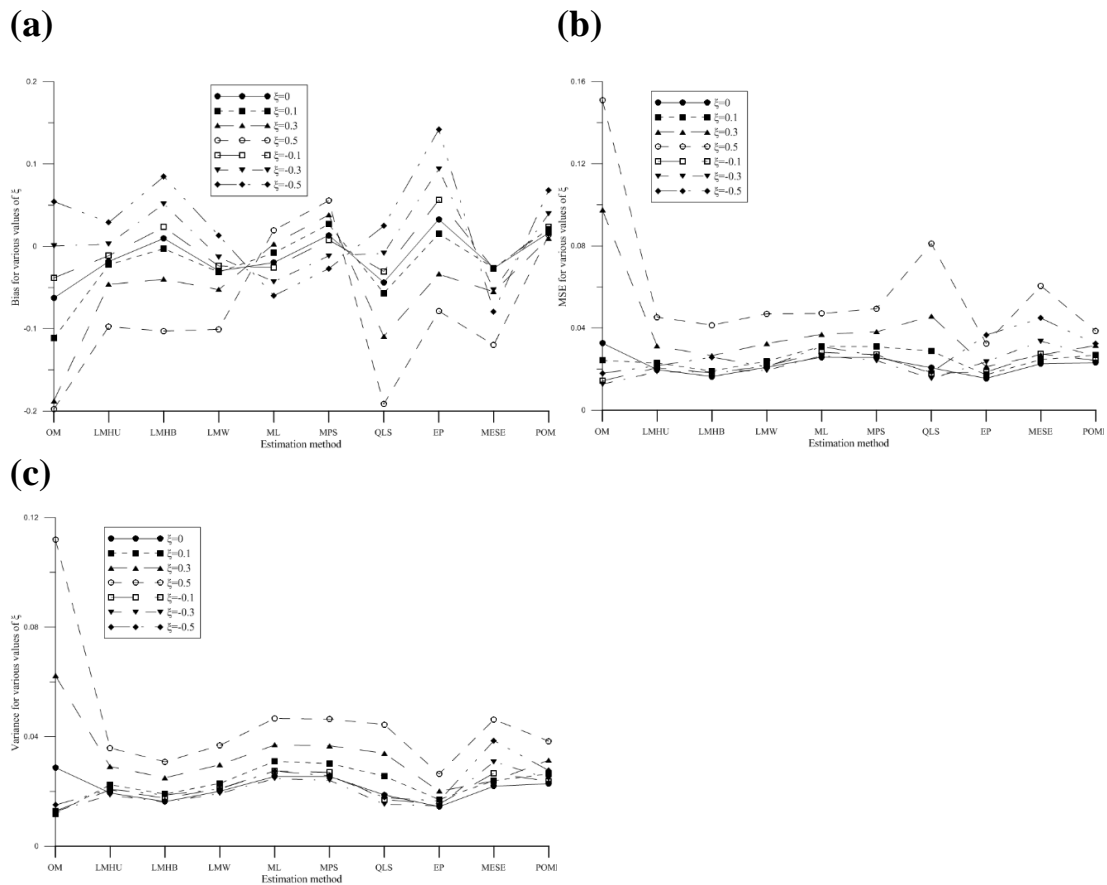


Figure 6.1: Bias (a), mean squared error (b) and variance (c) for the $\xi$ parameter obtained from simulation for various values of $\xi$. (Soukissian and Tsalis, 2015)

**(a)**

**(b)**



**(c)**
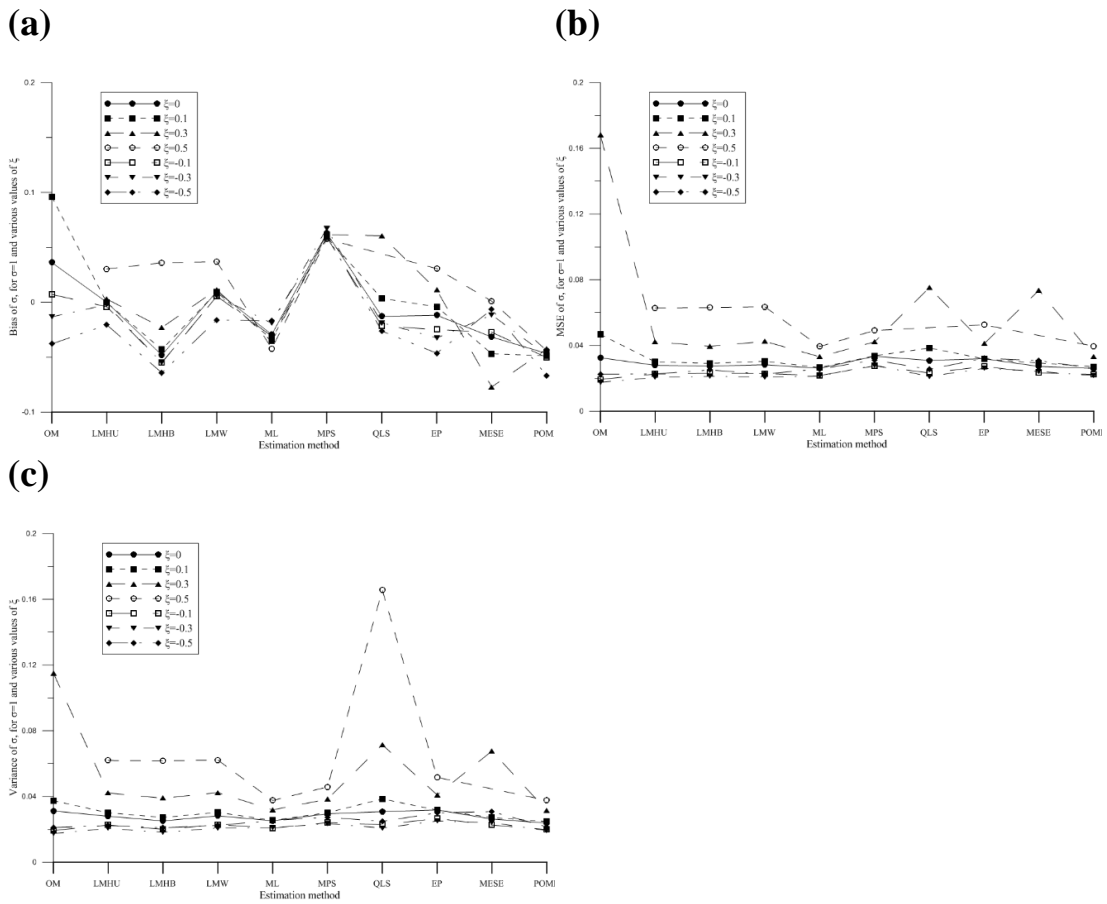


Figure 6.2: Bias (a), mean squared error (b) and variance (c) for the $\sigma$ parameter (for $\sigma = 1$) obtained from simulation for various values of $\xi$. (Soukissian and Tsalis, 2015)

**(a)**

**(b)**



91

**(c)**
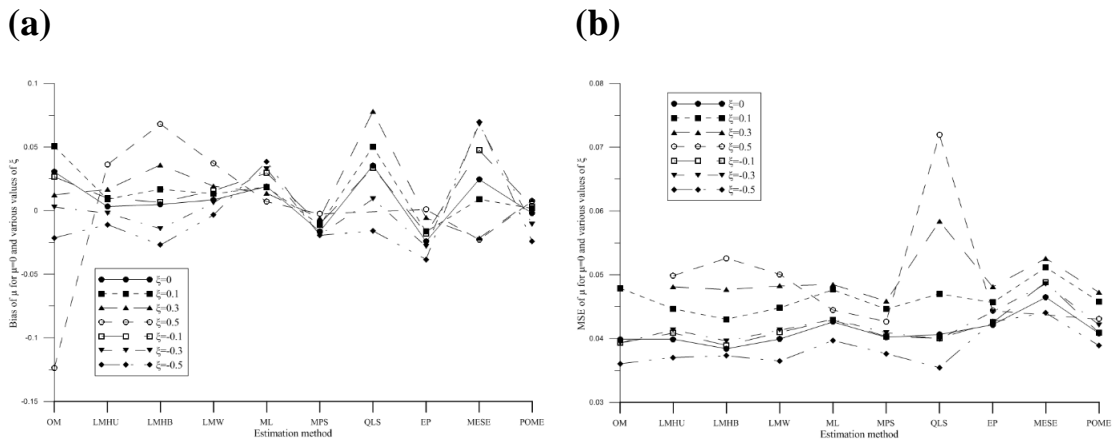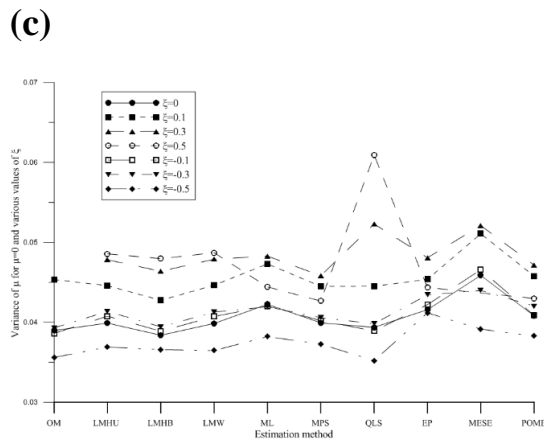


Figure 6.3: Bias (a), mean squared error (b) and variance (c) for the $\mu$ parameter (for $\mu = 0$) obtained from simulation for various values of $\xi$. (Soukissian and Tsalis, 2015)

As regards the bias in the estimation of the parameters, the following conclusions can be drawn:

- For the case of $\xi$ parameter (Figure 6.1, upper left panel), the ML, MPS and POME methods provide biases lying in a rather narrow strip of values (suggesting an almost constant bias), for all examined $\xi$ values. In the mean, the absolutely smallest biases are provided by the aforementioned methods for the entire range of $\xi$ values. In addition, the POME method provides the smallest values of bias for all $\xi$ apart from the cases $\xi = -0.3, -0.5$.
- For the case $\sigma = 1$ (Figure 6.2, upper left panel), the $LMH_U$ and LMW methods provide, in the mean, the absolutely smallest values of bias for the entire range of $\xi$ values. The method is not so efficient for the two extreme cases, $\xi = \pm 0.5$. On the other hand, the ML, MPS and POME methods provide almost constant biases for the entire range of $\xi$ values.
- For the case $\mu = 0$ (Figure 6.3, upper left panel), the MPS method provides an almost constant and very small bias (around -0.025), for the entire range of $\xi$ values. MPS and POME methods provide, in the mean, the absolutely smallest values of bias for the entire range of $\xi$ values. In addition, the POME method provides again the absolutely smallest values of bias (very close to 0) for all $\xi$ apart from the cases $\xi = -0.3, -0.5$.

As regards the mean squared error in the estimation of the GEV distribution parameters the following remarks can be derived:

- For the case of $\xi$ parameter (Figure 6.1, upper right panel), the smallest values of MSE are provided, in the mean, by the EP, POME, $LMH_U$ and $LMH_B$ methods, with EP method being the most efficient. These methods exhibit also the narrowest strips of MSE values.
- For the case $\sigma = 1$ (Figure 6.2, upper right panel), the ML, MPS, EP and POME methods are superior, providing, in the mean, the smallest MSE values among all methods for the entire range of $\xi$ values.
- For the case $\mu = 0$ (Figure 6.3, upper right panel), the ML, POME and MPS methods are the most efficient for the entire range of $\xi$ values, while EP method exhibits a fair behavior and the narrowest strip of MSE values.

As regards the variance in the estimation of the parameters the following conclusions can be drawn:

- For the case of $\xi$ parameter (Figure 6.1, lower left panel), the smallest values of variance, in the mean, are provided by the EP and LMH$_B$ methods. POME, LMH$_U$ and LMW methods also exhibit a fair behavior.
- For the case $\sigma = 1$ (Figure 6.2, lower left panel), the ML, POME, MPS and EP methods are superior, providing the smallest variances among all methods for the entire range of $\xi$ values.
- For the case $\mu = 0$ (Figure 6.3, lower left panel), many methods provide small variances. The behavior of LMH$_U$ and LMW methods is very similar. On the other hand, the ML, POME, EP and MPS methods provide, in the mean, the smallest variances among all methods for the entire range of $\xi$ values.

From the simulation analysis and the statistical parameters considered for fixed sample size inference is made for the optimum parameter estimation methods:

- Considering the bias, the most efficient estimation methods are MPS and POME. Furthermore, for the mean squared error, the most efficient estimation methods are ML, EP, MPS and POME, whist for the variance, the most efficient estimation methods are ML, POME, EP and MPS.
- Focusing on samples of wind speed where prior evidence exists of the $\xi$ parameter as negative (Brabson and Palutikof, 2000), it seems that EP, POME, MPS, and LMH$_U$ methods and, in a smaller degree, the ML method, are very reasonable solutions for all the cases and criteria examined.

## Applications

In this sub-Section $n -$year $(n = 10, 20, ..., 100)$ design values of wind speed are provided for measured data obtained from four buoys, where two buoys are located in the Pacific coast of central America and two buoys located in the North West coast of the Atlantic Ocean (see Figure 5.1). The relevant wind speed time series are available from the National Oceanic and Atmospheric Administration (NOAA). The code numbers of the buoys, the corresponding geographical locations and the measurement periods are the following:

- 41001 (34°33'40" N 72°37'50" W, 1976-2012),
- 44004 (38°29'2" N 70°25'57" W, 1977-2008),
- 46006 (40°45'16" N 137°27'51" W, 1977-2012),
- 51003 (19°1'6" N 160°34'54" W, 1984-2012).

Based on the annual maxima extracted from the above time series, the $n -$ year ($n$=10,20,…,100) design values have been estimated using BM method. The sample sizes of the annual maxima obtained from the aforementioned buoys are greater than 20, as previously discussed in sub-Section 1.1. The basic statistics of the wind data for the entire measurement period is provided in Table 5.1 in sub-Section 5.1, where samples are approximated to a size of 30 years.

Using wind speed datasets from the four locations (41001, 44004, 46006, and 51003) the GEV parameters are estimated using the methods from the simulation study. In order to obtain estimates of the standard errors and confidence intervals of the GEV parameters, we have also implemented a bootstrap approach. Though for some estimation methods confidence intervals and standard errors can be directly provided by analytic formulas, in order to treat the results in a uniform way, we prefer to provide the standard error by using a common technique for all methods. Specifically, 1000 random samples have been generated from the annual maxima data sets for each buoy using the standard non-parametric bootstrap approach; (see

sub-Section 2.4.2). Furthermore, the estimates of the standard errors as obtained from the bootstrap method for each estimation method is given in Table 6.1 (in parentheses).

Table 6.1: Parameters and 95% bootstrap standard errors (in parenthesis) of the GEV distribution for each estimation method and each buoy.

| Buoy No. Method of Estimation | 41001 | | | 44004 | | | 46006 | | | 51003 | | |
|---|---|---|---|---|---|---|---|---|---|---|---|---|
| | $\hat{\xi}$ | $\hat{\sigma}$ | $\hat{\mu}$ | $\hat{\xi}$ | $\hat{\sigma}$ | $\hat{\mu}$ | $\hat{\xi}$ | $\hat{\sigma}$ | $\hat{\mu}$ | $\hat{\xi}$ | $\hat{\sigma}$ | $\hat{\mu}$ |
| OM | -0.3563 | 4.0415 | 21.0555 | -0.0424 | 2.4564 | 21.1969 | -0.1140 | 3.0545 | 21.0228 | 0.0635 | 1.0302 | 13.8228 |
| | (0.139) | (0.710) | (0.671) | (0.074) | (0.382) | (0.468) | (0.093) | (0.468) | (0.566) | (0.097) | (0.199) | (0.208) |
| $LMH_U$ | -0.2999 | 3.8826 | 20.9699 | 0.0012 | 2.3874 | 21.1346 | -0.0804 | 2.9854 | 20.9717 | 0.1483 | 0.9436 | 13.7807 |
| | (0.139) | (0.657) | (0.658) | (0.114) | (0.364) | (0.465) | (0.126) | (0.481) | (0.566) | (0.142) | (0.175) | (0.209) |
| $LMH_B$ | -0.2616 | 4.0237 | 20.8220 | -0.0126 | 2.6504 | 21.0185 | -0.0760 | 3.1929 | 20.8551 | 0.0865 | 1.1759 | 13.6980 |
| | (0.127) | (0.636) | (0.663) | (0.098) | (0.345) | (0.459) | (0.112) | (0.452) | (0.561) | (0.117) | (0.168) | (0.208) |
| LMW | -0.2558 | 3.7929 | 20.8919 | 0.0693 | 2.2325 | 21.0634 | -0.0275 | 2.8562 | 20.9007 | 0.2633 | 0.8092 | 13.7377 |
| | (0.146) | (0.683) | (0.656) | (0.110) | (0.368) | (0.459) | (0.126) | (0.490) | (0.562) | (0.122) | (0.174) | (0.204) |
| ML | -0.3174 | 3.9891 | 21.0054 | -0.0171 | 2.3505 | 21.1905 | -0.1379 | 3.0559 | 21.0828 | 0.1499 | 0.9225 | 13.8005 |
| | (0.151) | (0.706) | (0.693) | (0.147) | (0.342) | (0.478) | (0.158) | (0.512) | (0.562) | (0.186) | (0.146) | (0.223) |
| MPS | -0.3061 | 4.3940 | 20.8388 | 0.0110 | 2.5828 | 21.1113 | -0.1216 | 3.3749 | 20.9751 | 0.2043 | 1.0076 | 13.7682 |
| | (0.156) | (0.771) | (0.687) | (0.148) | (0.368) | (0.473) | (0.158) | (0.561) | (0.561) | (0.189) | (0.158) | (0.218) |
| QLS | -0.3098 | 3.6101 | 21.1035 | -0.0537 | 2.3332 | 21.2575 | -0.1251 | 2.9062 | 21.0972 | 0.1485 | 0.9158 | 13.8077 |
| | (0.125) | (0.621) | (0.671) | (0.092) | (0.407) | (0.474) | (0.098) | (0.493) | (0.568) | (0.140) | (0.208) | (0.215) |
| EP | -0.1639 | 3.6936 | 20.7921 | 0.0137 | 2.5019 | 21.0772 | -0.0606 | 3.1954 | 20.8310 | 0.2414 | 0.9827 | 13.7634 |
| | (0.136) | (0.570) | (0.663) | (0.116) | (0.380) | (0.487) | (0.121) | (0.511) | (0.579) | (0.131) | (0.181) | (0.209) |
| MESE | -0.3844 | 4.4447 | 21.3780 | -0.0191 | 2.3683 | 21.2079 | -0.1597 | 3.2223 | 21.2304 | 0.1387 | 0.9028 | 13.7774 |
| | (0.270) | (1.278) | (0.717) | (0.142) | (0.442) | (0.512) | (0.180) | (0.685) | (0.612) | (0.145) | (0.141) | (0.219) |
| POME | -0.3895 | 4.1855 | 21.1924 | -0.0118 | 2.3505 | 21.1856 | -0.1700 | 3.1199 | 21.1480 | 0.1609 | 0.9178 | 13.7945 |
| | (0.182) | (0.774) | (0.644) | (0.147) | (0.327) | (0.477) | (0.182) | (0.540) | (0.547) | (0.164) | (0.134) | (0.218) |

The most intractable parameter in the relevant wind speed extremes literature (but also for other geophysical parameters) is undoubtedly $\xi$. There are a lot of controversies as regards the values that this parameter may or is feasible to take. In the relevant discussion in Palutikof et al., (1999), it is stated that "In the light of these conflicting views, it is difficult to offer advice on the choice of distribution type". In addition, the same authors note that "if the assumption that the distribution type is FT-I rather than FT-III is incorrect, then the resulting errors should lead to an overestimate of return period extremes, which, from the safety point of view, is desirable". The estimation of the standard error and the 95 % bootstrap confidence interval (CI) for $\xi$ parameter in particular may also provide further suggestions as regards the specific type of the asymptotic extreme distribution. As regards to the estimates of the GEV distribution parameters in Table 6.1 the following remarks can be derived:

- For the examined cases, all estimation methods seem to provide consistent results as regards the $\xi$ values. $\xi$ is clearly lower than 0 for buoy 41001, almost 0 and very close to 0 for buoys 44004 and 46006, respectively, and slightly above 0 for buoy 51003. However, for all buoys (except for 41001), the 95 % bootstrap CIs obtained by all estimation methods include zero. For buoy 41001, the 95 % bootstrap CIs obtained by OM, LMHU, LMHB, ML, QLS and MESE methods do not include zero.
- As a remark, it would be risky to overlook the results that are provided consistently by all estimation methods and select another type of extreme value distribution. Moreover, it should be reminded that the present work emphasizes in evaluating the performance of the various parameter estimation methods and not in the estimation of the inherent uncertainties.

From the simulation analysis of the parameter estimation methods and application in extremes of wind speed for the four buoys respectively, return levels (design values) at the corresponding return periods from 10 to 100 years are obtained in Figure 6.4.

**(e)**



**(f)**



**(g)**



**(h)**
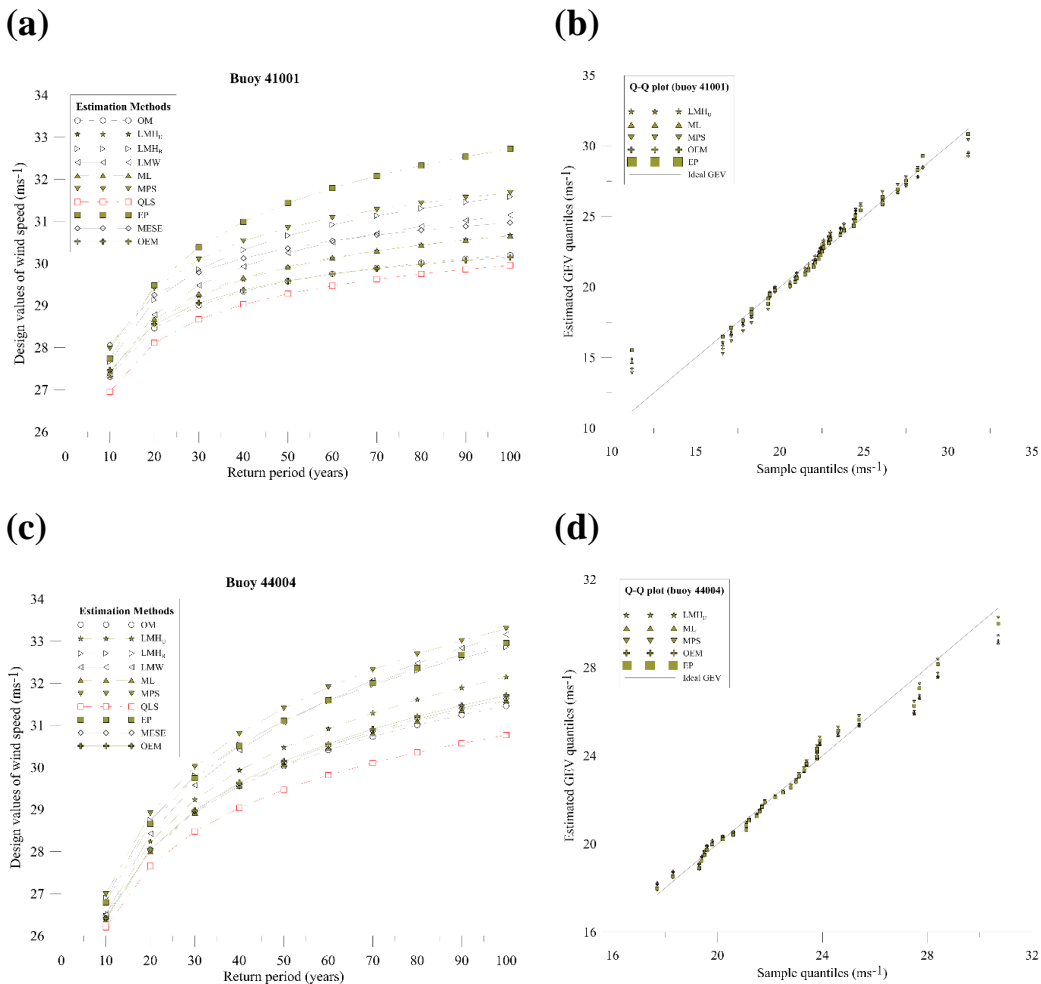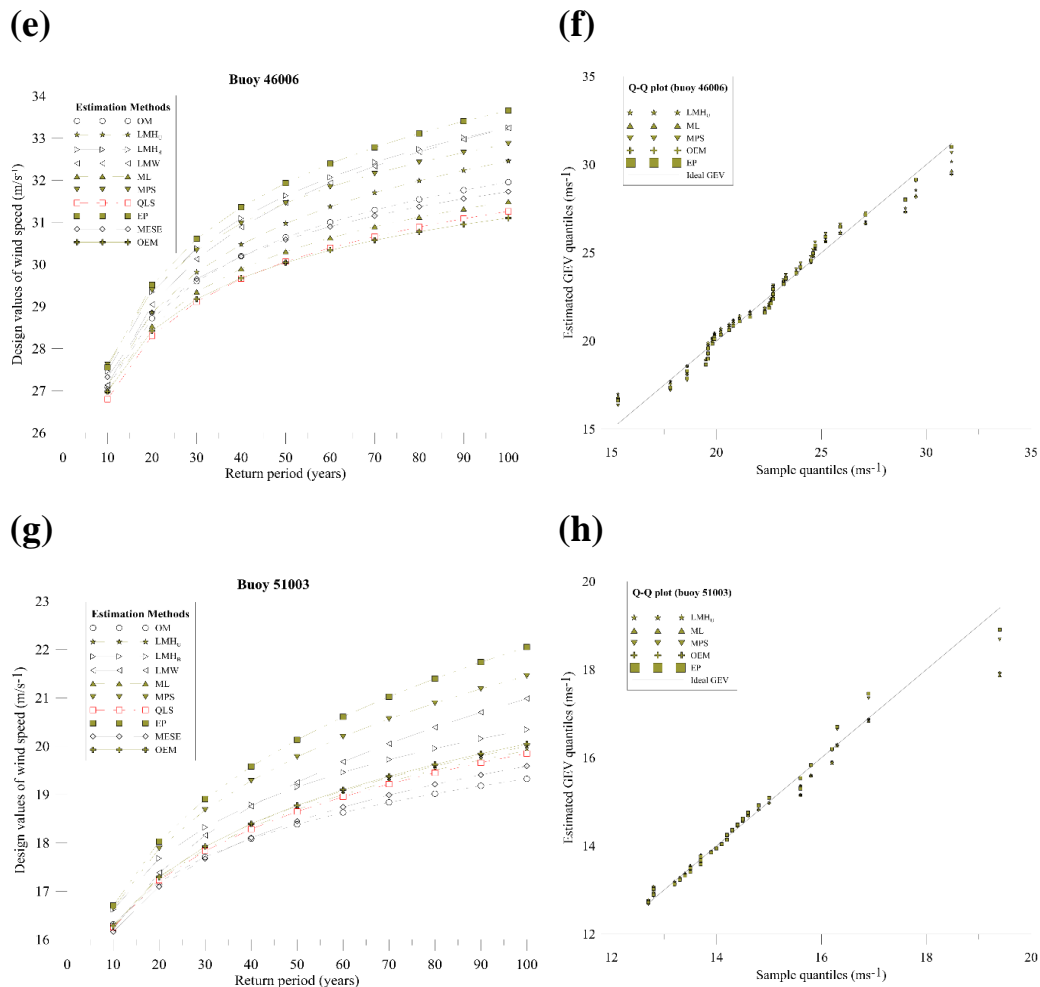


Figure 6.4: Design values of wind speed and associated return periods for buoys 41001, 44004, 46006 and 51003 in (a,c,e and g) and the corresponding Q–Q plots in (b, d, f and h) respectively. The colored red dot line outlines the QLS as the parameter estimation method that underestimates the return levels. The colored olive lines outline the optimum parameter estimation methods derived from the simulation study. (Soukissian and Tsalis, 2015)

In the right panels of the same figures of 6.4 (b,d,f and h), the Q–Q plots of OEM, $LMH_U$, ML, MPS and EP methods are provided. If the empirical data align closely with the modelled estimates, then it is likely that the chosen parameter method for the samples of wind speed is a good representation of the true extreme asymptotic form for these samples. As regards to the design value estimates of Figure 6.4 the following remarks can be derived:

- Regarding the extreme quantiles of the GEV distribution (right tail), the MPS and EP methods provide results that are systematically closer to the theoretical GEV line than the other methods (except for buoy 51003, where EP and MPS methods perform better only for the most extreme quantile)
- for buoy 41001, all methods perform sufficiently well for the entire range of quantiles;
- for buoys 44404 and 46006, all methods perform well for the left tail and the medium range of quantiles, while only EP and MPS methods perform well for the right tail with respect to to the theoretical GEV line
- for buoy 51003, all methods perform very well for the left tail; for the right tail with respect to to the theoretical GEV line, $LMH_U$, ML and OEM methods perform fair

(except for the most extreme quantile), providing very similar quantile values, while MPS and EP methods perform better for the most extreme quantile.

In addition to the Q–Q plots of the performance of the parameter estimation methods the statistical goodness-of-fit criteria provided below reveal some additional features of good performance. For the overall numerical evaluation of the obtained fits via the different estimation methods, two different measures of the goodness of fit are implemented:

a)  the standard error of fit (SEF) is defined as, (Kite, 1988):

$$SEF = \sqrt{\frac{\sum_{i=1}^{N}(x_i - \hat{x}_i)^2}{N - n_P}}, \qquad (6.5)$$

and

b)  the mean absolute relative deviation (MARD) that is defined as, (Jain and Singh, 1987):

$$MARD = \frac{100}{N}\sum_{i=1}^{N}\left|\frac{x_i - \hat{x}_i}{x_i}\right|, \qquad (6.6)$$

where $x_i$ are the available values of the sample (i.e., the sample annual maxima), $\hat{x}_i$ are the values estimated by the fitted distribution corresponding to the same return periods of the sample values, $N$ is the size of the available sample, and $n_P$ is the number of parameters of the GEV distribution function (i.e., $n_P = 3$).

In Table 6.2, the values of the aforementioned measures of goodness of fit are provided. The minimum values of the above parameters are shown in bold. Regarding the MARD criterion, EP method provides the best fit for two buoys (41001, 51003) and the second best fit for the other two buoys, MPS method provides the best fit for buoy 44004 and the second best fit for buoy 51003, and LMW method provides the best fit for buoy 46006 and the second best fit for buoy 41001. Regarding the SEF criterion, EP method provides the best fit for two buoys (46006, 51003) and the second best fit for buoy 44004, LMHB method provides the best fit for buoy 41001 and the second best fit for buoy 46006, and MPS method provides the best fit for buoy 44004 and the second best fit for buoy 51003. Taking into account the above results, it can be concluded that EP and MPS methods provide the overall best fits to the examined annual maxima wind speeds.

Table 6.2: Values of SEF and MARD goodness of fit criteria for all GEV parameter estimation methods.

| Buoy No. | 41001 | | 44004 | | 46006 | | 51003 | |
|---|---|---|---|---|---|---|---|---|
| Method of estimation | SEF | MARD | SEF | MARD | SEF | MARD | SEF | MARD |
| OM | 0.778 | 2.486 | 0.524 | 1.301 | 0.584 | 1.778 | 0.355 | 0.942 |
| LMH$_U$ | 0.785 | 2.357 | 0.483 | 1.287 | 0.563 | 1.688 | 0.320 | 0.850 |
| LMH$_B$ | **0.760** | 2.506 | 0.421 | 1.272 | 0.509 | 1.705 | 0.288 | 1.262 |
| LMW | 0.794 | 2.317 | 0.473 | 1.400 | 0.558 | **1.653** | 0.318 | 1.138 |
| ML | 0.769 | 2.420 | 0.544 | 1.347 | 0.625 | 1.844 | 0.334 | 0.891 |
| MPS | 0.794 | 3.097 | **0.391** | **1.162** | 0.539 | 1.978 | 0.208 | 0.826 |
| QLS | 0.905 | 2.408 | 0.638 | 1.469 | 0.690 | 1.861 | 0.342 | 0.912 |
| EP | 0.833 | **2.287** | 0.405 | 1.201 | **0.504** | 1.687 | **0.195** | **0.806** |
| MESE | 0.899 | 3.284 | 0.532 | 1.328 | 0.611 | 2.125 | 0.381 | 1.032 |
| POME | 0.790 | 2.600 | 0.532 | 1.335 | 0.654 | 1.979 | 0.324 | 0.872 |

Taking into consideration over- and under-design criteria for the behavior of the parameter estimation methods of the GEV distribution, the corresponding 50- and 100-year wind speed design values for each examined buoy are presented in Table 6.3. The differences between the maximum and the minimum 100-year design values are shown for the examined locations along with the estimation methods in parentheses. The methods that seem to provide higher 100-year design values (with respect to the other methods) are the EP (for buoys 41001, 46006 and 51003) and the MPS (for buoy 44004). The method that generally provides lower 100-year design values is QLS (for buoys 41001, 44004). The relative differences between the maximum and the minimum 100-year design values are the following: for buoy 41001, 8.46 %, for buoy 44004, 7.6 %, for buoy 46006, 7.59 %, and for buoy 51003, 12.36 %. On the other hand, the method that provides results lying in-between the results provided by all estimation methods is $LMH_U$ for buoys 44004 and 46006, LMW for buoy 41001 and $LMH_B$ for buoy 51003.

Table 6.3: The 50 and 100-years design values for wind speed (ms$^{-1}$) calculated with various GEV parameter estimation methods in buoys 41001, 44004, 46006 and 51003.

| Buoy no. | 41001 | | 44004 | | 46006 | | 51003 | |
|---|---|---|---|---|---|---|---|---|
| **50 and 100 years design values (ms$^{-1}$)** | | | | | | | | |
| Estimation methods | **50** | **100** | **50** | **100** | **50** | **100** | **50** | **100** |
| OM | 29.574 | 30.196 | 30.031 | 31.463 | 30.643 | 31.957 | 18.384 | 19.326 |
| $LMH_U$ | 29.906 | 30.667 | 30.473 | 32.149 | 30.974 | 32.457 | 18.764 | 20.000 |
| $LMH_B$ | 30.661 | 31.586 | 31.110 | 32.864 | 31.636 | 33.250 | 19.156 | 20.342 |
| LMW | 30.255 | 31.149 | 31.067 | 33.160 | 31.468 | 33.242 | 19.251 | 20.984 |
| ML | 29.931 | 30.655 | 30.063 | 31.590 | 30.305 | 31.493 | 18.692 | 19.911 |
| MPS | 30.846 | 31.682 | 31.409 | 33.298 | 31.460 | 32.865 | 19.781 | 21.458 |
| QLS | 29.278 | 29.954 | 29.471 | 30.768 | 30.070 | 31.263 | 18.649 | 19.851 |
| EP | 31.439 | 32.724 | 31.106 | 32.958 | 31.936 | 33.660 | 20.134 | 22.051 |
| MESE | 30.360 | 30.967 | 30.113 | 31.638 | 30.587 | 31.728 | 18.451 | 19.588 |
| POME | 29.587 | 30.146 | 30.149 | 31.710 | 30.046 | 31.104 | 18.778 | 20.048 |
| Diff. max-min of 100-year design value | | 2.770 (EP-QLS) | | 2.530 (MPS-QLS) | | 2.556 (EP-POME) | | 2.725 (EP-OM) |

As regards to the design value estimates the following remarks can be derived for ML method, which is the most commonly used in GEV parameter estimation and the MPS and EP methods, which are rather unknown to the engineering community. Taking as reference the mean value of all 100-year design wind speeds as provided by all the examined estimation methods, ML provides results that are systematically below the mean, i.e., 1.03 % for buoy 41001, 1.77 % for buoy 44004, 2.50 % for buoy 46006 and 2.19 % for buoy 51003. On the contrary, the MPS method provides results that are systematically greater than the mean, i.e., 2.24 % for buoy 41001, 3.42 % for buoy 44004, 1.71 % for buoy 46006 and 5.14 % for buoy 51003. Similarly, the EP method also provides results that are systematically greater than the mean, i.e., 5.35 % for buoy 41001, 2.42 % for buoy 44004, 4.03 % for buoy 46006 and 7.69 % for buoy 51003.

It can be also concluded that for the 100-year design values, the corresponding relevant absolute differences between ML and MPS methods are 3.24 % for buoy 41001, 5.13 % for buoy 44004, 4.18 % for buoy 46006 and 7.21 % for buoy 51003. The relevant absolute

differences between ML and EP methods are 6.32 % for buoy 41001, 4.15 % for buoy 44004, 6.44 % for buoy 46006 and 9.71 % for buoy 51003. The above results suggest that the relevant differences between ML and MPS are generally smaller than the differences between ML and EP methods.

The aim of this part of this study was the assessment of the most popular, along with some less popular, (or even unknown to the wider ocean and coastal engineering communities), methods for the estimation of the parameters of the GEV distribution. The analysis was based on a simulation study for fixed sample size and application of the estimation methods to wind speed datasets from four buoys located in the Atlantic and Pacific Ocean basins. From a statistical point of view, MPS, EP and POME methods meet important requirements satisfactorily, but when the design values are of significance importance, these three methods lead to over-design. In this respect, ML and LMH$_U$ method leads to slight under-design.

## 6.1.2 Variable sample size (simulation study and applications)

In this Section, the simulation and comparison of ML, MPS, EP and LMOM estimators is performed for different sample sizes ranging from 20 to 50. The considered small to medium sample sizes roughly correspond to the usually available sample sizes in relevant met-ocean applications. The LMOM method is also included since it has been suggested by other authors that it is more suitable, especially for small sample sizes; see e.g. (Hosking et al., 1985 and Hosking, 1990). For the evaluation of each estimation method performance four statistical criteria are adopted. Two of these criteria refer to the evaluation of each parameter estimate; in this respect, let it be noted that it is common ground in the relevant literature to evaluate one-by-one the parameter estimates of the GEV distribution. The other two criteria that are adopted (average absolute difference and average of the maximum absolute difference) refer to the overall evaluation of the combined effects of all parameter estimates with respect to the true and the estimated GEV cdf. The simulation part of this work essentially complements and completes the work of (Soukissian and Tsalis, 2015) and prepares the ground for the assessment of wind speed design values.

Simulation Study

In this section, the simulation study is presented in detail with the obtained results. The aim of the simulation is to assess and evaluate the performance of each examined estimation method with respect to the available sample size of maxima. Since the acquired sample sizes of AM in wind energy and metocean applications is usually of the order of 20–30, and the required return periods are of the order of 30–50 years, design values in the particular range (i.e. 20, 25, …, 50) are considered.

Each simulation run produces $N = 1000$ random samples of size $n_B = 20, 25, …50$, drawn from a GEV cdf $F(x; n_B, \boldsymbol{\theta})$, with fixed location and scale parameters ($\mu = 0$, $\sigma = 1$). The shape parameter $\xi$ lies in the range $[-0.25, 0.25]$ with a 0.05 step. The limits of this range are derived according to the EVA of wind speed presented in the latter Sections. For each considered value of $\xi$, $\widehat{\boldsymbol{\theta}}$ is estimated from each of the 1000 random samples (of size $n_B$) produced and the corresponding sample mean values and variances (of $\widehat{\boldsymbol{\theta}}$) are calculated. The metrics adopted for the evaluation of the performance of each method with respect to sample size, are the bias and the mean squared error. $\widehat{F}(x; n_B, \widehat{\boldsymbol{\theta}})$ denotes the corresponding estimated GEV distribution function.

Specifically, the simulation analysis can be described as follows:

**Step 1:** Specify a value for the sample size $n_B(n_B = 20,25, \ldots, 50)$ and another one for the shape parameter $\xi \in [-0.25, 0.25]$.

**Step 2:** Generate $N = 1000$ random samples each of size $n_B$ from a GEV distribution (with fixed $\mu = 0$, $\sigma = 1$ and $\xi$ as was selected in Step 1).

**Step 3:** Evaluate $\hat{\theta}_{j,n_B}$, $j = 1,2, \ldots, 1000$, for the considered sample, by implementing the examined estimation methods. $\hat{\theta}_{j,n_B}$ denotes any of the three parameters of the GEV distribution (i.e. location $\mu$, scale $\sigma$ or shape $\xi$ parameter) as is estimated from the $j$ −th random sample, $j = 1,2, \ldots, 1000$, with size $n_B$.

**Step 4:** From the obtained samples of the distribution parameters ($\hat{\theta}_{j,n_B}$, $j = 1,2, \ldots, 1000$) estimate the corresponding sample means and variances, i.e.

$$\bar{\bar{\theta}}_{n_B} = \frac{1}{N}\sum_{j=1}^{N}\hat{\theta}_{j,n_B}, \text{ and } s_{\hat{\theta}_{n_B}}^2 = \frac{1}{N-1}\sum_{j=1}^{N}\left(\hat{\theta}_{j,n_B} - \bar{\bar{\theta}}_{n_B}\right)^2, \tag{6.7}$$

where $\bar{\bar{\theta}}_{n_B}, s_{\hat{\theta}_{n_B}}^2$ denote the sample mean and the corresponding sample variance, respectively. Using the estimates from **Step 4** confidence intervals covering the parameters are derived as

$$\left(\bar{\bar{\theta}}_{n_B} - 1.96\frac{s_{\hat{\theta}_{n_B}}}{\sqrt{N}}, \bar{\bar{\theta}}_{n_B} + 1.96\frac{s_{\hat{\theta}_{n_B}}}{\sqrt{N}}\right). \tag{6.8}$$

**Step 5:** Evaluate the bias and the mean squared error (MSE) for each distribution parameter, and estimation method, as follows:

$$Bias(n_B) = \hat{\theta}_{n_B} - \theta, \ MSE(n_B) = s_{\hat{\theta}_{n_B}}^2 + \left(Bias[\hat{\theta}_{n_B}]\right)^2, \tag{6.9}$$

for $\theta = \mu = 0$ and $\theta = \sigma = 1$.

In order to consider the combined effects of all parameter estimates along with the examined sample sizes, the following measures, suggested by (Castillo and Hadi, 1995 a,b), are also considered:

1) The average absolute difference $D_{abs}$ between the true (initial) and the estimated distribution function taking into consideration all the randomly generated samples, i.e.:

$$D_{abs} = \frac{1}{Nn_B}\sum_{j=1}^{N}\sum_{\text{for all }n_B}\left|F(x_j; n_B, \boldsymbol{\theta}) - \hat{F}(x_j; n_B, \hat{\boldsymbol{\theta}})\right|, \tag{6.10}$$

and

2) the average of the maximum absolute difference $D_{\max}$ between the true and the estimated distribution function within each sample, i.e.:

$$D_{\max} = \frac{1}{N}\sum_{j=1}^{N}\max_{n_B}\left|F(x_j; n_B, \boldsymbol{\theta}) - \hat{F}(x_j; n_B, \hat{\boldsymbol{\theta}})\right|. \tag{6.11}$$

**Step 6:** If the considered values of $\xi$ are exhausted, then select a different value for $n_B$ and repeat the procedure. Otherwise, repeat the procedure for a different value of $\xi$.

At the end of the simulation, the behaviour of bias and MSE is obtained along with the values of $D_{abs}$ and $D_{\max}$ with respect to the examined parameter estimation methods and sample sizes. Implementing the above described procedure, the results of the numerical simulation study with respect to the different values of $\xi$ are obtained. Firstly, the results regarding the estimates of the parameters $\mu, \sigma$ and $\xi$ are presented and evaluated by using bias

and MSE. Secondly, the results regarding the performance of the total GEV fits derived by using $D_{abs}$ and $D_{\max}$ are provided and discussed.

The effects of the sample size on the estimation of location parameter

In Figure 6.5, the bias (left panel) and the MSE (right panel) of the location parameter $\mu$ (as estimated by the examined methods) with respect to sample size is shown. Let it be reminded that the random samples are generated from a GEV distribution with $\mu = 0$. It can be noted that bias and MSE curves follow fairly the same trend with respect to the examined estimation methods. Regarding the absolute bias, it seems that it does not tend in a definite way towards zero. Therefore, the simulation study was extended to larger sample sizes (not presented here) and the decrease of the absolute bias was eventually more pronounced for all methods.

**(a)**



**(b)**



**(c)**



**(d)**



**(e)**



**(f)**

**(g)**                                **(h)**
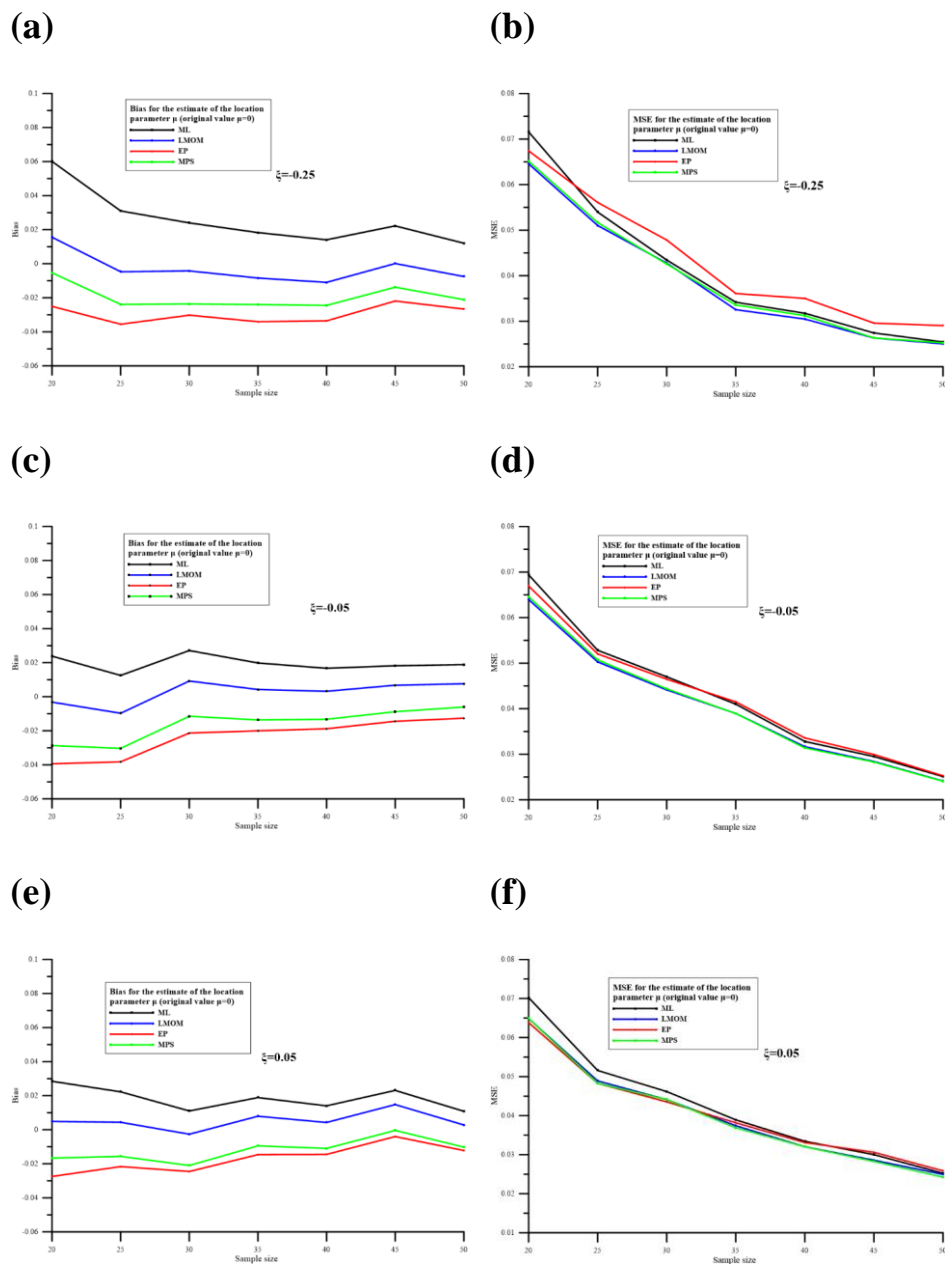


Figure 6.5: Bias in (a,c,e, and g) and MSE in (b,d,f, and h) of location parameter $\mu$ (for $\xi = -0.25, -0.05, 0.05, 0.25$) with respect to sample size obtained from all parameter estimation methods. (Soukissian and Tsalis, 2018)

Moreover, it can be concluded that for all examined values of $\xi$, LMOM performs better, since it provides the smallest absolute bias. This is also true for the smaller sample sizes examined. For $\xi = 0.25$, LMOM performs better for sample sizes up to 40, while for sample sizes greater than 40, EP and MPS perform slightly better. Finally, MPS provides systematically positive values for bias, while EP and ML provide negative.

Regarding MSE, its behaviour is much more systematic. It exhibits a clearly decreasing trend towards zero for all estimation methods and values of $\xi$, as the sample size increases. This behaviour suggests that the effect of the variance in Equation (6.7) plays a major role in the calculation of MSE (Equation (6.9), shaping in a great extent, its clearly decreasing behaviour. The provided curves suggest that LMOM provides overall the smallest values of MSE. Another interesting feature is that, for small sample sizes, ML provides the greatest values of MSE. For increasing values of $\xi$ and sample size, the MSE curves corresponding to the different estimation methods are hardly distinguishable.

From the simulation study considering $\xi \in [-0.25, 0.25]$, the mean values and the 95% confidence intervals (CI) of the mean (described in the previous Step 4) of location parameter $\mu$ are illustrated with respect to sample size in Figure 6.6. The narrowest 95% CI widths are provided by LMOM and MPS for all values of $\xi$. For $\xi = 0.25$, the CI widths become very similar. All methods have a clearly decreasing trend towards zero as the sample size increses. It is clear that for negative values of $\xi$ =-0.25 and -0.05, where strong evidence of negative values exists in modeling extreme wind speed (An and Pandey, 2007), ML and LMOM methods have a clearly decreasing trend towards zero following by the smoothly decreasing width of the CI as the sample size increases.

Figure 6.6: Mean values and 95% CI of location parameter $\mu$ (for $\xi = -0.25, -0.05, 0.05, 0.25$) in (a,b,c, and d) respectively to sample size obtained from all parameter estimation methods. (Soukissian and Tsalis, 2018)

The effects of the sample size on the estimation of scale parameter

In Figure 6.7, the bias (left panel) and the MSE (right panel) of the scale parameter $\sigma$ with respect to the sample size is shown (note that the random samples were generated from a GEV distribution with $\sigma = 1$). For the same reasons as stated above, the simulation study was extended to larger sample sizes and the decrease of the absolute bias was evident for all methods. It is concluded that LMOM performs clearly better for all values of $\xi$ and sample sizes (except for $\xi = 0.25$, where EP performs slightly better). MPS method provides, in absolute terms, the largest values of bias.

Regarding MSE, LMOM, and ML methods perform better providing very similar values of MSE for negative values of $\xi$; however, for $\xi = 0.25$, LMOM provides the largest values of MSE. For $\xi > 0$, ML method performs better for all examined sample sizes.

**(a)**

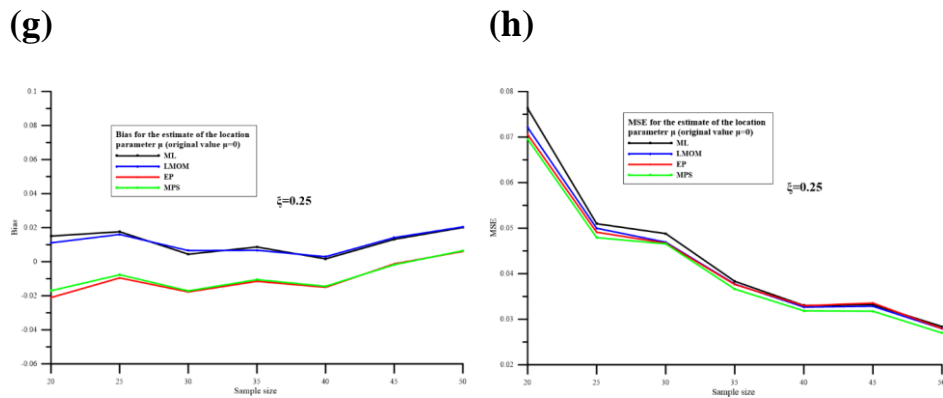**(b)**

**(c)**

**(d)**

**(e)**

**(f)**

**(g)**

**(h)**
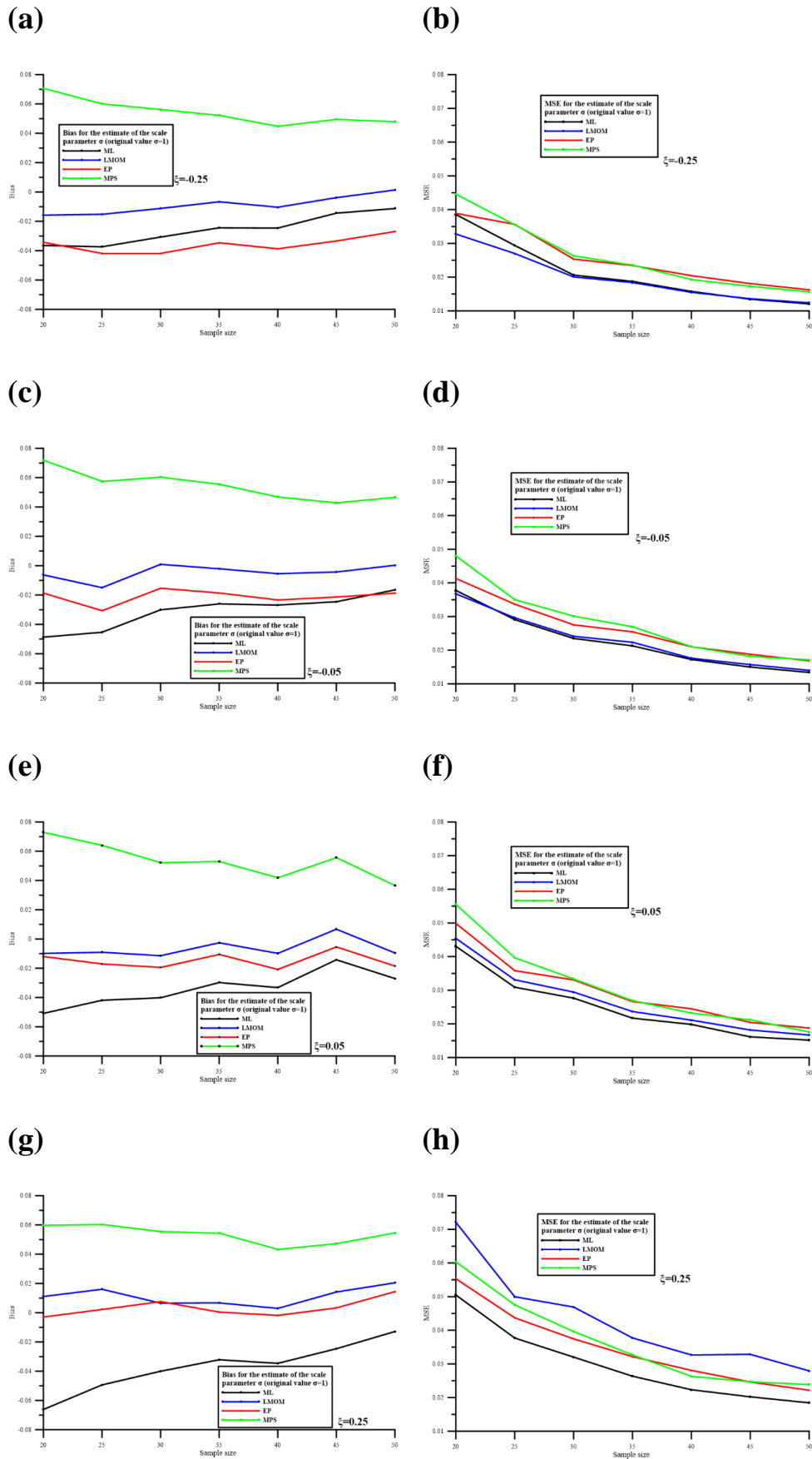
Figure 6.7: Bias in (a,c,e and g) and MSE in (b,d,f , and h) of scale parameter $\sigma$ (for $\xi = -0.25, -0.05, 0.05, 0.25$) with respect to sample size obtained from all parameter estimation methods. (Soukissian and Tsalis, 2018)

In the same context as in the parameter estimates of the location inferred in Figure 6.6, from the simulation study considering $\xi \in [-0.25, 0.25]$, the mean values and the 95% confidence intervals of the mean estimates of the scale parameter $\sigma$ are illustrated with respect to sample size in Figure 6.8. The narrowest 95% CI widths are provided by MLE and LMOM for $\xi = -0.25, -0.05, 0.05$, and MLE and MPS for $\xi = 0.25$. MLE method provides systematically the narrowest 95% CI. All methods assessed in this setting have a clearly decreasing trend towards $\sigma=1$ as the sample size increses. The decreasing trend in the scale estimates indicates a successfully simulation as the random samples enforced to all methods are generated from a GEV distribution of scale parameter set to unit value. The demonstration of LMOM shows the smoother decreasing rate towards $\sigma=1$ as the sample size increases. Inference is also made to the statndard ML method demonstrating a smooth decreasing rate of the scale parameter for sample sizes greater than 35 indicating the intractable problem of inference for smaller sample sizes, i.e., samples of 20 to 35; (Kharin and Zwiers, 2000; Kunz et al., 2010).
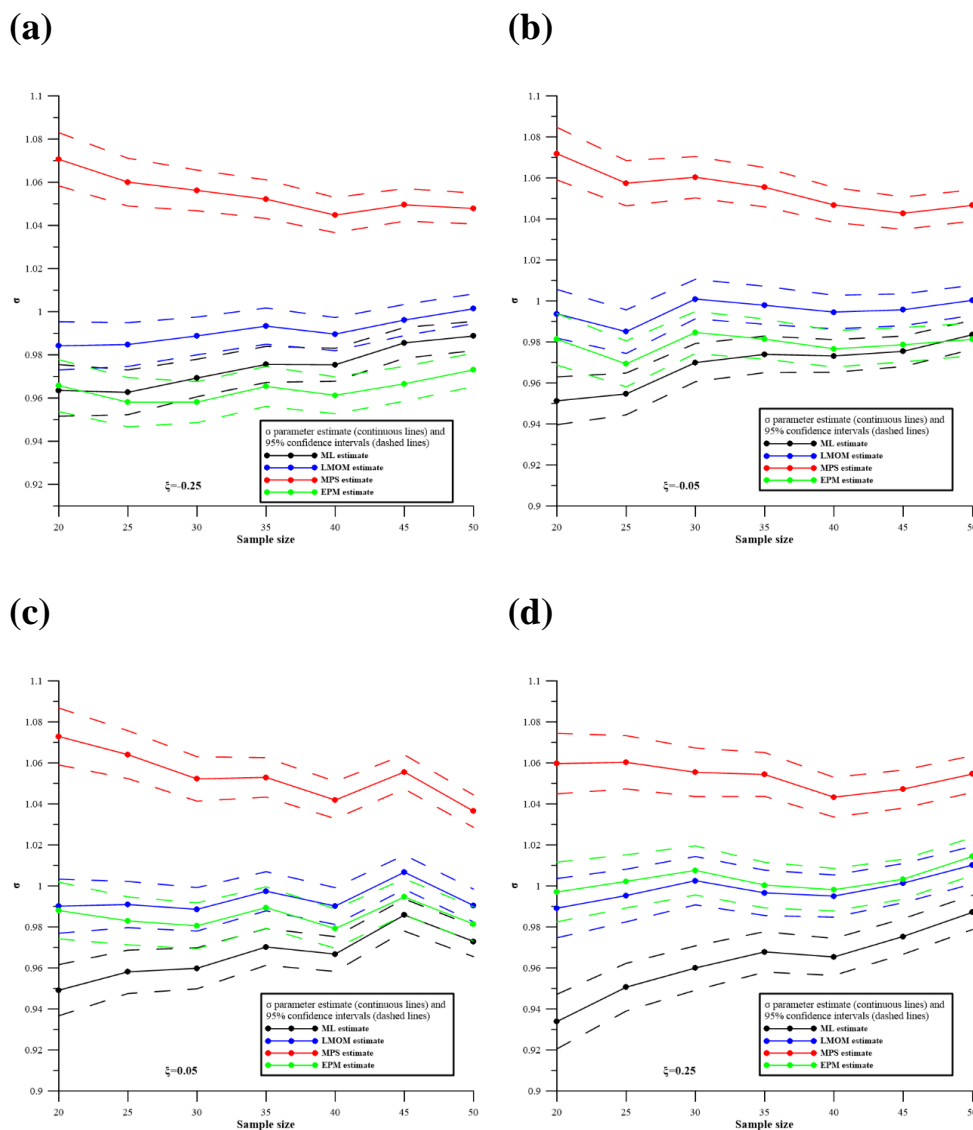


Figure 6.8: Mean values and 95% CI of scale parameter $\sigma$ (for $\xi = -0.25, -0.05, 0.05, 0.25$) in (a,b,c, and d) with respect to sample size obtained from all parameter estimation methods. (Soukissian and Tsalis, 2018)

The effects of the sample size on the estimation of shape parameter

The GEV distribution is essentially governed by the shape parameter $\xi$. In Figure 6.9, the bias (left panel) and the MSE (right panel) of this parameter with respect to sample size is shown. For $\xi$= -0.25 and -0.05, LMOM and MPS provide the smallest absolute bias and, in general, LMOM performs better for small sample sizes. For $\xi$= 0.05 and 0.25, ML provides overall the smallest bias. Regarding MSE, its behaviour is more systematic, i.e. it clearly decreases with increasing sample size, tending to zero. The smallest values of MSE are provided by LMOM and EP, while the largest ones by ML and MPS.

**(a)**



**(b)**



**(c)**



**(d)**



**(e)**



**(f)**

**(g)**                                    **(h)**
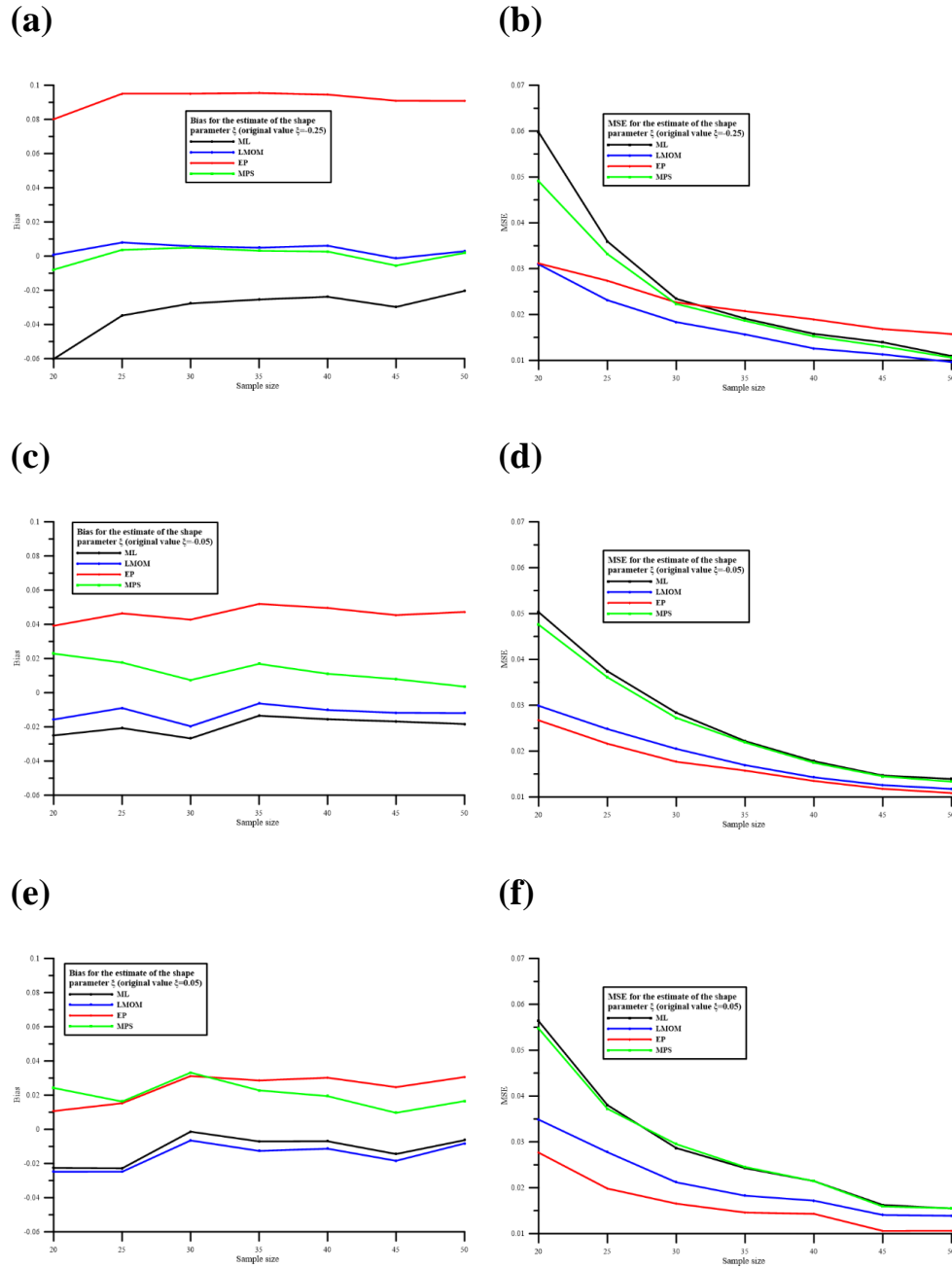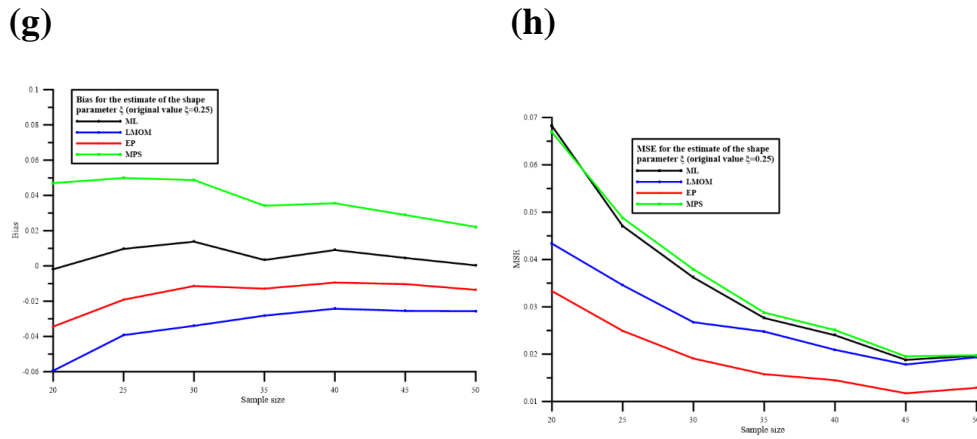


Figure 6.9: Bias in (a,c,e and g) and MSE in (b,d,f, and h) of shape parameter estimate (for $\xi = -0.25, -0.05, 0.05, 0.25$) with respect to sample size obtained from all parameter estimation methods. (Soukissian and Tsalis, 2018)

In Figure 6.10, the mean values and the 95% CI of shape parameter $\xi$ are depicted with respect to sample size. The narrowest CI widths are provided by EPM and LMOM for all examined values of $\xi$. EPM method provides systematically the narrowest 95% CI. It is clear that for negative values of $\xi$ =-0.25 and -0.05, where great interest is in modeling extreme wind speed, ML and LMOM methods have a clearly convergence trend towards the initialy fixed $\xi$ values of the simulation. The demonstration of LMOM shows the smoother decreasing rate as the sample size increases, outlining the fast converegence rate of the latter method to the shape parameter set for evaluation specifically for the relatively small sample sizes of 20 to 30. For the four methods inference is also made of the smoothly decreasing width of the CI as sample size increases pointing out the acceptable behavior of these parameter estimation methods.

**(a)**                                    **(b)**
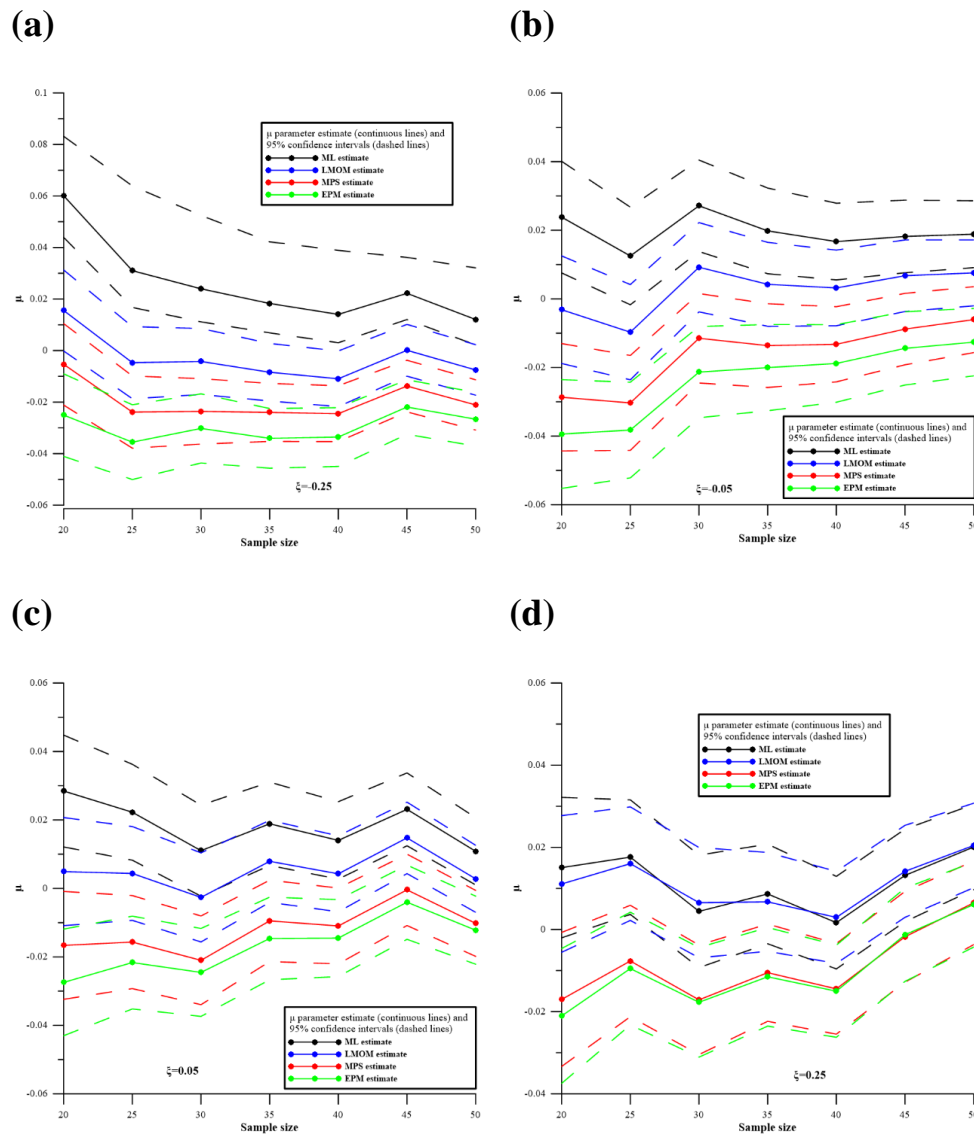
**(c)**

**(d)**
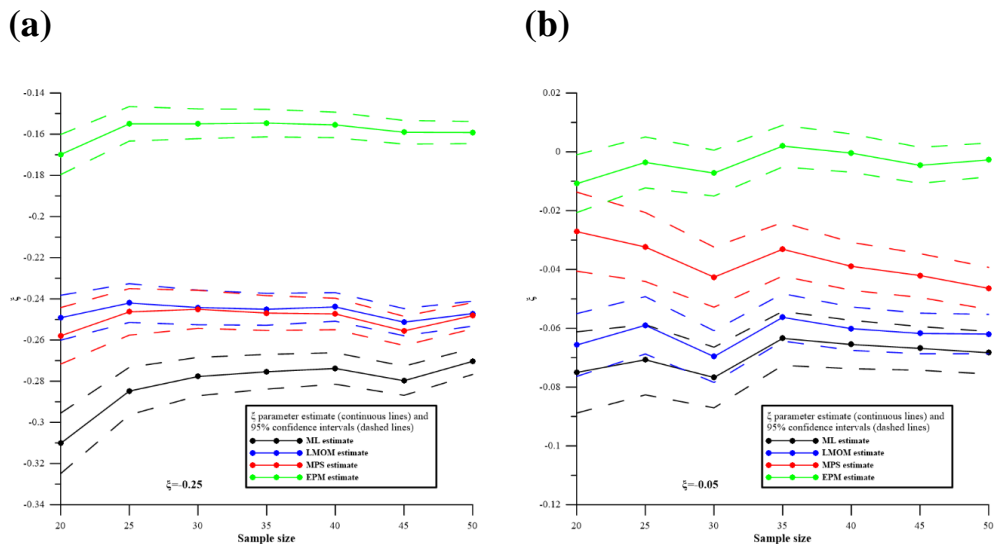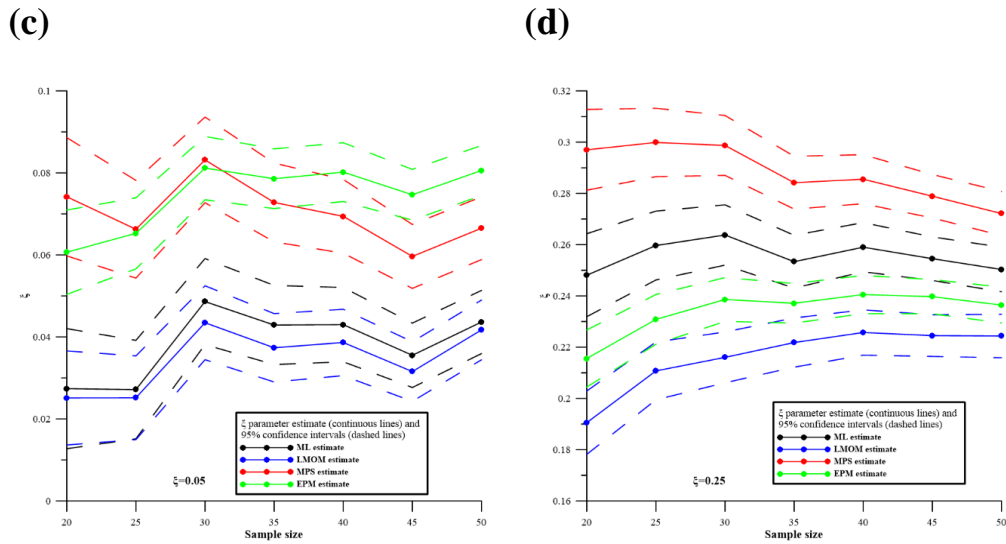


Figure 6.10: Mean values and 95% CI of shape parameter estimate (for $\xi = -0.25, -0.05, 0.05, 0.25$) in (a,b,c, and d) with respect to sample size obtained from all parameter estimation methods. (Soukissian and Tsalis, 2018)

Evaluation of the effects of sample size and estimation method to the GEV distribution

In order to evaluate the overall effects of both the sample size and of the particular estimation method, the results of the metrics $D_{abs}$ and $D_{max}$ are presented for different values of $\xi$. Note that these metrics evaluate the GEV distribution overall fit. Specifically, in Figure 6.11, $D_{abs}$ (left panel) and $D_{max}$ (right panel) are shown with respect to sample size. Regarding $D_{abs}$, LMOM performs clearly better for all examined values of $\xi$, while for $\xi = -0.25$ and 0.25, the values provided by ML method are fairly close to the values provided by the LMOM, especially for larger sample sizes. For small sample sizes, the superiority of LMOM method is more pronounced. With respect to $D_{max}$, LMOM performs clearly better for all examined values of $\xi$. The performance of ML is very close to LMOM's for larger values of $\xi$ and greater sample sizes. It is also evident that the values of both metrics tend to zero as the sample size increases.

**(a)**

**(b)**

**(c)**



**(d)**



**(e)**



**(f)**



**(g)**



**(h)**
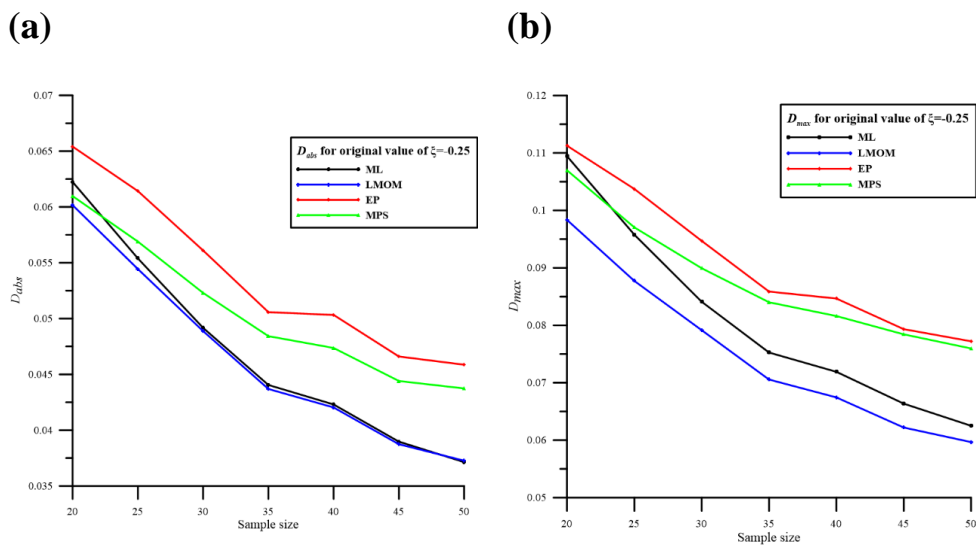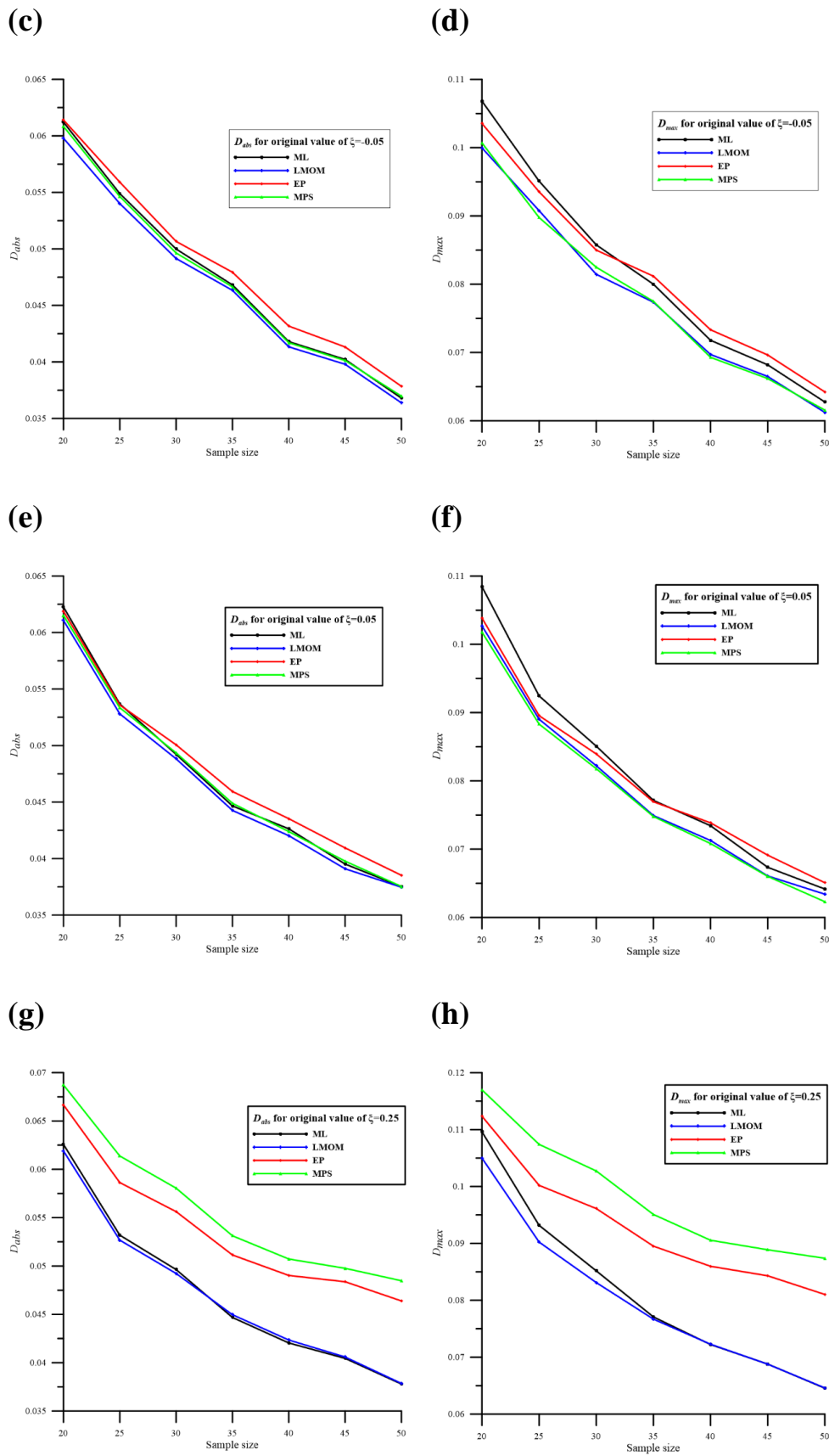


Figure 6.11: $D_{abs}$ in (a,c,e and g) and $D_{max}$ in (b,d,f, and h) for $\xi = -0.25, -0.05, 0.05, 0.25$ with respect to the sample size and the parameter estimation method. (Supplementary image of Soukissian and Tsalis, 2018)

From the simulation study considering a variable sample size of (20,25,30,35,40,45, and 50 years) the following remarks are outlined:

1. With respect to the <u>location parameter $\mu$</u>, LMOM method provides the smallest values of bias for small sample sizes and the smallest values of MSE overall.
2. Regarding the <u>scale parameter $\sigma$</u>, LMOM method provides overall the smallest values of bias while LMOM and ML methods provide the smallest values for MSE.
3. With respect to the <u>shape parameter $\xi$</u>, LMOM performs better with respect to bias for small sample sizes, while LMOM and EP methods provided the smallest values for MSE. For the initialy fixed $\xi$ values (-0.25 and -0.05) of the simulation, the ML and LMOM methods showed a smoother convergence rate towards the initially fixed $\xi$ parameters for sample sizes larger than 35 and to a lower extent for samples larger than 30. From the simulation assessment, the ML method fails to perform better than the other examined estimation methods.
4. Considering the overall behaviour of the estimation methods (for all three parameters simultaneously) a systematic behaviour is observed. Specifically, LMOM method performed clearly better with respect to both metrics $D_{abs}$ and $D_{\max}$, for the majority of the examined sample sizes and in particular, for the smaller ones.
5. Regarding the 95% CI with respect to $\mu$, the narrowest CI widths are provided by LMOM and MPS methods. With respect to $\sigma$, the narrowest CI widths are provided by ML method and in terms of $\xi$, the narrowest CI widths are provided by EPM.

In this regard, according to the above discussion, a rather safe choice is to select the LMOM method for the estimation of the GEV distribution parameters, particularly when the available sample size is relatively small.

## Applications

In the second part of this work, the optimum methods MLE and LMOM from the simulation analysis are applied to wind speed datasets of different sample size and different direction step of sampling to assess the effect of the latter characteristics to the estimators of the GEV parameters. Specifically, the wind data used in this work are in the form of 50 years long time series at four locations (L1,2,3, and 4) in the offshore region of the North Sea obtained from the suitable ERA-20C reanalysis dataset utilizing gridded analysis wind speed data sets of coarse resolution. The statistical analysis of the wind data for the four locations is presented in sub-Section 5.2.1 with respect to different time series lengths. The regional locations selected in this study are in the offshore area of the North Sea and far away one from each other in order to alleviate any correlation effect.

The Mann-Kendall test is applied to the corresponding subsamples of annual BM in order to secure that the relevant time series are non-monotonic. Then the effects of the GEV parameter estimation methods and the sample size and type on the 50- and 100-year design values for wind speed are studied in detail. Since the effects of the wind data sample size can be considered in two ways, i.e.,

i) for increasing sample sizes from the past to the future (F-samples), and
ii) from the current period ("now") to the past (B-samples), both types of effects are assessed (Soukissian and Tsalis; 2019). Specifically, the $n$-year design values of wind speed (for $n = 10,20,...100$ years) for the examined locations are provided for different time series lengths and the deviations between the corresponding

estimates are commented. In addition, the relative confidence intervals is estimated and discussed.

Before proceeding to the GEV parameter and the design value estimation using the methods ML and LMOM to the ERA-20C datasets, Stationarity tests are required. The period 1961–2010 lies within the climate change era and potentially includes climate change signals. Therefore, it is likely that time series statistics, and in particular annual maxima, are affected and thereby cancel out the stationarity assumption under which the BM approach is valid. Consequently it is necessary to examine whether the examined time series are stationary; for this purpose, the non-parametric rank-based Mann-Kendall (M-K) test is implemented, at a significance level $\alpha = 0.05$. In the frame of the M-K test, it is examined whether there is a monotonic upward or downward trend; in other words, assuming a linear trend, the M-K test is used to test whether the slope of the regression line is different from zero. The null hypothesis is $H_0$: *No monotonic trend is present*, against the alternative $H_1$: *There is a monotonic trend present*. The M-K test for trend detection and implementation is described in Appendix F. The main M-K test results (i.e. M-K score $S$, its variance $Var(S)$, and $p$–value for each examined location with respect to the different time series lengths of B– and F–samples) are shown in Table 6.4. The results were produced using the R Kendall package; (see https://cran.r-project.org/web/packages/Kendall/Kendall.pdf).

Table 6.4: Results of the Mann-Kendall test for all examined locations and time series lengths.

| Location | Time series length in years and period examined | $S_F$ | $S_B$ | $Var(S_F)$ | $Var(S_B)$ | $p_F$ | $p_B$ |
|---|---|---|---|---|---|---|---|
| | 20 (1961-1980, 1991-2010) | -16 | -34 | 950.000 | 950.000 | 0.626 | 0.284 |
| | 25 (1961-1985, 1986-2010) | 42 | -48 | 1833.333 | 1833.333 | 0.338 | 0.272 |
| | 30 (1961-1990, 1981-2010) | 57 | -107 | 3141.667 | 3141.667 | 0.318 | 0.059 |
| L1 | 35 (1961-1995, 1976-2010) | 85 | -71 | 4958.333 | 4958.333 | 0.233 | 0.320 |
| | 40 (1961-2000, 1971-2010) | 140 | -14 | 7366.667 | 7366.667 | 0.105 | 0.880 |
| | 45 (1961-2005, 1966-2010) | 86 | -2 | 10450.000 | 10450.000 | 0.406 | 0.992 |
| | 50 (1961-2010) | 15 | | 14291.67 | | 0.907 | |
| | 20 (1961-1980, 1991-2010) | 36 | -42 | 950.000 | 950.000 | 0.256 | 0.183 |
| | 25 (1961-1985, 1986-2010) | 62 | -70 | 1833.333 | 1833.333 | 0.154 | 0.107 |
| | 30 (1961-1990, 1981-2010) | 105 | -79 | 3141.667 | 3141.667 | 0.064 | 0.164 |
| L2 | 35 (1961-1995, 1976-2010) | 133 | -113 | 4958.333 | 4958.333 | 0.061 | 0.112 |
| | 40 (1961-2000, 1971-2010) | 150 | -68 | 7366.667 | 7366.667 | 0.083 | 0.435 |
| | 45 (1961-2005, 1966-2010) | 158 | -10 | 10450.000 | 10450.000 | 0.125 | 0.930 |
| | 50 (1961-2010) | 57 | | 14291.67 | | 0.639 | |
| | 20 (1961-1980, 1991-2010) | 22 | 14 | 950.000 | 950.000 | 0.496 | 0.673 |
| | 25 (1961-1985, 1986-2010) | 20 | 0 | 1833.333 | 1833.333 | 0.657 | 1.000 |
| L3 | 30 (1961-1990, 1981-2010) | 57 | 3 | 3141.667 | 3141.667 | 0.318 | 0.972 |
| | 35 (1961-1995, 1976-2010) | 39 | -11 | 4958.333 | 4958.333 | 0.589 | 0.887 |

| | | | | | | | |
|---|---|---|---|---|---|---|---|
| | 40 (1961-2000, 1971-2010) | 88 | -24 | 7366.667 | 7366.667 | 0.311 | 0.789 |
| | 45 (1961-2005, 1966-2010) | 34 | 66 | 10450.000 | 10450.000 | 0.747 | 0.525 |
| | 50 (1961-2010) | 55 | | 14291.67 | | 0.651 | |
| L4 | 20 (1961-1980, 1991-2010) | 16 | 4 | 950.000 | 950.000 | 0.626 | 0.922 |
| | 25 (1961-1985, 1986-2010) | 52 | 8 | 1833.333 | 1833.333 | 0.234 | 0.870 |
| | 30 (1961-1990, 1981-2010) | 63 | -29 | 3141.667 | 3141.667 | 0.269 | 0.617 |
| | 35 (1961-1995, 1976-2010) | 65 | -41 | 4958.333 | 4958.333 | 0.363 | 0.570 |
| | 40 (1961-2000, 1971-2010) | 112 | 38 | 7366.667 | 7366.667 | 0.196 | 0.666 |
| | 45 (1961-2005, 1966-2010) | 114 | 96 | 10450.000 | 10450.000 | 0.269 | 0.353 |
| | 50 (1961-2010) | 109 | | 14291.67 | | 0.366 | |

Evidently, all $p-$ values for all examined locations, time series lengths and sample types are not significant, since $p > 0.06$. Therefore, the assumption of no monotonic trend in the AM time series cannot be rejected. In (Orimolade et al., 2016) it was also found that the long-term time series of significant wave height for the Barents Sea (based on the Norwegian reanalysis data set NORA10) did not suggest a temporal trend.

Inference of the sample size effect to the GEV parameter estimates

For the estimation of the GEV distribution parameters, ML and LMOM methods are implemented. ML is used since it is a standard parameter estimation technique, while LMOM has been suggested as the overall best estimation method by the results of the simulation study described in the foregoing section. In Figure 6.12, the location, scale, and shape parameters of the GEV distribution are provided with respect to the available number of annual maxima considered for the F–samples (continuous lines) and B–samples (dashed lines).



112

**(c)** **(d)**

**(e)** **(f)**
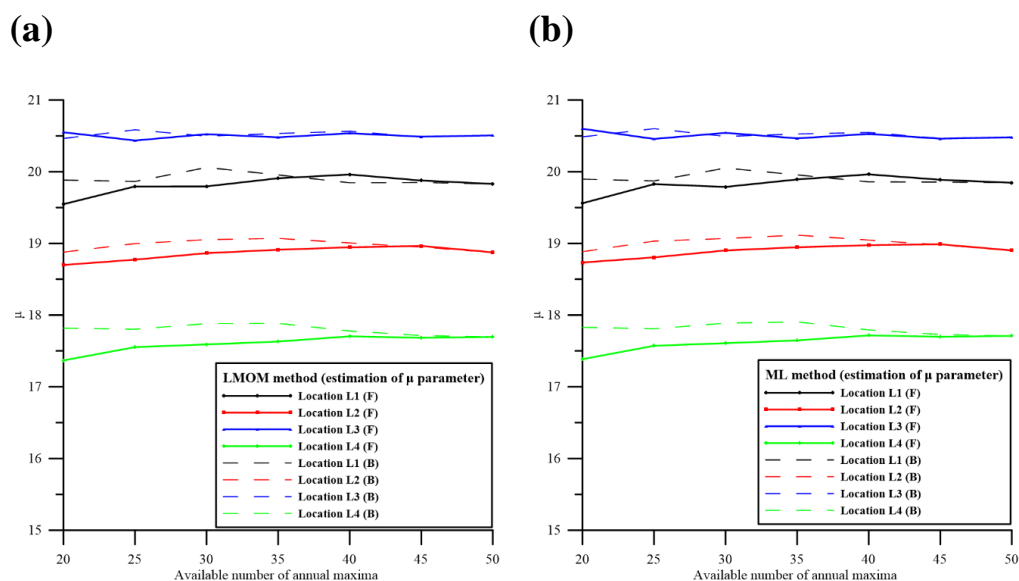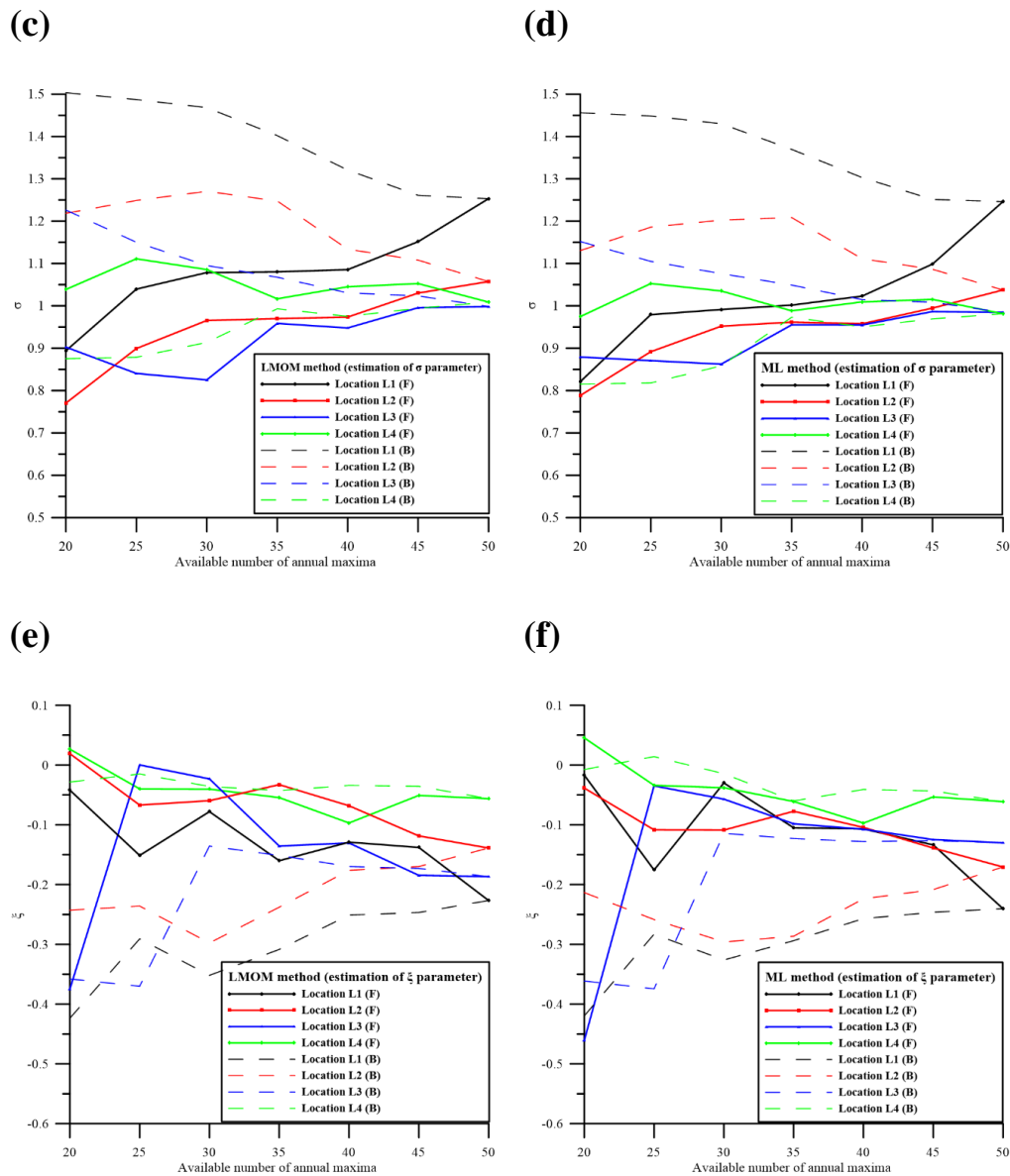


Figure 6.12: Estimation of the GEV distribution parameters according to LMOM method in (a,c, and e) and ML in (b,d, and f) for various sample sizes of annual maxima. Continuous lines correspond to F–samples and dotted lines correspond to B–samples. (Soukissian and Tsalis, 2019)

As can be seen from Figure 6.12 there is a strong variation of the estimated parameters for each examined case, depending on the sample size and type (F– or B–sample), and the estimation method. For locations L1, L2 and L3, the values of the estimated parameters $\sigma$ and $\xi$ are strongly dependent on the sample type. The fluctuation of $\xi$ is of most importance, since it affects the specific asymptotic form of the GEV distribution. In this respect, a significant jump (increase) in the estimated value of $\xi$ is observed for L3; for F–sample size 20, the values provided by the LMOM and ML were -0.375 and -0.461, respectively, while for sample size 25, the corresponding values of $\xi$ were 0.0001 and 0.0348. This abrupt shift is due to the appearance of the new maximum (24.662 m/s) to the 25 years long data-set, with value well above the existing AM values. On the contrary, the corresponding shift is almost negligible for $\mu$ and $\sigma$.

Although the challenging results, some general remarks can be pointed out and summarized as follows:

1   It seems that only $\mu$ parameter is rather insensitive to the sample type;
2   For location L4 where the extreme wind profile in the German Bight is related to the low sea level pressure pattern over Scandinavia (Sušelj et al., 2010; Befort et al., 2014) it seems that the sample type has minor effects to all estimated parameters;
3   The estimates of the parameters obtained from F– and B–samples converge to a stronger rate as sample size increases (larger than 40 and to a lower extent larger than 35), which was an expected behaviour;
4   The general trends for each location and estimated parameters with respect to the examined estimation method are much alike. For example, the trends of the two black lines (for both sample types) providing the fluctuation of $\xi$ as estimated by the LMOM and the ML method for location L1, are identical;
5   $\xi$ parameter estimates obtained from the F–samples are systematically greater than the corresponding estimates obtained from the B–samples (except for location L4 where both estimates are very close);
6   $\sigma$ parameter estimates obtained from the B–samples are systematically greater than the estimates obtained from the F–samples (except for location L4).

For the evaluation of the obtained GEV fits, let $x_N \leq \cdots \leq x_2 \leq x_1$ denote the ordered sample of AM, and $N$ the corresponding sample size. Let also $T$ denote the corresponding return periods obtained by means of an appropriate plotting position formula, such as the Weibull plotting position formula:

$$T = \frac{i}{N+1}, \qquad i = 1, 2, \ldots, N, \tag{6.12}$$

where $i$ denotes the order of the particular value in the sample. Moreover, let $\hat{x}_N \leq \cdots \leq \hat{x}_2 \leq \hat{x}_1$ denote the values estimated by the fitted GEV distribution that correspond to the same return periods. For a quantitative evaluation of the obtained fits with respect to the different sample sizes and types, and parameter estimation methods, two different goodness-of-fit measures are implemented, thestandard error of fit (SEF) and the mean absolute relative deviation (MARD) (see expressions previously stated in Equations (6.5) and (6.6).

In Table 6.5, the values of SEF and MARD criteria are summarized for different sample sizes and types and for both estimation methods. Results shown with boldface numbers denote minimum values for the F– and B–samples (with respect to estimation method). Boldface and italics numbers denote overall minimum values (with respect to estimation method and sample type). From this table, the following conclusions can be summarized:

Table 6.5: Values of MARD and SEF criteria for different sample sizes, sample types (F and B) and estimation methods. Boldface numbers denote minimum values for the F– and B–samples. Boldface and italics numbers denote overall minimum values.

| Location | Criterion | Estimation method | Sample type | Sample size | | | | | | |
|----------|-----------|-------------------|-------------|------|------|------|------|------|------|------|
| | | | | 20 | 25 | 30 | 35 | 40 | 45 | 50 |
| L1 | SEF | ML | F | 0.213 | 0.200 | 0.222 | 0.223 | 0.177 | 0.172 | 0.181 |
| | | | B | 0.335 | 0.311 | 0.247 | 0.199 | 0.188 | 0.189 | |
| | | LMOM | F | *0.171* | *0.155* | *0.197* | **0.214** | *0.155* | *0.147* | **0.174** |
| | | | B | **0.319** | **0.300** | **0.239** | *0.191* | **0.179** | **0.186** | |
| | MARD | ML | F | 0.698 | 0.797 | 0.756 | 0.771 | 0.651 | 0.641 | 0.616 |
| | | | B | 1.223 | 1.148 | 0.870 | 0.634 | 0.592 | 0.608 | |
| | | LMOM | F | *0.527* | *0.563* | *0.700* | **0.767** | **0.593** | *0.570* | **0.599** |

| | | | | | | | | | | |
|---|---|---|---|---|---|---|---|---|---|---|
| | | | B | **1.148** | **1.101** | **0.836** | *0.604* | *0.576* | *0.596* | |
| L2 | SEF | ML | F | 0.280 | 0.197 | 0.200 | 0.180 | 0.147 | 0.138 | 0.124 |
| | | | B | 0.239 | 0.202 | 0.190 | 0.173 | 0.157 | 0.138 | |
| | | LMOM | F | **0.259** | **0.168** | **0.173** | **0.152** | *0.117* | *0.107* | **0.095** |
| | | | B | *0.204* | *0.157* | *0.160* | *0.134* | **0.125** | **0.108** | |
| | MARD | ML | F | 0.837 | 0.715 | 0.750 | 0.686 | 0.585 | 0.574 | 0.495 |
| | | | B | 0.862 | 0.866 | 0.814 | 0.732 | 0.647 | 0.566 | |
| | | LMOM | F | **0.811** | *0.654* | *0.663* | **0.600** | *0.475* | *0.440* | **0.386** |
| | | | B | *0.739* | **0.656** | *0.642* | *0.519* | **0.498** | **0.449** | |
| L3 | SEF | ML | F | 0.176 | 0.375 | 0.317 | **0.283** | **0.247** | **0.244** | **0.213** |
| | | | B | 0.201 | 0.177 | *0.265* | *0.234* | *0.224* | *0.220* | |
| | | LMOM | F | *0.155* | **0.370** | **0.314** | 0.296 | 0.259 | 0.263 | 0.229 |
| | | | B | **0.159** | *0.155* | 0.269 | 0.241 | 0.236 | 0.234 | |
| | MARD | ML | F | 0.637 | **0.792** | 0.659 | 0.683 | 0.611 | 0.664 | 0.541 |
| | | | B | 0.733 | 0.636 | 0.646 | 0.538 | 0.545 | 0.569 | |
| | | LMOM | F | *0.556* | 0.796 | **0.648** | **0.646** | **0.589** | **0.594** | **0.473** |
| | | | B | **0.580** | *0.560* | *0.632* | *0.522* | *0.508* | *0.526* | |
| L4 | SEF | ML | F | 0.295 | 0.243 | 0.203 | 0.188 | 0.152 | 0.146 | 0.134 |
| | | | B | 0.238 | 0.194 | 0.179 | 0.185 | 0.166 | 0.151 | |
| | | LMOM | F | **0.261** | **0.206** | **0.167** | **0.165** | *0.128* | *0.116* | **0.111** |
| | | | B | *0.209* | *0.165* | *0.152* | *0.159* | **0.143** | **0.127** | |
| | MARD | ML | F | 1.026 | 0.958 | 0.804 | 0.664 | 0.552 | 0.602 | 0.528 |
| | | | B | 0.823 | 0.746 | 0.732 | 0.692 | 0.599 | 0.570 | |
| | | LMOM | F | **0.959** | **0.859** | **0.706** | **0.629** | *0.474* | *0.495* | **0.463** |
| | | | B | *0.729* | *0.631* | *0.623* | *0.617* | **0.543** | **0.509** | |

- **F–samples**: For locations L1, L2, and L4 both MARD and SEF criteria take their minimum values for LMOM method, for all sample sizes. For location L3, SEF criterion takes its minimum values for LMOM for small sample sizes (up to 30) and for ML for sample sizes (35–50). The minimum values of MARD criterion are obtained from LMOM for all sample sizes (except for sample size 25).

- **B–samples**: For locations L1, L2, and L4, both MARD and SEF criteria take their minimum values for LMOM method, for all sample sizes. For location L3, SEF criterion takes its minimum values for LMOM for small sample sizes (up to 25) and for ML for the sample sizes between 30 and 50. The minimum values of MARD criterion are obtained from LMOM for all sample sizes.

- Failling of definitive conclusions as regards of the performance of ML and LMOM estimation methods with respect to the sample types (F and B). The criteria with respect

to sample size, location and estimation method do not exhibit a strong systematic behaviour.

## Inference of the sample size effect to the wind speed design values of the GEV distribution

In this section, the particular effects of the available number of AM and the parameter estimation methods on the design values of wind speed are assessed. For the sake of simplicity, the $n$-years design values of wind speed (for $n$=10,20,...,100) obtained from the time series of $N$-year length ($N$= 20, 30, 40 and 50) are denoted by $U_D(n; N)$. Along with the obtained wind speed design values in Figure 6.13, the corresponding 95% CI were also estimated and presented. For the MLE method the usual normal approximation to the likelihood is implemented and for the LMOM method, the 95% CI was estimated using the parameteric bootstrap method, (see sub-Section 2.6.2.1). The main steps for the parameteric bootstrap method used are the following:

   i)   Generate $K = 2000$ random samples of AM each of size $N$, all derived from the fitted examined GEV pdf. The value $K = 2000$ has been selected by a trial and error procedure as is suggested in the R extRemes package (https://cran.r-project.org/web/packages/extRemes/extRemes.pdf). For this value of $K$, the results regarding CI are clearly stabilized;
   ii)  Estimate the GEV parameters of the $K$ random samples by means of the LMOM method, and;
   iii) Calculate the 95% CI of the parameters of interest directly from the bootstrap samples.

For the evaluation of the obtained results regarding CI, the relative CI ($RCI$) and width of CI ($WCI$) is introduced. Denoting by $\left[U_{D,L}, U_{D,U}\right]$ the 95% CI of $U_D$, $RCI$ and $WCI$ is defined as follows:

$$\begin{cases} RCI = \frac{U_{D,U} - U_{D,L}}{U_D}, \\ WCI = U_{D,U} - U_{D,L}. \end{cases} \tag{6.13}$$

In Figure 6.13, $U_D(n; N)$ is illustrated for locations L1, L2, L3 and L4, whereas the parameters of the GEV distribution are estimated by the LMOM method (left column) and the ML method (right column). An interesting behaviour that is illustrated from this figure refers to location L3 where the design values provided by the 20 years long time series are clearly outside the bulk of the rest curves. This is inferred from the abrupt change in the estimated value of $\xi$ parameter from the 20 and 30 years of time series. This effect at the NW location of the North Sea is somehow explained by the inability of the low-resolution product to capture the influence of the local circulation patterns into the relatively small sample period of 20 years (Sušelj et al., 2010). The high deviations of extremes extrapolated between the 20 and 30 years sample period from L3 confirms the disadvantage of the low-resolution dataset to resolve the local characteristics that influence the extreme wind profile at that region.

For a comprehensive statistical analysis in terms of the variation of each estimation method, in Figure 6.14 RCI of the 50- year design value DV(50) and the WCI of the estimated parameters ($\mu, \sigma, \xi$) are illustrated for the four locations assigning in (continuous lines) the Forward count samples for LMOM and ML, and in (dotted lines) the Backward samples respectively.

**(a)**



Location L1

**(b)**



Location L1

**(c)**



Location L2

**(d)**



Location L2

**(e)**



Location L3

**(f)**



Location L3

**(g)**



**(h)**
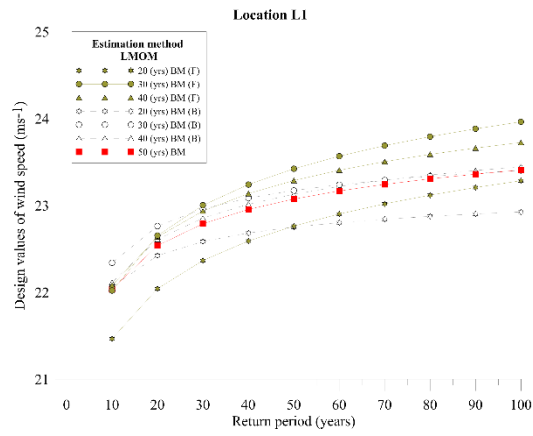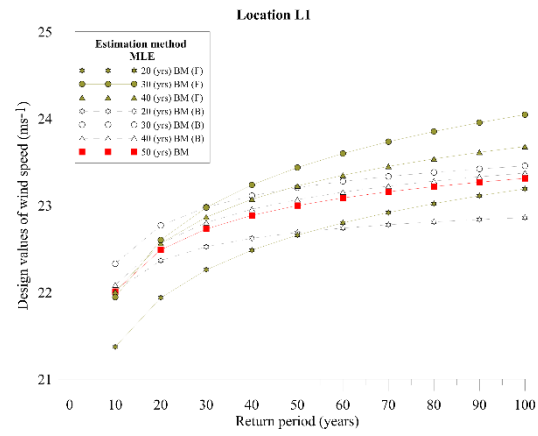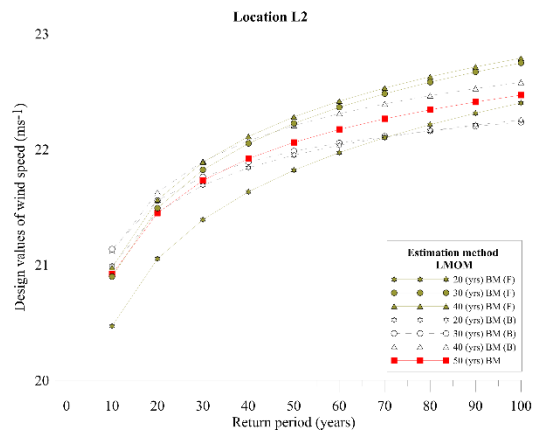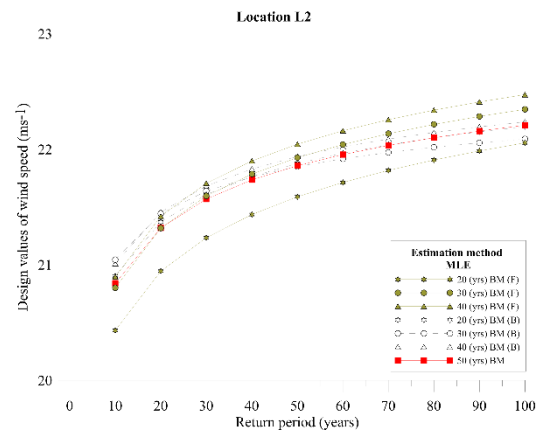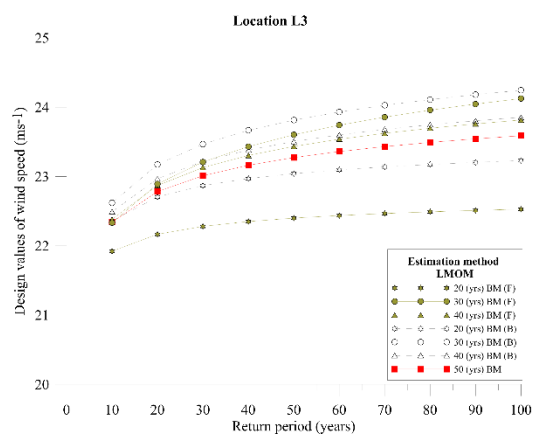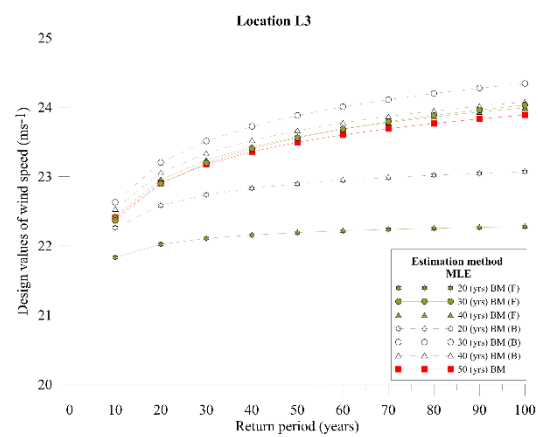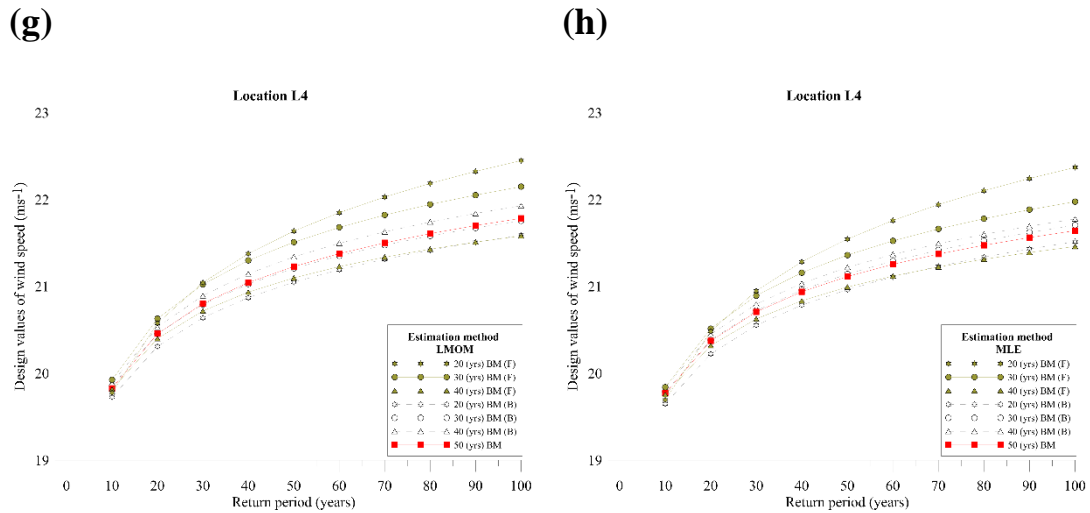


Figure 6.13: The $n$-year ($n = 10, 20, \cdots, 100$years ) design values of wind speed at locations L1, L2, L3, and L4, for different annual maxima sample sizes and sample types using LMOM method (a,c,e, and g), and ML method (b,d,f, and h). Continuous lines correspond to F–samples and dotted lines correspond to B–samples. (Soukissian and Tsalis, 2019)

**(a)**



**(b)**



**(c)**



**(d)**



118

**(e)**



RCI for 50 (yrs) Design Value
Location L2

**(f)**



Width of CI for location (μ)
Location L2

**(g)**



Width of CI for scale (σ)
Location L2

**(h)**



Width of CI for shape (ξ)
Location L2

**(i)**



RCI for 50 (yrs) Design Value
Location L3

**(j)**



Width of CI for location (μ)
Location L3

**(k)**

**(l)**



**(m)**

**(n)**



**(o)**

**(p)**
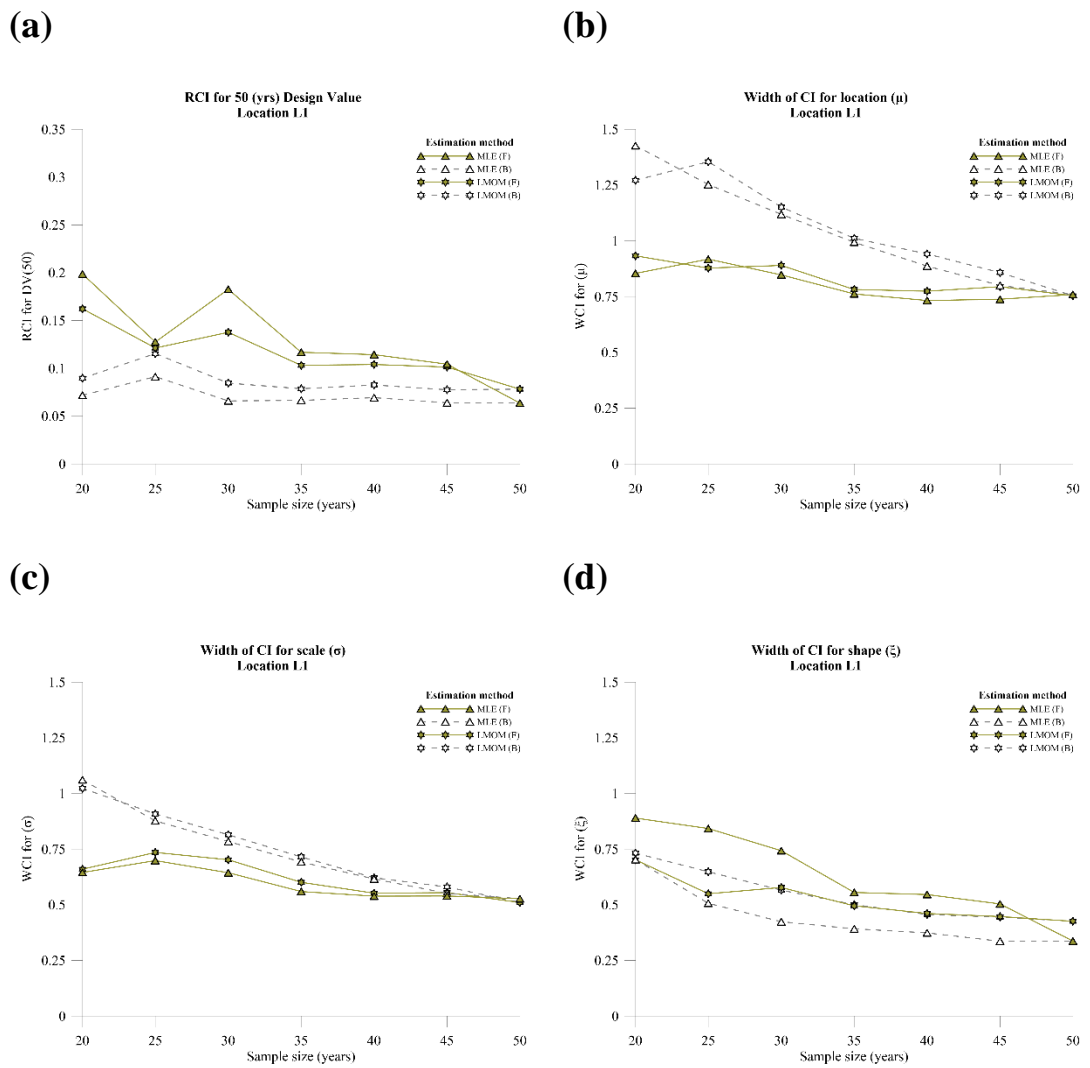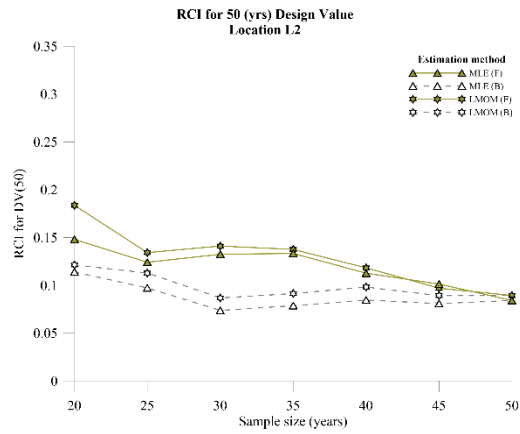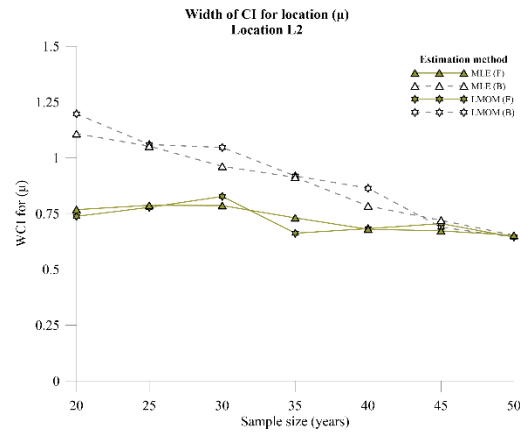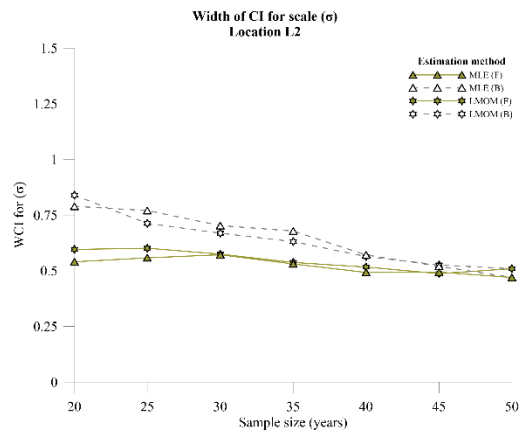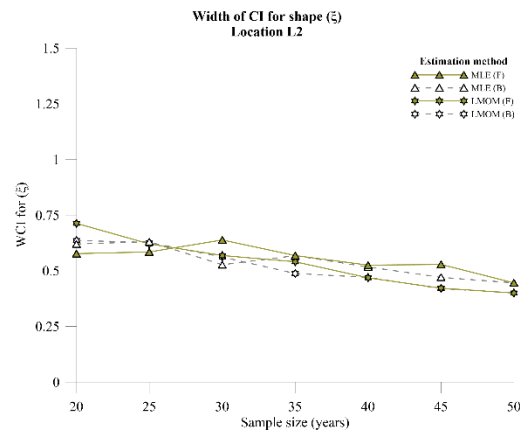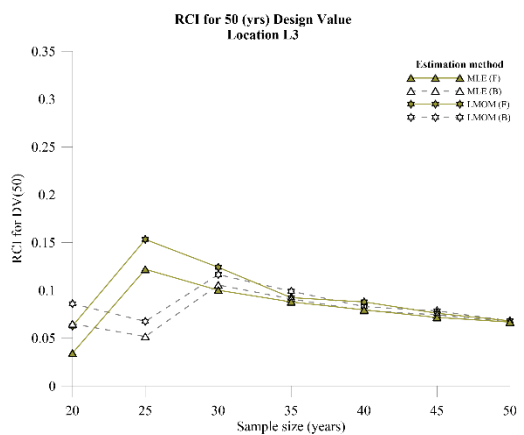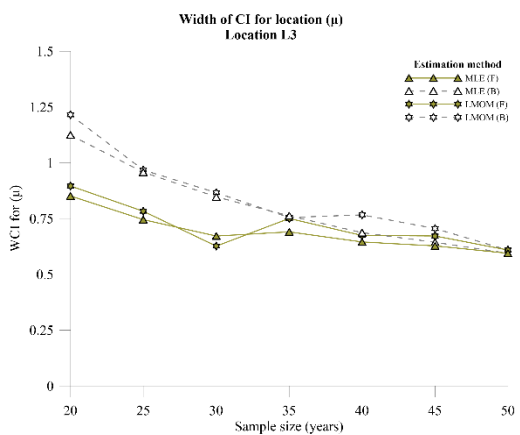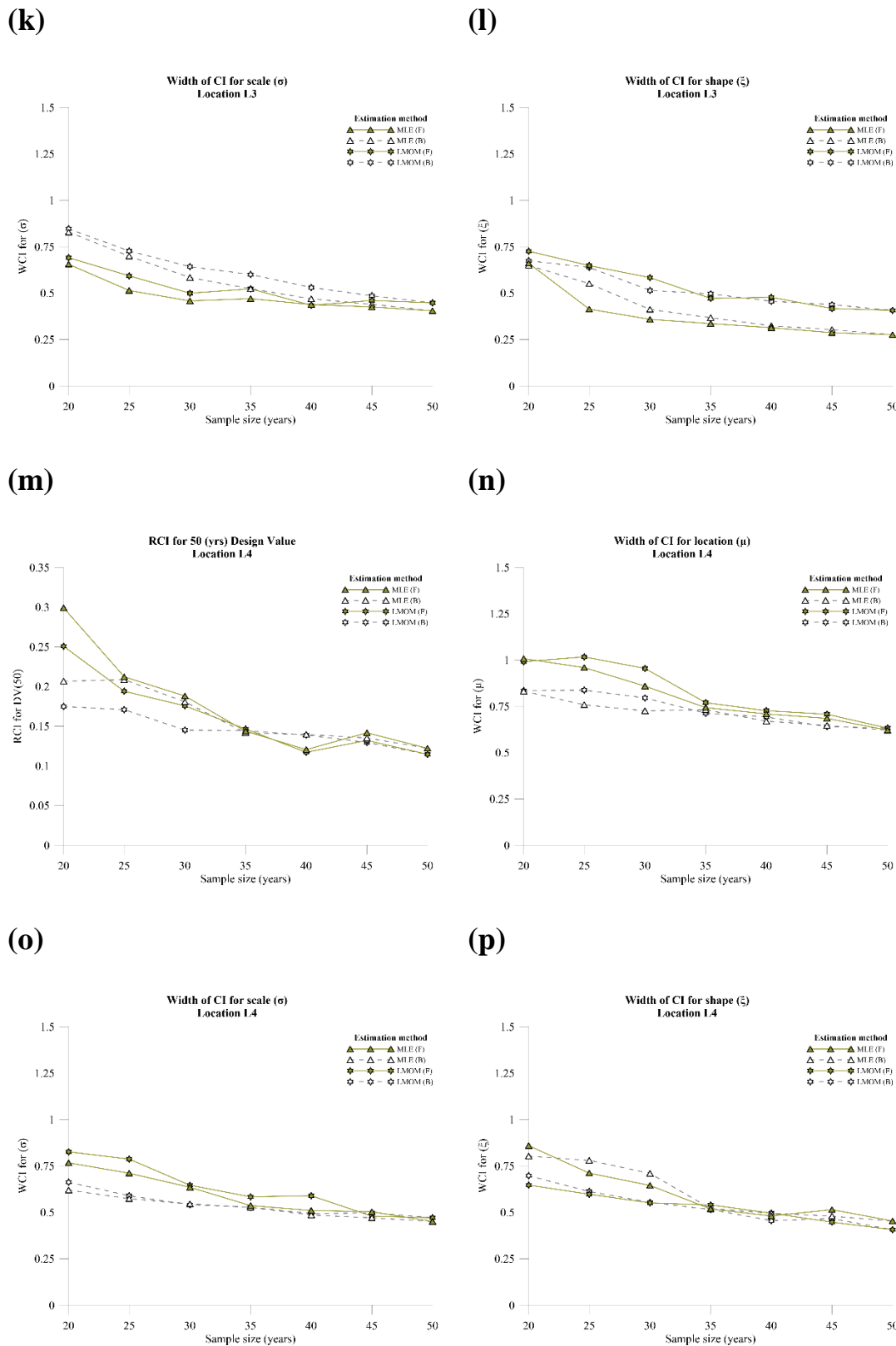


Figure 6.14: RCI for the DV(50) of wind speed and WCI for the estimated parameters at locations L1 (a,b,c, and d), L2 (e,f,g, and h), L3 (i,j,k, and l) and L4 (m,n,o, and p) for different annual maxima sample sizes using LMOM and ML methods. (Supplementary image of Soukissian and Tsalis, 2019)

As regards to the parameter estimation methods ML and LMOM of the GEV distribution for the variable sample size and the direction step of sampling, the following remarks from Figures 6.13 and 6.14 can be derived as following:

- The general behavior of the design value curves for each location is the same for LMOM and ML methods.
- The design values provided by B–samples (size 40), are systematically closer to the design values provided by the sample of 50 AM than the corresponding values provided by the F–samples. This is also true for the corresponding samples of size 30 (except for L3).
- The dispersion of the design values provided by the B–samples for different sample sizes, is, in the mean, smaller than the one provided by the F–samples.
- The F–samples with sizes 20 or 30 do not provide design values comparable to the design values provided by the samples of size 50.
- In general, as the sample size increases, RCI and WCI values decrease
- For sample sizes greater than 40 and to a lower extent graeter than 35, the values of RCI of F- and B-samples corresponding to the same return periods are similar from LMOM and ML.
- The largest values of RCI (for both F– and B–samples) correspond to the smallest sample sizes
- With respect to sample size, the scatter of the values of RCI obtained from the B–samples is smaller than the one obtained from the F–samples.

The aim of this part of this study was the assessment of the most popular methods for the estimation of the parameters of the GEV distribution considering the combined effects of variable sample size and the different direction step of sampling. The analysis was based on a simulation study for variable sample sizes and application of the estimation methods MLE and LMOM to wind speed datasets from the ERA-20C reanalysis at regional locations in the North Sea. Considering the variable sample size, inference is made from the simulation study pointing out that, in general to the estimated parameters ($\mu, \sigma$, and $\xi$), LMOM performs better with respect to bias for small sample sizes, while LMOM and EP methods provide the smallest values for MSE. Inference of the design values to wind speed datasets pointed out that for small sample sizes (size 20 and 30), the extremes extrapolated from the analysis based on the B–samples are, in general to the F–samples, closer to the extrapolated extremes based on the samples of size 50 especially for low return periods (up to 50 years). The latter argument is in some measure supported from the significant positive trend in ERA-20C in the number of extratropical cyclones in the North European regions (Befort et al., (2016) and Varino et al., (2018)). The B–samples are, in general to the F–samples, found with stronger wind profile.

## 6.2 Non Stationary approach

The study of extremes through the classical method of BM is more complicated when the stationarity assumption is not valid. In practical applications, under the presence of non-stationarity the parameters of the GEV distribution are considered time dependent and time is taken as a covariate. The underlying assumption of this approach is that the probability of occurrence of the considered extreme events evolves in time and the associated GEV parameters are considered time-dependent and the properties of the distribution vary with time; (see sub-Section 2.5.1). This is often the case when time series under climate change conditions are considered; (e.g., see Vanem, 2015). For this assessment, four steps summarize the non-stationary approach as follows:

    i.    First Step, the annual wind speed data series from the atmospheric weather reanalysis product ERA-20C is considered.

    ii.    Secondly, for each examined location L (1, 2, 3, 4, and 5) illustrated in Figure 5.6 with their descriptive statistics in Table 5.3, Trend and Stationarity test are implemented setting p-value<0.05.

    iii.    Third, the likelihood is formulated for the various non-stationary GEV parametric models, following from the estimation of the minimum model selection criteria of the AIC, BIC and LR test respectively for each location.

    iv.    Finally, in Step four the effective design values of each optimum parametric GEV model is estimated.

In the present work, the location parameter and the scale parameter are modelled as polynomial functions of time. The exponential in the scale parameter is used to ensure positivity for all values of time $t$. Shape parameter is of most importance for the distribution and due to its difficulty to be estimated with accuracy, we keep shape parameter time independent, following the work from Nogaj et al., (2007), El Adlouni et al., (2007) and Cannon (2010). In the following Table 6.6, the various time dependent forms of the parametric models are presented.

Table 6.6: Basic models of various functional forms of $(\mu(t), \sigma(t), \xi(t))$ for the non-stationary analysis.

| Model | Functional form of $\mu(t)$ | Functional form of $\sigma(t)$ | $\xi(t)$ |
|---|---|---|---|
| 1 | $\mu_0$ | $\sigma_0$ | $\xi_0$ |
| 2 | $\mu_0 + \mu_1 t$ | | |
| 3 | $\mu_0 + \mu_1 t + \mu_2 t^2$ | | |
| 4 | $\mu_0$ | $\exp(\sigma_0 + \sigma_1 t)$ | |
| 5 | $\mu_0 + \mu_1 t$ | | |
| 6 | $\mu_0 + \mu_1 t + \mu_2 t^2$ | | |
| 7 | $\mu_0 + \mu_1 \sin\left(\frac{2\pi}{365.25}t\right) + \mu_2 \cos\left(\frac{2\pi}{365.25}t\right)$ | $\exp\left(\sigma_0 + \sigma_1 \sin\left(\frac{2\pi}{365.25}t\right) + \sigma_2 \cos\left(\frac{2\pi}{365.25}t\right)\right)$ | |

## 6.2.1 Trend and unit root tests

In this assessment, two tests are first applied to verify the presence of trend to extremes of annual wind speed in the North Sea region. The first test is the Mann-Kendall (MK) non-parametric trend test and second the Cox Stuart (CS) trend test (see sub-Section (2.5.2)), in order to assess whether the considered time series are characterized by an increasing, decreasing or stationary trend. Secondly, two additional unit root tests are implemented referred to as the Kwiatkowski-Phillips-Schmidt-Shin (KPSS) stationarity test and the Augmented Dickey-Fuller (ADF) unit root test (see also sub-Section (2.5.2) and Appendix F). The KPSS test makes inquiries about the stationarity of the considered time series around a fixed level (level stationarity) and the ADF test examines if the process is stationary or not from the presence of a unit root. The null hypothesis of the MK and CS tests is no monotonic trend present, and the null hypothesis of KPSS is level stationarity. However, the null hypothesis of the ADF test is of the presence of a unit root (i.e., non-stationary process set as null). The extreme value analysis in this setting based on the nonstationary approach considers data of length 40 years corresponding to annual maxima wind speed records from the ERA-20C data product, covering the period (1961-2000).

The annual maxima of wind speed at the selected locations meet the requirements of the MK, CS, KPSS, and ADF tests presented in Table 6.7. Specifically, the trend tests MK and CS regarding the absence of a monotonic upward trend over time cannot be rejected at the significance level of 0.05. In the same context, the level stationarity test of the non existence of a unit root (i.e., indicating a stationary process) cannot be rejected at the significance level of 0.05 for the KPSS, where for the ADF test the presence of a unit root (i.e., indicating a non-stationary process) cannot be rejected at the same significance level of 0.05.

Table 6.7: The p – values testing for non-stationarity per location.

| p-values/ Location | L1 | L2 | L3 | L4 | L5 |
|---|---|---|---|---|---|
| MK-Test | 0.028 | 0.003 | 0.010 | 0.003 | 0.043 |
| CS-Test | 0.003 | 0.003 | 0.018 | 0.018 | 0.003 |
| KPSS-Test | 0.021 | 0.010 | 0.010 | 0.010 | 0.017 |
| ADF-Test | 0.436 | 0.099 | 0.078 | 0.134 | 0.350 |

## 6.2.2 AIC & BIC test

In the following Figure 6.15, the AIC and BIB model criteria are illustrated for each location. It is apparent that Model 2 and 3 derive the lowest AIC per location in (a) and considering the BIC values in (b) the Model 2 derived the lowest respectively.

**(a)**
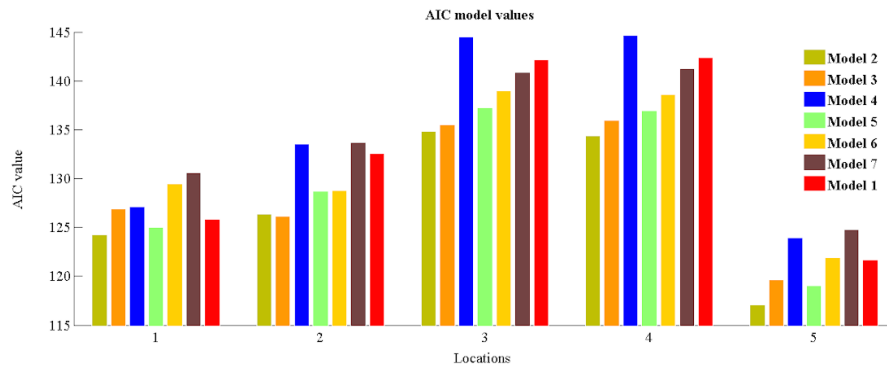


**(b)**
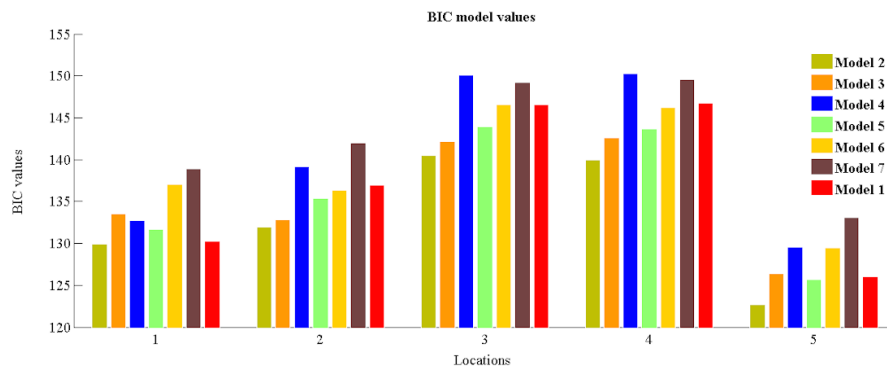
Figure 6.15: The AIC and BIC parametric model criteria for each location in (a) and (b) respectively. (Tsalis and Kallos, 2017)

## 6.2.3 LR test for optimum Models

In this sub-Section inference is made from the acception or rejection of the likelihood-ratio test of the six nested extreme value distribution models as a better representation of the extremes of wind speed when the stationarity assumption (demonstrated from Model 1) is violated. When the objective of the nonstationary analysis is how to incorporate effectively covariates into an extreme value analysis model, one method is to incorporate them into the parameters of the extreme value distributions themselves in a regression-like manner (Coles, 2001; Reiss and Thomas, 2007). In order to statisticaly justify whether or not the specific inclusion of the order of covariates into the model is significant or not is to apply the likelihood-ratio test (Wilks et al., 2011). The test is only valid for comparing nested models. That is, the parameters of Models (2,3,4,5, and 6) are undertaken as a subset of the parameters of the stationary Model 1.

The likelihood-ratio statistic (or deviance statistic) formulared in sub-Section (2.5.4) is inferred to the (1 - alpha) quantile of the chi-square distribution with degrees of freedom equal to the difference in the number of model parameters for alpha= 0.05. Specifically, the null hypothesis of the likelihood-ratio test to the optimum models obtained from the AIC and BIC criteria (i.e., Models 2 and 3) is challenged of rejection or not in favor of the stationary Model 1. The LR-statistic presented in Table 6.8 of the null hypothesis challenging the stationary Model 1 at the significance level of 0.05 infer that Model 2 is a better representation of GEV based on the nonstationary analysis of extremes of wind speed for the five locations.

Table 6.8: LR test for Model 1 vs Model 2 in (a) and LR test for Model 1 vs Model 3 in (b).

## (a)

| Model 1 vs Model 2 | LR Statistic | p-value <0.05 |
|---|---|---|
| L1 | 4.032 | 0.045 |
| L2 | 8.692 | 0.003 |
| L3 | 9.822 | 0.002 |
| L4 | 10.474 | 0.001 |
| L5 | 7.076 | 0.008 |

## (b)

| Model 1 vs Model 3 | LR Statistic | p-value <0.05 |
|---|---|---|
| L1 | 4.076 | 0.130 |
| L2 | 11.545 | 0.003 |
| L3 | 11.785 | 0.003 |
| L4 | 11.512 | 0.003 |
| L5 | 7.093 | 0.029 |

In the same context, the rejection of the null hypothesis at the significance level of 0.05 of Model 2 against the alternative parametric Model 3 is presented in Table 6.9.

Table 6.9: LR test for Model 2 vs Model 3.

| Model 2 vs Model 3 | LR Statistic | p-value <0.05 |
|---|---|---|
| L1 | 0.044 | 0.834 |
| L2 | 2.853 | 0.091 |
| L3 | 1.963 | 0.161 |
| L4 | 1.038 | 0.308 |
| L5 | 0.017 | 0.897 |

To alleviate any evidence of the use of the Gumbel distributions to fit extremes, many studies suggest a likelihood ratio test and if not rejected the latter distribution could alternatively model the extremes of wind speed; (e.g., An and Pandey, 2005 and Perrin et al., 2006). Spesifically, in Table 6.10 the LR-test results of the null hypothesis at the significance level of 0.05 inference that there is strong evidence that the stationary Gumbel distribution (except L1) is challenged from the parametric Models 2 and 3 as the best fit to the annual extremes of wind speed. Moreover, a possible underestimation of the extremes extrapolated at these locations (except L5) is expected from the stationary Model 1 (three parameters), since the stationary Gumbel distribution (two parameters) which is in the domain of attraction of the GEV distribution, is known to normally give higher extremes for a given return period than the stationary Type III form; (Palutikof et al., (1999)). However, it is arguably preferable to always allow the shape parameter to be non zero even if the LR-test results supports the Gumbel hypothesis. This recommendation is based on practical considerations as given in Coles et al., (2003) and on penultimate approximations in extreme value theory (Reiss and Thomas, 2007). Specifically, Coles (2001) and Coles and Pericchi (2003) showed that even in cases where a reduction to the Gumbel class (i.e., infer to narrower confidence bounds) is justifiable based on standard statistical tests, is a risky strategy instead of the more general GEV (i.e., infer to wider confidence bounds).

Table 6.10: LR test for Gumbel distr. vs Model 1,2, and 3 in (a), (b), and (c) respectively.

**(a)**

| Stationary Gumbel distr. vs Model 1 | LR Statistic | p-value <0.05 |
|---|---|---|
| L1 | 0.407 | 0.523 |
| L2 | 0.362 | 0.547 |
| L3 | 0.973 | 0.324 |
| L4 | 0.458 | 0.499 |
| L5 | 6.401 | 0.011 |

**(b)**

| Stationary Gumbel distr. vs Model 2 | LR Statistic | p-value <0.05 |
|---|---|---|
| L1 | 4.440 | 0.109 |
| L2 | 9.054 | 0.011 |
| L3 | 10.795 | 0.005 |
| L4 | 10.932 | 0.004 |
| L5 | 13.477 | 0.001 |

**(c)**

| Stationary Gumbel distr. vs Model 3 | LR Statistic | p-value <0.05 |
|---|---|---|
| L1 | 4.484 | 0.214 |
| L2 | 11.907 | 0.008 |
| L3 | 12.758 | 0.005 |
| L4 | 11.970 | 0.007 |
| L5 | 13.493 | 0.004 |

Summarizing the results in this sub-Section:

1. Model 1 is rejected compared to Model 2 for all locations,
2. Model 1 is rejected compared to Model 3 except for L1,

3. Model 2 cannot be rejected compared to Model 3 for all locations,
4. Stationary Gumbel distribution is rejected compared to Models 2 and 3 except for L1, and finally,
5. Stationary Gumbel distribution is not rejected in favor of Model 1 except for L5

## 6.2.4 Effective design values and Q-Q Plot diagrams

In addition to the assessment based on the nonstationary approach at the regional locations in the North Sea, extrapolations from all models are made for the better understanding of wind speed variability in potentially reducing risk at such regions. At this point it is important to outline the challenging findings associating the influence of natural climate variability in extreme wind speeds in the evaluated studies on projected changes of the NAO and storm track characteristics reported over the North Sea (e.g., Wang et al., 2004; Kumar et al., 2016 and Mölter et al., 2016). The inference of the latter studies (which is inline in this assessment) found evidence of a slight increase in the frequency of high wind speeds over regional locations at midlatitudes in the Northern Europe challenging the modeling of extremes.

The primarily interset of this assessment is to inference which model represents effectively the extremes in wind speed when the stationarity of the process is violated in order to alleviate the bias effect from the attempt of de-trending the process before the time series is used. Based on the likelihood ratio tests of Models 2 and 3 in this setting fitting better the nonstationary GEV distribution, influences of climate variability on extremes of wind speed are found to occur largely through the location parameter (i.e., Model 2 and 3) with negligible influences on scale and shape parameters (i.e., Models 4,5,6, and 7). Specifically, the design values for the n-th year (10,20,…,100) is illustrated in Figure 6.16 for locations L(1,2,3,4, and 5) in the North Sea to infer the demonstration of all considered parametric models.

To assess the fit of the stationary Model 1 with the fit of the outlining parametric Models 2 and 3, the Q-Q plots are illustrated in Figure 6.16 visualising the good representation of the extremes from these models. If the empirical data align closely with the modelled estimates, then it is likely that the chosen model is a good representation of the true extreme asymptotic form for these samples. It is outlined that Model 2 shows the better fit in terms of the quantile estimates for all locations. These findings are inline with the study from Cheng et al., 2014 in the NEVA assessment (see Apendix D) and from Smith, (2003) manifesting that the simple representation of the trend in the parameterization of the location parameter (i.e., the most likely observed extremes) allows estimating return values in a more realistic way consistent with the climatic variability of extremes. However, Model 2 is challenged at L1 where although the null hypothesis is regected compared to Model 1 (stationary 3 parameters), it is not rejected compared to the Gumbel model (stationary 2 parameters). This is somehow reasonable from the intractable problem of inference of the maximum likelihood estimator to distributions of more parameters to be estimated (Model 1 of three parameters) than less parameters estimated such as the Gumbel distribution of two parameters. However, the extrapolations made at L1 inference the underestimation of Model 1 as a stationary model of 2 parameters. The uneffectiveness of Model 1 as a stationary model of 3 parameters is also demonstrated at L5 in comparison to the return level estimates made from the parametric Models 2 and 3.

The dataset used is ERA-20C and the estimations of the parametric GEV is based on the Maximum Likelihood Estimator. The statistical software package (extRemes) in R (Gilleland and Katz, 2016) is used for the estimation of the associated parameters. Inference from the effective design values pointed out that the stationary model of 2 or 3 parameters in general, underestimates the extrapolations made of the extremes of wind speed.

**(a)**



Location L1

**(b)**



QQ plot Location L1

**(c)**



Location L2

**(d)**



QQ plot Location L2

**(e)**



Location L3

**(f)**



QQ plot Location L3

**(g)**

**(h)**



**(i)**

**(j)**
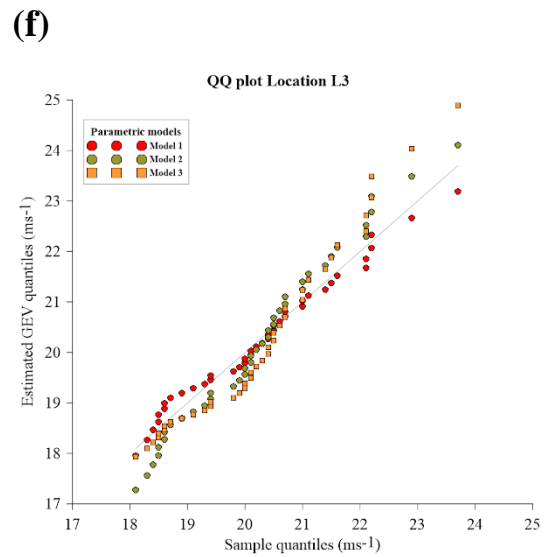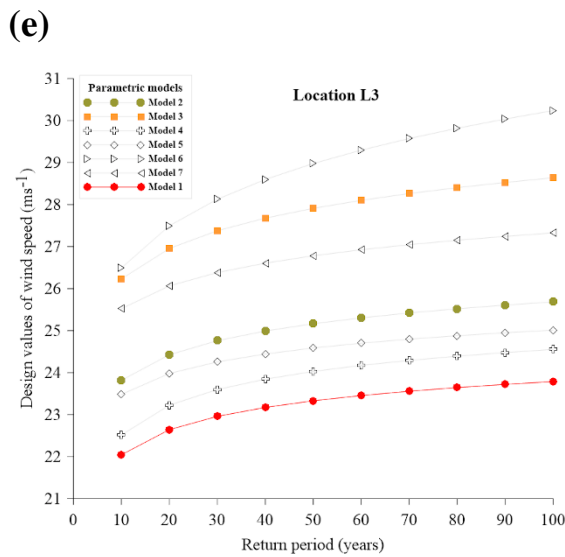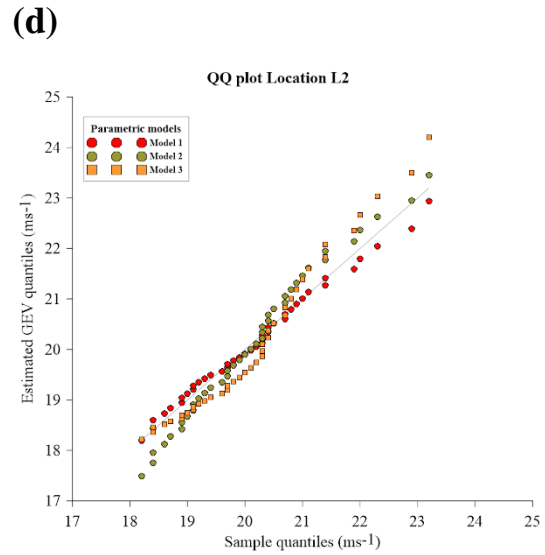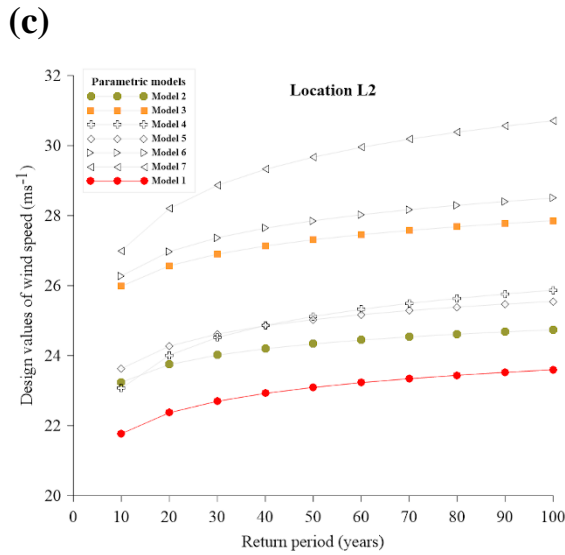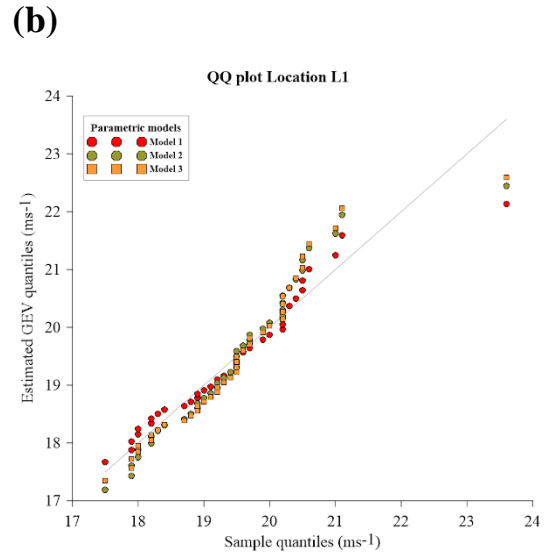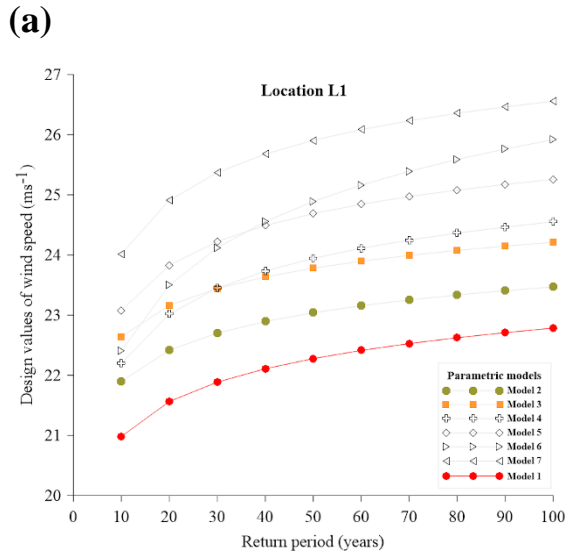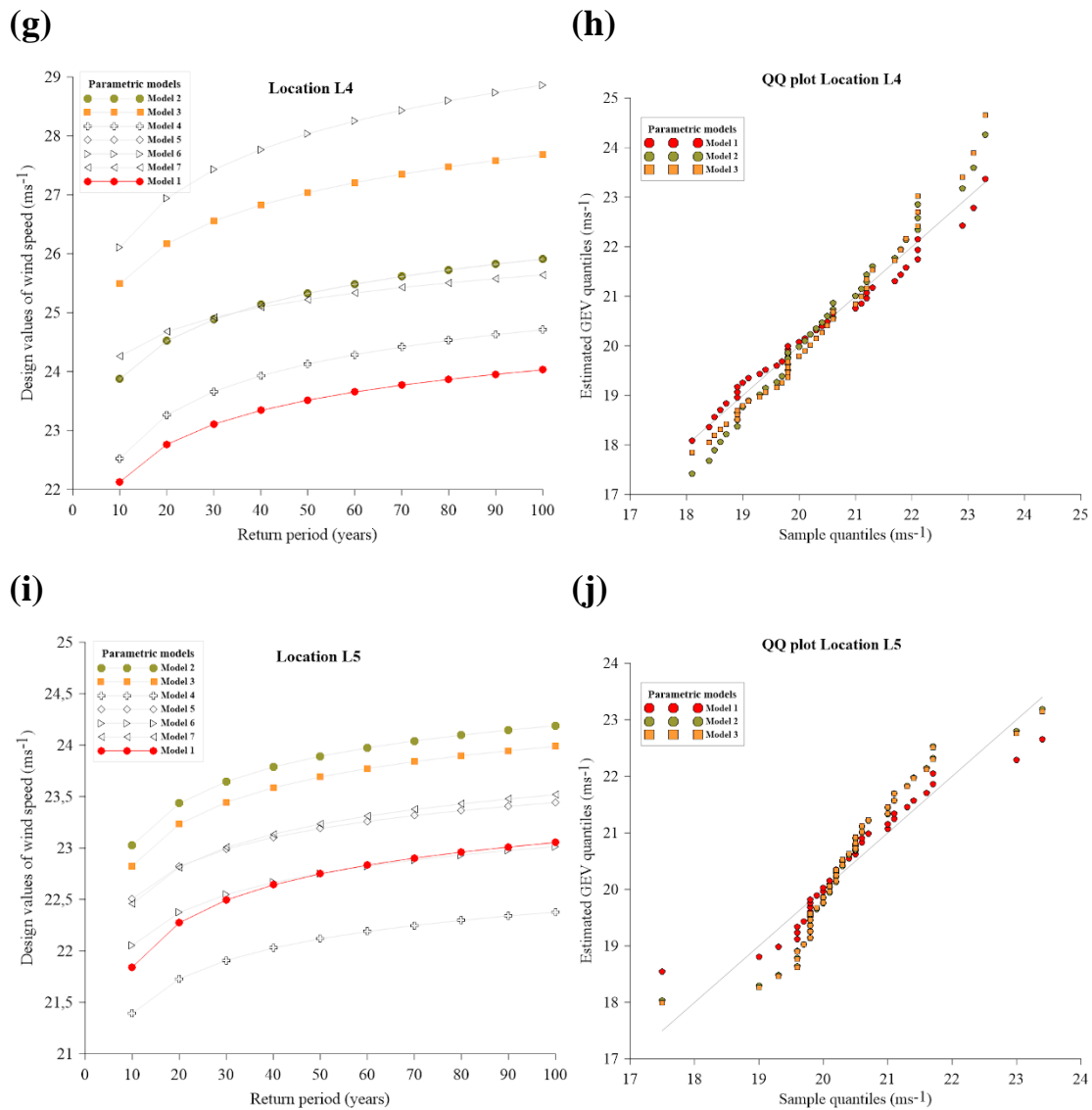


Figure 6.16: Estimation of the Design Values for the parameterized GEV distribution parameters in (a,c,e,g, and i) and the Q-Q Plots for Models 1,2 and 3 in (b,d,f,h, and j). (Tsalis and Kallos, 2017)

In addition, the parameter estimates of the parametric Model 2 is presented in Table 6.11 as the effective model with the simplest form representing the trend of the most likely observed extremes in a time dependent climate. The similar force mechanism previously discussed (i.e., associated to the NAO and the srorm track changes) that influences the climate variability on extremes of wind speed is obtained at locations where the parametric model represents the trend in a similar way. Specifically, the Model 2 at locations L (2,3, and 4) is a good representaion of the trend based on the parameterization of $\mu_0$ and $\mu_1$ of the same magnitude. However, in L1 and L5 parameter $\mu_0$ is of the same magnitude as in L(2,3,and 4) but less similar estimates is obtained for parameter $\mu_1$. This intractable problem of inference is somehow explained from the different forcing mechanism that suggests different patterns of climate variability between regional location in the Northern and Central North Sea (Kumar et al., 2016). To this effect, we recall the previous discussion made in sub-Section 5.2.2 where the tail extremity of the time series in L1 and L5 suggested more intense extremes than in L(2,3, and 4). As also discussed in Wang et al., (2004), in the strong forcing cases obtained at the Northern and Central North Sea locations a simple linear representation of the trend (i.e., Model 2) is probably not the best representation indicating a faster increase of the trend such as a

quadratic form (i.e., Model 3). However, given the powerful statistical tests applied to several parametric models and the long period (40 years) of data, Model 2 inferred as an effective model that represents the trend in extremes of wind speed in a simple linear form when the stationarity of the process is violated.

Table 6.11: Parameters and (SE) in parenthesis of the linear trend in location from Model 2.

| Locations | $\mu_0$ | $\mu_1$ | $\sigma_0$ | $\xi_0$ |
|---|---|---|---|---|
| L1 | 18.455 | 0.027 | 0.929 | -0.096 |
|  | (0.313) | (0.014) | (0.112) | (0.089) |
| L2 | 18.794 | 0.045 | 0.954 | -0.119 |
|  | (0.337) | (0.015) | (0.117) | (0.109) |
| L3 | 18.648 | 0.053 | 1.033 | -0.077 |
|  | (0.378) | (0.016) | (0.135) | (0.130) |
| L4 | 18.720 | 0.053 | 1.007 | -0.044 |
|  | (0.354) | (0.015) | (0.133) | (0.133) |
| L5 | 19.310 | 0.036 | 0.891 | -0.174 |
|  | (0.308) | (0.013) | (0.101) | (0.076) |

Numerus authors however resulted similar wind speed positive trend estimations with the present analysis in the North Sea. For example, Siegismund and Schrum (2001) detected an increase of the annual mean wind speed of about 10 % over the North Sea based on the NCEP/NCAR Reanalysis dataset (NCEP) (Kalnay et al., 1996) over the period 1958 - 1997. Also based on NCEP, Pryor and Barthelmie (2003) found increased wind speeds at 850 hPa over the Baltic Sea during the latter half of the 20th century in both mean and extreme wind speeds. Alexander et al., (2005) used pressure values to show a similar increase in the number of storms over the UK since 1950. However, updated time series show that an increase until 1990 was followed by a decrease since the 1990s (e.g. Matulla et al., 2007; Alexandersson et al., 2000).

The main scope of the present analysis was to effectively model non stationary GEV distribution parameters, as linear or nonlinear functions of the covariates on which the data show dependence. The basic remarks from the demonstration of these parametric models are the following:

- The linear Model 2 and quadratic Model 3 are overall evident models of detecting significant trends of the extremes of wind speed in the North Sea.
- The stationary Model 1 generally provided relatively small 50 and 100-year design values over all locations.

This approach in extreme environmental studies considers estimations in design values in a more realistic way under the assumption of a time changing climate. In addition to the study of existing trends in reanalysis or hindcast data, climate scenarios are tested for the occurrence of future trends. Evidence of future trends influencing the wind profile in the North Sea can be found in the literature. Most of them are connected to changes in the North-Atlantic storm track. Rockel and Woth (2007) identified increases in the storm climate with most significant trends for regions, influenced by the North Atlantic extra-tropical storms. Carnell et al., (1996) resulted a progressive rise in storm activity in the North-East Atlantic. This is linked to a northern shift of the North Atlantic storm track (Bengtssonet et al., 2006; Knippertz et al., 2000). A more detailed view of observed trends and variability in the wind climate of the North Sea during the last decades, is still lacking and further examination is mandatory.

## 6.3 The response of DeCAUn using the MARINA Platform database

The response of the DeCAUn model in applications considering a limited availability in data is one key factor in this part of the results. Therefore, the assessment is carried out for relatively small datasets of annual wind speed time series, corresponding to four sample periods of 10, 15, 20 and 25 years long. The performance of the re-sampled models DeCAUn.1 and DeCAUn.2, are compared within the quantile estimates from the standard de-clustering Runs in a POT selection, the DeCA model and the BM model at equally correspondent sample size.

For this evaluation the standard MLE method was implemented to the proposed and existing models. Furthermore, the quantile estimations of all models is evaluated based on estimates from the BM approach with block size of one year and assuming the available records are of at least 20 years. This BM will be regarded as the reference model (BM Ref.) considering the maximum available time series extending from 1979-2016 (38 years long) originated from the ERA-Interim product, from the ERA-20C extending from 1961-2010 (50 years long) and for the period 1996–2015 (20 years) from the MARINA Platform database.

The second key factor illustrated and discussed henceforth, is the response of the proposed model with regards to the return levels (design values) and return periods of wind speed originated from a high resolution dataproduct for locations selected over the North Sea, the Atlantic Ocean and the Mediterranean Sea. The findings of the model response from the statistical analysis will be discussed in the following sub-Sections summarizing the performance of DeCAUn for the selected 30 locations of the MARINA Platform database.

The criteria of the regional locations selected in this study are related to storm-related losses as evidence of increasing vulnerability to wind extremes in the offshore study region (Schwierz et al., 2010). In this analysis a high resolution dataset is used for a better representation of the wind climate at locations that are exposed to topographically complex regions especially near the coastline in this study. The effects on the simulation of wind climates from the increase in horizontal resolution is discussed from Pryor et al., (2010). In their study, the increase in model resolution increased the domain-averaged mean wind speed at 10 (m) height and the extrapolated 50 year return levels. In addition to their findings, the impact effect of the increase in model resolution is considerable in wind climate extremes rather than the effect in the mean wind speed. However it is important to stress that the high resolution product such as the MARINA Platform database is limited to the number of historical data where this effect is alleviated using reanalysis products such as the ERA-Interim or the ERA-20.

Considering the restrictions of re-sampling a relatively small sample, a dependent sample of extremes was reconstructed successfully by DeCAUn to an efficient independent sample converging to the i.i.d limitations. In addition, the number of the re-sampled extremes for each location is in agreement with the extreme wind variability at these sites of interest.

All re-samples from the DeCAUn model assume that an average of at least 1.65 peaks per year should be selected in a POT approach in order to gain advantage over BM (Cunnane, 1973; Tanaka and Takara, 2002; Serinaldi and Kilsby, 2014). The $nrmse$ measure of the re-samples was evaluated for all DEP reduction levels (60,65,70,75,80,85,90 and 95), normalized bandwidths $C \in [0.125,1]$ with a 0.125 step and statistical threshold considerations. In addition, the $nrmse$ measure of performance was applied for samples of 10 and 15 years, regarding sample periods from 1996-2005 and 1996-2010 respectively. Furthermore, the quantile estimates from DeCAUn were compared to the corresponding estimates obtained by the reference model (BM Ref.), employing to the latter the maximum available series extending from 1996 to 2015 (20 years).

Estimations in terms of the optimum DEP levels will be presented for the physical de-clustering DeCA approach at each sample period for the 30 selected locations in sub-Section 6.3.1. In addition to the results for these locations, estimations of the normalized bandwidth $C$ and the desired lag $(k)$-apart value of observations are included in sub-Sections 6.3.2 - 6.3.3 for the optimum performance of the Gaussian Kernel estimator and the optimum irregular re-sampling process used, respectively. Moreover, the associated $nrmse$ measure of performance

is also presented in sub-Section 6.3.4 for the optimum re-sample of the DeCAUn model at each location and in sub-Section 6.3.5 the estimates are summarized for the 30 locations.

Furthermore, for a comprehensive analysis, one characteristic location from each examined area (locations L2, L16, and L21) was selected for the evaluation in terms of the quantile projection and variability of the DeCAUn model. The foregoing estimations are highlighted in sub-Sections 6.3.6-6.3.8 respectively.

## 6.3.1 DEP level estimates

Beginning with the estimated DEP level of energy reductions for the physical de-clustering approach from DeCA, the results are presented in Figure 6.17 by means of colored dots assigned to the eight % levels (60,…,95) with a 5% step. The DEP level estimates per sample period resulted a safe range for DeCA to cluster events without the loss of valuable information. In general, the increase in sample size lead to reductions in the DEP level for the majority of the locations. Specifically, as the sample period increased from 10 to 15 years the modal value estimate of DEP was slightly reduced for the 10 locations (L1, L2, … L9, and L10) in the North Sea. Additionally, reductions of the mode estimate of the DEP level is obtained for the 10 locations in the Atlantic (L11, L12, … L19, and L20) and the 10 locations (L21, L22, … L29, and L30) in the Mediterranean respectively. The increase in sample size does not necessarily follow the large increase in the number of extreme events as expected. The approximate stable or reduced DEP level estimates as the sample size increased controlled the DeCA model to encompass the largest number of events as possible. The response of DeCAUn to the modal value estimates of the DEP levels is illustrated in the following Figure 6.17 (a,b) at the 30 regional locations of interest. Inference is made for the number of observations of the samples of DeCA that are irregularly spaced in time and most likely to be sampled from these locations.
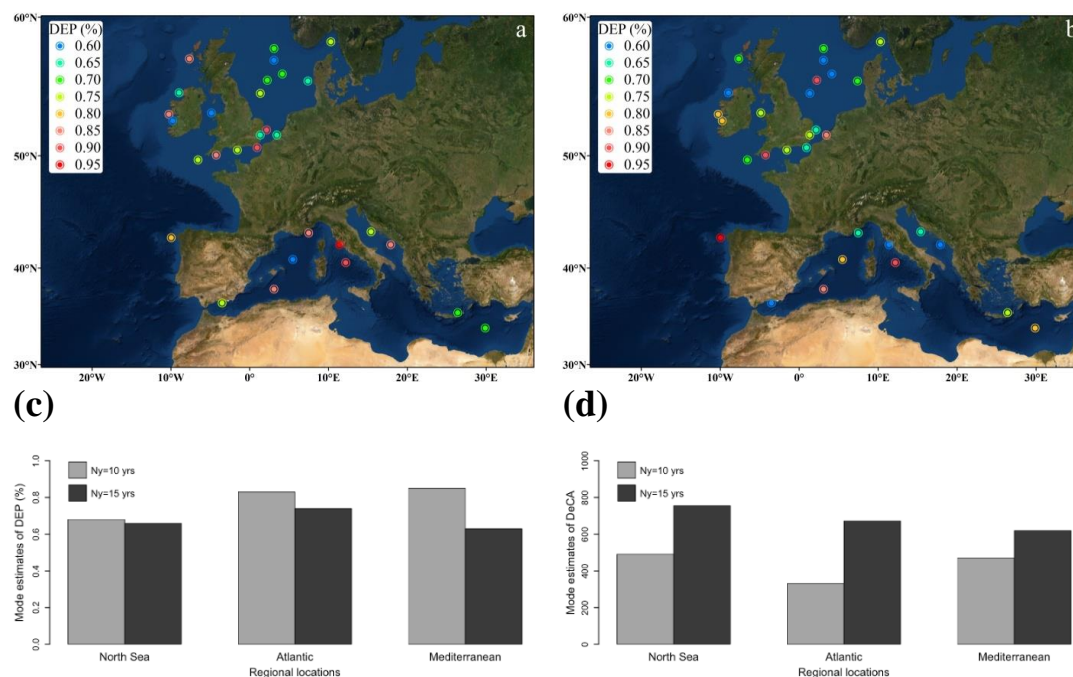


Figure 6.17: DEP (%) level estimates of energy reductions for the physical de-clustering approach from DeCA using samples of (a) 10 and (b) 15 years. The modal value estimates of the DEP (%) reduction level to the 10 locations in each region for sample periods of 10 and 15 years illustrated in (c) and the likely number of events from DeCA to these locations in (d). (Tsalis et al., 2021)

The moderate to low mode value estimates of the DEP levels for the 10 locations in the North Sea (0.68 for the 10 years and 0.66 for the 15 years) are in line with the variability of

extreme winds over this region. One key point of this agreement is the influence described by the large-scale circulation patterns such as the North Atlantic oscillation (NAO) on the wind speed over the North Sea. The index of the North Atlantic oscillation (NAOI) is strongly correlated with the wind speed over northern Europe, having an impact on the cyclones generating in this area by shifting the westerly zonal flow. However, an increase in the NAOI and the mean wind speeds from the 1960s to the mid-1990s does not necessarily increase the extreme wind profile (Sušelj et al., 2010). Thus, the DEP estimates for these locations are controlled by DeCA to a moderate to low level in order to enlarge as much as possible the number of extreme wind storm events.

Considering the Atlantic where strong extra-tropical storms can cause massive storm surges affecting the 10 locations there, the moderate to high mode value estimates of DEP (0.83 for the 10 years and 0.74 for the 15 years) is somewhat reasonable. It is well known that the extra-tropical cyclones travel eastward along the polar jet stream, e.g. (the Icelandic Low and Azores High.). Thus, the prevailing westerlies affecting the locations (L16, L19, L14, L17, and L20) in the North Atlantic (Feser et al., 2015), justify the moderate to high DEP estimates from a large number of extreme wind storm events obtained over these sites. On the other hand, locations (L15, L12, L11, and L18) in the Central and location L13 in the South Atlantic are also influenced by the strong pressure centers over the Atlantic Ocean. Specifically, the number of atmospheric circulation patterns that govern the extreme wind speed variability at these locations are influenced by the atmospheric dynamics in the North Atlantic as discussed in Pascual et al., (2013), justifying the DEP estimates at this region.

For the 10 locations in the Mediterranean, the mode value estimates of the DEP level is characterized as moderate to high (0.85 for the 10 years) and low (0.63 for the 15 years). The nature of the storms in this semi-enclosed basin is subjected to many external factors, like land–sea contrasts, near-surface temperatures, atmospheric waves and large-scale weather patterns (Flaounas et al., 2015 b; Campins et al., 2011). Although the windiest areas of the Mediterranean Sea are located in the NW- SW part e.g. locations (L25, L26, L21, and L27) and the SE part e.g. locations (L22 and L23) the DEP level estimations at these locations are characterized as moderate. This effect is due to the large but constant wind conditions at these sites, where DeCA is controlled by a moderate level of DEP in order to encompass the largest number of extreme wind storm events as possible. On the contrary, locations (L28, L29, L24, and L30) at the Central and North Mediterranean are characterized by a high DEP level as expected, where the largest number of explosive cyclogenesis is observed.

From the demonstration of DeCAUn to the MARINA Platform database the assessment yielded the most likely DEP reduction level to range approximately from 0.68 to 0.85 with regards to the sample period of 10 years and from 0.63 to 0.74 for the sample of 15 years.

## 6.3.2 Bandwidth estimates

In this Section, the results of the optimum normalized bandwidths for the 30 locations are presented from the empirical selection procedure as described previously in sub-Section 4.4. The most likely optimal normalized bandwidth estimates illustrated in Figure 6.18 (a,b) range in a bound from 0.126 to 0.267 avoiding over or under smoothing Kernel adjustments. It is apparent that as the sample period increased from 10 to 15 years, the optimal normalized bandwidth was reduced for the majority of the locations.

Given the relatively small sample period of data such as 10 years, it is not surprising that we obtain a limited number of events from the DeCA model. Thus, the irregular sample of DeCA will be characterized by a limited amount of values surrounding the mean width of the time intervals. As a consequence, the Gaussian weight function adjusted accordingly to the largest bandwidth for the sample period of 10 years. In this way, for the estimator of the irregular ACF in Equation (4.21) the largest possible number of higher weights is assigned to the inter-sampling time intervals closer to the given time lag ($k$). In other words, the weight function stretched out to a wider bandwidth scale in sample periods where little information is

available. Conversely, as the sample period increased from 10 to 15 years the optimal normalized bandwidth reduced, leading accordingly to a less wide bandwidth adjustment of the weight function. For locations characterized of strong but stable wind profile the increase of the sample period increased the bandwidth as a response of DeCAUn to the inconsistent increase of extremes as the sample size increased. In general, as the sample size increased the bandwidth estimates reduced as shown from the Gaussian–based correlation analysis of the ACF estimator SIMILARITY in the irregular DeCA samples. The reduced trend of the most likely optimal normalized bandwidth estimates to smaller values as the sample size increased is systematically obtained in the regional locations at the North Sea and the Mediterranean and to a lower extent obtained at the Atlantic as illustrated in Figure 6.18 (c).
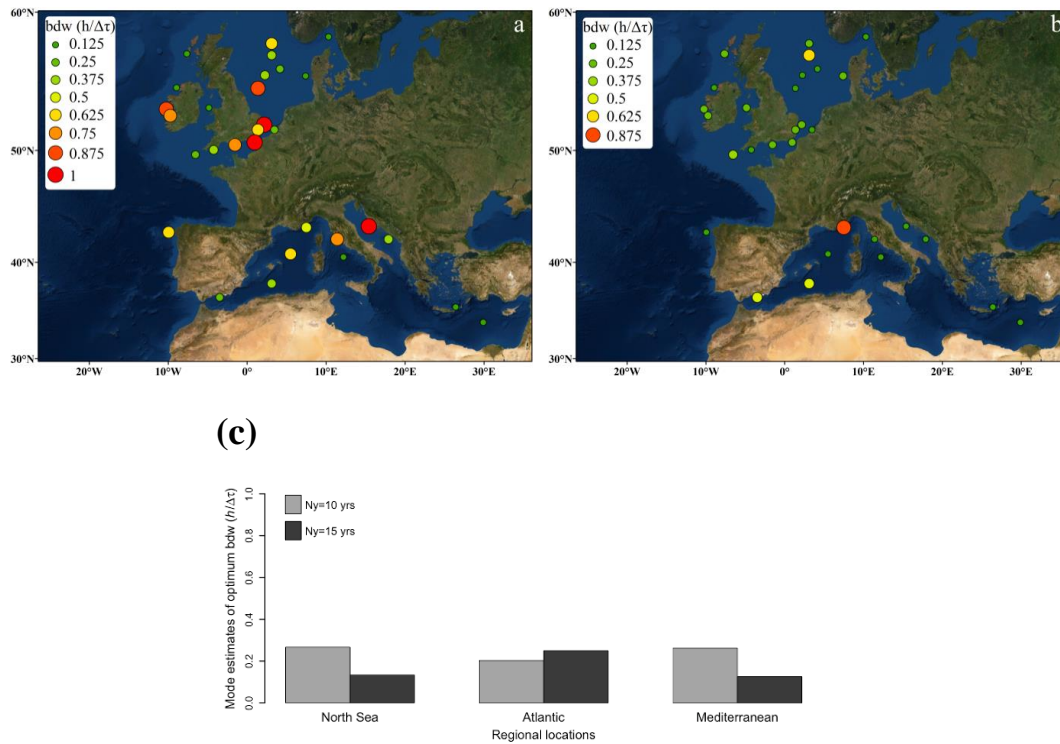


Figure 6.18: Optimum normalized bandwidth estimates of the Gaussian Kernel weight function applied to the irregular ACF estimator using samples of (a) 10 and (b) 15 years. The modal value estimates of the optimum normalized bandwidth considering the 30 regional locations are illustrated for sample periods of 10 and 15 years in (c). (Tsalis et al., 2021)

For inference of DeCAUn to the bandwidth response using the MARINA Platform database at the 30 regional locations, estimations of the most likely optimal normalized bandwidths pointed out to range approximately from 0.203 to 0.267 for the sample of 10 years and from 0.126 to 0.25 for the sample of 15 years.

## 6.3.3 Lag ($k$) estimates

The required lag($k$)-apart value of observations is presented for the re-sampling procedure at each location. The desired lag value estimates of $k$ will assign the statistically independent events from the optimum re-sample of DeCAUn at each sample period.

With an increasing sample period, the lag($k$) also increased for the majority of the examined locations illustrated in Figure 6.19 (a,b). In general, for the sample period of 10 years, the lower lag value estimate of $k$ ensures a successful trade-off between excluding events and loss of information. Thus, in order to increase the number of events and consequently the associated inter-sampling time intervals of the weights to be applied, a lower lag($k$) is selected.

Conversely, as the sample period increased from 10 to 15 years the irregular ACF estimator was adjusted to a larger lag($k$). As a consequence, the ACF estimator included a sufficient amount of independent events more efficiently at the larger sample period. The effect of DeCAUn to the mode estimates of the desired lag($k$) is illustrated in Figure 6.19 (c), where generally an increment of the mode estimates is obtained as the sample size increases. Inference is also made illustrating DeCAUn.2 to the most likely re-sampling scheme from the demonstration of DeCAUn at each sample period and region in Figure 6.19 (d).



**(c)**

**(d)**
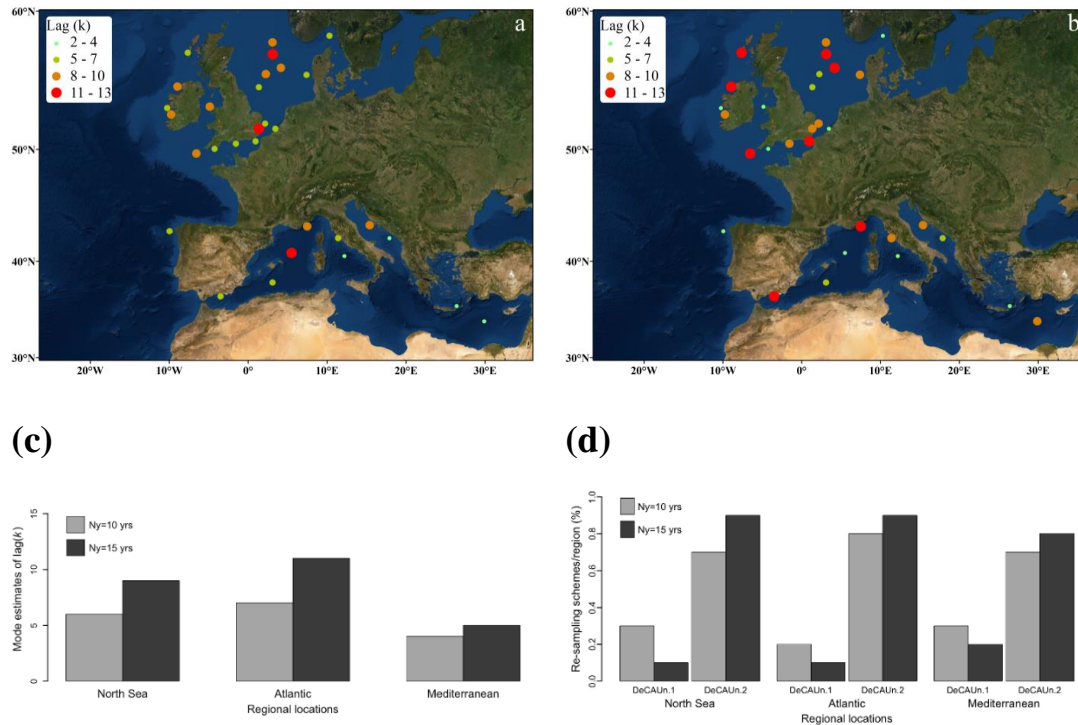


Figure 6.19: Lag($k$)-apart value of observations for re-sampling the irregular DeCA samples from DeCAUn using samples of (a) 10 and (b) 15 years. The modal value estimates of the desired lag($k$) to each region illustrated for sample periods of 10 and 15 years in (c). The re-sampling scheme performance of DeCAUn as a percentage (%) to the regional locations and at each sample period is illustrated in (d). (Tsalis et al., 2021)

The response of DeCAUn to the lag($k$) estimates is also closely related to the DEP% estimates that form the samples of DeCA. Specifically, for locations of strong winds and low volatility in extremes, the demonstration of DeCAUn in the increase of sample period resulted to higher DEP and to relatively smaller lag($k$). When little information of extremes is apparent at these locations, the lower lag($k$) is preferable to form clusters efficiently of larger length and consequently derive samples of higher DEP. To this effect, an example is presented in the following Table 6.12 for one case at the two sample periods of examination.

Table 6.12: DeCAUn model response using samples of 10 and 15 years for the NW location L21 in the Mediterranean

| Ny | $nrmse$ | DEP | No. DeCA cluster | bdw | re-sampling scheme | AIC-MSE | lowest | lag($k$) | No. DeCAUn cluster | $u$(m/s) | No. Thres. Exceedances |
|---|---|---|---|---|---|---|---|---|---|---|---|
| **10 yrs** | 0.011 | 60% | 635 | 0.625 | DeCAUn.1 | MSE | 64.700 | 11 | 57 | 0.000 | 57 |
| **15 yrs** | 0.007 | 80% | 737 | 0.125 | DeCAUn.2 | MSE | 9.420 | 3 | 200 | 16.997 | 90 |

Inference based on the lag value estimates of $k$ at the associated DEP level is also made for the number of the asymptotically independent events from DeCAUn. Under the DeCAUn.2 scheme for the locations in the North Sea, the likely number of re-sampled events is

approximated at (3.8/year) for the sample period of 10 years, and at (3.9/year) events for the 15 years respectively. Similarly, for the locations in the Atlantic the likely number of re-sampled events under the DeCAUn.2 scheme, is approximated at (4.8/year) for the 10 years and at (3.7/year) for the 15 years. Finally, for the locations in the Mediterranean DeCAUn.2 re-sampled approximately a number of (5.4/year) events for the 10 years and a number of (5.2/year) for the 15 years respectively. As a remark also discussed in 6.3.1 and 6.3.3, the increase in sample size does not necessarily follow the large increase in the number of extreme events, setting the estimated range of events in line with the variability of extreme winds over these regions.

## 6.3.4 The *nrmse* measure for DeCAUn

The estimation of the *nrmse* measure and its relation to the sample period resulted in something unsurprising for the majority of locations. Increase in the sample period increased the precision of *nrmse* to the quantile estimates of DeCAUn. To this effect, the re-sampled models and their fit to the GPD distribution are based on a larger amount of values containing more information about the tail behavior. Therefore, the quantile estimates of DeCAUn to a GPD fit converged with the increase in sample period to the quantile estimates of the BM Ref. fit to the GEV. This is illustrated in Figure 6.20(a) where the quantitative measure of performance of the optimum re-sampled models from DeCAUn generally reduced as the sample period increased. It is also outlined at the bar chart of Figure 6.20(b) that as the sample size increased from 10 to 15 years the most likely observed *nrmse* statistic of DeCAUn reduced smoothly considering the 30 regional locations of the MARINA Platform database.

**(a)**
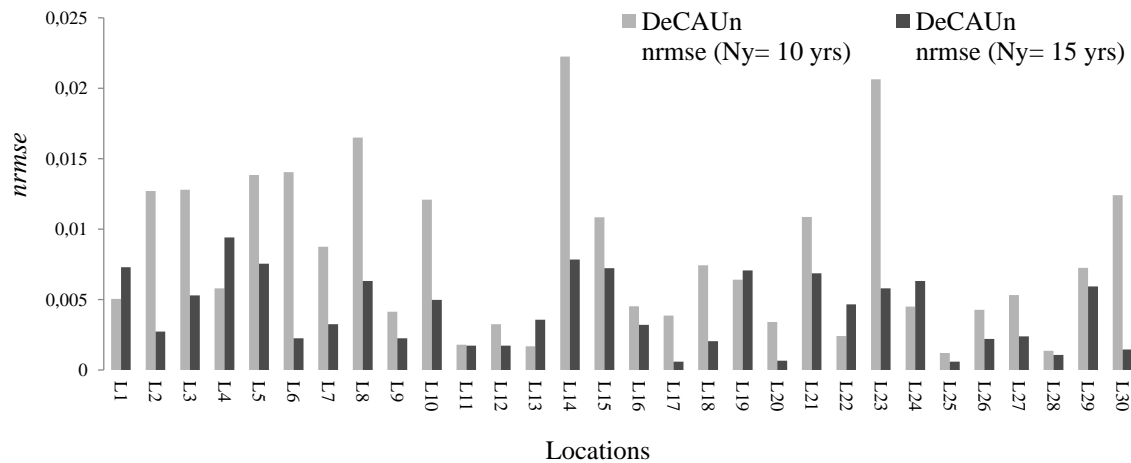


**(b)**
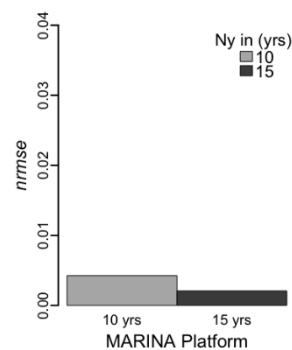
Figure 6.20: *nrmse* for the optimum re-sample of the DeCAUn model regarding the 30 locations (L1,..,L29, and L30). The increase in sample period reduced the *nrmse* measure for the majority of locations in (a). (Tsalis et al., 2021). The modal value estimates of the *nrmse* measure illustrated for sample periods of 10 and 15 years in (b). (Supplementary material of Tsalis et al., 2021)

The increase in sample period does not reduce the *nrmse* measure for all locations. This reverse proportional behavior of the measure is possible explained by the weak performance of the reference model BM Ref. at the locations (L1, L4, L13, L19, L22, and L24). The over-under quantile estimates from the reference model using small samples such as the available sample of 20 years, is also discussed in (An and Pandey, 2007; Ceppi et al., 2008; and Della-Marta et al., 2009). However, high wind speeds are frequently apparent at these locations as obtained in Table 5.7. To this effect, the available samples will probably force the fit of the extremes to the GEV to lie near the mode of the distribution and hence away from the tail area of interest. Hence, the reference model described by the BM approach will probably not give the best fit to the tail of the distribution at these locations. For samples of limited information in extremes, the validity of the asymptotic form is challenged. To assess the fit of the reference model BM Ref. to the GEV and the DeCAUn model to the GPD, the Q-Q, P-P and Kernel Density plots is illustrated in Figure 6.21 for one case (L13). If the empirical data align closely with the modelled estimates, then it is likely that the chosen model for relatively small samples of wind speed is a good representation of the true extreme asymptotic form for these samples. In addition, the 95% confidence bands are also provided based on the Kolmogorov-Smirnov statistic (Doksum and Sievers, 1976).
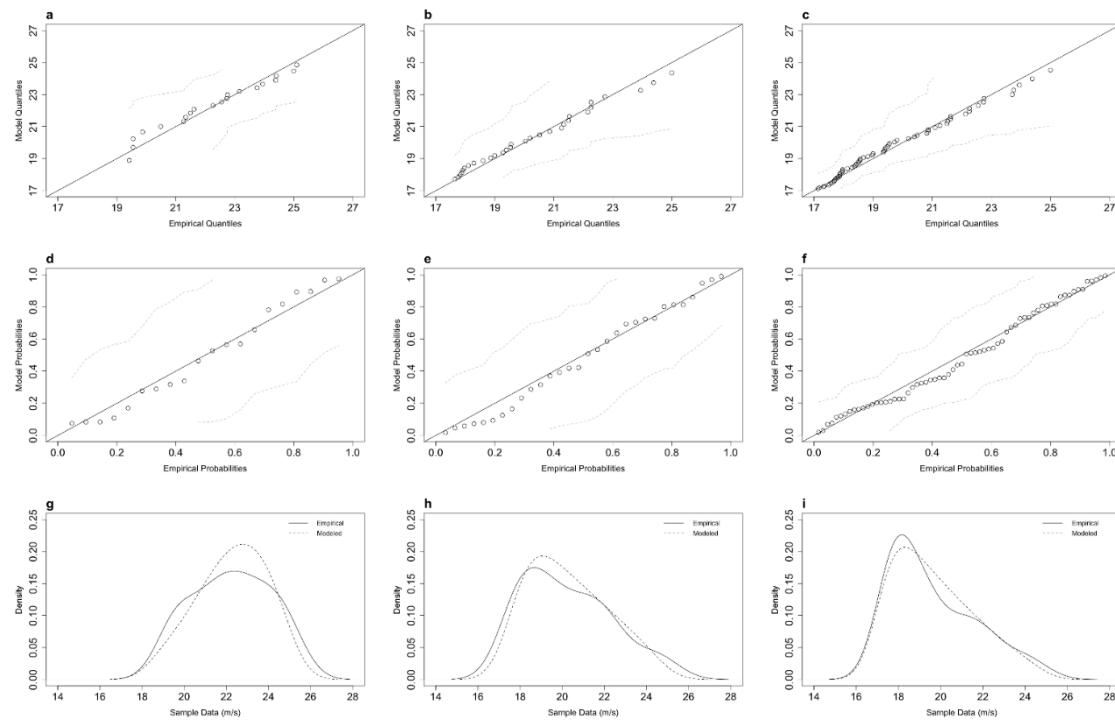


Figure 6.21: Visual inspection of the Q-Q, P-P and Kernel Density plot for L13 using the reference model BM Ref. for samples of 20 years in (a, d, g) and the proposed model DeCAUn for samples of 10 years in (b, e, h) and 15 years in (c, f, and i). For the Kernel Density plots of the BM Ref. model the bandwidth is set at 0.918 for the Empirical Density and at 0.8066 for the Modeled Density. Considering the DeCAUn model at 10 and 15 years the bandwidth is set at 0.9635 and 0.8052 for the Empirical and at 0.8542 and 0.7473 for the Modeled Density respectively. Dashed light grey lines in (a, b, c, d, e, and f) show the 95% pointwise tolerance intervals. The statistical software package (extRemes) in R (Gilleland and Katz, 2016) is used for the estimation of the associated parameters and diagram illustration. Illustrated also in Tsalis et al., (2021).

## 6.3.5 Summarizing DeCAUn model estimates

Estimations from the DeCAUn model are presented for the 30 locations with regards to the sample period of 10 and 15 years, obtaining design values of the 50 years return period $DV(50)$ and the confidence intervals denoted in italics, (Table 6.13 and 6.14). As a comparable measure we also denote the design value estimates $DV$ from the BM Ref. model at the same return period. The number of cluster maxima before and after the irregular modeling is also provided, the re-sampled models of DeCAUn, the lowest AIC and MSE statistic measures of the models, and finally the associated total number of peak exceedances fitting the GPD distribution.

Table 6.13: Model estimations for DeCAUn with regards to the sample period of 10 years extending from 1996 to 2005.

| Location | $DV(50)$ BM Ref. | Width of (CI) BM Ref. | $DV(50)$ DeCAUn | Width of (CI) DeCAUn | No.DeCA cluster | re-sampling scheme | AIC-MSE | lowest | No. DeCAUn cluster | $u$(m/s) | No. Thres. Exceedances |
|---|---|---|---|---|---|---|---|---|---|---|---|
| L1 | 25.894 | 0.945 | 25.793 | 1.980 | 513 | DeCAUn.2 | AIC | 238.075 | 68 | 15.007 | 51 |
| L2 | 26.592 | 4.835 | 26.841 | 5.989 | 225 | DeCAUn.2 | AIC | 100.512 | 30 | 16.852 | 22 |
| L3 | 25.836 | 5.397 | 26.154 | 7.652 | 528 | DeCAUn.1 | MSE | 15.720 | 106 | 12.142 | 53 |
| L4 | 26.093 | 6.010 | 26.086 | 4.495 | 419 | DeCAUn.2 | AIC | 78.251 | 64 | 19.273 | 22 |
| L5 | 28.433 | 4.657 | 28.226 | 8.381 | 545 | DeCAUn.1 | MSE | 73.450 | 45 | 0.000 | 45 |
| L6 | 23.930 | 1.796 | 23.576 | 3.854 | 406 | DeCAUn.2 | AIC | 153.035 | 51 | 16.068 | 38 |
| L7 | 24.331 | 2.643 | 24.350 | 7.011 | 514 | DeCAUn.1 | MSE | 55.100 | 43 | 0.000 | 43 |
| L8 | 28.669 | 4.947 | 28.940 | 5.557 | 465 | DeCAUn.2 | MSE | 20.140 | 35 | 17.110 | 26 |
| L9 | 26.686 | 2.845 | 26.660 | 3.629 | 467 | DeCAUn.2 | MSE | 16.700 | 34 | 16.387 | 25 |
| L10 | 27.805 | 4.303 | 28.065 | 4.726 | 448 | DeCAUn.2 | MSE | 20.510 | 32 | 16.748 | 24 |
| L11 | 24.266 | 0.997 | 24.284 | 2.700 | 431 | DeCAUn.2 | MSE | 8.740 | 50 | 17.040 | 25 |
| L12 | 24.767 | 1.122 | 24.826 | 4.214 | 298 | DeCAUn.2 | AIC | 82.652 | 34 | 17.703 | 20 |
| L13 | 25.174 | 2.055 | 25.172 | 4.969 | 375 | DeCAUn.2 | AIC | 119.096 | 61 | 17.574 | 30 |
| L14 | 28.200 | 5.343 | 28.800 | 5.840 | 289 | DeCAUn.2 | AIC | 109.212 | 32 | 18.443 | 24 |
| L15 | 26.827 | 3.061 | 26.919 | 7.304 | 400 | DeCAUn.1 | AIC | 293.395 | 44 | 0.000 | 44 |
| L16 | 28.721 | 2.403 | 28.859 | 7.353 | 315 | DeCAUn.2 | MSE | 10.150 | 52 | 20.659 | 23 |
| L17 | 26.110 | 1.869 | 26.036 | 5.710 | 600 | DeCAUn.1 | MSE | 69.920 | 75 | 0.000 | 75 |
| L18 | 25.632 | 2.859 | 25.808 | 4.275 | 250 | DeCAUn.2 | AIC | 74.992 | 35 | 17.403 | 17 |
| L19 | 28.542 | 4.625 | 28.751 | 7.501 | 540 | DeCAUn.2 | MSE | 6.540 | 45 | 19.433 | 24 |
| L20 | 24.830 | 0.960 | 24.773 | 1.771 | 600 | DeCAUn.2 | MSE | 7.460 | 53 | 18.470 | 26 |
| L21 | 25.791 | 3.672 | 25.786 | 4.282 | 635 | DeCAUn.1 | MSE | 64.700 | 57 | 0.000 | 57 |
| L22 | 20.875 | 1.968 | 20.929 | 2.374 | 444 | DeCAUn.2 | MSE | 6.400 | 187 | 12.129 | 140 |
| L23 | 20.910 | 3.048 | 20.610 | 4.785 | 490 | DeCAUn.1 | AIC | 419.345 | 245 | 10.266 | 112 |
| L24 | 23.727 | 4.748 | 23.785 | 5.759 | 547 | DeCAUn.2 | AIC | 58.360 | 54 | 17.983 | 20 |
| L25 | 20.700 | 0.904 | 20.724 | 2.070 | 653 | DeCAUn.2 | MSE | 5.080 | 103 | 14.075 | 57 |
| L26 | 21.429 | 1.754 | 21.366 | 2.702 | 308 | DeCAUn.2 | AIC | 57.326 | 43 | 16.784 | 18 |
| L27 | 23.886 | 3.955 | 24.012 | 4.789 | 531 | DeCAUn.2 | AIC | 66.129 | 48 | 18.529 | 21 |

| Location | DV (50) BM Ref. | Width of (CI) BM Ref. | DV (50) DeCAUn | Width of (CI) DeCAUn | No.DeCA cluster | re-sampling scheme | AIC-MSE | lowest | No. DeCAUn cluster | u(m/s) | No. Thres. Exceedances |
|---|---|---|---|---|---|---|---|---|---|---|---|
| L28 | 19.174 | 0.498 | 19.170 | 2.770 | 301 | DeCAUn.2 | AIC | 98.418 | 37 | 13.442 | 27 |
| L29 | 21.219 | 2.404 | 21.101 | 3.003 | 383 | DeCAUn.1 | MSE | 9.720 | 127 | 11.788 | 57 |
| L30 | 21.427 | 0.968 | 21.155 | 4.023 | 428 | DeCAUn.2 | MSE | 5.470 | 115 | 15.012 | 45 |

Table 6.14: Model estimations for DeCAUn with regards to the sample period of 15 years extending from 1996 to 2010.

| Location | DV (50) BM Ref. | Width of (CI) BM Ref. | DV (50) DeCAUn | Width of (CI) DeCAUn | No.DeCA cluster | re-sampling scheme | AIC-MSE | lowest | No. DeCAUn cluster | u(m/s) | No. Thres. Exceedances |
|---|---|---|---|---|---|---|---|---|---|---|---|
| L1 | 25.894 | 0.945 | 25.745 | 3.994 | 720 | DeCAUn.2 | MSE | 10.510 | 71 | 18.202 | 34 |
| L2 | 26.592 | 4.835 | 26.672 | 6.033 | 778 | DeCAUn.2 | AIC | 129.915 | 66 | 18.164 | 33 |
| L3 | 25.836 | 5.397 | 25.890 | 5.854 | 454 | DeCAUn.1 | MSE | 13.990 | 227 | 13.678 | 103 |
| L4 | 26.093 | 6.010 | 25.839 | 4.540 | 900 | DeCAUn.2 | AIC | 87.682 | 104 | 20.024 | 29 |
| L5 | 28.433 | 4.657 | 28.541 | 5.487 | 864 | DeCAUn.2 | AIC | 111.829 | 51 | 19.113 | 25 |
| L6 | 23.930 | 1.796 | 23.942 | 2.278 | 635 | DeCAUn.2 | AIC | 243.521 | 130 | 16.252 | 62 |
| L7 | 24.331 | 2.643 | 24.403 | 3.057 | 610 | DeCAUn.2 | AIC | 102.150 | 52 | 17.252 | 26 |
| L8 | 28.669 | 4.947 | 28.788 | 6.148 | 704 | DeCAUn.2 | AIC | 114.597 | 53 | 19.787 | 27 |
| L9 | 26.686 | 2.845 | 26.720 | 3.365 | 878 | DeCAUn.2 | AIC | 124.461 | 57 | 18.653 | 30 |
| L10 | 27.805 | 4.303 | 27.818 | 4.113 | 347 | DeCAUn.2 | AIC | 185.238 | 56 | 16.411 | 39 |
| L11 | 24.266 | 0.997 | 24.258 | 1.177 | 645 | DeCAUn.2 | AIC | 86.283 | 50 | 19.114 | 25 |
| L12 | 24.767 | 1.122 | 24.811 | 1.498 | 368 | DeCAUn.2 | AIC | 105.115 | 77 | 19.207 | 30 |
| L13 | 25.174 | 2.055 | 25.163 | 2.677 | 298 | DeCAUn.2 | AIC | 251.810 | 130 | 17.057 | 65 |
| L14 | 28.200 | 5.343 | 28.106 | 5.970 | 541 | DeCAUn.1 | MSE | 18.980 | 180 | 14.318 | 90 |
| L15 | 26.827 | 3.061 | 26.939 | 2.727 | 712 | DeCAUn.2 | MSE | 10.580 | 50 | 18.029 | 37 |
| L16 | 28.721 | 2.403 | 28.644 | 1.844 | 742 | DeCAUn.2 | MSE | 17.910 | 47 | 18.325 | 35 |
| L17 | 26.110 | 1.869 | 26.111 | 2.345 | 582 | DeCAUn.2 | AIC | 94.653 | 51 | 19.767 | 25 |
| L18 | 25.632 | 2.859 | 25.676 | 3.457 | 843 | DeCAUn.2 | AIC | 120.108 | 60 | 17.974 | 30 |
| L19 | 28.542 | 4.625 | 28.662 | 5.210 | 918 | DeCAUn.2 | MSE | 5.890 | 54 | 19.811 | 27 |
| L20 | 24.830 | 0.960 | 24.834 | 1.685 | 677 | DeCAUn.2 | MSE | 7.540 | 140 | 17.681 | 64 |
| L21 | 25.791 | 3.672 | 25.865 | 2.831 | 737 | DeCAUn.2 | MSE | 9.420 | 200 | 16.997 | 90 |
| L22 | 20.875 | 1.968 | 20.864 | 1.795 | 617 | DeCAUn.2 | MSE | 7.010 | 127 | 12.928 | 95 |
| L23 | 20.910 | 3.048 | 20.789 | 4.602 | 598 | DeCAUn.2 | AIC | 120.056 | 61 | 14.013 | 33 |
| L24 | 23.727 | 4.748 | 23.577 | 4.383 | 996 | DeCAUn.2 | AIC | 88.248 | 77 | 17.816 | 30 |
| L25 | 20.700 | 0.904 | 20.693 | 1.132 | 1237 | DeCAUn.2 | AIC | 77.223 | 76 | 16.975 | 29 |
| L26 | 21.429 | 1.754 | 21.437 | 2.691 | 509 | DeCAUn.2 | AIC | 63.457 | 67 | 17.625 | 25 |
| L27 | 23.886 | 3.955 | 23.916 | 4.427 | 1087 | DeCAUn.2 | MSE | 3.380 | 62 | 18.703 | 27 |
| L28 | 19.174 | 0.498 | 19.154 | 0.797 | 1189 | DeCAUn.2 | AIC | 160.306 | 91 | 13.474 | 45 |
| L29 | 21.219 | 2.404 | 21.107 | 2.084 | 606 | DeCAUn.1 | MSE | 11.410 | 303 | 10.902 | 148 |
| L30 | 21.427 | 0.968 | 21.399 | 1.825 | 1054 | DeCAUn.1 | AIC | 1058.479 | 175 | 0.000 | 175 |

In line with the aforementioned remarks, design value estimations $DV(50)$ for the 30 locations are illustrated in Figure 6.22 (a) for inference of the wind speed projections of the DeCAUn model. The variability of the design value estimates $DV(50)$ of DeCAUn with the increase of the sample period is illustrated in Figure 6.22 (b).

**(a)**



**(b)**
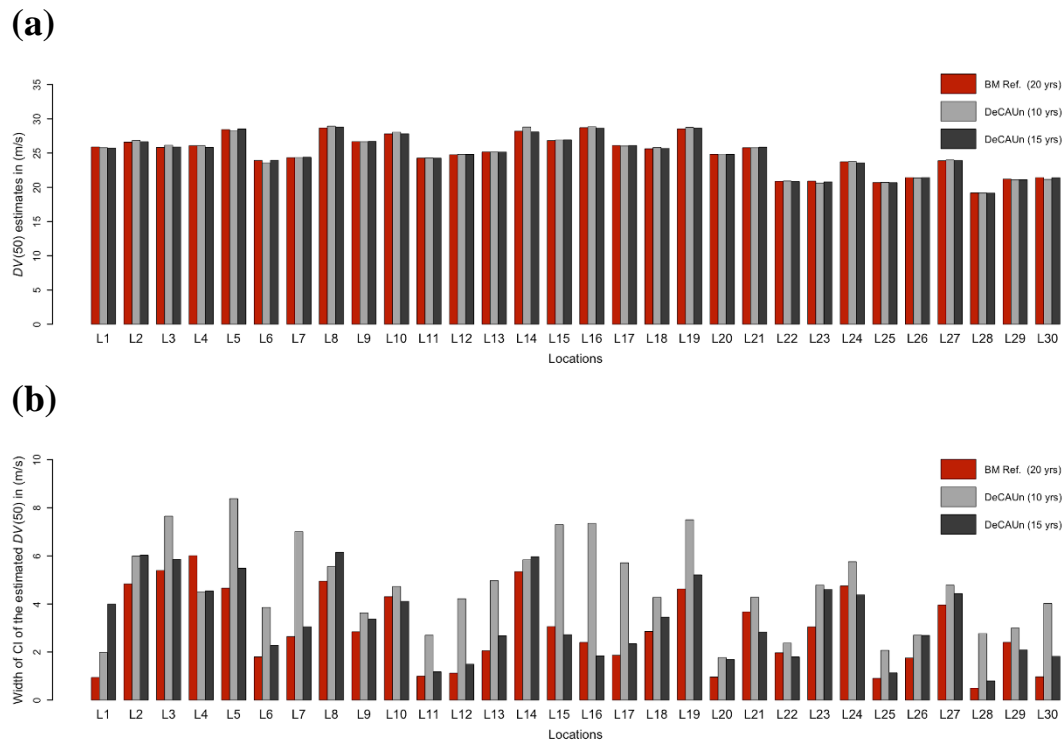


Figure 6.22: The $DV(50)$ estimates of the reference BM Ref. model for sample periods of 20 years (from 1996 to 2015) and DeCAUn for sample periods of 10 years (from 1996 to 2005) and 15 years (from 1996 to 2010) for the 30 locations illustrated in (a). Width of the 95% CI for the $DV(50)$ of DeCAUn for sample periods of 10 years (from 1996 to 2005) and 15 years (from 1996 to 2010) for the 30 locations illustrated in (b). The standard non-parametric bootstrap method (Percentile) is applied to DeCAUn and the normal approximation applied to the BM Ref. model for sample period of 20 years (from 1996 to 2015). Illustrated also in Tsalis et al., (2021)

The most important findings from the assessment of the proposed re-sampling procedure for the 30 locations using wind speed data from the MARINA Platform database can be summarized as follows:

- The assessment yielded the most likely DEP reduction level to range approximately from 0.68 to 0.85 with regards to the sample period of 10 years and from 0.63 to 0.74 for the sample of 15 years.
- Furthermore, estimations in terms of the most likely optimal normalized bandwidths are summarized approximately to range from 0.203 to 0.267 for the sample of 10 years and from 0.126 to 0.25 for the sample of 15 years.
- Although the 50 years return levels of DeCAUn are reasonable for both sample periods of 10 and 15 years in comparison to the extrapolation made from the BM Ref. model based on samples of 20 years, the proposed model is confounded by large variability followed by the reduction in sample size from the proposed re-sampling procedure.
- Inference is made on the most likely re-sampled number of independent events which is in line with the variability of extreme wind speed over the 30 regional locations. Specifically, based on the re-sampling strategy from DeCAUn the number of approximated events range from 3.8 to 3.9/year over the locations in the North Sea, from 3.7 to 4.8/year for the locations over the Atlantic and from 5.2 to 5.4/year for the regional locations over the Mediterranean. It is evident that to alleviate any chanse of bias estimations of the return levels based on the modeling of DeCAUn to the GPD

distribution, a data length longer than 15 years seems sufficient for these sites to include more than 50 events in total; (Larsén, 2013; Jonathan and Ewans, 2013).

- The extremes extrapolated based on the re-sampling strategy of DeCAUn is also strengthened from the high resolution wind database used for the analysis, ensured as possible the extreme efficient characteristics primarily near the coasts and in narrow straits and basins where applied, avoiding the apparent underestimation of the extreme variability of wind speed.

## 6.3.6 Design Values

Design value estimations *(DV* in (m/s))* for various return periods are presented for the two relatively small sample periods of examination (10 and 15 years). Henceforth, all results will be referring to the selected locations L2, L16, and L21. The use of a high resolution database at these sites will challenge the requirements of the resampling strategy of DeCAUn to short and irregularly samples where the meteorological model of lower resolution is not able to reproduce the underlying terrain and capture the wind speed variations sufficiently. Specifically, the three representative locations of the strong wind conditions observed within each area are located in the Southern part of the North Sea (L2 with highest wind speed 26.704 m/s), the Northern part of the Atlantic (L16 with 28.671 m/s the highest wind speed) and the Western part of the Mediterranean (L21 with 25.901 m/s the highest wind speed) respectively. The intensity of the extreme wind profile at these sites is reinsured from the systematically positive excess kurtosis parameter to these three locations indicating heavy-tailed distributions for the wind speed (see also Table 5.7 in sub-Section 5.4).

Alongside the *DV* estimations of the optimal re-samples from the DeCAUn model we include estimations from the initial de-clustering approach, the DeCA model for inference. The performance of the Runs is also presented as the standard comparable model at each sample period of examination. Moreover, the BM model refers to sample periods of (10 and 15 years) and the BM Ref. at the maximum available sample period (20 years).

Regarding L2, *DV* estimates of the 50 years return period *DV*(50) for BM Ref. (the reference model for both sample periods of examination) yielded 26.59 m/s(see Figure 6.22). DeCAUn provided *DV*(50) estimates at 26.84 m/s with an *nrmse* measure at 0.013 with regards to the sample period of 10 years (Figure 6.23a) and 26.67 m/s followed by a reduction of the *nrmse* measure to 0.003 for the 15 years (Figure 6.23b).

Proceeding with the estimates from the other models, the *DV*(50) obtained from DeCA pointed out 26.61 m/s with an *nrmse* at 0.020 and 26.28 m/s followed by a reduction of *nrmse* to 0.014 respectively for the two sample periods. Runs yielded *DV*(50) at 28.09 m/s and 26.50 m/s with *nrmse* at 0.053 and followed by a considerable reduction to 0.007 respectively.

Furthermore, BM yielded *DV*(50) at 29.81 m/s with an *nrmse* at 0.121 and 27.49 m/s followed by a considerable reduction of *nrmse* to 0.035 respectively for the two sample periods of examination.
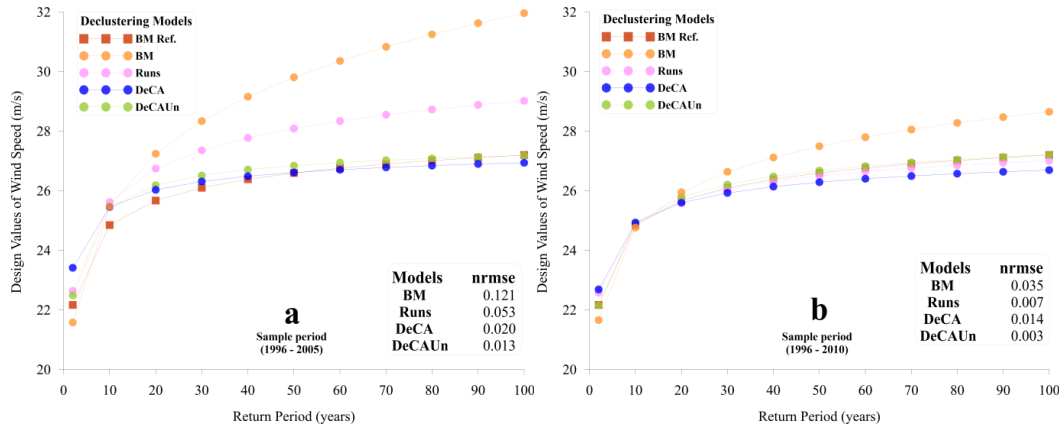
Figure 6.23: Design values using the de-clustering models for sample periods of (a) 10 and (b) 15 years regarding L2. (Tsalis et al., 2021)

The $DV(50)$ for BM Ref. regarding L16 was estimated at 28.72 m/s. Subsequently the estimations for L16 with regards to the $DV(50)$ and *nrmse* measure illustrated in Figure 6.24 are outlined in the same context as previously.

DeCAUn provided $DV(50)$ estimates at 28.86 m/s with an *nrmse* measure at 0.005 with regards to the sample period of 10 years (Figure 6.24a) and 28.64 m/s followed by a reduction of the *nrmse* measure to 0.003 for the 15 years (Figure 6.24b).

Proceeding with the estimates from the other models, the $DV(50)$ obtained from DeCA pointed out 28.60 m/s with an *nrmse* at 0.007 and 28.84 m/s followed by a slight reduction of *nrmse* to 0.006 respectively for the two sample periods. Runs yielded $DV(50)$ at 29.92 m/s and 30.04 m/s with *nrmse* at 0.040 and followed by a slight increment to 0.044 respectively.

Furthermore, BM yielded $DV(50)$ at 28.32 m/s with an *nrmse* at 0.018 and 28.77 m/s followed by a considerable reduction of *nrmse* to 0.004 respectively for the two sample periods of examination.
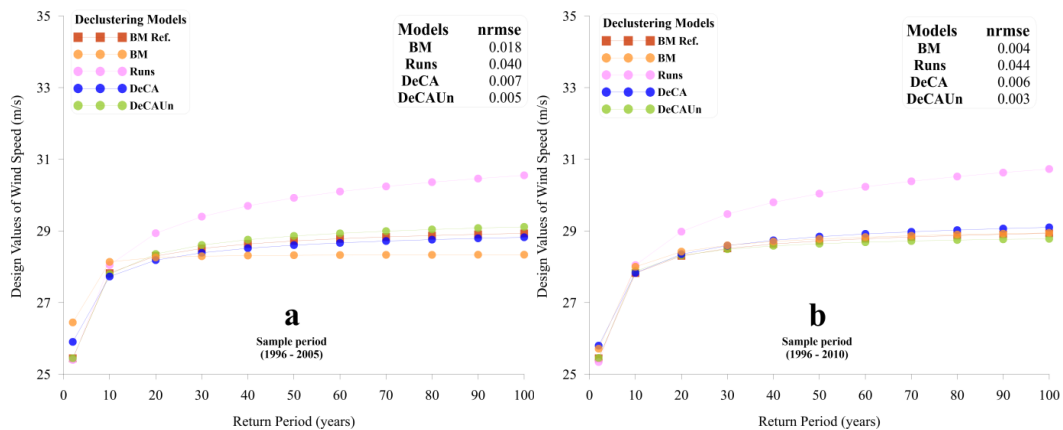


Figure 6.24: Design values using the de-clustering models for sample periods of (a) 10 and (b) 15 years regarding L16. (Tsalis et al., 2021)

Finally, the $DV(50)$ for BM Ref. regarding L21 was estimated at 25.79 m/s. In the same context as before we subsequently outlined the estimations for L21 with regards to the $DV(50)$ and *nrmse* measure.

DeCAUn provided $DV(50)$ estimates at 25.79 m/s with an *nrmse* measure at 0.011 with regards to the sample period of 10 years (Figure 6.25a) and 25.86 m/s followed by a reduction of the *nrmse* measure to 0.007 for the 15 years (Figure 6.25b).

Proceeding with the estimates from the other models, the $DV(50)$ obtained from DeCA pointed out 26.00 m/s with an *nrmse* at 0.013 and 25.72 m/s followed by a reduction of *nrmse* to 0.008 respectively for the two sample periods. Runs yielded $DV(50)$ at 26.25 m/s and 26.07 m/s with *nrmse* at 0.018 and followed by a reduction to 0.011 respectively.

At last, BM yielded $DV(50)$ at 31.72 m/s with an *nrmse* at 0.244 and 26.16 m/s followed by a considerable reduction of *nrmse* to 0.014 respectively for the two sample periods of examination.
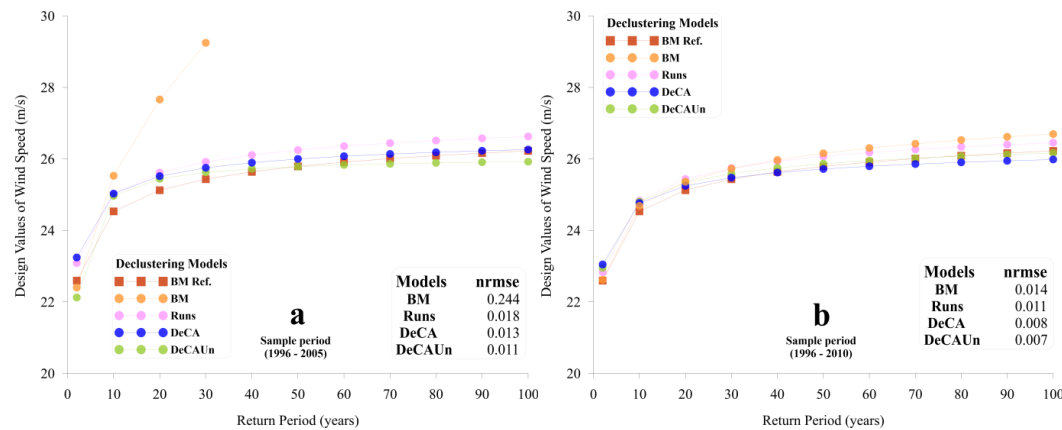


Figure 6.25: Design values using the de-clustering models for sample periods of (a) 10 and (b) 15 years regarding L21. (Tsalis et al., 2021)

As a general remark of the $DV$ estimates made from the DeCAUn model, the proposed model slightly overestimated the quantile projection (with regards to BM Ref.) for small-scale return periods of 50 years, as obtained for all three locations. This effect is more obvious considering the sample period of 10 years in Figure 6.23a, Figure 6.24a and Figure 6.25a. On the contrary, for the larger sample period of 15 years there is a remarkable convergence of DeCAUn towards the BM Ref. model. Moreover, Runs failed to provide reliable $DV$ estimates for the sample of 10 years yielding quantile overestimates in comparison to those made from the reference model. Finally, we anticipated weak performance from the BM model for the two sample periods, although the latter model was supplied as a weak comparable measure of prediction. For completeness in terms of the quantile projection of the DeCAUn model considering the design value estimations $DV(50)$ for the 30 locations see (Tables 6.13 and 6.14).

## 6.3.7 Confidence bounds

For locations (L2, L16, and L21) and to each sample period of examination, only the confidence bound of the estimated $DV(50)$ of the 50 years return period for each model is demonstrated. The interval estimates are supported by two methods. The first method is the normal approximation and is applied only to the BM Ref. model. The second method is the standard non-parametric bootstrap method (Percentile) and is applied to the models BM, Runs, DeCA and DeCAUn.

The DeCAUn model for L2 (Figure 6.26a) yielded a slight increment in the width of the 95% confidence interval (Width of CI) at +0.044 m/s with the increase of the sample period from 10 to 15 years. On the contrary, a considerable reduction in the Width of CI at -5.509 m/s and -1.451 m/s is obtained for L16 (Figure 6.26b) and L21 (Figure 6.26c) respectively.

Proceeding with the variability of DeCA within the same context as before, the model provided an increment in the Width of CI at +0.798 m/s for L2 with the increase of the sample period, followed by a considerable reduction in Width at -0.630 m/s and -0.780 m/s respectively for L16 and L21.

At last, Runs model derived a considerable reduction in the Width of CI at -4.111 m/s with the increase of the sample period, followed by a reduction in Width at -0.716 m/s for L16 and -0.083 m/s for L21 respectively.

**(a)**
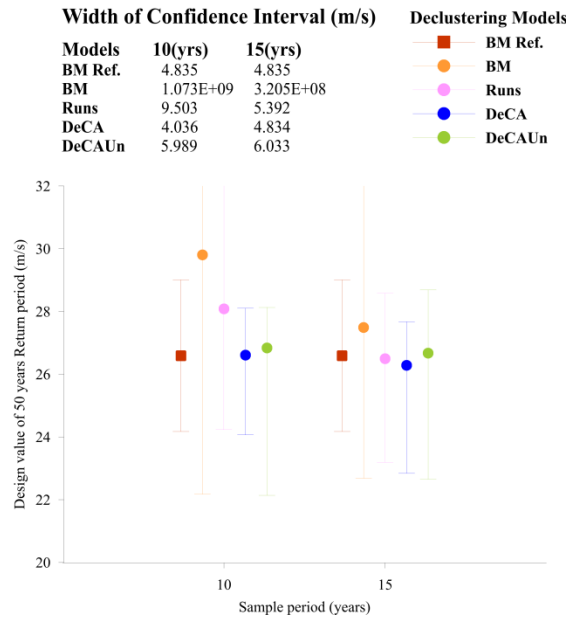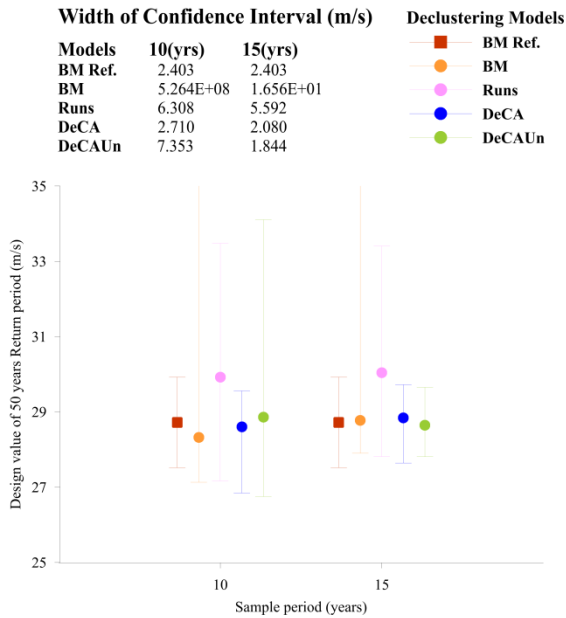


**(b)**                                                         **(c)**
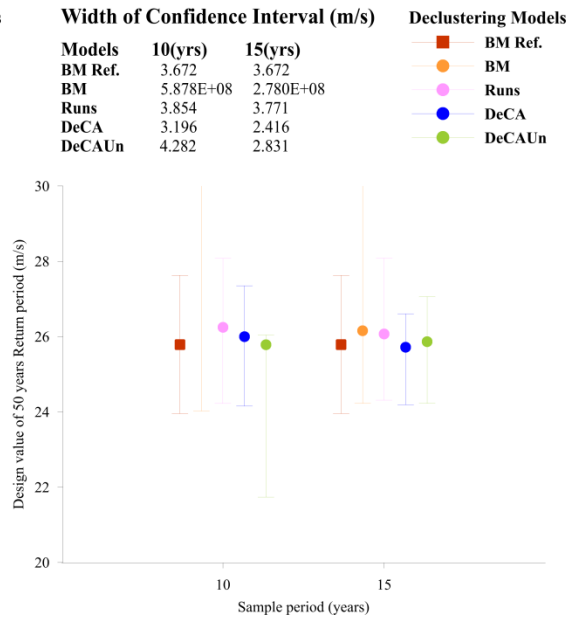


Figure 6.26: Width of CI for the *DV* (50) of all models for sample periods of 10 and 15 years regarding (a) L2, (b) L16, and (c) L21. (Tsalis et al., 2021)

With regards to the DeCAUn model the confidence bounds are considerably wider in comparison to DeCA for all three locations. The estimations confirmed the wider bound effect that was expected. Despite the fact that a bootstrap approach was performed for a reliable inference in terms of variability, it failed to overcome the weakness of small samples such as

the irregular re-samples from DeCAUn. The inevitable high variability of the proposed model is caused by the reduction in the sample size as a repercussion from re-sampling at the associated DEP levels. Moreover, the increase of the sample period to 15 years positively affected DeCA, DeCAUn and Runs, yielding narrower confidence bounds. Finally, BM confirmed the inability to provide trustful bounds in comparison to the other models. For completeness regarding the variability of the DeCAUn model for the 30 locations see (Tables 6.13 and 6.14) and Figure 6.22.

## 6.3.8 Model Parameters

For easier representation of the asymptotic distributional behavior in sample observations derived from each model, only the estimated shape parameter ($\hat{\xi}$) is provided at the three locations. The 95% confidence intervals of the estimated parameters of the GEV and GPD distributions at each sample period are derived by two methods in the same context as previously presentedin sub-Section 6.3.7. For this analysis, the MLE method was implemented setting the discussion within the most popular framework for stationary BM and POT samples. This way, all results are easily comparable with those reported in the relevant literature. The regularity conditions of the GEV and GPD exist when the shape parameter which is equal for the two distributions is restricted (see the discussion in sub-Section 2.3.1). Specifically, the MLE is valid when $\xi > -1$, although the asymptotically normal properties of the parameters are valid for $\xi > -0.5$. When $\xi < -1$, the estimators generally do not exist (Davison and Smith, 1990; Grimshaw, 1993; Tajvidi, 2003). In practice, for the modeling of extremes of wind speed, it is likely to obtain more often zero and negative estimates (i.e., indicating right-tail distributions of an exponential type or short and light-tailed respectively with an infinite or finite right endpoint), rather than positive value estimates of the shape parameter (Jonathan and Ewans, 2013; Brabson and Palutikof, 2000).

Assuming that the shape parameter estimation with regards to the BM Ref. model ($\hat{\xi}_{Ref}$) has a reduced degree of uncertainty, it will be considered as the reference estimation for the comparisons made in the parameter ($\hat{\xi}$) for both sample periods of examination. In general, DeCAUn estimates of $\hat{\xi}$ resulted a width reduction of the 95% CI in the increase of the sample period from 10 to 15 years for the three locations L2, L16, and L21 illustrated in Figure 6.27.

**(a)**

| Width of Confidence Interval | | |
|---|---|---|
| **Models** | **10(yrs)** | **15(yrs)** |
| **BM Ref.** | 0.668 | 0.668 |
| **BM** | 7.082E+00 | 6.621E+00 |
| **Runs** | 0.481 | 0.354 |
| **DeCA** | 0.278 | 0.383 |
| **DeCAUn** | 1.037 | 1.028 |

**Declustering Models**
- ■ BM Ref.
- ● BM
- ● Runs
- ● DeCA
- ● DeCAUn

**(b)**

| Width of Confidence Interval | | |
|---|---|---|
| **Models** | **10(yrs)** | **15(yrs)** |
| **BM Ref.** | 0.912 | 0.912 |
| **BM** | 7.126E+00 | 2.016E+00 |
| **Runs** | 0.437 | 0.361 |
| **DeCA** | 0.216 | 0.189 |
| **DeCAUn** | 1.434 | 0.993 |

**Declustering Models**
- ■ BM Ref.
- ● BM
- ● Runs
- ● DeCA
- ● DeCAUn

**(c)**

| Width of Confidence Interval | | |
|---|---|---|
| **Models** | **10(yrs)** | **15(yrs)** |
| **BM Ref.** | 0.747 | 0.747 |
| **BM** | 7.152E+00 | 6.955E+00 |
| **Runs** | 0.376 | 0.498 |
| **DeCA** | 0.306 | 0.230 |
| **DeCAUn** | 0.977 | 0.473 |

**Declustering Models**
- ■ BM Ref.
- ● BM
- ● Runs
- ● DeCA
- ● DeCAUn



Figure 6.27: Estimates of the $\hat{\xi}$ parameter with the 95% Width of CI to all models for sample periods of 10 and 15 years regarding locations (a) L2, (b) L16, and (c) L21. The parameter interval estimate of $\hat{\xi}$ for the BM Ref. model is inferred from the normal approximation method. The interval estimates for the models BM, Runs, DeCA and DeCAUn is infered from the standard non-parametric bootstrap method (Percentile). (Tsalis et al., 2021)

The estimates of the shape parameter of DeCAUn for locations (L2, L16, and L21) ranged from -0.471 to -0.771 and even wider for the associated bounds. However, as the sample period increased we observed $\hat{\xi}$ estimates converging to the $\hat{\xi}_{Ref}$. This convergence confirmed the unique relationship between the distributions of GEV and GPD fitting successfully the samples of the reference and proposed model respectively. In this implementation, the residual RESID $(\hat{\xi}) = \hat{\xi}_{Ref} - \hat{\xi}$ will be used as a visual metric for comparison of the DeCAUn model for

145

each location respectively. The $\hat{\xi}_{Ref}$ parameter estimates to locations L2, L16 and L21 are at -0.168, -0.473 and -0.170 respectively shown in (Figure 6.27a, Figure 6.27b and Figure 6.27c).

DeCAUn yielded RESID ($\hat{\xi}$) at 0.303, 0.018 and 0.601 with a Width of CI at 1.037, 1.434 and 0.977 for the sample period of 10 years from the three locations. With regards to the 15 years, the RESID is followed by a reduction at 0.121 (converging to $\hat{\xi}_{Ref}$), increment at 0.243 (diverging negatively from $\hat{\xi}_{Ref}$) and reduction at 0.178 (converging to $\hat{\xi}_{Ref}$). In the same context regarding the 15 years, the Width of CI are obtained as reductions at 1.028, 0.993 and 0.473 respectively.

For inference of the shape parameter estimates of DeCAUn to the 30 locations, Figure 6.28 is given. In general, the RESID ($\hat{\xi}$) metric reduced to zero (converging to $\hat{\xi}_{Ref}$) as the sample period increased for the majority of the locations.
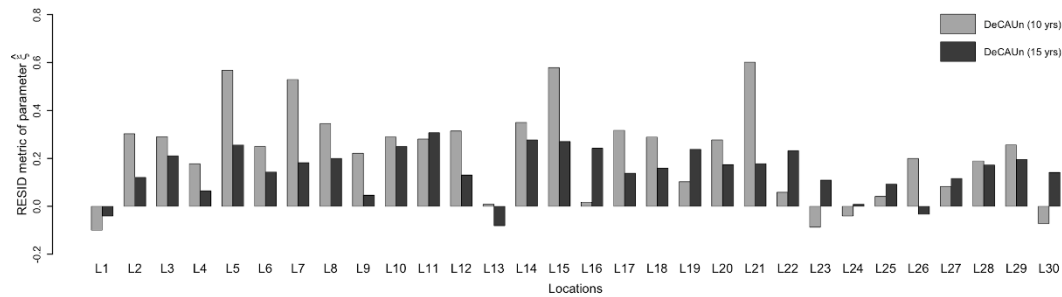


Fig. 6.28: The RESID metric estimates of $\hat{\xi}$ from the DeCAUn model regarding the 30 locations for sample periods of 10 and 15 years. Parameter estimates of $\hat{\xi}_{Ref}$ and $\hat{\xi}$ are derived from the standard MLE method to models BM Ref. and DeCAUn fitting the GEV and GPD distributions respectively. (Tsalis et al., 2021)

As a remark, the parameter assessment from the proposed model derived almost week asymptotically normal properties especially for the sample periods of 10 years (i.e., L5, L7, L15, and L21). A possible explanation is given from the over/underestimation of $\hat{\xi}$ under the standard MLE method considering the relatively small number of observation at these locations. In addition, the inverse proportional behavior of the metric measure RESID in the increase of sample period (e.g., location L13) is also possible related to the intractable problems of inference for the $\hat{\xi}_{Ref}$ parameter of GEV under MLE. However, for the relatively small samples, using the LMOM method according to Hosking and Wallis (1997) would probably model in a better way the statistical weakness of the small re-samples obtained from DeCAUn.

We close our results in the following sub-Section 6.3.9 with the threshold selection for the Runs model at the three aforementioned locations.

## 6.3.9 Threshold diagnostics for the Runs model

The effective threshold to the Runs model and the selection criteria is thoroughly discussed in sub-Sections 3.4 and 3.5. This part of the results highlights the detailed demonstration of the Runs model used, providing an optimum threshold $u$ from the Multiple-Threshold Model by the NC diagnostics. The threshold range for the Score test of the NC diagnostics is limited between the 60% and 99.5% sample quantile of the daily wind speed maxima with a step of 0.01. As a remark, the threshold from NC required less subjectivity and experience to detect in comparison to alternative diagnostics also discussed previously in sub-Section 3.4. Inference of the Multiple-Threshold Model by the NC diagnostics confirmed the advantage against the standard PS plot.

The NC diagnostics is presented for the sample periods of 10 (diagrams b, f and j) and 15 years (diagrams d, h and l), with the standard Parameter Stability (PS) plot (see sub-Section

2.7.2) as a comparative measure (diagrams a, e and i for 10 years and diagrams c, g and k for 15 years respectively) in Figure 6.29. For the diagnostics, Score test is performed for the shape parameter over multiple thresholds to the three locations (L2, L16 and L21). The empirical threshold selection is depicted as the value associated to the sharpest p-value increase at the significance level of 0.05. For easier representation, peak p-values and threshold are located on the vertical dashed line on the diagram of the NC diagnostics. Furthermore, threshold exceedances are also denoted on the top scale of the same diagram. The threshold setting for the samples of wind speed at the 30 locations is in line with the suggestions of Jonathan and Ewans (2013) for threshold adjustments of clustering no fewer than 50 events totally.
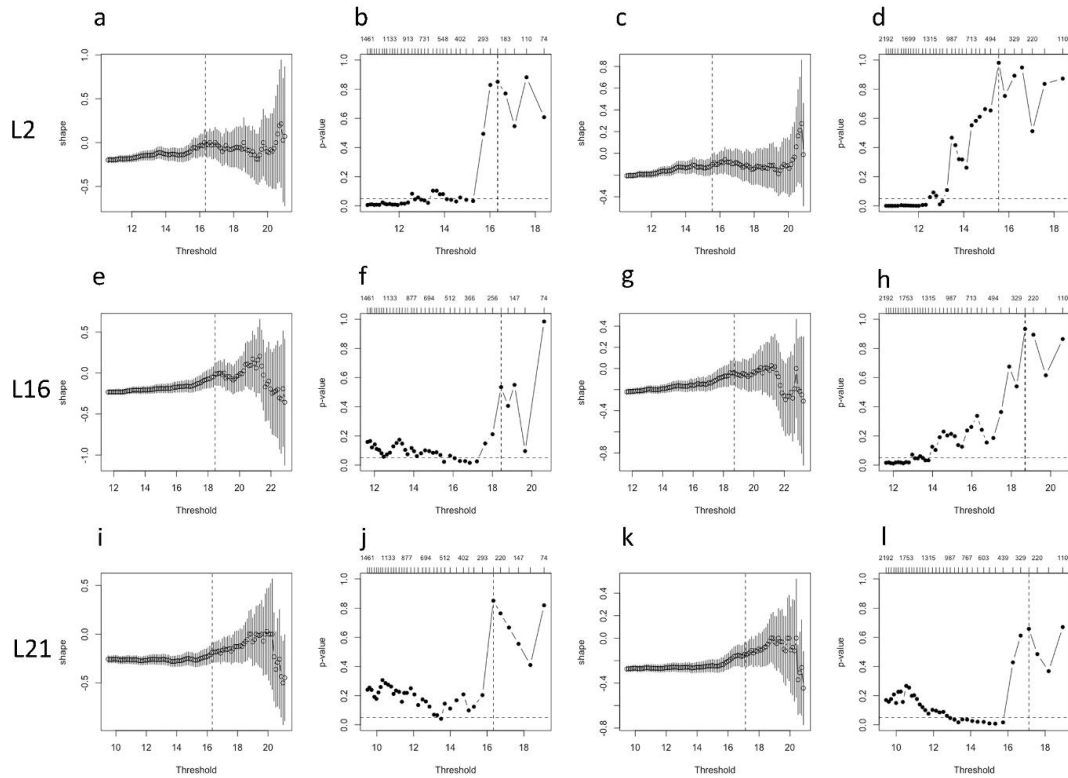


Figure 6.29: Threshold model diagnostics for the Runs model. Diagrams of PS plot in (a,c,e,g,i,k) and NC diagnostics in (b,d,f,h,j,l) for sample periods of 10 and 15 years respectively. The threshold selection from the NC diagnostics is transferred onto the PS plot as a comparative measure. The NC threshold obtained from the PS plot is located on the diagram as the solid dot line highlighting empirical estimation for the shape parameter and as vertical solid lines at the same diagram the approximate point wise Wald 95% confidence intervals. (Tsalis et al., 2021)

Additional diagnostics of the Runs model to the threshold from NC are summarized considering the three locations. Specifically, the p-value estimates, threshold and No. of cluster peak exceedances over threshold from the NC diagram are summarized in Table 6.15.

Table 6.15: Threshold diagnostics for the de-clustering scheme of the Runs model.

| Locations | Ny= 10 yrs | | | Ny= 15 yrs | | |
|---|---|---|---|---|---|---|
| | *p*-value | *u*(m/s) | No. Peak exceedances | *p*-value | *u*(m/s) | No. Peak exceedances |
| L2 | 0.851 | 16.342 | 70 | 0.981 | 15.550 | 121 |
| L16 | 0.535 | 18.439 | 71 | 0.934 | 18.701 | 104 |
| L21 | 0.851 | 16.341 | 92 | 0.658 | 17.124 | 90 |

As regards to the estimates of the NC diagnostics for the threshold setting the following remarks can be derived:

- The number of cluster peak exceedances over threshold yielded in a range from 70 to 121 with regards to the sample period of 10 and 15 years.
- The threshold of wind speed is set in a range from 15.55 (m/s) to 18.70 (m/s) with regards to the sample period of 10 and 15 years.

## 6.4 The response of DeCAUn using the ERA 20C and ERA Interim database

In this analysis, we assess the performance of the most reasonably de-clustering models discussed in 6.3 using relatively small annual wind speed time series, in a range of 10, 15, 20 and 25 years long. The examined locations for applying all models are 32 in total, denoted as L1, L2,…, L31, and L32 respectively, addressing two different data products, the ERA-Interim and ERA-20C covering the North Sea, Atlantic, Mediterranean and Black Sea.

In the same context as in the MARINA Platform in sub-Section 6.3, all re-samples from the DeCAUn model obtained using the ERA-Interim and ERA-20C assume that an average of at least 1.65 peaks per year should be selected in a POT approach in order to gain advantage over BM. The $nrmse$ measure of the re-samples was evaluated also in this setting for all DEP reduction levels (60,65,70,75,80,85,90 and 95). However, the DeCAUn model reconstructed the dependent sample of extremes to an efficient independent sample, using a normalized bandwidth value at $C$=0.25 for the Gaussian Kernel estimator. The bandwidth value was set for the resampling procedure at this value based on the work of (Rehfeld et al., 2011) on Asian monsoon records.

We assessed the performance of all de-clustering models in terms of the extreme wind speed quantile estimates and compared all results to the estimates of the BM model regarding the longest available time series from each data product. Specifically, the maximum available time series extending from 1979-2016 (38 years long) originated from the ERA-Interim product, or from the ERA-20C extending from 1961-2010 (50 years long). Our implementation is highlighted on the Intervals Estimate method for estimating the runs length, addressing a threshold value from the Multiple-Threshold Model when performing the GPD analysis via the Runs model. Standard errors and confidence intervals for the estimated parameters and return values of the GEV and GPD distribution parameters are derived by two approaches, the normal approximation to the distribution of the MLE estimator and by the non-parametric bootstrap method (Percentile), (see sub-Section 2.4 on the discussion of the confidence bound estimates). Before proceeding to our analysis, a summary Table 6.16 is presented with the basic characteristics of the models used in this part of our study.

Table 6.16: Models and basic characteristics

| Models | Characteristics |
|---|---|
| BM Ref. | Annual-Block Maximum sampling approach. This BM will be regarded as the reference model counted upon the largest available sample of 38 years from 1979 to 2016 (ERA-Interim) and sample of 50 years from 1961 to 2010 (ERA 20C) . |
| BM | Annual-Block Maximum sampling approach. This BM will be regarded as the model counted upon the samples of 10, 15, 20, and 25 years of the ERA-Interim and ERA-20C . |
| Runs | Standard de-clustering model which samples approximately independent events (Smith and Weissman, 1994) |
| DeCA | The physical De-Clustering Algorithm (DeCA model) forming samples of events approximately independent and irregularly spaced in time. The samples from DeCA are formed assuming physical considerations from energy reduction levels DEP at % values (60,65,70,75,80,85,90 and 95). |
| DeCAUn | The proposed DeCA Uncorrelated (DeCAUn) model. The model performs re-sampling taking into account the correlation effect in the irregular samples of DeCA. The response of DeCAUn to the irregular correlation analysis considering Gaussian Kernel functions is assessed at the normalized bandwidth value of $C$=0.25. |

It is important at this point to emphasize the potential usefulness for the large-scale wind energy applications the use of reanalysis data products such as ERA-20C and ERA-Interim of relatively small special scale manifested in the study of Torralba, et al., (2017b). The sample sizes of long-term wind speed larger than 30 that are found with relative ease at these dataproducts, has set a sound base for studying the various factors that cause the uncertainties in the estimation of return level estimates based on the asymptotic model formulation of GEV and GPD in extremes (e.g., Larsén et al., 2013).

The demonstration of DeCAUn reconstructing irregularly wind speed samples is primarily challenged from the sample size effect as previously discussed in sub-Section 6.3. However, the demonstration of the resampling strategy was controled to relatively small sample sizes of 10 and 15 years based on the available time series of wind speed originated from the MARINA Platform database of high resolution. The asymptotic properties of GPD modelling DeCAUn is challenged to samples of very small sizes (Holmes and Moriarty, 1999; Galambos and Macri, 1999; Katz et al., 2002; Jonathan and Ewans, 2013; and Wang and Holmes, 2020). Therefore, to assess the effect of larger sample sizes to the asymptotic properties of GPD will infer effectively the modelling of DeCAUn in line to the i.i.d limitations. In this respect, larger wind speed sample sizes from a fairly coarse resolution database such as the ERA-20C and ERA-Interim are required to evaluate the demonstration of DeCAUn.

However, the proposed resampling strategy is challenged from the intractable problems of inference associated to the distribution of wind speed from these dataproducts suggesting light-tails for the majority of the midlatitude regional locations used in this part of the assessment; (see also the discussion made in sub-Section 5.3). It is important to outline that if the parent distribution is characterized of being heavy tailed responsible of the natural forcing mechanism reconstructing the wind speed time series, then extremes of wind speed are modelled from a distribution with a bounded tail (e.g., FT-III or reverse Weibull class); (see Katz, 2002; Holmes, 2015; Pinheiro and Ferrari, 2015). The light-tails of wind speed originated from ERA-20C and ERA-Interim will challenge the modelling of DeCAUn to samples of less extremes at different sample periods (i.e., 10, 15, 20, and 25 years). The demonstration of DeCAUn to these relatively small datasets is also challenged from the bias effect to the return level estimates when the modelling at different periods is strongly influenced from the extreme wind climate changes obtained at each sample period (e.g., Larsén and Mann, 2009).

To infer the effect of the relatively short sample periods from 10 to 25 years of ERA-20C and ERA-Interim to the response of DeCAUn, the design value estimates in (m/s) corresponding to the 50 years return period are illustrated in the following Figures 6.30 and 6.31. It is importatnt to outline that the demonstration of DeCAUn is compared to the DeCA model and BM model at equally correspondent sample size based on the *nrmse* statistic. Only optimum model estimates based on the minimum *nrmse* value and reference model BM Ref. in parenthesis is illustrated in a,b,c, and d respectively to the sample periods of 10, 15, 20, and 25 years using ERA-20C (from 1961 to 1985 of a 5 years step forward) and ERA-Interim (from 1979 to 2003 respectively). In this setting, DeCAUn manifested as the optimum model particularly at sample periods of 10 and 15 years.
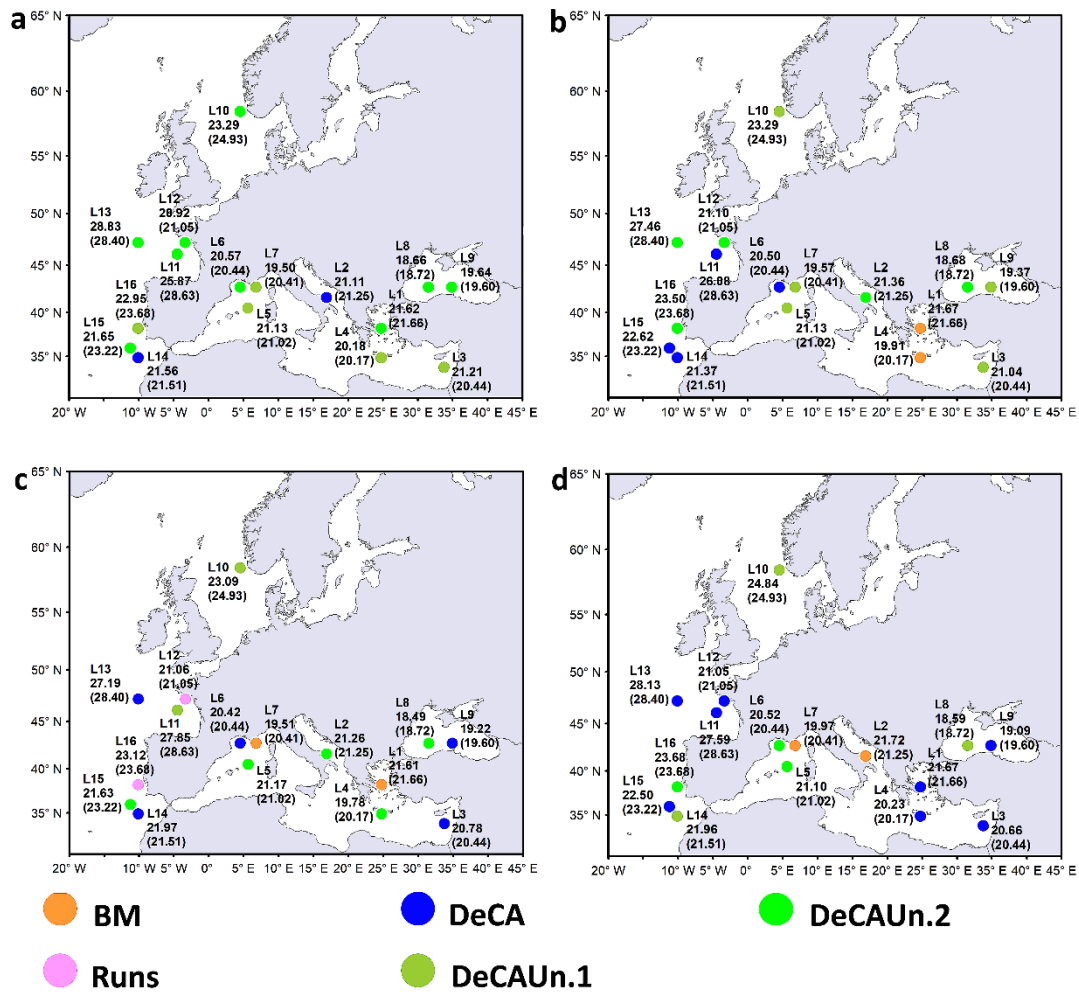
Figure 6.30: Optimum model estimates based on the minimum *nrmse* statistic and reference model BM Ref. in parenthesis of the 50 years design value respectively. Design value estimates are in (m/s) in (a,b,c, and d) respectively to the sample periods of 10, 15, 20, and 25 years of wind speed from the ERA-20C data product. (Tsalis et al., 2019)
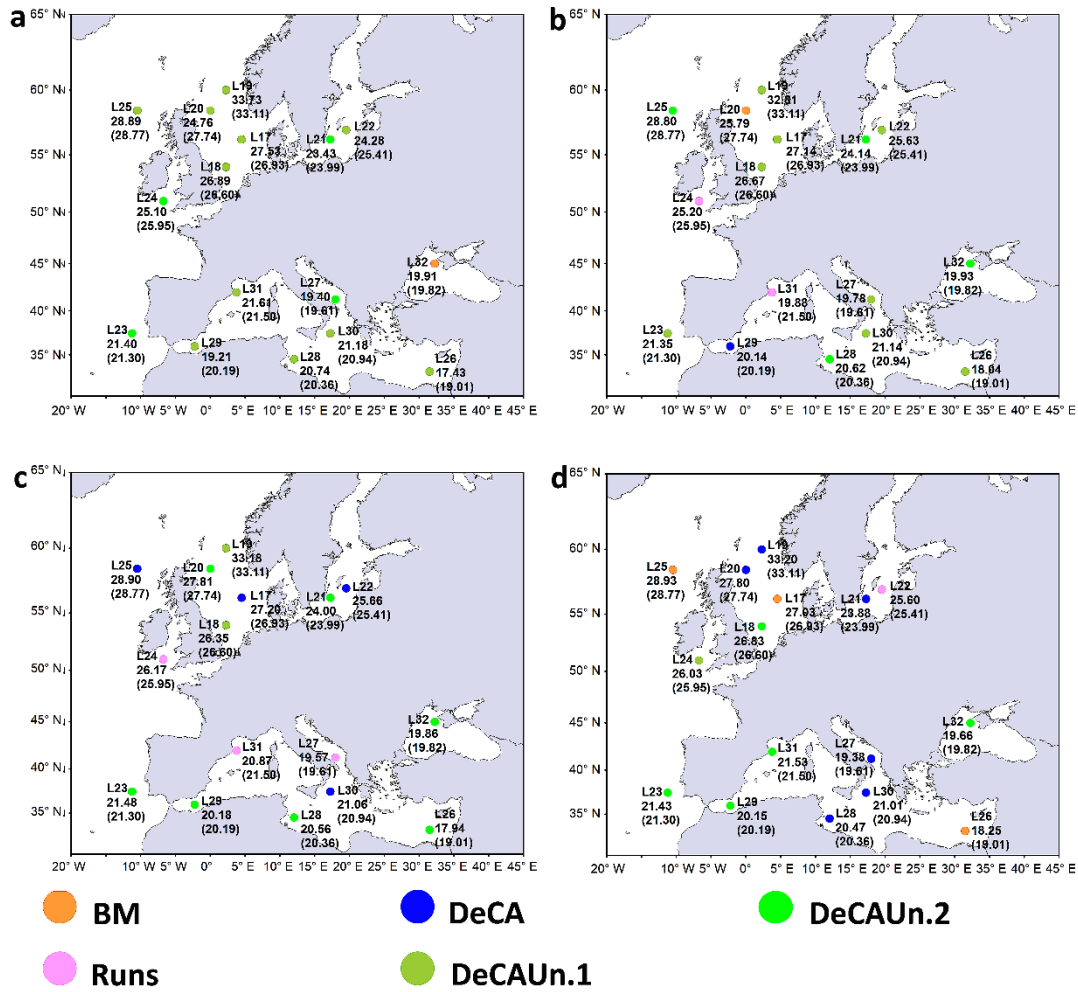
Figure 6.31: Optimum model estimates based on the minimum *nrmse* statistic and reference model BM Ref. in parenthesis of the 50 years design value respectively. Design value estimates are in (m/s) in (a,b,c, and d) respectively to the sample periods of 10, 15, 20, and 25 years of wind speed from the ERA-Interim data product. (Tsalis et al., 2019).

The number of the effective models that infer closer to the stability properties of the GEV limit distribution that modeled BM Ref. is presented in the following Table 6.17(a) summarizing the demonstration of each model in terms of the *nrmse* based criteria at each sampling period and data product respectively. Particularly, the demonstration of the optimum re-samples DeCAUn.1 and DeCAUn.2 modelling the GPD threshold model is assessed to the return level estimates made from DeCA, Runs and BM model at equally correspondent sample size based on the minimum *nrmse* value. It is outlined at the bar chart of Table 6.17(b) that as the sample size increased the most likely observed *nrmse* statistic of DeCAUn reduced smoothly and at a higher rate degree in regards to the 16 regional locations of ERA-Inrerim and to a lower extent regarding the 16 locations of ERA-20C. The strong bias effect to the return level estimates is rather reasonable to ERA-20C as the modelling of DeCAUn is strongly influenced from the inability of the data product to reproduce the extreme wind changes at the relatively small sample periods. The *nrmse* statistic of DeCAUn shows a smoother response to the increase of sample period when the modelling of extremes is originated from samples of ERA-20C (greater than 20 years) and ERA-Interim (greater than 15 years).

In addition, inference is also made for the DEP levels of the resampling strategy of DeCAUn based on the ERA-20C and ERA-Interim data products. In general, the increase in sample size from 10 to 25 years lead to small reductions of the most likely observed DEP level for the majority of the regional locations of ERA-Interim and to a small increase of the mode

estimate of DEP from 10 to 15 years for ERA-20C and to a smaller increase from 20 to 25 years. Specifically, in line with the previous results of the model based on the MARINA Platform in sub-Section 6.3, the increase in sample size does not necessarily follow the large increase in the number of extreme events as expected. The approximate stable or reduced modal value estimate of the DEP level of the irregular DeCA samples at locations from ERA-Interim controlled DeCAUn to encompass the largest number of events as possible as the sample size increased from 10 to 25 years. However, the reduction of the modal value estimate of the DEP level is clear for samples larger than 15 years for the ERA-20C challenging the inability of the ERA-20C to reproduce to a reasonable certainty the extreme wind changes at the relatively small sample periods up to 15 years. The response of DeCAUn to the modal value estimates of the DEP levels is illustrated at the bar chart of Table 6.17(c) considering the 16 regional locations of interest from the ERA-20C and ERA-Interim respectively.

The response of DeCAUn to the lag($k$)-apart estimates is also closely related to the DEP estimates that form the samples of DeCA (see discussion in sub-Section 6.3.3). Specifically, for the majority of locations the demonstration of DeCAUn in the increase of sample period resulted to larger (lower) DEP level and to relatively smaller (larger) lag($k$). Clearly, for locations e.g., in the NW and central part of the Mediterranean Sea that are characterized of having strong winds and relatively low volatility in extremes (i.e., larger DEP and relatively smaller lag($k$)), the DEP and lag($k$)-apart estimates of L5 of ERA-20C is illustrated in Table 6.17 (d and f) and the estimates of L30 of ERA-Interim illustrated in Table 6.17 (e and g); (see changes in the frequency and intensity of cyclones and associated windstorms affecting the extremes into the Mediterranean region from Nissen et al., (2014)). When little information of extremes is apparent at these locations, the lower lag($k$) is preferable to form clusters efficiently of larger length and consequently derive samples of higher DEP. The effect of the DEP increase (reduction) and reduction (increase) in the lag($k$)-apart value of observations of DeCAUn as the sample size increased in illustrated in the bar chart of Table 6.17 (f and g) for locations of ERA-20C and ERA-Interim respectively.

Following the mode estimates of the DEP in Table 6.17 (c), inference is also made for the mode estimates of the lag($k$)-apart value of observations of DeCAUn as the sample size increased in Table 6.17 (h). Specifically, the small reduction of the mode estimate of DEP as the sample size increased from 10 to 25 years in Table 6.17 (c) for the ERA-Interim locations, derived in general a small increase of the mode estimate of the lag($k$) illustrated in Table 6.17 (h). However, for the locations of ERA-20C the reverse proportional relation of the DEP and lag($k$) is more pronounced for samples larger than 15 years.

Table 6.17: The number of optimum models based on the minimum *nrmse* statistic of good performance presented in (a) infer closer to BM Ref. at the regional locations from ERA-20C and ERA-Interim. The mode estimate of the minimum *nrmse* statistic of DeCAUn to each data product is illustrated in (b) for the sample periods of 10, 15, 20, and 25 years of wind speed. In addition, the most likely value estimates of the DEP (%) reduction level of DeCAUn to the 16 locations in each region of the ERA-20C and ERA-Interim data products for sample periods of 10, 15, 20, and 25 years is illustrated in (c) and DEP estimates for each location respectively in (d and e). The lag($k$)-apart value of observations of DeCAUn as the sample size increased in illustrated in the bar chart of (f and g) for locations of ERA-20C and ERA-Interim respectively, with the mode estimates of the lag($k$)-apart value of observations of DeCAUn as the sample size increased in (h); (supplementary image of Tsalis et al., 2019). All models and parameter estimates are derived by the extRemes package (Ver. 2.0) in R; (Gilleland and Katz, 2016)

**(a)**

| Models | No. of Optimum models from ERA-20C **16 Locations** | | | | No. of Optimum models from ERA-Interim **16 Locations** | | | |
|---|---|---|---|---|---|---|---|---|
| | 1961 - 1970 (10 Years) | 1961 - 1975 (15 Years) | 1961 - 1980 (20 Years) | 1961 - 1985 (25 Years) | 1979 - 1988 (10 Years) | 1979 - 1993 (15 Years) | 1979 - 1998 (20 Years) | 1979 - 2003 (25 Years) |
| BM | 0 | 2 | 2 | 2 | 1 | 1 | 0 | 3 |
| Runs | 0 | 0 | 2 | 0 | 0 | 2 | 3 | 1 |
| DeCA | 2 | 4 | 5 | 8 | 0 | 1 | 4 | 6 |
| DeCAUn.1 | 5 | 5 | 2 | 3 | 11 | 8 | 2 | 1 |
| DeCAUn.2 | 9 | 5 | 5 | 3 | 4 | 4 | 7 | 5 |

**(b)**



**(c)**



**(d)**



153

**(e)**



**(f)**



**(g)**



**(h)**
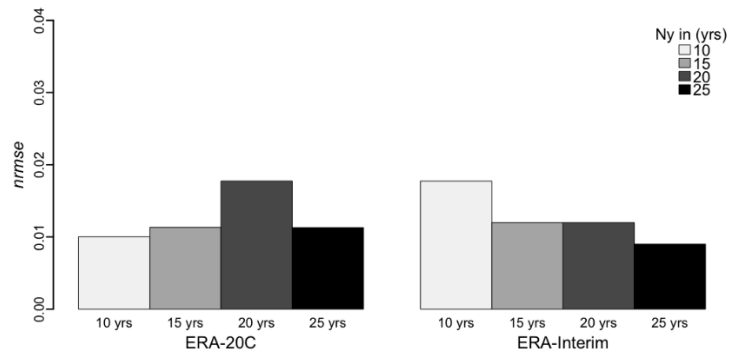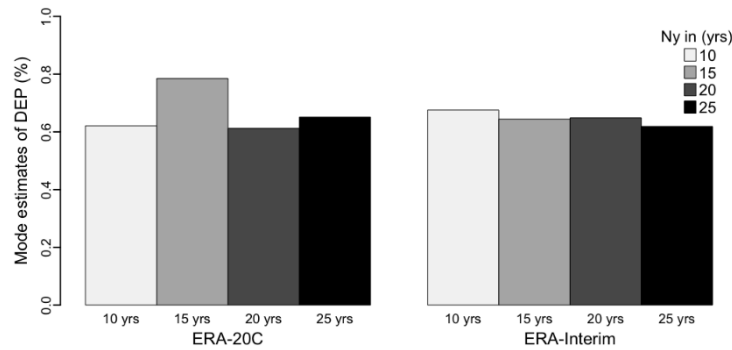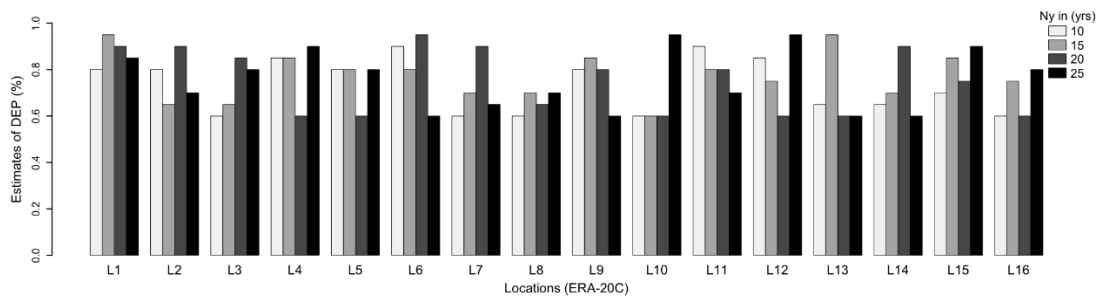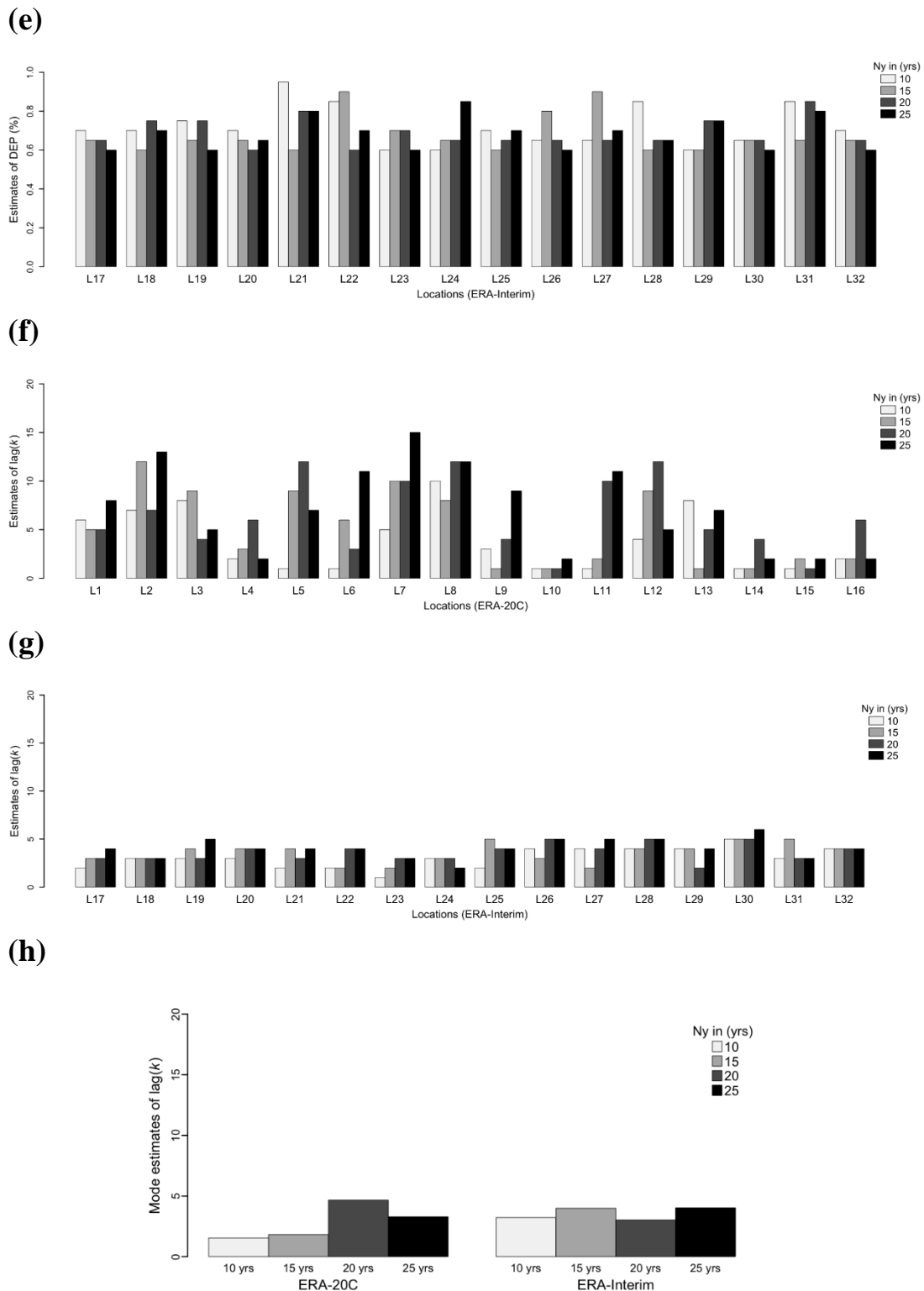


The major remarks of the sample size effect to the demonstration of DeCAUn in terms of the return level estimates are outlined in the following:

- The DeCAUn model succeeds as the optimum model based on the *nrmse* statistical criteria of good performance compared to DeCA, Runs, and BM for sample sizes of 10 and 15 years of wind speed at the regional locations from ERA-20C and ERA-Interim (see Figures 6.30 and 6.31 and Table 6.17(a)).

154

- The Runs and DeCA models seem to converge closely to DeCAUn for sample sizes greater than 20 years.
- The most likely observed *nrmse* statistic of DeCAUn reduced smoothly and at a higher rate degree as the sample size increased in regards to the regional locations of ERA-Inrerim and to a lower extent to locations of ERA-20C (see the bar chart of Table 6.17(b)).
- The resampling strategy DeCAUn showed systematically stronger rate of convergence to the stability properties of GEV that modeled BM Ref. particularly at regional locations from ERA-Interim and a less stronger rate of convergence at locations from ERA-20C.
- BM systematically inferred as a model of great instability particularly of sample sizes up to 25 years.
- The resampling strategy DeCAUn.2 to wind speed for sample periods of 10 and 15 years succeded when data are originated using ERA-20C and DeCAUn.1 when using ERA-Interim. DeCAUn.2 is also outlined as the best re-sampling strategy using the MARINA Platform database at the relatively small sample periods of 10 and 15 years. The assessment to the irregularly samples obtained from the high resolution product controled the bandwidth of the Gaussian Kernel effectively to DeCAUn rather better than the assessment made using the low resolution product having a constant bandwidth.
- It is evident from the bar charts illustrated in Table 6.17(b) and Figure 6.20(b) that as the sample size increases, the most likely observed *nrmse* statistic of DeCAUn at the regional locations reduced smoothly and at a higher rate degree in regards to the datasets of the MARINA Platform database and to a lower extent regarding datasets from ERA-20C and ERA-Interim. Particularly, the resampling strategy proposed showed systematically stronger rate of convergence to the asymptotic properties of the extreme value distribution for wind speed datasets of high spatial resolution and to a less stronger rate of convergence for datasets of lower resolution.
- From the demonstration of DeCAUn to the ERA-20C and ERA-Interim the most likely DEP (%) reduction level yield to range approximately from 0.61 to 0.78 with regards to the sample period from 10 to 25 years for the ERA-20C, and from 0.62 to 0.68 for the ERA-Interim respectively (see bar chart in Table 6.17(c)).
- From the demonstration of DeCAUn to the ERA-20C and ERA-Interim the most likely $\text{lag}(k)$-apart value of observations of DeCAUn as the sample size increased from 10 to 25 years yield to range approximately from 2 to 5 for the ERA-20C, and from 3 to 4 for the ERA-Interim respectively (see bar chart in Table 6.17(h)).
- Based on the most likely observed *nrmse* statistic of DeCAUn as the sample period increases (i.e., reduction in general of *nrmse* as sample increases), DeCAUn shows stronger rate of convergence to the asymptotic forms for samples larger than 20 from ERA-20C and larger than 15 from ERA-Interim.

At this point we outline the primarily interest of this study is to assess the effect of the sample period to the asymptotic properties of GPD that modeled DeCAUn and not the response of the proposed re-sampling strategy to the specific features responsible to bias samples originated from data products of low resolution. It is reasonable for assessing risk associated to extreme wind speed episodes to use high-resolution simulations especially in the coastal areas (Sušelj et al., 2010). Allthough modelled wind speed patterns differ between models they are usually small when compared to natural variability. Assessments made from Nikulin et al (2011) avoiding any statistical downscaling showed no significant changes in the 20 year return wind speed over the North Sea, and Pryor et al (2012) found no changes in the strength of wind gusts. These results strengthens the use of a low-resolution reanalysis data product such as ERA-Interim or ERA-20C when the primarily target is on the large-scale forcing of the wind field and not on the local effects.

Under the proviso of the statistical downscaling, two representative location from the ERA-20C (L5 and L10) and the ERA-Interim (L18 and L30) database is selected for the demonstration of DeCAUn in terms of the return level estimates and variability of the proposed model to each sample period. The locations L5 and L30 are a good representative of the strong wind climate in the Mediterranean also discussed in Flaounas et al., (2015 b) and locations L10 and L18 model typically the extreme wind characteristics obtained in the North Sea also studied from Sušelj et al., (2010).

The return level estimates of the DeCAUn model in association with the extrapolations made from BM, Runs and DeCA models for the four sample periods of 10, 15, 20, and 25 years from each data product respectively is illustrated in the following Figures. Specifically, Figures (6.32 and 6.33) inference the stability properties of the limit distributions in extremes that modeled all resampling strategies based on wind speed samples originated from ERA-20C and Figures (6.34 and 6.35) from ERA-Interim respectively. The demonstration of DeCAUn showed the systematically model convergence to BM Ref. particularly at sample periods of 10 and 15 years. The modelling of DeCAUn was extended to larger sample sizes (not presented here) and the decrease of the absolute return level estimates to each return period was eventually more pronounced to the estimations made based on BM Ref. Additional diagnostics of the DeCAUn response to the sample period for the four locations (L5, L10, L18, and L30) using the low resolution data products is presented in Appendix I. The diagnostics of all models are inferred to the four sample periods of ERA-20C and ERA-Interim set from 1961 to 1985 and from 1979 to 2003 with a 5 years step forward to each data product respectively.
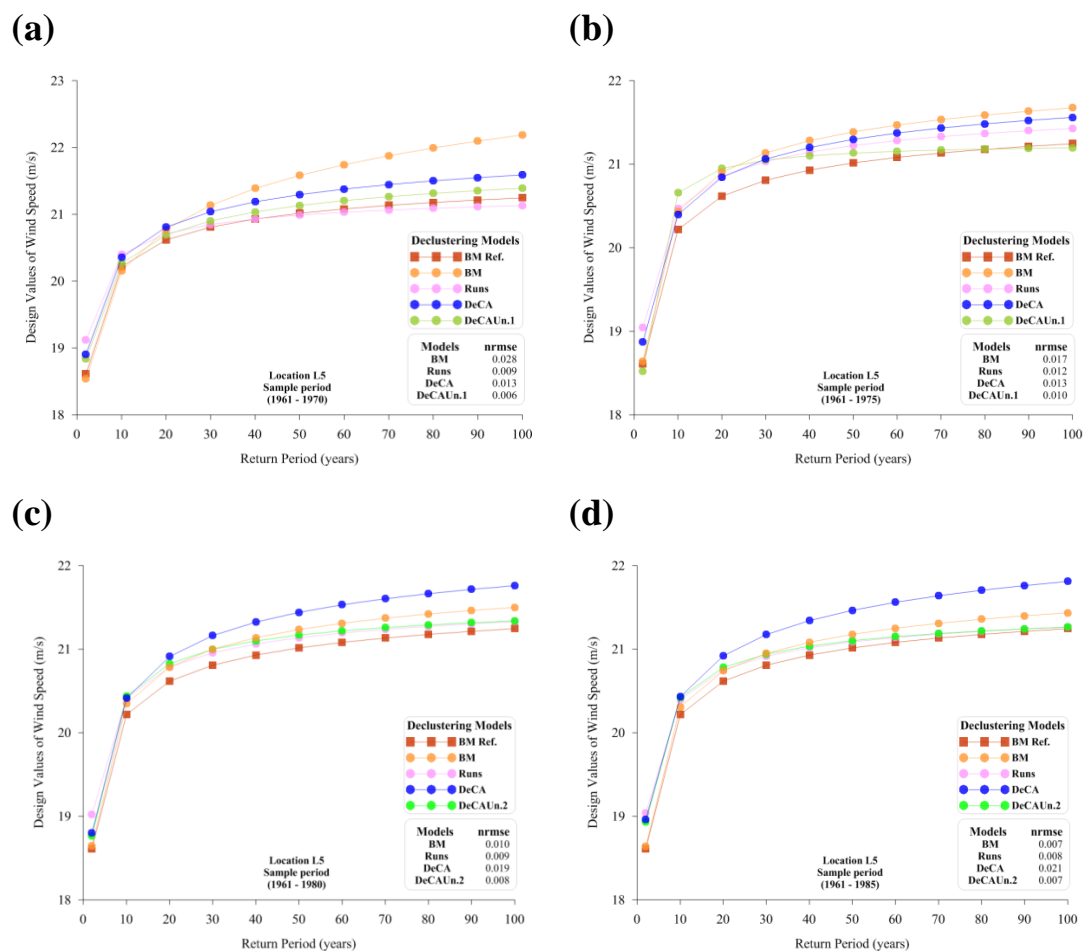


Figure 6.32: Design value estimates based on the resampling strategies of BM, Runs, DeCA, and DeCAUn regarding location L5 of the ERA-20C data product. Estimates of all models are in (m/s) and shown in (a,b,c, and d) respectively to the sample periods of 10, 15, 20, and 25 years of wind speed. (Tsalis et al., 2019).

**(a)**



**(b)**



**(c)**



**(d)**
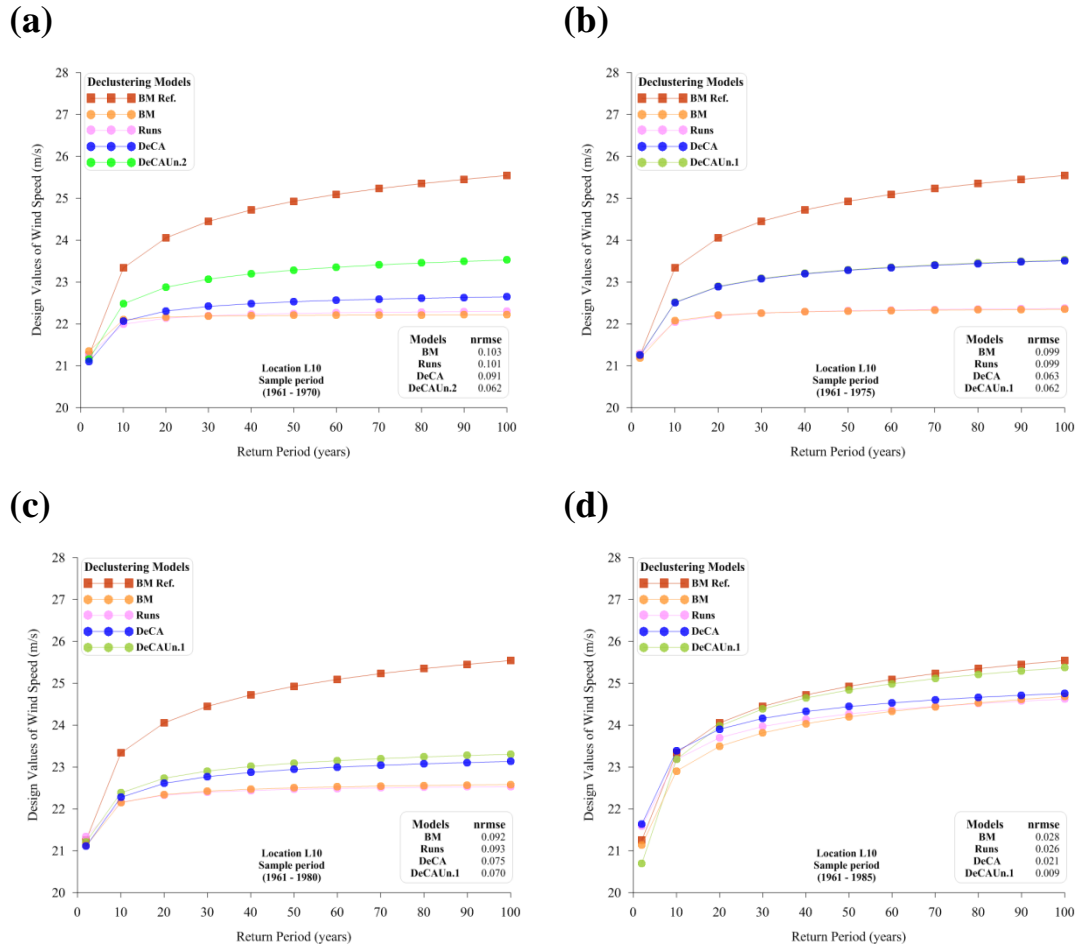


Figure 6.33: Design value estimates based on the resampling strategies of BM, Runs, DeCA, and DeCAUn regarding location L10 of the ERA-20C data product. Estimates of all models are in (m/s) and shown in (a,b,c, and d) respectively to the sample periods of 10, 15, 20, and 25 years of wind speed. (Tsalis et al., 2019).

The inability of ERA-20C to capture the extreme wind climate changes at different periods is systematically influencing the demonstration of the Runs, DeCA and DeCAUn models particularly in L10. However, DeCAUn inferred as the model with the fastest convergence rate as the sample period increased. All models demonstrated a rather smoother convergence to BM Ref. for sample sizes greater than 20 years.

**(a)**



**(b)**

**(c)**



**(d)**
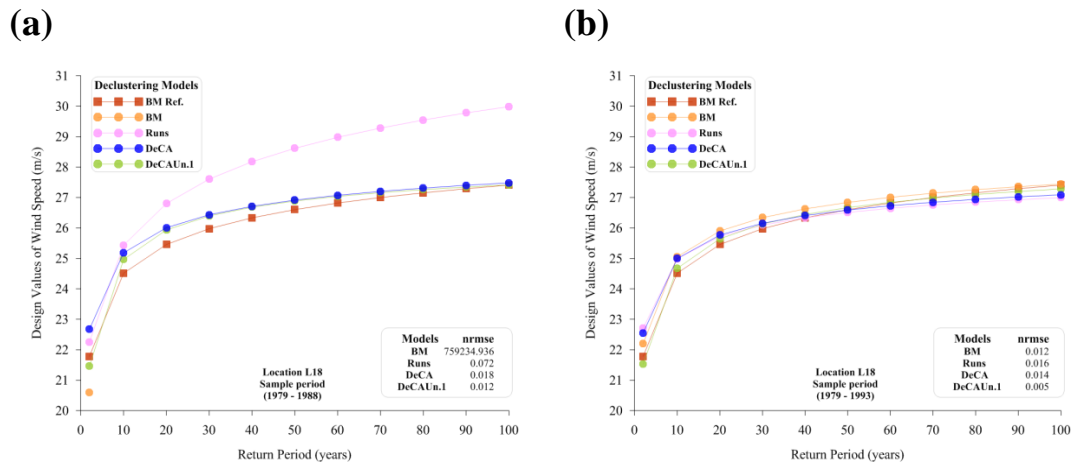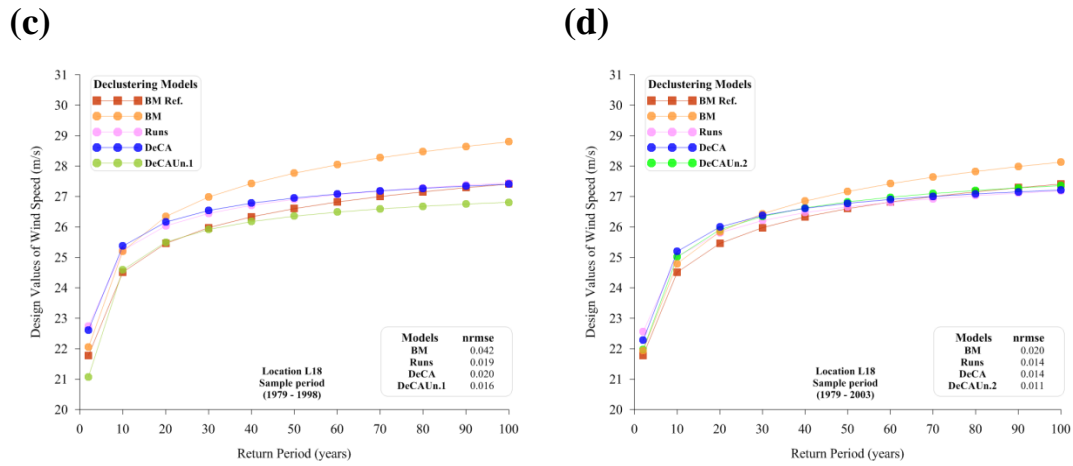


Figure 6.34: Design value estimates based on the resampling strategies of BM, Runs, DeCA, and DeCAUn regarding location L18 of the ERA-Interim data product. Estimates of all models are in (m/s) and shown in (a,b,c, and d) respectively to the sample periods of 10, 15, 20, and 25 years of wind speed. (Tsalis et al., 2019).

**(a)**



**(b)**



**(c)**



**(d)**
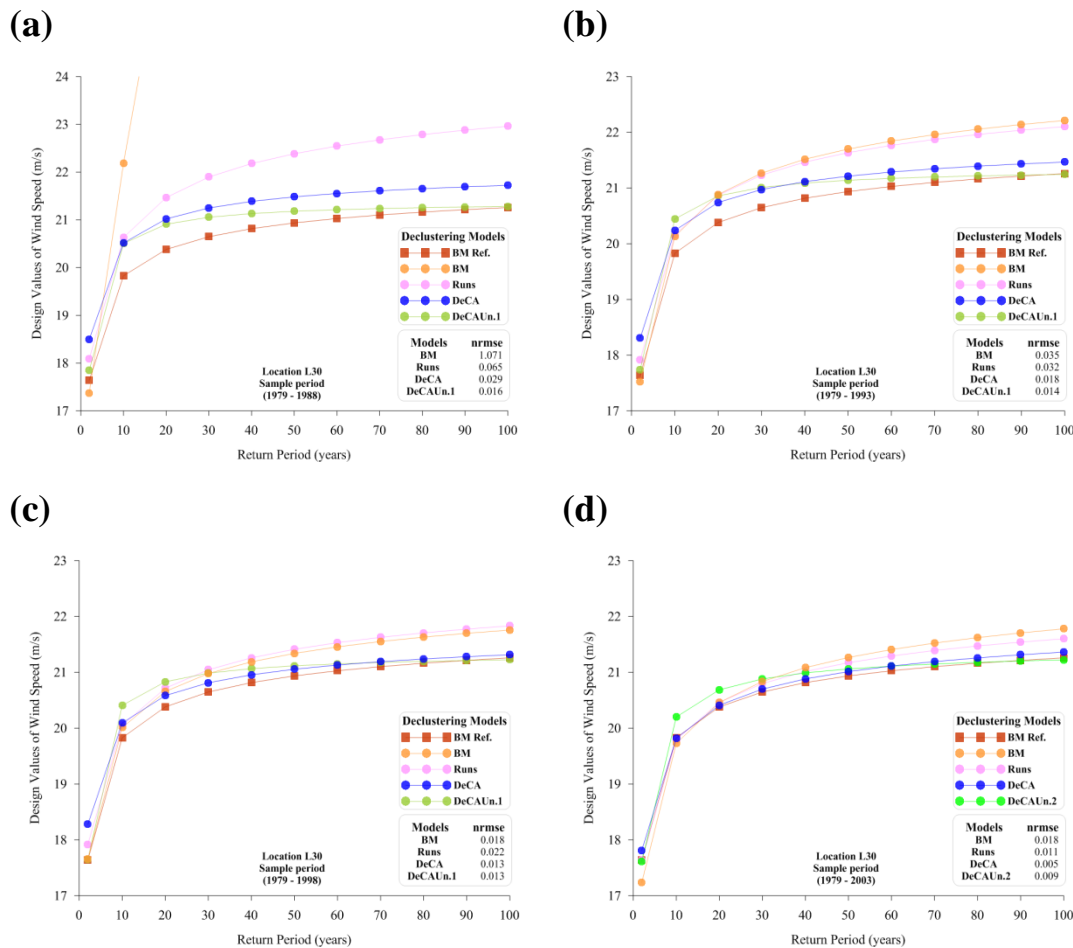


Figure 6.35: Design value estimates based on the resampling strategies of BM, Runs, DeCA, and DeCAUn regarding location L30 of the ERA-Interim data product. Estimates of all models are in (m/s) and shown in (a,b,c, and d) respectively to the sample periods of 10, 15, 20, and 25 years of wind speed. (Tsalis et al., 2019).

In regards to the sample size effect of the model demonstration in terms of the return level estimates the following remarks can be derived:

158

- For sample size greater than 20 all models converge to the extrapolations made from the BM Ref.
- DeCAUn show the higher convergence rate to the BM Ref. especially considering sample sizes of 10 and 15 years
- The resampling strategy DeCAUn.1 shows better convergence to the extrapolations made from BM Ref. for return periods lower than 50 years and DeCAUn.2 for return periods higher than 50 years
- For a sample period greater than 15 and 20 years DeCA and DeCAUn models show similar extrapolation behavior
- The relatively stronger flunctuations of the *nrmse* statistic is obtained at locations from ERA-20C and to a lower extent at locations from ERA-Interim. The bias effect of the inability of ERA-20C to capture the extreme wind variability at different periods is systematically more intence than at the regional locations from ERA-Interim influencing accordingly the return level estimates of all models.
- BM failed to converege to the BM Ref. especially for relatively small sample periods of 10 and 15 years.

In addition, inference of the variability of DeCAUn to the design value estimates at return period of 50 years is made using two approaches for the confidence bound estimates. The first approach namely the normal approximation (delta method) and the second the non-parametric bootstrap method (Percentile) for locations (L5, L10, L18, and L30) as illustrated in Figure 6.36. The sample period of 10, 15, 20, and 25 years data is set on the x axis challenging all model estimates with the width of CI on the y axis respectively. However, the standard approach to infer the approximate normality of the maximum likelihood estimator is challenged for small sample sizes pointing out very high quantile estimation variances that are not physically plausible as evidence in (a, c, e, and g) of Figure 6.36. To this effect an alternative approach to alleviate the intractable problem of inference of the uncertainty analysis based on small datasets is using the non-parametric bootstrap approach in (b, d, f, and h) of Figure 6.36; (see also the discussion of Pandey et al., 2003). Under the proviso of the two confidence bound estimate approximations inference is made pointing out the following:

- The confidence bound estimates of DeCA and DeCAUn are systematically of larger width using the normal approximation to the likelihood in panel (a, c, e, and g) of Figure 6.36 than the estimates made using the non-parametric bootstrap approach illustrated in panel (b, d, f, and h) respectively.
- The maximum width of CI in (m/s) of the design value estimates of DeCAUn using the non-parametric bootstrap approach for locations (L5, L10, L18, and L30) is reduced to (4.201, 4.248, 6.954, and 5.273) from the non physically plausible estimates of (14.551, 6.352, 15.100, and 49.706) of the normal approximation.
- The high variance effect to the return level estimates using the non-parametric bootstrap approach influenced at a greater extent locations of lower bias. Specifically, L18 and L30 of ERA-Interim illustrated in b, d, f, and h show larger width of the bound estimates than L5 and L10 of ERA-20C in panel a, c, e, and g respectively.
- The intractable problems of inference related to the normal approximation as the sample size increased showed larger inconsistencies of the bound estimates for DeCAUn and to a lower extent when using the non-parametric bootstrap approach. The smoother bound estimates from the bootstrap approach is also notable for the models DeCA and Runs.
- The normal approximation to the likelihood showed symmetric bound estimates to all models and the non-parametric approach assymetric bounds with the upper design value estimate considerable narrower than the lower estimate respectively.
- BM failed to demonstrate reasonable bound estimates from both approximations to the relatively small sample periods.

- DeCAUn show the greater rate of converegence to BM Ref. especially based on the bound approximation of the non parametric approach for samples greater than 15 or 20 years. The demonstration of DeCA showed a more smoother convergence at smaller sample sizes. However, estimates in extremes based on sample sizes smaller than 10 years is probably unrealistic (not demonstrated in this setting) as samples of such small sizes is reported to bias strongly the design value estimates of the 50 years return period (e.g., Larsén et al., 2013).

- Despite the fact that a non parametric bootstrap approach was performed to alleviate in some degree the large variability, it failed to overcome the weakness of small samples such as the irregularly re-samples from DeCAUn. The inevitable high variability of the proposed model is caused by the reduction in the sample size as a repercussion from re-sampling at the associated DEP levels. To a lower extent however this effect is also obtained at datasets originated from the MARINA Platform database.

**(a)**



Width of Confidence Interval (m/s) — Location L5

| Models | 10(yrs) | 15(yrs) | 20(yrs) | 25(yrs) |
|---|---|---|---|---|
| BM Ref. | 1.147 | 1.147 | 1.147 | 1.147 |
| BM | 7.358 | 2.745 | 2.127 | 1.854 |
| Runs | 1.426 | 1.774 | 1.445 | 1.195 |
| DeCA | 4.850 | 5.915 | 3.711 | 2.351 |
| DeCAUn.1 | 6.533 | 0.361 | - | - |
| DeCAUn.2 | - | - | 14.551 | 11.657 |

**(b)**



Width of Confidence Interval (m/s) — Location L5

| Models | 10(yrs) | 15(yrs) | 20(yrs) | 25(yrs) |
|---|---|---|---|---|
| BM Ref. | 1.147 | 1.147 | 1.147 | 1.147 |
| BM | 6.024E+08 | 4.355E+120 | 1.656E+162 | 4.954E+35 |
| Runs | 2.307 | 2.493 | 2.215 | 1.616 |
| DeCA | 3.510 | 2.637 | 2.420 | 1.823 |
| DeCAUn.1 | 3.185 | 4.201 | - | - |
| DeCAUn.2 | - | - | 2.306 | 1.473 |

**(c)**



Width of Confidence Interval (m/s) — Location L10

| Models | 10(yrs) | 15(yrs) | 20(yrs) | 25(yrs) |
|---|---|---|---|---|
| BM Ref. | 3.008 | 3.008 | 3.008 | 3.008 |
| BM | 1.408E-07 | 0.627 | 0.791 | 2.758 |
| Runs | 0.741 | 0.635 | 0.529 | 1.804 |
| DeCA | 19.464 | 4.072 | 5.533 | 4.072 |
| DeCAUn.1 | - | 3.858 | 4.163 | 4.843 |
| DeCAUn.2 | 6.352 | - | - | - |

**(d)**



Width of Confidence Interval (m/s) — Location L10

| Models | 10(yrs) | 15(yrs) | 20(yrs) | 25(yrs) |
|---|---|---|---|---|
| BM Ref. | 3.008 | 3.008 | 3.008 | 3.008 |
| BM | 2.697E+97 | 4.110 | 2.130 | 2.144E+49 |
| Runs | 0.927 | 0.874 | 0.569 | 2.939 |
| DeCA | 1.825 | 1.799 | 1.484 | 2.774 |
| DeCAUn.1 | - | 1.826 | 1.626 | 4.248 |
| DeCAUn.2 | 3.153 | - | - | - |

**(e)**

Width of Confidence Interval (m/s)

| Models | 10(yrs) | 15(yrs) | 20(yrs) | 25(yrs) |
|---|---|---|---|---|
| BM Ref. | 4.278 | 4.278 | 4.278 | 4.278 |
| BM | 145481.017 | 6.158 | 8.021 | 6.056 |
| Runs | 13.387 | 4.000 | 3.797 | 3.237 |
| DeCA | 7.542 | 6.583 | 8.966 | 10.621 |
| DeCAUn.1 | 15.100 | 9.020 | - | 7.538 |
| DeCAUn.2 | - | - | | |

Declustering Models: BM Ref. · BM · Runs · DeCA · DeCAUn.1 · DeCAUn.2

Location L18

**(f)**

Width of Confidence Interval (m/s)

| Models | 10(yrs) | 15(yrs) | 20(yrs) | 25(yrs) |
|---|---|---|---|---|
| BM Ref. | 4.278 | 4.278 | 4.278 | 4.278 |
| BM | 1252896468.629 | 6.158 | 36.892 | 10.480 |
| Runs | 11.178 | 4.534 | 4.471 | 4.195 |
| DeCA | 5.850 | 4.744 | 4.273 | 3.939 |
| DeCAUn.1 | 6.954 | 5.943 | 5.426 | |
| DeCAUn.2 | - | - | - | 4.133 |

Declustering Models: BM Ref. · BM · Runs · DeCA · DeCAUn.1 · DeCAUn.2

Location L18

**(g)**

Width of Confidence Interval (m/s)

| Models | 10(yrs) | 15(yrs) | 20(yrs) | 25(yrs) |
|---|---|---|---|---|
| BM Ref. | 1.923 | 1.923 | 1.923 | 1.923 |
| BM | 152.826 | 5.472 | 3.636 | 3.833 |
| Runs | 7.786 | 4.424 | 3.562 | 3.054 |
| DeCA | 23.164 | 13.917 | 9.224 | 5.857 |
| DeCAUn.1 | 1.156 | 0.871 | 0.669 | |
| DeCAUn.2 | - | - | - | 49.706 |

Declustering Models: BM Ref. · BM · Runs · DeCA · DeCAUn.1 · DeCAUn.2

Location L30

**(h)**

Width of Confidence Interval (m/s)

| Models | 10(yrs) | 15(yrs) | 20(yrs) | 25(yrs) |
|---|---|---|---|---|
| BM Ref. | 1.923 | 1.923 | 1.923 | 1.923 |
| BM | 663287856.321 | 33.607 | 9.994 | 3.600 |
| Runs | 8.288 | 4.361 | 3.193 | 2.983 |
| DeCA | 4.266 | 2.900 | 2.378 | 2.539 |
| DeCAUn.1 | 5.273 | 4.785 | 4.578 | |
| DeCAUn.2 | - | - | - | 1.748 |

Declustering Models: BM Ref. · BM · Runs · DeCA · DeCAUn.1 · DeCAUn.2

Location L30

Figure 6.36: CI estimations from the normal approximation (delta method) in the left panel (a,c,e, and g) and from the non-parametric bootstrap (Percentile) method in the right panel (b,d,f, and h), for locations L5, L10, L18 and L30. (supplementary image of Tsalis et al., 2019)

## 6.5 Inference of DeCAUn to datasets of different scale resolution

Finally, inference can be made of the effective sample size and the influence of the data product to the resampling strategy of DeCAUn. At this point we recall that this is not the primarily interest of this study however interesting remarks can be outlined of the response of DeCAUn to wind speed datasets originated from the three data products (ERA-20C, ERA-Interim, and the MARINA Platform database) at regional locations that are closely arranged in the Northern North Sea, the Central Atlantic Ocean, and the Western Mediterranean Sea.

The regional locations from each data product in this setting are based on the similar forcing mechanism that suggest similar patterns of wind variability to each site of interest. However, the resampling strategy of DeCAUn is challenged from the effectiveness of the different datasets in scale resolution in simulating regional aspects of climate variability and forcing scenario uncertainty to provide reliable information of extremes at the same sample period.

Particularly, in the following Tables 6.18 and 6.19 the effective DEP (%) reduction level, the resampling scheme (i.e., DeCAUn.1 or DeCAUn.2), the likely number of the approximately independent events resampled from DeCAUn, the lag ($k$)-apart value of observations and $\xi$ parameter estimates, are presented for samples of different statistical resolution based on the response of DeCAUn to sample periods of 10 years (from 1996 to 2005) and 15 years (from 1996 to 2010). In the same context of the previous evaluation of DeCAUn

161

in 6.3 and 6.4 the standard MLE method is set as the parameter estimator of the GPD distribution that models the resamples of the proposed model. Furthermore, the response of DeCAUn is evaluated based on estimates regarded the reference model BM Ref. considering the maximum available time series extending from 1979-2016 (38 years long) originated from the ERA-Interim product, from the ERA-20C extending from 1961-2010 (50 years long) and for the period 1996–2015 (20 years) from the MARINA Platform database.

Table 6.18. Estimates of DeCAUn using statistical high and downscaled resolution datasets of wind speed. The sample period of 10 years is set at (1996-2005) respectively for the datasets originated from the ERA-20C, ERA-Interim, and the MARINA Platform database.

| | **10 years** | Lat. | Long. | DEP (%) | re-sampling scheme | No. DeCAUn cluster | $DV$ (50) (m/s) | WCI (50) (m/s) | lag ($k$) | $\hat{\xi}$ | bdw |
|---|---|---|---|---|---|---|---|---|---|---|---|
| Northern North Sea | ERA-20C | 58.500N | 4.500E | 90 | DeCAUn.1 | 209 | 24.803 | 4.668 | 1 | -0.271 | 0.125 |
| | ERA-Interim | 60.000N | 2.250E | 80 | DeCAUn.2 | 32 | 32.556 | 17.201 | 3 | -0.081 | 0.125 |
| | MARINA Platform | 57.95 N | 3.1 E | 70 | DeCAUn.2 | 35 | 28.940 | 5.557 | 10 | -0.523 | 0.625 |
| Central Atlantic Ocean | ERA-20C | 47.250N | 10.125W | 75 | DeCAUn.2 | 41 | 27.608 | 11.137 | 7 | -0.162 | 0.5 |
| | ERA-Interim | 51.000N | 6.750W | 60 | DeCAUn.1 | 58 | 26.498 | 7.092 | 3 | -0.325 | 0.125 |
| | MARINA Platform | 42.85 N | 9.95 W | 80 | DeCAUn.2 | 61 | 25.172 | 4.969 | 5 | -0.497 | 0.625 |
| Western Med/nean Sea | ERA-20C | 42.750N | 4.500E | 65 | DeCAUn.2 | 38 | 20.419 | 2.798 | 9 | -0.443 | 0.75 |
| | ERA-Interim | 42.000N | 3.750E | 60 | DeCAUn.1 | 65 | 21.838 | 4.481 | 4 | -0.403 | 0.125 |
| | MARINA Platform | 40.8 N | 5.5 E | 60 | DeCAUn.1 | 57 | 25.786 | 4.282 | 11 | -0.771 | 0.625 |

Table 6.19. Estimates of DeCAUn using statistical high and downscaled resolution datasets of wind speed. The sample period of 15 years is set at (1996-2010) respectively for the datasets originated from the ERA-20C, ERA-Interim, and the MARINA Platform database.

| | **15 years** | Lat. | Long. | DEP (%) | re-sampling scheme | No. DeCAUn cluster | $DV$ (50) (m/s) | WCI (50) (m/s) | lag ($k$) | $\hat{\xi}$ | bdw |
|---|---|---|---|---|---|---|---|---|---|---|---|
| Northern North Sea | ERA-20C | 58.500N | 4.500E | 65 | DeCAUn.1 | 140 | 24.198 | 4.011 | 5 | -0.275 | 0.125 |
| | ERA-Interim | 60.000N | 2.250E | 80 | DeCAUn.2 | 36 | 31.726 | 8.938 | 4 | -0.488 | 0.125 |
| | MARINA Platform | 57.95 N | 3.1 E | 70 | DeCAUn.2 | 53 | 28.788 | 6.148 | 10 | -0.378 | 0.25 |
| Central Atlantic Ocean | ERA-20C | 47.250N | 10.125W | 65 | DeCAUn.1 | 249 | 27.430 | 8.460 | 3 | -0.128 | 0.125 |
| | ERA-Interim | 51.000N | 6.750W | 60 | DeCAUn.2 | 56 | 26.460 | 4.741 | 4 | -0.355 | 0.125 |
| | Marina Platform | 42.85 N | 9.95 W | 95 | DeCAUn.2 | 130 | 25.163 | 2.677 | 2 | -0.408 | 0.125 |
| Western Med/nean Sea | ERA-20C | 42.750N | 4.500E | 90 | DeCAUn.2 | 188 | 20.543 | 1.829 | 2 | -0.369 | 0.125 |
| | ERA-Interim | 42.000N | 3.750E | 95 | DeCAUn.1 | 82 | 21.725 | 2.151 | 2 | -0.497 | 0.125 |
| | MARINA Platform | 40.8 N | 5.5 E | 80 | DeCAUn.2 | 200 | 25.865 | 2.831 | 3 | -0.349 | 0.125 |

The major remarks that is outlined from the resampling strategy of DeCAUn to irregularly samples of wind speed originated from databases of different scale resolution are pointed out in the following:

- The response of the Gaussian weight function confirmed the effect of stretching out to a wider bandwidth scale in sample periods of 10 years where little information is available (bdw estimates of Table 6.18). Conversely, as the sample period increased from 10 to 15 years the optimal normalized bandwidth reduced, leading accordingly to a less wide bandwidth adjustment of the weight function; (see bdw estimates of Table 6.19).
- The approximate stable or reduced DEP level estimates as the sample size increased controlled the irregularly DeCA samples to encompass the largest number of events as possible. The response of DeCAUn to the increase in sample size does not necessarily follow the large increase in the number of extreme events as expected for all product types. Specifically, for locations characterized of strong winds and low volatility in extremes (e.g., locations at the Western Med/nean Sea), the demonstration of DeCAUn in the increase of sample period resulted to higher DEP and to relatively smaller lag(k). When little information of extremes is apparent at these locations, the lower lag(k) is

preferable to form clusters efficiently of larger length and consequently derive samples of higher DEP.

- In general, for sample period set at 15 years it is evident that from the No. of the DeCAUn clusters in Table 6.19, any chanse of bias estimations of the return levels based on the modeling of DeCAUn to the GPD distribution is alleviated at these sites where the reconstruction process derived more than 50 events in total. To a lower extent the latter is challenged for location (60.00N and 2.25E) of the ERA-Interim database.

- The resampling scheme DeCAUn.2 handles effectively the irregularly samples for larger sample periods in comparison to DeCAUn.1. This also is confirmed from the findings of the assessment made using the high resolution product (Figure 6.19 (d)) and the low resolution product (Table 6.17 (a)). Although DeCAUn.1 succeeds for samples of 10 and 15 years only using the ERA-Interim, for samples larger than 15 years DeCAUn.2 is strongly recommended as the effectively resampling strategy.

- The parameter assessment from the DeCAUn model derived almost weak asymptotically normal properties especially for the sample periods of 10 years for all data products. This is the major drawback of the inconsistency of the standard MLE method considering the relatively small number of observation at these locations. For moderate or small samples, the anomalous behavior of the likelihood when sampling from the GPD distribution is also discussed in (Davison and Smith, 1990; Castillo and Hadi, 1997; and Castillo and Daoudi, 2009). The intractable problems of inference of the parameters of GPD under MLE for small samples challenged DeCAUn especially for samples of 10 years. However, using the LMOM method according to Hosking and Wallis (1997) would probably model in a better way the statistical weakness of the small re-samples obtained from DeCAUn.

- The estimations confirmed the wider bound effect that was expected. Despite the fact that a bootstrap approach was performed for a reliable inference in terms of variability, it failed to overcome the inconsistency of small samples from DeCAUn. The inevitable high variability of the proposed model to samples originated from all dataproducts is caused by the reduction in the sample size as a repercussion from re-sampling at the associated DEP levels.

Finaly, to assess the fit of the DeCAUn model to GPD when samples of wind speed are of different scale resolution, return level estimates, Q-Q and Kernel Density plots are illustrated in Figures 6.37, 6.38, and 6.39 for the regional locations closely arranged at the Northern North Sea, Central Atlantic Ocean, and Western Mediterranean Sea. The sample period is equally set to all datasets at 10 years (from 1996 to 2005) and 15 years (from 1996 to 2010). If the empirical data in the Q-Q and Kernel Density plots align closely with the modelled estimates, then it is likely that the chosen model for relatively small samples of wind speed is a good representation of the true extreme asymptotic form for these samples.

**(a)**                                                    **(b)**
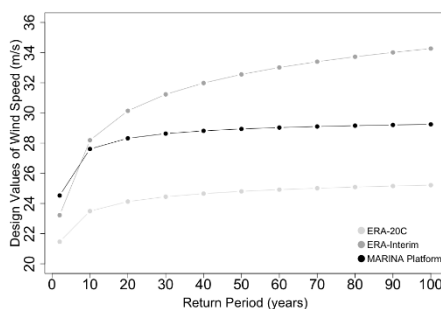
10 (yrs)                                                  15 (yrs)

Figure 6.37: Visual inspection of the return level estimates in (a) and (b) of DeCAUn, with the Q-Q plot diagrams in (c,d,e,i, j, and k) and Kernel Density plot diagrams in (f,g,h,l,m, and n) for samples of 10 and 15 years for regional locations closely arranged in the Northern North Sea. Dashed light grey lines of the Q-Q plots show the 95% pointwise tolerance intervals. The statistical software package (extRemes) in R (Gilleland and Katz, 2016) is used for the estimation of the associated parameters and diagram illustration. (Supplementary material of Tsalis et al., 2021)

As regards in relation to the demonstration of DeCAUn for samples of 10 and 15 years of different scale resolution at the three regional locations closely arranged in the Northern North Sea, the following remarks can be derived from this setting:

- Regarding the extreme quantiles of the GPD distribution (right tail), the response of DeCAUn to datasets originated from the Marina Platform and ERA-20C provide results that are systematically closer to the theoretical GPD line and to a lower extent from ERA-Interim as illustrated in the Q-Q diagrams of Figure 6.37.
- DeCaUn reconstructed the irregularly samples more easily for sample period of 15 years using datasets of larger scale resolution as obtained in the comparison of the Q-Q diagrams in (i,j, and k) of Figure 6.37. The response of DeCAUn is also controlled from the maximum available dataset of each dataproduct. Although the high resolution data product succeds in scale, ERA-20C succeds in long records setting the latter dataset also effective for DeCAUn as obtained in diagrams (k) and (n) of Figure 6.37.
- The relatively small datasets originated from ERA-Interim challenged the reconstruction of DeCAUn in a better scale resolution than of ERA-20C but controlled the DEP and bandwidth parameters from a less available maximum data record. To this effect, the demonstration of DeCAUn is characterized less effective to these samples as illustrated in the Q-Q diagram (j) and Kernel density diagram (m) of Figure 6.37, particularly for the smaple period of 15 years.
- The non parametric bootstrap approach to the bound estimate of the 50 years return levels from the modelling of DeCAUn yield extremely wide confidence/credible intervals regarding the samples of ERA-Interim, and to a lower extent from the modelling of DeCAUn to samples of ERA-20C and MARINA Platform; (see Table 6.18 and 6.19).
- In general, return level estimates from the modelling of DeCAUn to these regional locations of ERA-20C and ERA-Interim yielded under and over estimates as illustrated in (a) and (b) of Figure 6.37.

**(a)**　　　　　　　　　　　　　　　　　　**(b)**
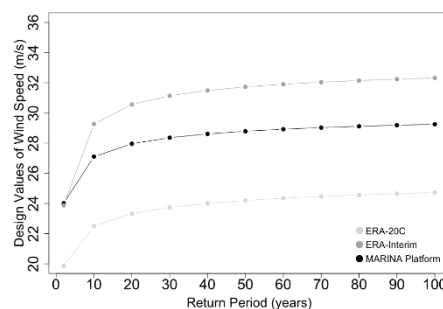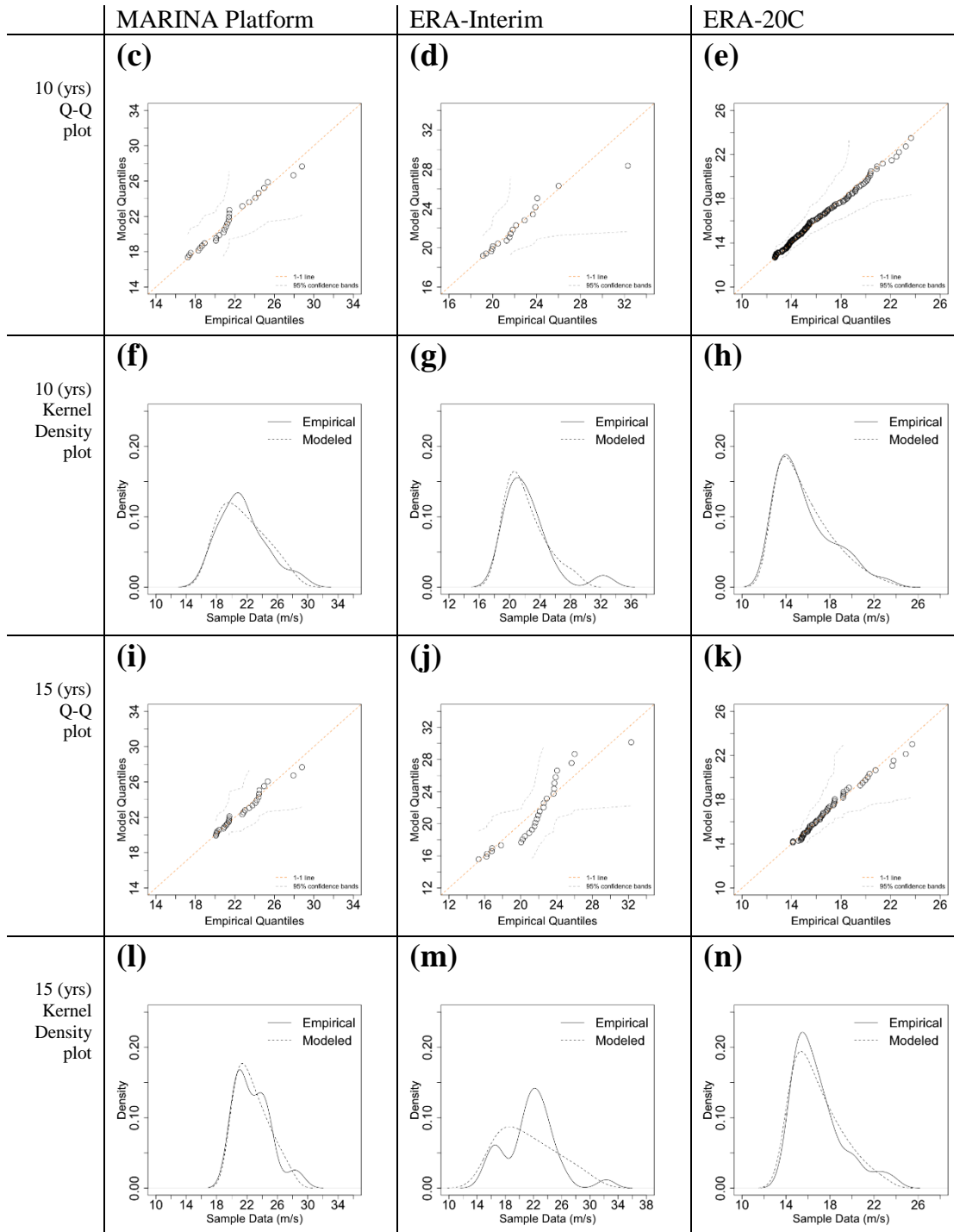
10 (yrs)　　　　　　　　　　　　　　　　15 (yrs)

Figure 6.38: Visual inspection of the return level estimates in (a) and (b) of DeCAUn, with the Q-Q plot diagrams in (c,d,e,i, j, and k) and Kernel Density plot diagrams in (f,g,h,l,m, and n) for samples of 10 and 15 years for regional locations closely arranged in the Central Atlantic Ocean. Dashed light grey lines of the Q-Q plots show the 95% pointwise tolerance intervals. (Supplementary material of Tsalis et al., 2021)

As regards to the demonstration of DeCAUn at the three regional locations closely arranged in the Central Atlantic Ocean the following remarks can be derived from this setting:

- The asymptotic properties of the maximum likelihood estimator at these regional locations are less challenged from the modelling of DeCAUn to samples of different

scale resolution. The model-based curve and empirical estimates are in reasonable agreement for all samples as obtained in the Q-Q and Kernel density diagrams of Figure 6.38. The shape parameter estimates are $\xi > -0.5$ for all samples assigning valid the regularity conditions that are required for the usual asymptotic properties associated with the maximum likelihood estimator (Smith, 1985).

- The response of DeCAUn at these locations is less influenced from the land-sea topography. Particularly, the different scale-resolution datasets effectively reproduced the large-scale forcing on the wind field alleviating any inconsistencies in the nearshore areas. However, the extreme quantiles of the GPD distribution are systematically closer to the theoretical GPD line regarding the high resolution datasets of the MARINA Platform as illustrated in the Q-Q diagrams (c) and (i) of Figure 6.38, and to a lower extent from the low-resolution datasets of ERA-Interim in (d and j), and of ERA-20C in (e and k), respectively.

- The wind speed data usually show a skewness to the right (i.e., right-skewed distribution of a long right tail) and the modeled shape parameter is usually negative; (see also Jonathan and Ewans, 2013; Marcos et al., 2019). The right-skewed distribution effect is also demonstrated in this setting illustrated in the Kernel density diagrams of Figure 6.38 and the modeled shape parameter is clearly negative as shown in Table 6.18 and 6.19.

- The high variance effect of the maximum likelihood estimator to the 50 years return levels is obtained strongly for the samples of ERA-20C and to a lower extent for the samples of ERA-Interim and the MARINA Platform. The intractable problems of inference in terms of the strong variability from the modelling of DeCAUn to the relatively small samples of ERA-20C in this setting, set difficulties to verify that the ML estimator meets the desired asymptotic properties.

- Return level estimates illustrated in (a) and (b) of Figure 6.38 show small bias effect to the modelling of DeCAUn to samples from the MARINA Platform in comparison to the modelling made to samples of lower scale resolution. However, the large scale distance of the locations in this setting show difficulties to verify inference of under or over-estimation in the return level estimates from the modelling of DeCAUn to these samples.

**(a)**                                                      **(b)**
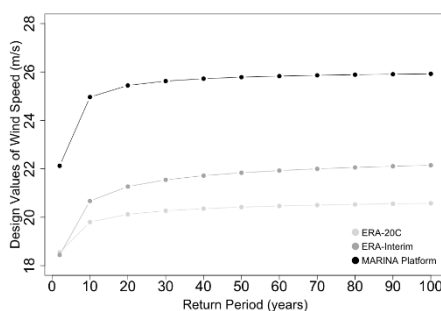
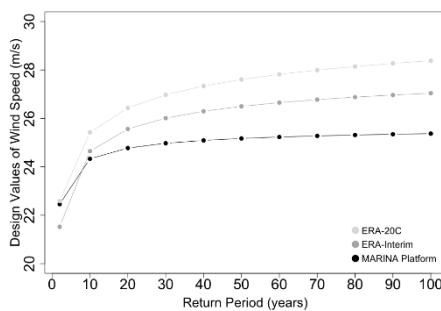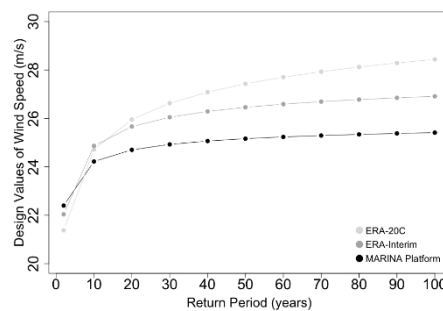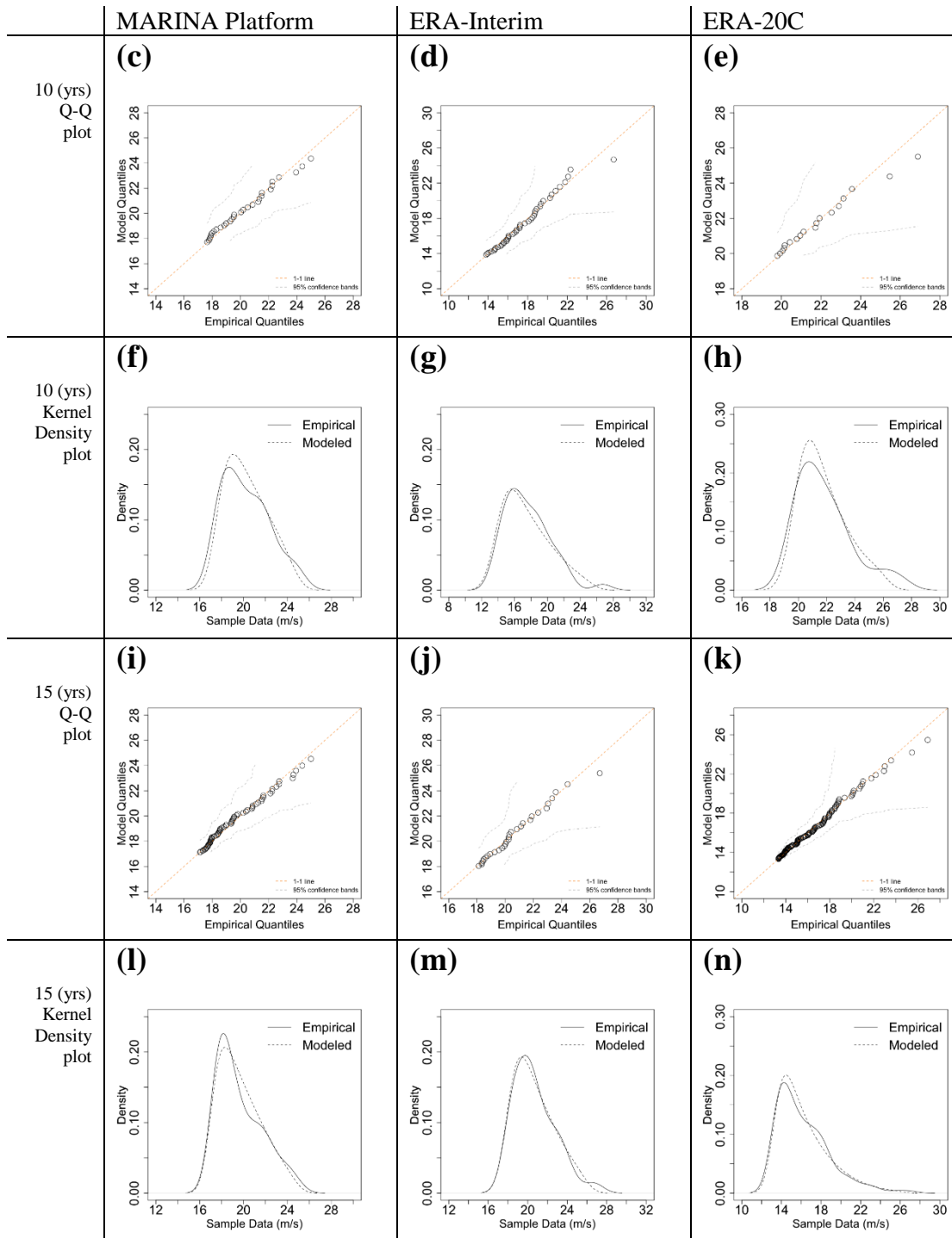10 (yrs)                                                     15 (yrs)
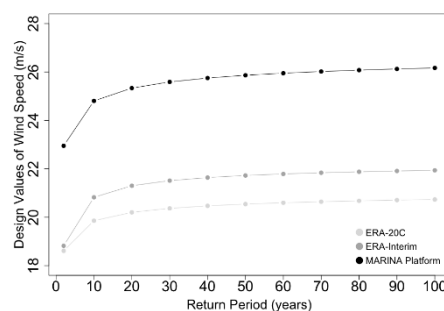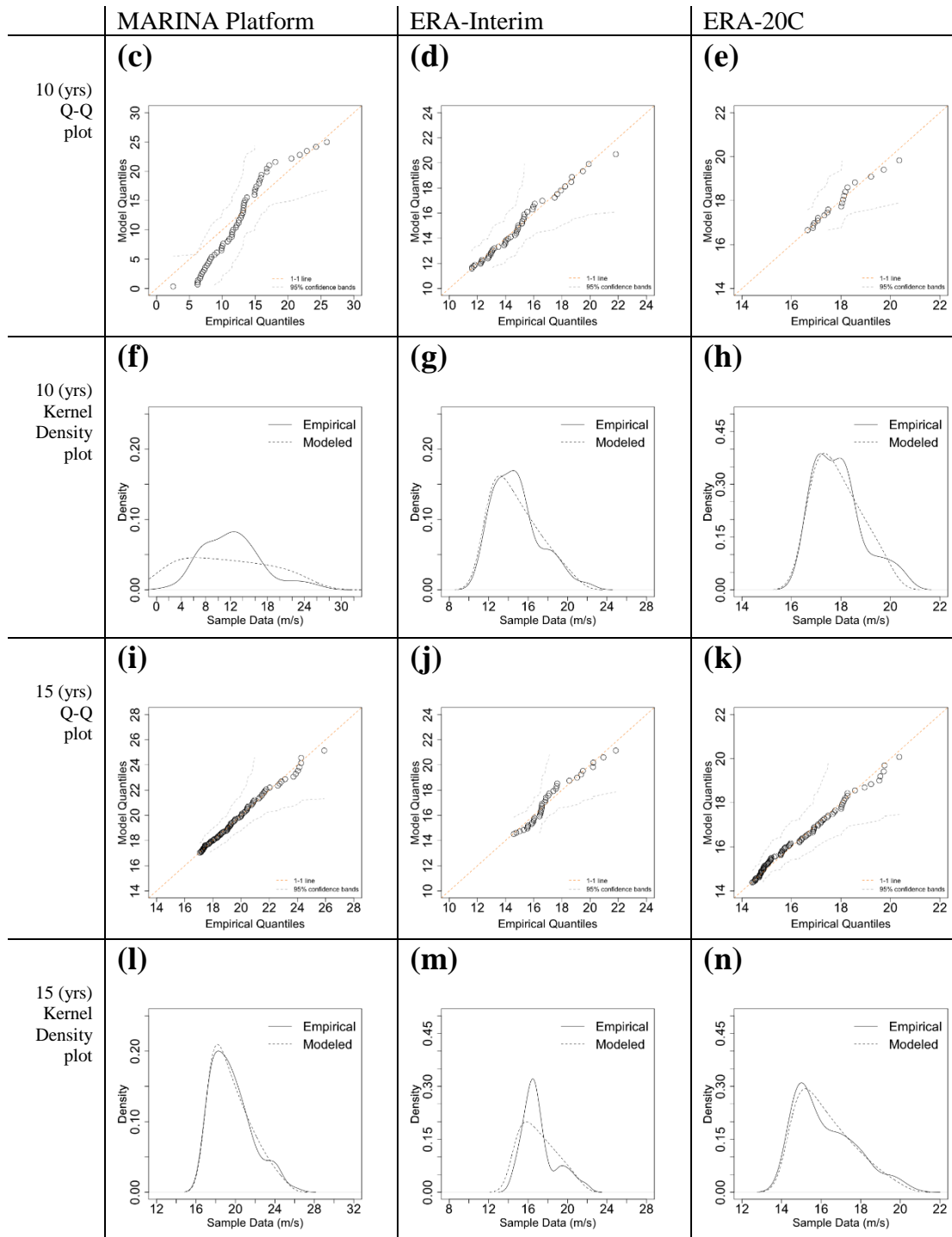
Figure 6.39: Visual inspection of the return level estimates in (a) and (b) of DeCAUn, with the Q-Q plot diagrams in (c,d,e,i, j, and k) and Kernel Density plot diagrams in (f,g,h,l,m, and n) for samples of 10 and 15 years for regional locations closely arranged in the Western Mediterranean Sea. Dashed light grey lines of the Q-Q plots show the 95% pointwise tolerance intervals. (Supplementary material of Tsalis et al., 2021)

As regards to the demonstration of DeCAUn at the three regional locations closely arranged in the Western Mediterranean Sea the following remarks can be derived from this setting:

- The response of DeCAUn at these locations is strongly influenced from the land-sea topography. Particularly, for the sample period of 15 years in the nearshore areas to

this setting the extreme quantiles of the GPD distribution are systematically closer to the theoretical GPD line regarding the high resolution datasets of the MARINA Platform as illustrated in the Q-Q diagram (i) of Figure 6.39, and to a lower extent from the low-resolution datasets of ERA-Interim in (j), and of ERA-20C in (k), respectively. The higher scale-resolution datasets reproduced the wind speed pattern effectively for the modelling of DeCAUn in comparison to the downscaled datasets as expected.

- The right-skewed distribution effect is also in line with the wind speed characteristics illustrated in the Kernel density diagrams of Figure 6.39. Specifically, for the sample period of 15 years the modeled density of DeCAUn based on samples of the MARINA Platform show stronger rate of convergence to the empirical density in the (l) diagram and to a lower extent from ERA-20C in (n), and to a less extent from ERA-Interim in (m).

- The inconsistency of the maximum likelihood estimator to the sample size of 10 years failed to infer the asymptotic properties particularly for the higher scale resolution dataset and to a lower extent for the downscaled datasets.

- The non parametric bootstrap approach to the bound estimate of the 50 years return levels from the modelling of DeCAUn yield normal confidence/credible intervals in respect to samples of all datasets, giving bounds that lie within the physical constraints of the wind speed variable studied as shown in Table 6.18 and 6.19.

- Return level estimates illustrated in (a) and (b) of Figure 6.39 show larger values from the modelling of DeCAUn to samples of the MARINA Platform in comparison to the estimates made to samples of lower scale resolution.

To sum up then, from this assessment the ML method confirmed the fact that may lead to very high quantile estimation variances and biased estimates when fitting the standard GPD distribution based on small sample sizes of 10 and 15 years (Davison and Smith, 1990; Fawcett and Walshaw 2015). The intractable problems of inference in terms of the strong variability from the modelling of DeCAUn to the relatively small samples of high and downscaled resolution datasets in this setting, set difficulties to verify that the ML estimator meets the desired asymptotic properties particularly for the sample sizes of 10 years. The inconsistencies from the estimator are alleviated when the sample period of wind speed is set no less than 15 years. However, despite the challenging problems of inference when the available sample is small, from this evaluation, the DeCAUn model is proposed as an alternative re-sampling strategy reconstructing a dependent sample of observations irregularly spaced in time to a sample based on the i.i.d limitations.

Recent work in Fawcett and Walshaw (2006a, 2007, 2012) and Eastoe and Tawn (2012) revealed estimation bias for the model parameters as well as the return levels. Specifically, from their assessment to the modelling of extremes based on the standard GPD, they showed in some cases significant under-estimation of the return levels. The major effect from the reconstruction procedure of DeCAUn is the considerable reduction of the available number of observations. To this effect, a challenging aim for the improvement of DeCAUn in future work is to investigate the use of methods that maximise the number of extremes from observations irregularly spaced in time. For example, Eastoe and Tawn (2012) and Fawcett and Walshaw (2012, 2015), proposed methods that can substantially reduce return level estimation uncertainty relative to the standard modelling of extremes based on GPD. Specifically, if DeCAUn is modelled to sample sizes less than 15 years an alternative to the standard GPD distribution will probably be the sub-asymptotic model as proposed from Eastoe and Tawn (2012), that will probably model more effectively the irregularly cluster maxima of the small resamples.

# Chapter 7
## Conclusions and future work

## 7.1 Main contributions and most important findings

The present study contributed on the modeling and extrapolation of extreme events based on simulation analysis and applications using historical data of wind speed. In particular,

- Identification of the combined effects of i) the sample size (along with the direction step of sampling) of the annual maxima and ii) the comparison of the parameter estimation methods to these effects to wind speed.
- Inference from the nonstationary modelling of extreme wind speed setting one or more of the parameters of the distribution as linear or nonlinear functions of the covariates on which the data show dependence in time.
- A proposed methodology for the modelling of extremes based on the asymptotic model formulation of the standard distributions when samples are irregularly spaced in time. Specifically, focusing on relatively small samples of wind speed the proposed model demonstrated as an alternative strategy for reconstructing a dependent sample of observations irregularly spaced in time to a re-sample in line to the i.i.d limitations.

The most important findings from this assessment in extremes are outlined in the following considering the distributional behavior of the two types of extreme wind speed sampling data used (the classical BM and the POT concept):

- Focusing on samples of wind speed where prior evidence exists of the estimated $\xi$ parameter of the GEV distribution as negative, it seems that the rather less known methods (EP, POME, and MPS) and, in a smaller degree, the well known ML and $LMH_U$ methods, are very reasonable solutions for modeling extremes. This is evident based on the statistical criteria assessed from the simulation and applications to wind speed setting fixed sample periods of 30 years.
- Based on the evaluation using different sample sizes of wind speed data, LMOM method outperforms, in many respects, compared to the MLE method. Overall, regarding the design values from both the simulation study and applications it is evident that sample sizes greater than 35 are necessary for a substantial reduction of epistemic uncertainty. On the other hand, LMOM method should be preferred for small sample sizes.
- Under the proviso of nonstationarity at locations in the North Sea, the stationary model generally provided the lowest return level estimates in comparison to the parametric models set to assess the trend in wind speed. The inference made of the models assessed to the likelihood is that linear and quadratic are overall evident models of detecting significant trends of the annual extremes in the North Sea.
- No definitive conclusions can be drawn as regards the performance of MLE and LMOM estimation methods with respect to the sample types (F or B), since the values of the criteria fluctuate with respect to sample size, location and estimation method and do not exhibit a systematic pattern. However, inference of the design values to wind speed pointed out that for small sample sizes (size 20 and 30), the extremes from the analysis based on the B–samples are, in general to the F–samples, closer to the extrapolations based on the samples of size 50 especially for low return periods (up to 50 years).

- The effective DEP level estimates and bandwidth response of the proposed resampling strategy to the irregularly sample of observations set the reconstructed range of events in line with the variability of extreme winds over the regional locations in this analysis.
- For sample periods of wind speed greater than 15 years the re-samples of DeCAUn modeled by the approximation to the GPD demonstrated effective projections in terms of precision and variability.
- With regards to the 50 year design values, DeCAUn yielded larger confidence bounds in comparison to the extrapolations made from the standard models within the POT concept. The samples of 10 and 15 years confirmed the inconsistency of MLE to BM to provide reasonable bound estimates resulting in a weak comparable measure of prediction to these samples.
- The high resolution database used for the analysis, ensured as possible the extreme efficient characteristics of the resamples of DeCAUn primarily near the coasts and in narrow straits and basins where applied, avoiding the apparent underestimation of the extreme variability of wind speed.
- However, the proposed model was confounded by large variability following by the reduction in sample size from the proposed sampling procedure. A more comprehensive investigation with regards to the optimization of the parameter estimation and the sampling uncertainties must be undertaken before the proposed model is widely applied.

## 7.2 Future improvements of this study

- A better approach, would require reducing the uncertainty of the return level estimates from GEV. Bias correction techniques such as the Bayesian hierarchical model have been introduced in order to improve predictions of extremes from global climate and ocean models, see Oliver et al., (2014). Future work could include the MPS and EP estimation methods along with the common estimation methods, for cases of advanced correction methods of this kind.
- It is suggested that further assessment is necessary to the response of sample types of different count for extrapolations, since different sample types are challenged in practical applications.
- Additional issues related to the proposed re-sampling procedure still remain and worth to be further assessed. For example, the L-moments (LMOM) method is probably more suitable for the modelling of extremes based on the relatively small sample periods (see application of LMOM in Pandey et al., 2001). Following the findings of the simulation study for large and small samples from Šimková and Picek (2016), LMOM succeeded for heavy or moderate tailed distributions, while MLE method is recommended for light-tailed distributions. Although the modelling of extremely high wind speeds in general supports a bounded tail, the use of the Gumbel type and LMOM for relatively small samples is strongly recommended in engineering design in practice (e.g., see Katz, 2002).
- Additionally, the use of the parametric bootstrap approach (Davison and Hinkley, 1997) for the DeCAUn model validation will probably improve the uncertainty bound effect of the estimates. This remark also follows the suggestion from Kyselý (2008) for inference based on the small to moderate sample sizes such as those reconstructed from DeCAUn.
- Finally, a modelling basis for the multivariate probabilistic assessment of DeCAUn considering the limiting distribution of more than one vector random variables that are extreme in at least one component based on the conditional extremes approach proposed by Heffernan & Tawn (2004) and later formalized by Heffernan & Resnick (2007), will address respectively all danger parameters in a more natural way to wind speed applications.

# Appendix

## A. Characteristic Function

A function$\varphi_X(t)$ is defined as a characteristic function(see Ochi, 1998),

$$\varphi_X(t) = E[\exp(itX)] = \int_R e^{itx} dF_X(x) = \int_R e^{itx} f_X(x) dx, \tag{A.1}$$

with properties:

I. $\varphi_X(t)$ must be continuous in $t$
II. $\varphi_X(t)$ is defined in every finite $t$ interval
III. $\varphi_X(0) = 1$
IV. $\varphi_X(t)$ and $\varphi_X(-t)$ are considered to be conjugate quantities.

## B. Gamma function and derivatives

The values of the derivatives of the Gamma function at the point 1, yields from the expansion of Gamma function

$$\Gamma(z+1) = \exp\left(-\gamma z + \sum_{k=2}^{\infty} \frac{(-1)^k \zeta(k) z^k}{k}\right), |z| < 1 \tag{B.1}$$

e.g., see (Rivoal 2009) and (Abramowitz and Stegun 1972) as follows:

$$\Gamma^{(s)}(n+1) = n! \sum_{j=0}^{s} \binom{s}{j} H_n^{[s-j]} \Gamma^{(j)}(1), \tag{B.2}$$

for any integers $n \geq 0$ and $s \geq 0$.

Function $H_n^{[s]}$ and Riemann Zeta function $\zeta(s)$ are defined recursively

$$H_n^{[s]} = s! \sum_{1 \leq i_1 < \dots < i_s \leq n} \frac{1}{i_1 i_2 \cdots i_s}, \text{ for } s \geq 0 \text{ and} \tag{B.3}$$

$$\zeta(s) = \frac{1}{\Gamma(s)} \int_0^{\infty} \frac{1}{e^x - 1} x^s \frac{dx}{x}, \text{ for } Re(z) > 1. \tag{B.4}$$

## C. Plotting position formulae

The plotting position problem has been discussed by many authors; see for example Cunnane (1978), Makkonen (2006, 2008), Kim et al., (2012),Gringorten (1963), Arnell et al., (1986), Inna et al., (1989), Goel and De (1993) and Goda (2011). By 1960 many new formulae had appeared, but there was no criterion by which a single formula could be chosen to give unique results over all distributions. In order to choose the best plotting position formula, the estimated quantile should be free from bias and should have minimum variance among graphical estimates. See also the relevant discussion in Makkonen (2006, 2008) about plotting position formulae in extreme value analysis. Since quantiles are an important ingredient in plotting position and return period calculations, there is a clear connection between them: First, the data (e.g., annual maxima) are ranked in increasing order of magnitude and a cumulative probability is associated to each point. Then, a best-fit line is fitted to the ranked values by some fitting procedure. An extrapolation of this line provides long-return periods of the extreme value of interest.

Let $x_{\min} = x_{1:n} \leq x_{2:n} \leq \cdots x_{n:n} = x_{\max}$ be an ordered random sequence. The most well-known plotting position formula is probably the Weibull formula, i.e.,

$$F(x_{i:n}) = \Pr[X < x_{i:n}] = p_{i:n} = \frac{i}{n+1}, i = 1,2,\dots,n. \tag{C.1}$$

In the above relation as well as for all plotting positions formulae, $F(x_{i:n})$ is the empirical estimate of the non-exceedance probability of the $i - th$ smallest member in an ordered sample. The plotting position provided by relation (C1) is the only one justified for return period calculations.

In (Cunnane, 1978) the following general representation for the plotting position formulae is proposed:

$$p_{i:n} = (i - a)/n, \text{ or } p_{i:n} = (i - a)/(n + 1 - 2a), \text{ for } 0 < a < 1. \tag{C.2}$$

The value of $a$ (plotting position parameter) in the above relation, yields approximately unbiased plotting positions for a variety of different distributions and determines the efficiency of the plotting position as regards the fit of a given theoretical distribution. For example, $a = 0$ is valid for all distributions (Weibull formula), $a = 0.44$ is valid for the GEV and exponential distributions (Gringorten formula), $a = 0.5$ for the GEV distribution (Hazen formula) and $a = 3/8$ for the normal distribution.

Recently, in (Kim et al., 2012), the authors using a genetic optimization method, proposed the following plotting position formula for the GEV distribution:

$$p_{j:n} = \frac{j - 0.32}{n + 0.0149g^2 - 0.1364g + 0.3225}, \quad j = 1,2,\dots,n, \tag{C.3}$$

where $g$ denotes the skewness coefficient. The authors compared also the proposed formula with the formulas provided in Cunnane (1978), Gringorten (1963), Arnell et al. (1986), In-na et al. (1989), Goel and De (1993).

# D. NEVA

The work from Cheng et.al., (2014), represents a computational platform for estimating stationary and non-stationary return levels, return periods and climatic extremes using Bayesian inference. The software package in MATLAB environment is named NEVA after Non-stationary Extreme Value Analysis. In a Bayesian approach, NEVA estimates the extreme value parameters with a Differential Evolution Markov Chain (DE-MC) approach for global optimization over the parameter space.

NEVA provides three different methods for estimation of return levels: (i) standard return levels (commonly used in hydrologic design) in which the exceedance probability is constant for any given return period during the life of the design (design exceedance probability); (ii) constant thresholds with time varying exceedance probability; and (iii) effective return levels. A unique feature of NEVA is that it estimates and provides the associated probability intervals and uncertainty bounds for the return level estimates under non-stationarity. NEVA offers a range of return levels, and the user can select the upper bound (low risk) or the lower bound (high risk) depending on the application at hand.

Furthermore, the function detects the presence of a trend by implementing the MK trend test at the choice of the significance level (default choice $a = 0.05$). If the null hypothesis is not rejected, NEVA will perform extreme value analysis under the stationary assumption. Upon detection of a trend at the 5 % significance level, the GEV parameters will be estimated under the non-stationary assumption.

Finally, NEVA is also used in studies for stationary and non-stationary extreme value analysis of annual temperature maxima from the Climatic Research Unit (New et al., 2000) gridded monthly temperature data (1901–2009).

# E. Spectrum Autocorrelation

## E.1 Parseval's identity for Fourier transforms-(Rayleigh's Theorem)

The contribution of each frequency $v(Hz)$ to a signal $f(t)$ is defined by the Fourier transform $\text{FT}(f)$ of the signal as follows:

$$F(v) = \text{FT}[f(v)] = \int_{-\infty}^{+\infty} f(t)e^{-2\pi vt \cdot i} dt\ , \quad -\infty \le v \le +\infty. \tag{E.1.1}$$

The function of Fourier transform $\text{FT}(f)$ is a complex valued function of frequency $v(Hz)$. The inverse Fourier transform $\text{F}^{-1}(F)$ is defined as follows:

$$f(t) = \text{F}^{-1}[F(t)] = \int_{-\infty}^{+\infty} F(v)e^{+2\pi vt \cdot i} dv\ , \quad -\infty \le t \le +\infty. \tag{E.1.2}$$

Considering together Fourier transform and its inverse, it is provided a way of passing between equivalent representations of a signal via the Fourier inversion theorem:

$$f(t) \rightleftarrows F(v) \tag{E.1.3}$$

An important relation between the energy of the signal in the time domain and the energy spectrum in the frequency domain is given by Parseval's identity for Fourier transforms or Rayleigh's Theorem, which relates the variances of a signal $f(t)$ and its Fourier transform $\text{FT}(f)$, by the equation

$$\int_{-\infty}^{+\infty} |f(t)|^2 dt = \int_{-\infty}^{+\infty} |F(v)|^2 dv. \tag{E.1.4}$$

The total power can therefore be expressed either in terms of the integral of the original function or its Fourier transform (Parseval's theorem), as follow (Priestley, 1981):

$$\text{total power} = \int_{-\infty}^{+\infty} |f(t)|^2 dt = \int_{-\infty}^{+\infty} |F(v)|^2 dv \tag{E.1.5}$$

The square magnitude of the Fourier transform of a signal $f(t)$ is called the power spectrum $P(v) = |F(v)|^2 = F(v) \cdot F^*(v)$, $-\infty \le v \le +\infty$ or the spectral power density, or the energy spectrum, and $F^*(v) = \text{FT}[f(-v)]$ is the complex conjugate of the Fourier transform.

## E.2 Convolution and Correlation Theorem

Referring to the Time Convolution Theorem, the Fourier transform $H(v)$ of the convolution $h(t)$ of two functions $f(t)$ and $g(t)$, equals to the product of Fourier transforms $F(v)$ and $G(v)$ of the two functions (e.g see Bronshtein and Semendyayev, 1985, p. 582).

Considering $f(t) \rightleftarrows F(v)$, $g(t) \rightleftarrows G(v)$ and $(f * g)(t) = h(t)$, the equivalent expressions are derived as follow:

$$h(t) \rightleftarrows F(v) \cdot G(v), \tag{E.2.1}$$

$$(f * g)(t) \rightleftarrows F(v) \cdot G(v), \text{ and} \tag{E.2.2}$$

$$\int_{-\infty}^{+\infty} f(t - \tau)g(\tau)d\tau \rightleftarrows F(v) \cdot G(v). \tag{E.2.3}$$

Closely related to the Time Convolution theorem, is the correlation theorem. Considering the time convolution theorem and Fourier inverse-transform properties

$$f(-t) \rightleftarrows F^*(v) \text{ and } F^*(v) = F(-v), \tag{E.2.4}$$

the product of a Fourier transform with the complex conjugate of its Fourier transform can be reduced to the form

$$\begin{cases} f(t) * f(-t) \rightleftarrows F(v) \cdot F^*(v), \\ f(t) * f(-t) \rightleftarrows F(v) \cdot F(-v), \\ \int_{-\infty}^{+\infty} f(t - \tau)f(-\tau)d\tau \rightleftarrows F(v) \cdot F(-v). \end{cases} \tag{E.2.5}$$

Substitution of $f(-\tau) = f(\tau)$ and $f(t - \tau) = f(t + \tau)$ into the expressions stated in (E.2.5), the Fourier transform of the correlation theorem is stated

$$\int_{-\infty}^{+\infty} f(t + \tau)f(\tau)d\tau \rightleftarrows F(v) \cdot F(-v), \tag{E.2.6}$$

since $f(t)$ is considered a real and even signal.

## E.3 Wiener-Khinchin Theorem

Considering the time Convolution theorem stated in Equation (E.17), the Correlation theorem and Fourier inverse-transforms in (E.20), the covariance and the spectrum function can be expressed as a Fourier transform pair,

$$\int_{-\infty}^{+\infty} f(t + \tau)f(\tau)d\tau \rightleftarrows F(v) \cdot F^*(v), \text{ and} \tag{E.3.1}$$

$$Cov_f(t) \rightleftarrows P(v). \tag{E.3.2}$$

Normalizing the Covariance and spectrum function dividing respectively by the total power or Parseval's Theorem,

$$Cov_f(0) = \sigma^2 = \int_{-\infty}^{+\infty} |f(t)|^2 dt = \int_{-\infty}^{+\infty} |F(v)|^2 dv = \text{total power}, \tag{E.3.3}$$

it is derived,

$$\frac{Cov_f(t)}{\text{total power}} \rightleftarrows \frac{P(v)}{\text{total power}}, \text{ and} \tag{E.3.4}$$

$$\frac{Cov_f(t)}{\int_{-\infty}^{+\infty}|f(t)|^2 dt} \rightleftarrows \frac{P(v)}{\int_{-\infty}^{+\infty}|F(v)|^2 dv}. \tag{E.3.5}$$

Therefore, the autocorrelation and the normalized expression of spectrum function can be expressed as a Fourier transform pair,

$$\rho(t) \rightleftarrows \frac{P(v)}{\sigma^2}. \tag{E.3.6}$$

## F. Trend and unit root tests

Mann-Kendall (MK) non-parametric trend test

The non-parametric MK test is commonly employed to detect monotonic trends in series of environmental data, climate data or hydrological data. The MK test for trend detection has also been mentioned in the work from (Cunderlik and Burn 2002; Hundecha et.al, 2008; van Belle G. and Hughes J.P., 1984; Kundzewicz and Robson, 2004). This aim of the MK test is to examine the hypothesis that there is a monotonic upward or downward trend of the variable. Assuming a linear trend, the MK test, in other words, is used to test whether the slope of the regression line is different from zero.

The null hypothesis of the test is expressed as follows:

$H_0$: No monotonic trend is present, i.e., data come from a population with independent realizations and are identically distributed, against the alternative,

$H_1$: There is a monotonic trend present.

The steps for the implementation of the test are described as follows; see also Gilbert (1987):

1.  Let $M_1, M_2, ..., M_N$ be the time series of the annual maxima for year $1, 2, ..., N$.

2.  Calculate all the possible differences $\Delta_{ji} = M_j - M_i$, for all $j > i$ and consider the sign indicator function $I(j, i)$ taking the values -1, 0 and 1 for $\Delta_{ji} < 0$, $\Delta_{ji} = 0$ and $\Delta_{ji} > 0$, respectively. The total number of differences is $N(N - 1)/2$.

3.  Estimate the MK score $S$ and the variance $Var(S)$ as follows:

    $$S = \sum_{i-1}^{N-1} \sum_{j-i+1}^{N} \Delta_{ji}, \tag{F.1}$$

    and the corresponding variance as follows:

    $$Var(S) = \frac{1}{18}\left[N(N-1)(2N+5) - \sum_{p=1}^{g} t_p(t_p+1)(2t_p+5)\right], \tag{F.2}$$

    where $g$ denotes the number of tied groups and $t_p$ is the number of observations (data) in the $p-$th group in the sample of the actual observations $M_1, M_2, ..., M_N$.

4.  Finally, by applying the following transformation:

$$z_{M-K} = \begin{cases} \dfrac{S-1}{\sqrt{Var(S)}}, & S > 0 \\ 0, & S = 0 \\ \dfrac{S+1}{\sqrt{Var(S)}}, & S < 0 \end{cases} \tag{F.3}$$

the test statistic (score) $S$ is approximately normally distributed. It is noted by (Hipel and McLeod, 1994) that the minimum acceptable value of $N$ for implementing this method is 10, unless the number of ties is significant. The null hypothesis of no trend is rejected if the p-value ($^9$) is less than a significance level ($a$ =0.05). In other words, the null hypothesis is rejected at the significance level if $|Z_{M-K}| > z_{a/2}$ where $z_{a/2}$ is the critical value obtained from the standard normal distribution with a probability of exceedance of $a/2$. Contrarily, when the estimated p-value is larger than 0.05 the null hypothesis cannot be rejected.

Cox Stuart (CS) trend test

The Cox–Stuart test belongs to the class of nonparametric tests, as the Mann–Kendall test and is a robust method to detect the presence of the trend regardless of the distribution of the data. The statistical hypothesis in testing for trend in a series of random variables are:

$H_0$: No monotonic trend exists in the series, against the alternative

$H_1$: The series is characterized by a monotonic trend.

Considering the independent series of data$\{y_t, t = 1, \cdots, n-1, n\}$. In the testing procedure, first the series are divided into three sequences of data. In this way, it is compared whether the data of the first third of the series are larger or smaller than the data of the last third of the series. Secondly, all paired differences $D = y_{n-c+1:n} - y_{1:c}$ are derived in respect to $c$, with the latter defined as the point index separating the first third of the data. The totals of the positive or negative sign in $D$ are denoted as $D^+$or $D^-$respectively. The z-statistic of the CS trend test is defined:

$$z = |D - n/6|/sqrt(n/12), \text{for } n > 30\,, \tag{F.4}$$

and including a continuity correction as

$$z = (|D - n/6| - 0.5)/sqrt(n/12), \text{for } n < 30. \tag{F.5}$$

The CS test is performed for a positive trend (increase) considering the $D^+$, negative trend (decrease) with the $D^-$, or as a two sided test with $D = \min(D^+, D^-)$. The $z$-statistic is normally distributed where p-values are estimated respectively. In order to REJECT the null hypothesis for this test, a p-value of less than 0.05 (or smaller) must be obtained.

Unit root

In probability theory and statistics, a unit root is a feature of some stochastic processes (such as random walks) that can cause problems in statistical inference involving time series models. A linear stochastic process has a unit root, if the process's characteristic equation has a root of value equal to one. Such a process is non-stationary but does not always have a trend.

---

($^9$) p-value $=\Pr\{|Z_{M-K}| > z\}=\Pr\{Z_{M-K} < -z \cup Z_{M-K} > z\}=\Pr\{Z_{M-K} < -z\}+\Pr\{Z_{M-K} > z\}=2\Pr\{Z_{M-K} > z\}$, where $\Pr\{Z_{M-K} > z\}$ is the probability from a standard normal distribution.

A discrete-time stochastic process $\{y_t, t = 1, 2, \cdots, \infty\}$ can be written as an autoregressive process of order $p$ as follows:

$$y_t = a_1 y_{t-1} + a_2 y_{t-2} + \cdots + a_p y_{t-p} + e_t, \tag{F.6}$$

where $\{e_t, t = 0, 1, \cdots, \infty\}$ is a serially uncorrelated, zero-mean stochastic process with constant variance. The component $e_t$ is also regarded as the (white noise) process. If $m = 1$ is a root of the characteristic equation:

$$m^p - m^{p-1} a_1 - m^{p-2} a_2 - \cdots - a_p = 0, \tag{F.7}$$

then the stochastic process has a unit root. Tests to check for the existence of a unit root is the primarily Dickey–Fuller test (DF) proposed by (Dickey and Fuller, 1979) or the augmented Dickey–Fuller (ADF) and the KPSS type tests that complement unit root tests such as the ADF test.

## Dickey-Fuller (DF) test

Considering a first order auto-regression model of the form

$$y_t = a + \beta t + \rho y_{t-1} + e_t, \tag{F.8}$$

the Dickey-Fuller test is testing the presence of a unit root $\rho = 1$ for this model. The presence of a unit root is also regarded as a non-stationary process. The coefficients $(a, \beta)$ denote the drift and the trend component respectively of the model. For the DF unit root test, the model is written as

$$\Delta y_t = y_t - y_{t-1} = a + \beta t + \gamma y_{t-1} + e_t, \tag{F.9}$$

where $\gamma = \rho - 1$ and $y_t$ is the data. The model is written this way in order to perform a linear regression of $\Delta y_t$ against $t$ and $y_{t-1}$, and test if $\gamma$ is different from 0. If $\gamma = 0$ then the process is considered nonstationary. A unique nonstationary process for $(a = 0, \beta = 0, \gamma = 0)$ is also regarded as a (random walk). Contrariwise, if $\gamma < 0$ and $(-2 < \gamma < 0)$, the process is considered stationary.

## Augmented Dickey-Fuller (ADF) unit root test

The Augmented Dickey-Fuller test examines higher-order autoregressive processes by including $\Delta y_{t-p}$ in the model. The number of lagged difference terms is denoted as $p$ and specified. The model is written as follow:

$$\Delta y_t = a + \beta t + \gamma y_{t-1} + \delta_1 \Delta y_{t-1} + \delta_2 \Delta y_{t-2} + \cdots + \delta_p \Delta y_{t-p} + e_t, \tag{F.10}$$

where the null hypothesis of the presence of a unit root is $H_0: \gamma = 0$ (non-stationary process) under the alternative hypothesis, $H_1: \gamma < 0$ (stationary process).

In order to REJECT the null hypothesis of this test, a p-value less than 0.05 (or smaller) must be obtained. The ADF test statistic is defined as ADF=$\hat{\gamma}/SE(\hat{\gamma})$, where $\hat{\gamma}$ is the least squares estimate and $SE(\hat{\gamma})$ the corresponding standard error. The p-value of the test is derived by interpolating the test statistics from the corresponding critical values in (Table 10.A.2 in Fuller (1996)). The DF test is a special case of the ADF test when $p = 1$.

## (KPSS) stationarity test

The Kwiatkowski-Phillips-Schmidt-Shin (KPSS) stationarity test by Kwiatkowski et al. (1992) examines if a time series is stationary around a mean (level stationary) or linear trend

stationary (trend stationary), or manifests the series under the alternative hypothesis as non-stationary due to a presence of a unit root. The series is expressed as the sum of a deterministic trend, random walk, and stationary error by the regression equation as follows:

$$y_t = a + \beta t + x_t + \varepsilon_t, \tag{F.11}$$

where the first part $\{a + \beta t\}$ considers the drift and trend into the model, $\{x_t, x_t = x_{t-1} + e_t\}$ is the component of a random walk process and finally the stationary error where $\{\varepsilon_t, t = 0,1, \cdots, \infty\}$ is a serially uncorrelated, zero-mean stochastic process with zero variance. The KPSS test performs the Score test of the hypothesis that the random walk has zero variance $H_0: \sigma_e^2 = 0$ (stationary process), under the alternative hypothesis $H_1: \sigma_e^2 > 0$ (non-stationary process). In order to REJECT the null hypothesis for this test, a p-value of less than 0.05 (or smaller) must be obtained. The KPSS statistic is defined as

$$\text{KPSS} = \left(\frac{1}{n^2}\sum_{t=1}^{n}\hat{S}_t^2\right)/\hat{\lambda}, \tag{F.12}$$

where $\hat{S}_t = \sum_{j=1}^{t}\hat{\varepsilon}_j$ and $\hat{\lambda} = \sum_{j=1}^{t}\hat{\varepsilon}^2/n$ for a given data sample of size $n$. The residuals of a regression of the $y_t$ data on the corresponding $t$ are denoted as $\hat{\varepsilon}_j$.

If the data are stationary the series will be stationary around a fixed level. The test uses the Ordinary Least Squares method (OLS) to estimate the residuals $\hat{\varepsilon}_j$, depending on whether to test for level stationarity or trend stationarity (Kočenda and Černý, 2007). A simplified version of the KPSS test without the time trend component is used to test level stationarity (see also Syczewska, 2010). Finally, the p-values are obtained by the interpolation of the test statistic from tables of critical values (Table 5, Hobijn et al., 2004).

## G. Kernel properties

1.  Expected value of $\hat{f}(x)$

$$E[\hat{f}(x)] = f(x) + \frac{1}{2}h^2 f''(x)\int_{-\infty}^{+\infty}z^2 K(z)dz + 0(h^2). \tag{G.1}$$

Proof:

$$E[\hat{f}(x)] = E\left[\frac{1}{nh}\sum_{i=1}^{n}K\left(\frac{x-x_i}{h}\right)\right] = \frac{1}{n}\sum_{i=1}^{n}E\left[\frac{1}{h}K\left(\frac{x-x_i}{h}\right)\right] = E\left[\frac{1}{h}K\left(\frac{x-x_i}{h}\right)\right]. \tag{G.2}$$

Using the integral of the expected value operator and the appropriate change of variables $z = \frac{x-t}{h}$, and $dt = |-h|dz$ into (G.2) yields,

$$E\left[\frac{1}{h}K\left(\frac{x-x_i}{h}\right)\right] = \frac{1}{h}\int_{-\infty}^{+\infty}K\left(\frac{x-t}{h}\right)f(t)dt = \int_{-\infty}^{+\infty}K(z)f(x-hz)dz. \tag{G.3}$$

Expanding $f(x - hz) = f(x) - hzf'(x) + \frac{1}{2}(hz)^2 f''(x) + 0(h)^2$ with Taylor series into (G.3), then

$$\int_{-\infty}^{+\infty}K(z)f(x-hz)dz =$$
$$= f(x)\int_{-\infty}^{+\infty}K(z)dz - hf'(x)\int_{-\infty}^{+\infty}zK(z)dz + \frac{1}{2}h^2 f''(x)\int_{-\infty}^{+\infty}z^2 K(z)dz + 0(h^2). \tag{G.4}$$

Substituting the Kernel pdf properties, (G.4) finally yields Silverman (1986, Ch. 3) or Wand and Jones (1995, Ch. 2)

$$\int_{-\infty}^{+\infty} K(z)f(x - hz)dz = f(x) + \frac{1}{2}h^2 f''(x)\int_{-\infty}^{+\infty} z^2 K(z)dz + 0(h^2). \tag{G.5}$$

Terms of the form $0(h^2)$ converge to zero faster than $h^2$ as $h \to 0$.

2. Bias of $\hat{f}(x)$

$$Bias\left(\hat{f}(x)\right) = E[\hat{f}(x)] - f(x) = \frac{1}{2}h^2 f''(x)\int_{-\infty}^{+\infty} z^2 K(z)dz + 0(h^2), \text{ and} \tag{G.6}$$

3. Variance of $\hat{f}(x)$

$$Var[\hat{f}(x)] \simeq f(x)\frac{1}{nh}\int_{-\infty}^{+\infty}(K(z))^2 dz + 0\left(\frac{1}{nh}\right). \tag{G.7}$$

Proof:

$$Var[\hat{f}(x)] = Var\left[\frac{1}{nh}\sum_{i=1}^{n} K\left(\frac{x-x_i}{h}\right)\right] = \frac{1}{n^2 h^2}\sum_{i=1}^{n} Var\left[K\left(\frac{x-x_i}{h}\right)\right]. \tag{G.8}$$

Considering $n$ real observations $(x_1, x_2, \dots, x_n)$ independent and identical distributed, the Variance of the Kernel estimator is derived:

$$Var\left[K\left(\frac{x-x_i}{h}\right)\right] = E\left[\left(K\left(\frac{x-x_i}{h}\right)\right)^2\right] - \left(E\left[K\left(\frac{x-x_i}{h}\right)\right]\right)^2. \tag{G.9}$$

Using the integral of the expected value operator into (G.9),

$$Var\left[K\left(\frac{x-x_i}{h}\right)\right] = \int_{-\infty}^{+\infty}\left(K\left(\frac{x-t}{h}\right)\right)^2 f(t)dt - \left(\int_{-\infty}^{+\infty} K\left(\frac{x-t}{h}\right)f(t)dt\right)^2, \tag{G.10}$$

and substituting correspondingly into (G.8) yields

$$\begin{aligned}
Var[\hat{f}(x)] &= \frac{1}{n^2 h^2}\sum_{i=1}^{n} Var\left[K\left(\frac{x-x_i}{h}\right)\right]\\
&= \frac{1}{nh^2}\left(\int_{-\infty}^{+\infty}\left(K\left(\frac{x-t}{h}\right)\right)^2 f(t)dt - \left(\int_{-\infty}^{+\infty} K\left(\frac{x-t}{h}\right)f(t)dt\right)^2\right)\\
&= \frac{1}{n}\int_{-\infty}^{+\infty}\left(\frac{1}{h}K\left(\frac{x-t}{h}\right)\right)^2 f(t)dt - \frac{1}{n}\left(\frac{1}{h}\int_{-\infty}^{+\infty} K\left(\frac{x-t}{h}\right)f(t)dt\right)^2\\
&= \frac{1}{n}\int_{-\infty}^{+\infty}\left(\frac{1}{h}K\left(\frac{x-t}{h}\right)\right)^2 f(t)dt - \frac{1}{n}(E[\hat{f}(x)])^2,
\end{aligned}$$

therefore,

$$Var[\hat{f}(x)] = \frac{1}{n}\int_{-\infty}^{+\infty}\left(\frac{1}{h}K\left(\frac{x-t}{h}\right)\right)^2 f(t)dt - \frac{1}{n}\left(Bias[\hat{f}(x)] + f(x)\right)^2. \tag{G.11}$$

Using the appropriate change of variables $z = \frac{x-t}{h}$ into (G.11), it is derived

$$Var[\hat{f}(x)] = \frac{1}{n} \int\limits_{-\infty}^{+\infty} \left(\frac{1}{h}K\left(\frac{x-t}{h}\right)\right)^2 f(t)dt - \frac{1}{n}\left(f(x) + \frac{1}{2}h^2 f''(x) \int\limits_{-\infty}^{+\infty} z^2 K(z)dz + 0(h^2)\right)^2$$

$$= \frac{1}{nh} \int\limits_{-\infty}^{+\infty} \left(K(z)\right)^2 f(x-hz)dz - \frac{1}{n}\left(f(x) + \frac{1}{2}h^2 f''(x) \int\limits_{-\infty}^{+\infty} z^2 K(z)dz + 0(h^2)\right)^2,$$

and expanding $f(x - hz)$ with Taylor series yields,

$$Var[\hat{f}(x)] = \frac{1}{nh} \int\limits_{-\infty}^{+\infty} \left(K(z)\right)^2 f(x-hz)dz - \frac{1}{n}\left(f(x) + \frac{1}{2}h^2 f''(x) \int\limits_{-\infty}^{+\infty} z^2 K(z)dz + 0(h^2)\right)^2$$

$$= \frac{1}{nh} \int\limits_{-\infty}^{+\infty} \left(K(z)\right)^2 \left(f(x) - hzf'(x) + \frac{1}{2}(hz)^2 f''(x) + 0(h^2)\right)dz - \frac{1}{n}\left(f(x) + \frac{1}{2}h^2 f''(x) \int\limits_{-\infty}^{+\infty} z^2 K(z)dz + 0(h^2)\right)^2.$$

$$(G.12)$$

Considering $n \to \infty$ and $h \to 0$, the latter stated in Equation (G.12) is derived as follow:

$$Var[\hat{f}(x)] \simeq f(x)\frac{1}{nh}\int_{-\infty}^{+\infty}\left(K(z)\right)^2 dz + 0\left(\frac{1}{nh}\right). \tag{G.13}$$

# H. Likelihood approximation for the $r$-largest order statistics

**Theorem H.1** (Convergence law of Point Processes for Extremes)

*We denote $M_n = max(X_1, \ldots, X_n)$ as the maximum of a random sample of size $n$ with independent and identical variables. If there exists sequences of constants $\{a_n > 0\}$ and $\{b_n \in R\}$, such that the sequence of point processes*

$$P_n = \left\{i/(n+1), \frac{(X_i - b_n)}{a_n} : i = 1,2,3,\ldots,n\right\} \to P, n \to \infty \tag{H.1}$$

*for some large value of $u_n$, then P follows a non-homogeneous Poisson process with integrated intensity measurein the time interval $[t_1, t_2] = [0,1]$ and over the region $[t_1, t_2] \times [u_n, \infty)$ as follows,*

$$\Lambda\left([t_1, t_2] \times [u_n, \infty)\right) = (t_2 - t_1)V(A), \tag{H.2}$$

*where $V(A)$ is the expected number of exceedances obtainedover the region $A = \{(0,1) \times [u_n, \infty)\}$.*

Moreover, considering the independent and identically distributed $M_n^{(r)} = r^{th}$ largest of $(X_1, X_2, \ldots, X_n)$ that exceed of a level $u_n$ denoted as

$$\left(\frac{X^{(1)} - b_n}{a_n}, \frac{X^{(2)} - b_n}{a_n}, \ldots, \frac{X^{(i)} - b_n}{a_n}, \ldots, \frac{X^{(r)} - b_n}{a_n}\right), \tag{H.3}$$

then for a fixed value of $r$ the expected number of exceedances in a time interval $(0,1)$ over the region $\{(0,1) \times [u_n, \infty)\}$ converge into (see Smith, 1990):

$$V\left(x^{(r)}; \xi, \sigma, \mu\right) = \left[1 + \xi\left(\frac{x^{(r)} - \mu}{\sigma}\right)\right]^{-1/\xi} = \left[1 + \xi\left(\frac{u_n - \mu}{\sigma}\right)\right]^{-1/\xi}, x^{(r)} = u_n. \tag{H.4}$$

The occurrence rate of points per unit region $\lambda\left(x^{(r)};\xi,\sigma,\mu\right)$, is just the negative derivative of the $V\left(x^{(r)};\xi,\sigma,\mu\right)$:

$$\lambda\left(x^{(r)};\xi,\sigma,\mu\right) = -\frac{\partial}{\partial x^{(r)}}V\left(x^{(r)};\xi,\sigma,\mu\right) = \frac{1}{\sigma}\left[1+\xi\left(\frac{x^{(r)}-\mu}{\sigma}\right)\right]^{-1/\xi-1}, x^{(r)} \geq u_n. \quad (H.5)$$

Making the appropriate substitutions of Equations (H.4) and (H.5) into the likelihood of the non-homogeneous Poisson process stated in Equation (3.1), the general form of the non-homogeneous Poisson process likelihood stated in Equation (3.2) is obtained for the $r^{th}$ largest ordered maxima that exceed over a high threshold level $u_n$.

## H.1 Likelihood approximation of the non-homogeneous Poisson process for the $r$-largest order statistics

At this point it is reasonable to point out that the likelihood obtained from the modeling derived by Coles (2001) is equivalent to the initial formulation made from Weissman (1978) or by Leadbetter et al. (1983, Chapter 2).

(Leadbetter 1983) associated the identical events, $\Pr\left[M_n^{(r)} \leq u_n\right] = \Pr[S_n < r]$, where $S_n$ denotes the number of $(X_1, X_2, \ldots, X_n)$ which exceed $u_n$. In other words, the probability of the $r^{th}$ largest of $(X_1, X_2, \ldots, X_n)$ which does not exceed $u_n$ is in the same sense as the probability of no more than $S_n$ number of exceedances exceeding $r$. Consequently, the distribution function of the $r^{th}$ largest order statistic is stated by the following Theorem H.2.

**Theorem H.2** (Leadbetter 1983):

*If the expected number of exceedances $V(A)$ in a time interval $(0,1)$ over the region $A = \{(0,1) \times [u_n, \infty)\}$ converge into a Poisson variable with mean $V(A) = V\left(x^{(r)};\theta\right) = \left[1+\xi\left(\frac{x^{(r)}-\mu}{\sigma}\right)\right]^{-1/\xi} = \left[1+\xi\left(\frac{u_n-\mu}{\sigma}\right)\right]^{-1/\xi}$, $\theta = (\mu,\sigma,\xi)$, then*

$$Pr\left[\frac{M_n^{(r)}-b_n}{a_n} \leq u_n\right] \to F_r(u_n), \quad (H.6)$$

*for a linear renormalization of the random variables with*

$F_r(u_n) = exp\{-V(A)\}\sum_{s=0}^{r-1}\frac{V(A)^s}{s!}$, *where $s$ denotes the number of $(X_1, X_2, \ldots, X_n)$ exceeding $u_n$.*

The latter stated Theorem H.2 gives information for the approximate distribution of each of the elements of $M_n^{(r)}$ in Equation (H.6), but does not guarantee the independency over the components of $M_n^{(r)}$, and does not formulate the full joint distribution of the $M_n^{(r)}$ exceedances.

Therefore, Tawn (1988) attempted a formulation of the limiting joint Generalized Extreme Value distribution for the r largest order statistics. The formulation therein suggested that from a sample of independent and identically distributed random variables exceeding of a level $u_n$ and a fixed $r$ value, the limiting joint distribution function for the $r$ largest order statistics considering $x^{(1)} \geq x^{(2)} \geq \cdots \geq x^{(i)} \geq \cdots \geq x^{(r)}$ with $x^{(r)} = u_n$ is:

$$\Pr\left\{\frac{X^{(1)}-b_n}{a_n}<x^{(1)},\frac{X^{(2)}-b_n}{a_n}<x^{(2)},\ldots,\frac{X^{(i)}-b_n}{a_n}<x^{(i)},\ldots,\frac{X^{(r)}-b_n}{a_n}<x^{(r)}\right\}$$

$$\rightarrow\sum_{s_1=0}^{1}\sum_{s_2=0}^{2-s_1}\cdots\sum_{s_{r-1}=0}^{r-1-s_1-\cdots-s_{r-2}}\frac{\left(V(x^{(2)};\theta)-V(x^{(1)};\theta)\right)^{s_1}}{s_1!}\cdots\frac{\left(V(x^{(r)};\theta)-V(x^{(r-1)};\theta)\right)^{s_{r-1}}}{s_{r-1}!}\exp\left(-V(x^{(r)};\theta)\right).$$

$$(H.7)$$

The limiting joint density of the $r$ largest order statistics is found to be:

$$f(x^{(1)},\ldots,x^{(r)};\mu,\sigma,\xi)=$$

$$\sigma^{-r}\exp\left\{-\left(1+\xi\left(\frac{x^{(r)}-\mu}{\sigma}\right)\right)^{-1/\xi}-(1+1/\xi)\sum_{j=1}^{r}\log\left(1+\xi\left(\frac{x^{(j)}-\mu}{\sigma}\right)\right)\right\}$$

$$(H.8)$$

where $1+\xi\left(\frac{x^{(j)}-\mu}{\sigma}\right)>0$ for $j=1,2,\ldots,r$.

## H.2 Statistical modeling of the r-largest Order Maxima

The likelihood of a non-homogeneous Poisson process for extremes is derived when all of the available data are grouped into $m$ blocks, selecting the $r^{th}$ largest ordered maxima in each block. It is usually to set equal $r^{th}$ largest number of maxima over all blocks as $r^{th}_{block1}=r^{th}_{block2}=\ldots=r^{th}_{block\ m}=r$. The optimum selection of the $r^{th}$ value is crucial due to the bias-variance trade-off effect ([10]). Assuming that data from separated blocks are independent, then the product of these joint densities is the appropriate joint density for the set of whole observations.

The general form of the non-homogeneous Poisson process likelihood for the $r^{th}$ largest ordered maxima that exceed over a high threshold level $u_n$, over all available $m$ blocks, is defined as follows:

$$L_{\{[t_1,t_2]\times(u_n,\infty),(m\ blocks)\}}\left(x^{(1)}_{block},\ldots,x^{(r)}_{block};\xi,\sigma,\mu\right)=$$

$$=\prod_{block=1}^{m}\left(\exp\left[-(t_2-t_1)\left[1+\xi\left(\frac{u_{n(block)}-\mu}{\sigma}\right)\right]^{-1/\xi}\right]\prod_{i=1}^{r}\left(\frac{1}{\sigma}\left[1+\xi\left(\frac{x^{(i)}_{block}-\mu}{\sigma}\right)\right]^{-1/\xi-1}\right)\right),$$

$$(H.9)$$

where $-\infty<\mu<\infty,\quad\sigma>0,\quad-\infty<\xi<\infty$. In addition,

$$\begin{cases}x^{(1)}_{block=1}\ge x^{(2)}_{block=1}\ge\ldots\ge x^{(i)}_{block=1}\ge\ldots\ge x^{(r)}_{block=1}=u_{n(block=1)}\\ x^{(1)}_{block=2}\ge x^{(2)}_{block=2}\ge\ldots\ge x^{(i)}_{block=2}\ge\ldots\ge x^{(r)}_{block=2}=u_{n(block=2)}\\ \ldots\ldots\ldots\ldots\ldots\ldots\ldots\ldots\ldots\ldots\ldots\ldots\ldots\ldots\ldots\ldots\ldots\ldots\ldots\ldots\ldots\\ x^{(1)}_{block=m}\ge x^{(2)}_{block=m}\ge\ldots\ge x^{(i)}_{block=m}\ge\ldots\ge x^{(r)}_{block=m}=u_{n(block=m)}\end{cases}$$

---

([10]) Small $r$ values will generate few data leading to a high variance. On the contrary, large values of $r$ leads to high bias.

provided $1 + \xi \left( x_{block}^{(i)} - \mu \right)/\sigma > 0$ for $i = 1,2,3,\ldots,r$.

When $\xi = 0$ the following form of the likelihood is considered:

$$L_{\{[t_1,t_2]\times(u_n,\infty),(m\ blocks)\}}\left( x_{block}^{(1)},\ldots,x_{block}^{(r)};\xi = 0,\sigma,\mu \right)=$$

$$=\prod_{block=1}^{m}\left( \exp\left[ -\exp\left( -(t_2 - t_1)\left( \frac{u_{n_{(block)}}-\mu}{\sigma} \right) \right) \right]\prod_{i=1}^{r}\left( \frac{1}{\sigma}\exp\left[ -\left( \frac{x_{block}^{(i)}-\mu}{\sigma} \right) \right] \right) \right). \qquad (H.10)$$

Special case $r = 1$ for each block in Equations (H.9) and (H.10), reduces to the likelihood family of GEV for BM. The $r^{th}$ largest order statistic model gives a likelihood whose parameters correspond to those of the GEV of BM, but uses more information from the data.

The corresponding log likelihood of the above expressions can be maximized numerically in order to obtain maximum likelihood estimates. The log likelihood is therefore:

$$l\left( x_{block}^{(1)},\ldots,x_{block}^{(r)};\mu,\sigma,\xi \right)=$$

$$-r\ln\sigma - m_{years}\left[ 1 + \xi\left( \frac{u_{n_{(block)}}-\mu}{\sigma} \right) \right]^{-1/\xi} - (1/\xi + 1)\sum_{i=1}^{r}\ln\left[ 1 + \xi\left( \frac{x_{block}^{(i)}-\mu}{\sigma} \right) \right], \qquad (H.11)$$

where $m_{years}$ denotes the number of years of observation.

## I.     Additional diagnostics

Additional diagnostics are presented for the four locations (L5, L10, L18, and L30) using the low resolution ERA-20C and ERA-Interim in sub-Section 6.4. Statistical estimates of DeCA and the proposed resampling strategy DeCAUn are outlined for the four locations, yielding AIC and MSE statistic measures, optima DEP values and the associated re-sampling factor $k$ −th lag from the Similarity function in Table I.1. For each sample period we also include the number of cluster maxima, threshold values and number of exceedances fitting the GPD. The four sample periods of the ERA-20C and the ERA-Interim are set from 1961 to 1985 and from 1979 to 2003 with a 5 years step forward respectively to each data product.

Table I.1: Model estimations for the DeCA and DeCAUn model using the ERA-20C and ERA-Interim database

| Ny | | | L5 DeCA | L5 DeCAUn | L10 DeCA | L10 DeCAUn | L18 DeCA | L18 DeCAUn | L30 DeCA | L30 DeCAUn |
|---|---|---|---|---|---|---|---|---|---|---|
| 10 Years | | Lowest AIC-MSE | MSE 8.660 | Un.1 MSE 8.650 | MSE 9.220 | Un.2 MSE 9.560 | MSE 8.140 | Un.1 MSE 16.490 | AIC 194.832 | Un.1 MSE 47.450 |
| | | DEP | 60% | 80% | 80% | 60% | 65% | 70% | 95% | 65% |
| | | Similarity (lag) | | 1 | | 1 | | 3 | | 5 |
| | | No. of clusters | 480 | 343 | 339 | 535 | 145 | 43 | 83 | 41 |
| | | u (m/sec) | 11.214 mode | 11.577 median | 13.712 mode | 13.233 mode | 16.248 mode | 13.669 25% | 11.786 mode | 0 |
| | | No. of Thres. exceedances | 252 | 170 | 169 | 264 | 62 | 32 | 45 | 41 |
| 15 Years | | Lowest AIC-MSE | AIC 810.727 | Un.1 MSE 38.670 | MSE 11.210 | Un.1 MSE 11.550 | MSE 9.580 | Un.1 MSE 10.990 | AIC 338.440 | Un.1 MSE 45.080 |
| | | DEP | 95% | 80% | 60% | 60% | 75% | 60% | 95% | 65% |
| | | Similarity (lag) | | 9 | | 1 | | 3 | | 5 |
| | | No. of clusters | 358 | 67 | 973 | 973 | 169 | 82 | 134 | 61 |
| | | u (m/sec) | 11.560 mode | 0 | 11.673 mode | 11.462 25% | 16.266 mode | 16.212 median | 11.514 mode | 0 |
| | | No. of Thres. exceedances | 206 | 67 | 688 | 727 | 83 | 41 | 80 | 61 |
| 20 Years | | Lowest AIC-MSE | AIC 1342.320 | Un.2 AIC 186.464 | MSE 9.420 | Un.1 MSE 8.850 | AIC 307.004 | Un.1 MSE 15.710 | MSE 10.670 | Un.1 MSE 46.690 |
| | | DEP | 95% | 60% | 80% | 60% | 90% | 75% | 85% | 65% |
| | | Similarity (lag) | | 12 | | 1 | | 3 | | 5 |
| | | No. of clusters | 533 | 84 | 933 | 1432 | 130 | 73 | 238 | 79 |
| | | u (m/sec) | 11.267 mode | 14.814 mode | 13.169 mode | 12.992 median | 16.366 mode | 13.630 25% | 10.954 mode | 0 |
| | | No. of Thres. exceedances | 347 | 52 | 508 | 713 | 71 | 54 | 148 | 79 |
| 25 Years | | Lowest AIC-MSE | MSE 7.500 | Un.2 AIC 217.820 | AIC 1779.529 | AIC | AIC 327.028 | Un.2 MSE 7.960 | MSE 8.060 | Un.2 AIC 245.641 |
| | | DEP | 60% | 80% | 95% | 95% | 95% | 70% | 90% | 60% |
| | | Similarity (lag) | | 7 | | 2 | | 3 | | 6 |
| | | No. of clusters | 1750 | 138 | 649 | 325 | 144 | 88 | 251 | 74 |
| | | u (m/sec) | 10.961 mode | 15.477 mode | 12.871 mode | 12.983 mode | 16.108 mode | 18.192 mean | 13.053 mode | 11.073 mode |
| | | No. of Thres. exceedances | 1035 | 66 | 423 | 211 | 74 | 44 | 100 | 53 |

Parameter model estimates are presented in Table I.2 as a demonstration of the standard MLE estimator to the asymptotic distributions of extremes in samples of different size for only one location (54.00 N 2.25 E in the North Sea corresponding to location L18 from the ERA-Interim database). Location L18 is also used for the threshold selection of the Runs model presented in Figure 3.3 for the 20 year time series (from 1979 to 1998). The 95% confidence intervals of the estimated parameters of the GEV and GPD distributions at each sample period (10,15,20, and 25 years) are derived by two methods using normal and non-parametric bootstrap approximations as previously discussed in sub-Section 2.4. The nonparametric bootstrap estimator is considered to be more robust relative to the parametric, when sampling uncertainties appear in relation to probabilities (return periods) and high quantiles (design/return values) of extreme climatological and hydrological events (see Kyselý, 2008).

Table I.2: Parameter estimation for location L18. CI are denoted in italics

| Ny | Model | Normal approximation | | | Nonparametric Bootstrap (Percentile) | | | p-value MK-test |
|---|---|---|---|---|---|---|---|---|
| | | μ | σ | ξ | μ | σ | ξ | |
| 10 Years | BM Ref. (GEV) | 21.202 | 1.604 | -0.077 | | | | 0.365 |
| | | *20.630* | *1.197* | *-0.306* | | | | |
| | | *21.775* | *2.010* | *0.152* | | | | |
| | BM (GEV) | 20.234 | 0.398 | 4.395 | 20.234 | 0.398 | 4.395 | 0.721 |
| | | *20.234* | *0.398* | *4.387* | *20.181* | *0.155* | *-1.564* | |
| | | *20.234* | *0.398* | *4.403* | *23.848* | *4.278* | *5.756* | |
| | Runs (GPD) | | 1.977 | 8.81E-08 | | 1.977 | 8.81E-08 | 0.392 |
| | | | *1.211* | *-0.294* | | *1.384* | *-0.304* | |
| | | | *2.744* | *0.294* | | *3.006* | *0.237* | |
| | DeCA (GPD) | | 3.371 | -0.233 | | 3.371 | -0.233 | |
| | | | *2.303* | *-0.437* | | *2.596* | *-0.543* | |
| | | | *4.438* | *-0.029* | | *4.623* | *-0.096* | |
| | DeCAUn.1 (GPD) | | 5.824 | -0.375 | | 5.824 | -0.375 | 0.983 |
| | | | *3.258* | *-0.677* | | *4.217* | *-1.172* | |
| | | | *8.391* | *-0.073* | | *9.928* | *-0.205* | |
| 15 Years | BM (GEV) | 21.516 | 1.932 | -0.190 | 21.516 | 1.932 | -0.190 | 0.767 |
| | | *20.391* | *1.109* | *-0.636* | *20.205* | *0.507* | *-1.236* | |
| | | *22.641* | *2.755* | *0.256* | *23.215* | *3.571* | *5.337* | |
| | Runs (GPD) | | 3.615 | -0.254 | | 3.615 | -0.254 | 0.683 |
| | | | *2.854* | *-0.388* | | *2.975* | *-0.456* | |
| | | | *4.376* | *-0.121* | | *4.563* | *-0.129* | |
| | DeCA (GPD) | | 3.540 | -0.266 | | 3.540 | -0.266 | |
| | | | *2.567* | *-0.447* | | *2.687* | *-0.521* | |
| | | | *4.514* | *-0.085* | | *4.718* | *-0.112* | |
| | DeCAUn.1 (GPD) | | 3.942 | -0.283 | | 3.942 | -0.283 | 0.898 |
| | | | *2.343* | *-0.563* | | *2.719* | *-0.775* | |
| | | | *5.541* | *-0.003* | | *6.533* | *-0.011* | |
| 20 Years | BM (GEV) | 21.406 | 1.769 | -0.042 | 21.406 | 1.769 | -0.042 | 0.626 |
| | | *20.520* | *1.125* | *-0.409* | *20.504* | *0.800* | *-0.551* | |
| | | *22.293* | *2.413* | *0.324* | *22.475* | *2.637* | *1.084* | |
| | Runs (GPD) | | 3.376 | -0.245 | | 3.376 | -0.245 | 0.656 |
| | | | *2.598* | *-0.389* | | *2.724* | *-0.474* | |
| | | | *4.153* | *-0.101* | | *4.156* | *-0.130* | |
| | DeCA (GPD) | | 4.389 | -0.345 | | 4.389 | -0.345 | |
| | | | *3.119* | *-0.535* | | *3.364* | *-0.633* | |
| | | | *5.658* | *-0.155* | | *5.838* | *-0.203* | |
| | DeCAUn.1 (GPD) | | 6.196 | -0.427 | | 6.196 | -0.427 | 0.764 |
| | | | *4.363* | *-0.598* | | *5.112* | *-1.090* | |
| | | | *8.030* | *-0.256* | | *10.235* | *-0.325* | |
| 25 Years | BM (GEV) | 21.371 | 1.576 | -0.031 | 21.371 | 1.576 | -0.031 | 0.469 |
| | | *20.682* | *1.087* | *-0.302* | *20.684* | *0.849* | *-0.341* | |
| | | *22.059* | *2.065* | *0.241* | *22.133* | *2.162* | *0.519* | |
| | Runs (GPD) | | 3.388 | -0.253 | | 3.388 | -0.253 | 0.892 |
| | | | *2.679* | *-0.382* | | *2.825* | *-0.490* | |
| | | | *4.097* | *-0.124* | | *4.102* | *-0.151* | |
| | DeCA (GPD) | | 4.774 | -0.381 | | 4.774 | -0.381 | |
| | | | *3.435* | *-0.566* | | *3.589* | *-0.649* | |
| | | | *6.114* | *-0.195* | | *6.352* | *-0.217* | |
| | DeCAUn.2 (GPD) | | 3.653 | -0.324 | | 3.653 | -0.324 | 0.291 |
| | | | *2.245* | *-0.589* | | *2.456* | *-0.701* | |
| | | | *5.060* | *-0.059* | | *5.377* | *-0.133* | |

Regarding the four locations, the estimated threshold values for the standard Runs model is obtained from the NC-diagnostics in Table I.3, with the corresponding p-values associated to the Score test. The threshold exceedances are considered as the peak De-clustered values from the Runs model. The GPD fit of daily max wind speeds, was performed for threshold values in a range from 11.2 to 18.6 m/s, or 91% to 98% sample quantiles, yielding total number of peak exceedances between 52 and 177.

Table I.3: Threshold model diagnostics for the Runs model using the ERA-20C and ERA-Interim database

| Ny | | L5 | L10 | L18 | L30 |
|---|---|---|---|---|---|
| **10 Years** | p-value (Score test) | 0.458 | 0.984 | 0.995 | 0.213 |
| | u (m/sec) | 13.267 | 16.344 | 17.474 | 12.207 |
| | u (quantile) | 92% | 95% | 97% | 94% |
| | No. of Peak exceedances | 65 | 64 | 56 | 52 |
| **15 Years** | p-value (Score test) | 0.187 | 0.750 | 0.683 | 0.732 |
| | u (m/sec) | 13.544 | 15.775 | 15.294 | 11.202 |
| | u (quantile) | 93% | 93% | 91% | 91% |
| | No. of Peak exceedances | 105 | 116 | 136 | 113 |
| **20 Years** | p-value (Score test) | 0.594 | 0.468 | 0.734 | 0.792 |
| | u (m/sec) | 14.097 | 15.338 | 16.590 | 11.499 |
| | u (quantile) | 95% | 91% | 95% | 92% |
| | No. of Peak exceedances | 114 | 177 | 112 | 138 |
| **25 Years** | p-value (Score test) | 0.962 | 0.463 | 0.801 | 0.718 |
| | u (m/sec) | 14.094 | 18.565 | 16.544 | 11.480 |
| | u (quantile) | 95% | 98% | 95% | 92% |
| | No. of Peak exceedances | 141 | 92 | 132 | 161 |

# References

1. 11th international conference on Extreme Value Analysis, at Faculty of Science, Univeristy of Zagreb, Croatia, 1-5 July 2019,

2. Abild, J., E. Y.Andersen, and D. Rosbjerg, 1992: The climate of extreme winds at the Great Belt of Denmark. J. Wind Eng.Ind.Aerodyn., 41-44,521-532.

3. Abramowitz, M. and Stegun, I. A. 1972. (Eds.). "Kelvin Functions." §9.9 in Handbook of Mathematical Functions with Formulas, Graphs, and Mathematical Tables, 9th printing. New York: Dover, pp. 379-381.

4. Agarwal, A., Venugopal, V., Harrison, G.P., 2013. The assessment of extreme wave analysis methods applied to potential marine energy sites using numerical model data. Renewable and Sustainable Energy Reviews 27, 244-257.

5. Akaike, Hirotugu, 1973. "Information Theory as an Extension of the Maximum Likelihood Principle." Pp. 267-281 in Second International Symposium on Information Theory, edited by B. N. Petrov and F. Csaki . Budapest: Akademiai Kiado.

6. Alexander, L.V., S.F.B. Tett and T Jonsson, 2005: Recent observed changes in severe storms over the United Kingdom and Iceland. Geophys. Res. Lett., 32, L13704, doi:10.1029/2005GL022371.

7. Alexandersson H, Tuomenvirta H, Schmith T, Iden K, 2000. Trends of storms in NW Europe derived from an updated pressure data set. Clim Res 14:71–73

8. Ali, S., Lee, S.-M., Jang, C.-M., 2017. Techno-Economic Assessment of Wind Energy Potential at Three Locations in South Korea Using Long-Term Measured Wind Data. Energies 10 (9), 1442.

9. Alves, J. H. G. M., and I. R. Young, 2003: On estimating extreme wave heights using combined Geosat, TOPEX/Poseidon and ERS-1 altimeter data. Appl. Ocean Res., 25, 167–186, https://doi.org/10.1016/j.apor.2004.01.002.

10. Amberg Brian, 2008. A range of different kernels in Python, CC BY-SA 3.0 <https://creativecommons.org/licenses/by-sa/3.0>, via Wikimedia Commons https://commons.wikimedia.org/wiki/File:Kernels.svg

11. An, Y., Pandey, M.D., 2005. A comparison of methods of extreme wind speed estimation. Journal of Wind Engineering and Industrial Aerodynamics 93 (7), 535-545.

12. An, Y., Pandey, M.D., 2007. The r largest order statistics model for extreme wind speed estimation. Journal of Wind Engineering and Industrial Aerodynamics95(3): 165-182. https://doi.org/10.1016/j.jweia.2006.05.008.

13. Anastasiades, G, McSharry, PE, 2014. Extreme value analysis for estimating 50 year return wind speeds from reanalysis data. J Wind Energ. 17(8): 1231-1245, http://dx.doi.org/10.1002/we.1630

14. Ancona-Navarrete, M.A. & Tawn, J.A., 2000. A comparison of methods for estimating the extremal index, Extremes, 3, 5–38.

15. Arnell NW, Beran M, Hosking JRM, 1986. Unbiased plotting positions for the general extreme value distribution. J Hydrol. 86: 59–69.

16. Arns A, Wahl T, Haigh ID, Jensen J, Pattiaratchi C, 2013. Estimating extreme water level probabilities: A comparison of the direct methods and recommendations for best practice. J Coastal Engineering 81:51–66.

17. Ashkar, F., Tatsambon, C.N., 2007. Revisiting some estimation methods for the generalized Pareto distribution. J. Hydrol. 346, 136–143.

18. Ashoori, F., Ebrahimpour, M., Bozorgnia, A., 2017. Modeling of maximum precipitation using maximal generalized extreme value distribution. Communications in Statistics - Theory and Methods 46 (6), 3025-3033.

19. Athanassoulis GA, Soukissian TH, Stefanakos ChN., 1995. Long-term variability and its impact to the extreme-value prediction from time series of significant wave height. In Fourth International Workshop on Wave Hindcasting and Forecasting: Climate Variability and Extremes, Swail VR (ed.). Atmospheric Environment Service: Banff, Alberta, Canada; 343–358.

20. Auld, G., Papastathopoulos, I., 2021. Extremal clustering in non-stationary random sequences, Extremes. https://doi.org/10.1007/s10687-021-00418-2

21. Babu, G.J., Feigelson, E.D., 1996. Astrostatistics. Taylor & Francis.

22. Babu, P., Stoica, P., 2010. Spectral analysis of nonuniformly sampled data – a review. Digital Signal Processing 20 (2), 359-378.

23. Balkema, A., and de Haan, L., 1974. "Residual life time at great age", Annals of Probability, 2, 792–804.

24. Barning, F. J. M. 1963. The numerical analysis of the light-curve of 12 Lacertae, Bulletin of the Astronomical Institutes of the Netherlands

25. Bartlett, M.S., 1946. On the Theoretical Specification and Sampling Properties of Autocorrelated Time-Series. Journal of the Royal Statistical Society Series B-Statistical Methodology 8 (1), 27-41.

26. Bauwens, L. and P. Giot, 2001. Econometric Modeling of Stock Market Intraday Activity, Advanced Studies in Theoretical and Applied Econometrics, Kluwer Academic Publishers: Dordrecht, 196 pages.

27. Bean S, Tsokos CP, 1980. Developments in nonparametric density estimation. Int Stat Rev 48(3):267–287

28. Befort D, Wild S, Kruschke T, Ulbrich U and Leckebusch G., 2016. Different long-term trends of extra-tropical cyclones and windstorms in ERA-20C and NOAA-20CR reanalyses Atmos. Sci. Lett. 17 586–95

29. Befort, D. & Peter, Madlen & Leckebusch, G.C. & Ulbrich, U. & Ganske, Anette & Rosenhagen, G. & Heinrich, Hartmut, 2014. Identification of storm surge events over the German Bight from atmospheric reanalysis and climate model data. Natural Hazards and Earth System Sciences Discussions. 2. 3935-3963. 10.5194/nhessd-2-3935-2014.

30. Begueria, S., M. Angulo-Martinez, S. M. Vicente-Serrano, J. I. Lopez-Moreno, and A. El-Kenawy, 2011. Assessing trends in extreme precipitation events intensity and magnitude using non-stationary peaks-over-threshold analysis: A case study in northeast Spain from 1930 to 2006, Int. J. Climatol., 31, 2102–2114, doi:10.1002/joc.2218.

31. Beirlant, J., Goegebeur, Y., Segers, J., Teugels, J., De Waal, D., Ferro, C., 2004. Statistics of Extremes: Theory and Applications. John Wiley & Sons, Hoboken.

32. Bendat, J. S., and Piersol, A. G., 1993. Engineering Applications of Correlation and Spectral Analysis, 2nd ed. Wiley-Interscience, New York.

33. Benedict, L.H., Nobach, H., Tropea, C., 2000. Estimation of turbulent velocity spectra from laser Doppler data. Measurement Science and Technology 11 (8), 1089-1104.

34. Bengtsson, L., Hodges, K. I. and Roeckner, E. 2006. Storm tracks and climate change. J. Clim. 19, 3518–3543.

35. Bernardara, P., Mazas, F., Kergadallan, X., Hamm, L., 2014. A two-step framework for over- threshold modelling of environmental extremes. Nat. Hazards Earth Syst. Sci. 14,635–647.

36. Bitner-Gregersen EM, Ewans KC, Johnson MC, 2014. Some uncertainties associated with wind and wave description and their importance for engineering applications. J Ocean Engineering 86:11-25.

37. Bitner-Gregersen, E.M., 2015. Joint met-ocean description for design and operations of marine structures. Applied Ocean Research 51, 279-292.

38. Bjornstad, O.N., Falck, W., 2001. Nonparametric spatial covariance functions: Estimation and testing. Environmental and Ecological Statistics 8 (1), 53-70, doi:10.1023/A:1009601932481.

39. Bommier, E., 2014. Peaks-over-threshold modelling of environmental data (Technical report). U.U.D.M. Project Report 2014:33.

40. Bonazzi, A., Cusack, S., Mitas, C., and Jewson, S., 2012. The spatial structure of European windstorms as characterized by bivariate extreme-value Copulas, Nat. Hazards Earth Syst. Sci.,12, 1769–1782, doi:10.5194/nhess-12-1769-2012.

41. Bowman, A., 1984. An alternative method of cross-validation for the smoothing of density estimates. Biometrika 71 353–360.

42. Brabson, B.B., Palutikof, J.P., 2000. Tests of the generalized pareto distribution for predicting extreme wind speeds. Journal of Applied Meteorology 39 (9), 1627-1640.

43. Bracewell, R.N., 2000. The Fourier Transform and Its Applications. 3rd Ed., McGraw-Hill, Boston, Mass., USA.

44. Broersen, P.M.T., 2009. Five Separate Bias Contributions in Time Series Models for Equidistantly Resampled Irregular Data. Ieee Transactions on Instrumentation and Measurement 58 (5), 1370-1379.

45. Broersen, P.M.T., S. de Waele and R. Bos, 2004a. Application of autoregressive spectral analysis to missing data problems. IEEE Trans. On Instrument. And Measurement, 53, pp. 981-986.

46. Broersen, P.M.T., S. de Waele and R. Bos, 2004b. Autoregressive spectral analysis when observations are missing. Automatica, 40, pp. 1495-1504.

47. Bronshtein I.N. and Semendyayev K.A. Handbook of Mathematics. (Springer, 1985).

48. Brunetti M, Buffoni L, Mangianti F, Maugeri M, Nanni T. 2004. Temperature, precipitation and extreme events during the last century in Italy. Global and Planetary Change 40(1–2): 141–149.

49. Burnham, Kenneth P. and David R. Anderson . 2002. Model Selection and Multimodel Inference: A Practical Information-Theoretical Approach. 2d ed. New York: Springer-Verlag.

50. Butler, A., Heffernan, J. E., Tawn, J. A., Flather, R. A., 2007. Trend estimation in extremes of syntheticNorth Sea surges. J. Roy. Statist. Soc. C 56, 395–414.

51. Cai, Y.Z., Hames, D., 2011. Minimum Sample Size Determination for Generalized Extreme Value Distribution. Communications in Statistics-Simulation and Computation 40 (1), 99-110.

52. Caires S, Sterl A, 2005. 100-Year Return Value Estimates for Ocean Wind Speed and Significant Wave Height from the ERA-40 Data. J of Climate 18:1032–1048.

53. Caires, S., 2016. A comparative simulation study of the annual maxima and the peaks-over-threshold methods. Journal of Offshore Mechanics and Arctic Engineering 138 (5).

54. Cannon, A.J., 2010. A flexible nonlinear modeling framework for nonstationary generalized extreme value analysis in hydroclimatology. Hydrological Process, v.24, p.673-685,. Available from:

<http://www.eos.ubc.ca/~acannon/GEVcdn/GEVcdn-paper.pdf>. Accessed: Jan 12, 2011. doi: 10.1002/hyp.7506.

55. Cannon, D.J., Brayshaw, D.J., Methven, J., Coker, P.J., Lenaghan, D., 2015. Using reanalysis data to quantify extreme wind power generation statistics: A 33 year case study in Great Britain. Renewable Energy 75, 767-778.

56. Carnell RE, Senior CA, Mitchell JFB, 1996. Assessment og measures of storminess: simulated changes in northern hemisphere winter due to increased CO2, Clim. Dyn., 12, 467-476

57. Casella G, Berger RL, 2002. Statistical Inference. 2nd edition, Duxbury: USA;.

58. Castillo E, Hadi AS, 1994. Parameter and quantile estimation for the generalized extreme-value distribution. J Environmetrics 5: 417-432.

59. Castillo E, Hadi AS, Balakrishnan N and Sarabia JM, 2005. Extreme Value and Related Models with Applications in Engineering and Science. John Wiley and Sons, Hoboken NJ.

60. Castillo Joan del, Daoudi Jalila, 2009. Estimation of generalized Pareto distribution. Statistics and Probability Letters, Elsevier, 79 (5), pp.684. 10.1016/j.spl.2008.10.021. hal-00508918

61. Castillo, E, Sarabia, JM, Hadi, AS, 1997. Fitting continuous bivariate distributions to data. Journal of the Royal Statistical Society, Ser. D 46:355-369.

62. Castillo, E. and Hadi, A., 1997. Fitting the Generalized Pareto Distribution to Data. Journal of the American Statistical Association, 92,1609-1620.

63. Castillo, E., Hadi, A.S., 1995a. A Method for Estimating Parameters and Quantiles of Distributions of Continuous Random-Variables. Computational Statistics & Data Analysis 20 (4), 421-439.

64. Castillo, E., Hadi, A.S., 1995b. Modeling Lifetime Data with Application to Fatigue Models. Journal of the American Statistical Association 90 (431), 1041-1054.

65. Ceppi, P., Della-Marta, P. M., and Appenzeller, C., 2008. Extreme Value Analysis of Wind Speed Observations over Switzerland, Arbeitsberichte der MeteoSchweiz, 219, 43 pp.

66. Chatfield, C., 1996. The Analysis of Time Series: An Introduction, Sixth Edition. Taylor & Francis.

67. Chavez-Demoulin, V., & Davison, A. C., 2012. Modelling time series extremes. REVSTAT - Statistical Journal, 10(1), 109+.

68. Chen, G., Bi, S.W., Ezraty, R., 2004. Global structure of extreme wind and wave climate derived from TOPEX altimeter data. International Journal of Remote Sensing 25 (5), 1005-1018.

69. Chen, Huey-Long & Rao, A.., 2002. Testing Hydrologic Time Series for Stationarity. Journal of Hydrologic Engineering - J HYDROL ENG. 7. 10.1061/(ASCE)1084-0699(2002)7:2(129).

70. Chen, X., Huang, G., 2010. Estimation of probabilistic extreme wind load effects: Combination of aerodynamic and wind climate data. Journal of Engineering Mechanics 136 (6), 747-760.

71. Cheng E, Yeung C, 2002. Generalized extreme gust wind speeds distribution. J Wind Eng Ind Aerodyn 90:1657–1669.

72. Cheng, L., AghaKouchak, A., Gilleland, E., Katz, R.W., 2014. Non-stationary extreme value analysis in a changing climate. Climatic Change 127 (2), 353–369.

73. Cheng, R.C.H., Amin, N.A.K., 1983. Estimating Parameters in Continuous Univariate Distributions with a Shifted Origin. Journal of the Royal Statistical Society Series B-Methodological 45 (3), 394-403.

74. Chiodo, E., Mazzanti, G., Karimian, M., Zoh, R., 2015. Comparison of two different estimation methods of wind speed extreme values, 5th International Conference on Clean Electrical Power: Renewable Energy Resources Impact, ICCEP 2015, pp. 653-659.

75. Coles S, Pericchi L, Sisson S, 2003. A Fully Probabilistic Approach to Extreme Value Modelling. Journal of Hydrology, 273, 35–50. doi:10.1016/s0022-1694(02)00353-0.

76. Coles, S., 2001. An Introduction to Statistical Modeling of Extreme Values. Springer-Verlag London.

77. Coles, S., and E. Simiu, 2003: Estimating uncertainty in the extreme value analysis of data generated by a hurricane simulation model. J. Eng. Mech., 129 (11), 1288-1294.

78. Coles, S.G. and Pericchi, L., 2003. Anticipating catastrophes through extreme value modelling, Appl. Stat. 25: 405-416.

79. Coles, S.G., Dixon, M.J., 1999. Likelihood-Based Inference for Extreme Value Models. Extremes 2 (1), 5-23.

80. Coles, S.G., Walshaw, D., 1994. Directional Modeling of Extreme Wind Speeds. Journal of the Royal Statistical Society Series C-Applied Statistics 43 (1), 139-157.

81. Cook N.J., 1982. Towards better estimation of extreme winds, J. Wind Eng. Ind. Aerodyn. 9 295-323.

82. Cook N.J., 1985. The designer's guide to wind loading of building structures. Part 1: Background, damage survey, wind data and structural classification. Butterworths.

83. Cooley, D., 2009. Extreme value analysis and the study of climate change. Climatic Change 97 (1-2), 77-83.

84. Cortesi, N., Torralba, V., González-Reviriego, N. et al., 2019. Characterization of European wind speed variability using weather regimes. Clim Dyn 53, 4961–4976. https://doi.org/10.1007/s00382-019-04839-5

85. Cox, D. R. and Stuart, A., 1955. Some quick sign test for trend in location and dispersion, Biometrika, 42, 80-95

86. Cumming A, Marcy G, Butler R, 1999. The Lick Planet Search: Detectability and Mass Thresholds. The Astrophysical Journal, 526(2), 890–915. doi:10.1086/308020.

87. Cunderlik, J.M. and D.H. Burn., 2003. "Non- Stationary Pooled Flood Frequency Analysis." Journal of Hydrology, 276: 210-223.

88. Cunderlik, J.M., Burn, D.H., 2002. Local and Regional Trends in Monthly Maximum Flows in Southern British Columbia. Canadian Water Resources Journal / Revue canadienne des ressources hydriques 27 (2), 191-212.

89. Cunnane C., 1978. Unbiased plotting positions - a review. J Hydrol. 37: 205-222.

90. Cunnane, C., 1973. A particular comparison of annual maxima andpartial duration series methods of flood frequency prediction. J.Hydrol. 18, 257–271.

91. Cunnane, C., 1979: A note on the Poisson assumption in partial duration series models, Water Resour. Res., 15, 489–494.

92. Daley, D. J. and Vere-Jones, D., 2008. An Introduction to the Theory of Point Pro- cesses, Volume II: General Theory and Structure. 2 edition. Springer.

93. Damaschke, N., Kühn, V., Nobach, H., 2018. A fair review of non-parametric bias-free autocorrelation and spectral methods for randomly sampled data in laser Doppler velocimetry. Digital Signal Processing 76, 22-33.

94. Davison, A.C. and Hinkley, D.V., 1997. Bootstrap Methods and Their Application. Cambridge University Press.

95. Davison, A.C., Smith, R.L., 1990. Models for Exceedances over High Thresholds. Journal of the Royal Statistical Society Series B-Methodological 52 (3), 393-442 (with discussion)

96. de Haan, L. and Ferreira, A., 2006. Extreme Value Theory: An Introduction. New York: Springer.

97. de Oliveira MMF, Ebecken NFF, de Oliveira JLF, Gilleland E., 2011. Generalized extreme wind speed distributions in South America over the Atlantic Ocean region. J Theor Appl Climatol 104:377–385.

98. de Oliveira, T., 1963. Estatística de Densidades; ResultadosAssintóticos. Revista da Faculdade de Ciências de Lisboa 2 (A, IX), 111-206.

99. de Winter R C, Sterl A and Ruessink B G, 2013. Wind extremes in the North Sea basin under climate change: an ensemble study of 12 CMIP5 GCMs J. Geophys. Res.1181601–12

100. Dee, D.P., et al., 2011. The ERA-Interim Reanalysis: Configuration and Performance of the Data Assimilation System. Quarterly Journal of the Royal Meteorological Society, 137, 553-597. https://doi.org/10.1002/qj.828

101. Deeming, T. J., 1975. 'Fourier Analysis with Unequally Spaced Data',Astrophys. Space Sci. 36, 137–158.

102. Della-Marta, P. M., Mathis, H., Frei, C., Liniger, M. A., and Kleinn, J., 2009. The return period of wind storms over Europe, Int. J. Climatol., 459, 437–459.

103. Deng Y, Ding Y, Li A, Zhou G., 2011. Prediction of extreme wind velocity at the site of the Runyang Suspension Bridge. J of Zhejiang University-SCIENCE A (Applied Physics & Engineering) 12(8):605-615.

104. Devis-Morales, A., Montoya-Sánchez, R.A., Bernal, G., Osorio, A.F., 2017. Assessment of extreme wind and waves in the Colombian Caribbean Sea for offshore applications. Applied Ocean Research 69, 10-26.

105. Dickey, D.A. and Fuller, W.A., 1979. Distribution of the Estimators for Autoregressive Time Series With a Unit Root. Journal of the American Statistical Association, 74(366): 427- 431.

106. Diebolt, J., Guillou, A., Naveau, P., Ribereau, P., 2008. Improving Probability-Weighted Moment Methods for the Generalized Extreme Value Distribution. Revstat-Statistical Journal 6 (1), 33-+.

107. Dixon, M. J. and Tawn, J. A., 1999. The effect of non-stationarity on extreme sea-level estimation, Appl. Statist., 48, 135-151.

108. Dodet, G., Bertin, X., Taborda, R., 2010. Wave climate variability in the North-East Atlantic Ocean over the last six decades, Ocean Modeling 31 120-131, http://dx.doi.org/10.1016/j.ocemod.2009.10.010.

109. Doksum, K.A. and G.L. Sievers, 1976. Plotting with confidence: graphical comparisons of two populations. Biometrika, 63 (3), 421–434.

110. Dukes, M.D.G., Palutikof, J.P., 1995. Estimation of Extreme Wind Speeds with Very Long Return Periods. Journal of Applied Meteorology 34 (9), 1950-1961.

111. DuMouchel, W.H., 1983. Estimating the stable index α in order to measure tail thickness: A critique, Ann. Statist., 11, 1019–1031.

112. Eastoe EF, Tawn JA., 2012. Modelling the distribution for the clustermaxima of exceedances of sub-asymptotic thresholds. Biome-trika 99(1):43–55

113. Edelson, R.A., Krolik, J.H., 1988. The discrete correlation function - A new method for analyzing unevenly sampled variability data. The Astrophysical Journal 333.

114. Efron, B. 1979. Bootstrap methods - another look at the jackknife. Annals of Statistics, 7(1), 1-26.

115. Efron, B., Tibshirani, R.J., 1994. An Introduction to the Bootstrap. Taylor & Francis.

116. Egozcue, J. J., Pawlowsky-Glahn, V., and Ortego, M. I., 2005. Wave - height hazard analysis in Eastern Coast of Spain – Bayesian ap- proach using generalized Pareto distribution, Adv. Geosci., 2, 25–30,.

117. El Adlouni, S., Ouarda, T. B. M. J., Zhang, X., Roy, R., and Bobée, B., 2007. Generalized maximum likelihood estimators for the nonstationary generalized extreme value model, Water Resour. Res., 43, W03410, doi:10.1029/2005WR004545.

118. Embrechts, P., Klüppelberg, C. & Mikosch, T., 1997. Modelling extremal events: for Insurance and Finance, Berlin, Heidelberg, Springer-Verlag.

119. Engeland, K., Hisdal, H., Frigessi, A., 2004. Practical Extreme Value Modelling of Hydrological Floods and Droughts: A Case Study. Extremes 7 (1), 5-30.

120. Engle R. F. and Russell J. R., 1998. Autoregressive Conditional Duration. A New Model for Irregularly Spaced Transaction Data, Econometrica 66, pp. 1127-1162.

121. Engle, R.F. and J.R. Russell, 2002. "Analysis of High Frequency Data," forthcoming in Handbook of Financial Econometrics, ed. by Y. Ait-Sahalia and L. P. Hansen, Elsevier Science: North-Holland.

122. Epanechnikov, V. A., 1969. "Non-Parametric Estimation of a Multivariate Probability Density". Theory Probab. Appl. 14 (1): 153–158. doi:10.1137/1114019

123. Fang, X.Q., Wang, A.Y., Fong, S.K., Lin, W.S., Liu, J., 2008. Changes of reanalysis-derived Northern Hemisphere summer warm extreme indices during 1948-2006 and links with climate variability. Global and Planetary Change 63 (1), 67-78.

124. Fawcett L, Walshaw D., 2008. Bayesian inference for clustered extremes. Extremes 11:217–233

125. Fawcett L, Walshaw D., 2012. Estimating return levels from serially dependent extremes. Environmetrics 23(3):272–283

126. Fawcett L., and Walshaw D., 2007. "Improved estimation for temporally clustered extremes", Environmetrics Vol. 18, pp. 173-188.

127. Fawcett, L. and Walshaw, D., 2006a. Markov chain models for extreme wind speeds. Environmetrics, 17: 795-809. doi:10.1002/env.794

128. Fawcett, L. and Walshaw, D., 2006b. A hierarchical model for extreme wind speeds. Journal of the Royal Statistical Society: Series C (Applied Statistics), 55: 631-646. doi:10.1111/j.1467- 9876.2006.00557.x

129. Fawcett, L., and D. Walshaw, 2015. Sea-surge and wind speed extremes: Optimal estimation strategies for planners and engineers, Stochastic Environ. Res. Risk Assess., 30, 463–480, doi:10.1007/s00477-015-1132-3.

130. Ferreira, A., 1997. Extreme Sea Level in Venice. In:Extreme Value Analysis with XTREMES (R.-D. Reiss and M. Thomas, Editors), Birkhäuser Verlag, Basel.

131. Ferreira, A., de Haan, L., 2015. On the Block Maxima Method in Extreme Value Theory: Pwm Estimators. Annals of Statistics 43 (1), 276-298.

132. Ferreira, A.; de Haan, L. & Peng, L., 2003. On optimising the estimation of high quantiles of a probability distribution, Statistics, 37, 401–434.

133. Ferro, C. A. T., A. Hannachi, and D. B. Stephenson, 2005. Simple nonparametric techniques for exploring changing probability distributions of weather. J. Climate, 18, 4344–4354.

134. Ferro, C.A.T., Segers, J., 2003. Inference for clusters of extreme values. Journal of the Royal Statistical Society Series B-Statistical Methodology 65, 545-556.

135. Fisher, R.A., Tippett, L.H.C., 1928. Limiting forms of the frequency distribution of the largest or smallest member of a sample. Proceedings of the Cambridge Philosophical Society 24, 180-190.

136. Fujino, Y., Kimura, K., Tanaka, H., 2012. Design Wind Speed, Wind Resistant Design of Bridges in Japan: Developments and Practices. Springer Japan, Tokyo, pp. 39-70.

137. Fuller, W., 1996. Introduction to Statistical Time Series, Second Edition. John Wiley, New York.

138. Galambos J., Macri N.J., 1999. Classical extreme value model and prediction of extreme winds J. Struct. Eng., 125 (7), pp. 792-794

139. Gilbert, R.O., 1987. Statistical Methods for Environmental Pollution Monitoring. Wiley.

140. Gilleland, E., Katz, R.W., 2011. New Software to Analyze How Extremes Change Over Time. Eos, Transactions American Geophysical Union 92 (2), 13--14.

141. Gilleland, E., Katz, R.W., 2016. extRemes 2.0: An Extreme Value Analysis Package in R. Journal of Statistical Software 72 (8), 1-39.

142. Gilleland, E.; Katz, R.W. & Young, G., 2010. extRemes: Extreme value toolkit. R package version 1.62.

143. Gnedenko, B., 1943. Sur La Distribution Limite Du Terme Maximum D'Une Serie Aleatoire. Annals of Mathematics 44 (3), 423-453.

144. Goda, Y., 2011. Plotting-Position Estimator for the L-Moment Method and Quantile Confidence Interval for the GEV, GPA, and Weibull Distributions Applied for Extreme Wave Analysis. Coastal Engineering Journal 53 (2), 111-149. https://doi.org/10.1142/S057856341100229X.

145. Goel NK, De M., 1993. Development of unbiased plotting position formula for general extreme value distribution. J Stoch. Env. Res. 7: 1–13.

146. Gomes, M.I., 1993. On the estimation of parameters of rare events in environmental time series. Statistics for the environment 2: Water Related Issues (V. Barnett and K.F. Turkman, eds) John Wiley & Sons, 225-241.

147. Gouldby B, Méndez FJ, Guanche Y, Rueda A, Mínguez R., 2014. A methodology for deriving extreme nearshore sea conditions for structural design and flood risk analysis.J Coastal Engineering 88:15–26.

148. Greenwood, JA, Landwehr, JM, Matalas, NC, Wallis, JR., 1979. Probability weighted moments: Definition and relation to parameters of several distributions expressable in inverse form, Water Resour. Res., 15(5), 1049-1054, http://dx.doi.org/10.1029/WR015i005p01049

149. Grimshaw, S.D., 1993. Computing Maximum-Likelihood-Estimates for the Generalized Pareto Distribution. Technometrics 35 (2), 185-191.

150. Gringorten II., 1963. A plotting rule for extreme probability paper. J Geophys. Res. 68 (3): 813–814.

151. Gross JL, et al., 1994. Novel extreme value procedures: application to extreme wind data. In: Galambos J, Lechner JA, Simiu E, editors. Extreme value theory and applications. Dordrecht: Kluwer Academic Publishers.

152. Haigh, I. D., Nicholls, R., and Wells, N., 2010. A comparison of the main methods for estimating probabilities of extreme still water levels, Coast. Eng., 57, 838–849.

153. Hall, P. and Marron, J. S., 1991. Local minima in cross-validation functions. J. Roy. Statist. Soc. Ser. B 53 245–252.

154. Hall, P., Fisher, N.I., and Hoffmann, B., 1994. On the Nonparametric Estimation of Covariance Functions, Ann.Stat., 22, 2115-2134.

155. Hall, P., Racine, J., and Li, Q., 2004. "Cross-Validation and the Estimation of Conditional Probability Densities," Journal of the American Statistical Association, 99, 1015-1026.

156. Hamon BV, Middleton JF., 1989. Return periods of extreme sea levels: the exceedance probability method. Int. Hydrogr. Rev. 66(2): 165–177.

157. Harris, R.I., 1996. Gumbel re-visited - a new look at extreme value statistics applied to wind speeds, J. Wind Eng. Ind. Aerodyn. 59 1-22.

158. Harris, R.I., 1999. Improvements to the `Method of Independent Storms'. Journal of Wind Engineering and Industrial Aerodynamics 80 (1), 1-30.

159. Hautsch, N., 2004. Modeling Irregularly Spaced Financial Data — Theory and Practice of Dynamic Duration Models, Lecture Notes in Economics and Mathematical Systems, Vol. 539, Springer: Berlin, 291 pages.

160. Heffernan, J. E. & Tawn, J. A., 2004. A conditional approach for multivariate extreme values (with discussions and reply by the authors), J. Roy. Statist. Soc., B 66(3), 1–34.

161. Heffernan, J. E. and Resnick, S. I., 2007. Limit laws for random vectors with an extreme component. Ann. Appl. Prob., 17, 537–571.

162. Hipel, K.W., McLeod, A.I., 1994. Time Series Modelling of Water Resources and Environmental Systems. Elsevier Science.

163. Hobijn, B., Franses, P. H., and Ooms, M., 2004. Generalizations of the KPSS-test for Stationarity. Statistica Neerlandica, 58(4):483–502.

164. Hocke, K., and Kämpfer, N., 2008. Gap filling and noise reduction of unevenly sampled data by means of the Lomb-Scargle periodogram. Atmos. Chem. Phys. 9, 4197–4206.

165. Holmes J.D., Moriarty W.W., 1999. Application of the generalized Pareto distribution to extreme value analysis in wind engineering, Journal of Wind Engineering and Industrial Aerodynamics, Volume 83, Issues 1–3, Pages 1-10, ISSN 0167-6105, https://doi.org/10.1016/S0167-6105(99)00056-2.

166. Holmes, J. D., 2015. Wind Loading of Structures. 3rd ed., CRCPress, 450 pp.

167. Holmes, JD, 2015. Wind Loading of Structures, 3rd edn. CRC Press, Boca Raton.

168. Horne, J. H. & Baliunas, S. L., 1986. A prescription for period analysis of unevenly sampled time series. Astrophysical Journal, Part 1 (ISSN 0004- 637X), vol. 302, p. 757-763.

169. Hosking JRM, Wallis JR, Wood EF., 1985. Estimation of the generalized extreme value distribution by the method of probability weighted moments. J Technometrics 27(3): 251-261.

170. Hosking JRM, Wallis JR., 1997. Regional Frequency Analysis: An Approach based on L-Moments. Cambridge University Press

171. Hosking JRM., 1986. The theory of probability weighted moments. Research Report RC 12210. IBM Research Division Yorktown Heights NY.

172. Hosking JRM., 1990. L-moments: analysis and estimation of distributions using linear combinations of order statistics. J of the Royal Statistical Society, Series B 52: 105–124.

173. Hosking, J.R.M., 1985. Maximum-Likelihood-Estimation of the Parameters of the Generalized Extreme-Value Distribution. Journal of the Royal Statistical Society Series C-Applied Statistics 34 (3), 301-310.

174. Houghton, J. T., Ding, Y., Griggs, D. J., Noguer, M., van der Linden, P. J., Dai, X., Maskell, K. & Johnson, C. A. (eds), 2001. IPCC Third assessment report: climate change 2001. Cam- bridge University Press.

175. Hsing, T., Hüsler, J. and Leadbetter, M., 1988. 'On the exceedance point process for a stationary sequence', Probab. Theory Reltd Flds 78, 97–112.

https://doi.org/10.1016/j.oceaneng.2018.09.017

https://web.math.pmf.unizg.hr/eva2019/application/files/6415/6163/8771/AllSpeakersEVA2019.pdf.

https://www.aimspress.com/article/10.3934/energy.2017.2.268

176. Hundecha, Y., St-Hilaire, A., Ouarda, T.B.M.J., Adlouni, S.E., Gachon, P., 2008. A Nonstationary Extreme Value Analysis for the Assessment of Changes in Extreme Annual Wind Speed over the Gulf of St. Lawrence, Canada. Journal of Applied Meteorology and Climatology 47 (11), 2745-2759.

177. Hyndman, R.J., Fan, Y.N., 1996. Sample quantiles in statistical packages. American Statistician 50 (4), 361-365.

178. Ian Harris, 2005. Generalised Pareto methods for wind extremes. Useful tool or mathematical mirage?, Journal of Wind Engineering and Industrial Aerodynamics 93 (5), 341-360

179. In-na N, Nyuyen Van-Thanh-Van, 1989. An unbiased plotting position formula for the generalized extreme value distribution. J Hydrol. 106: 193–209.

180. Jain, D, Singh, VP., 1987. Estimating of EV1 distribution for flood frequency analysis, Wat. Res. Bull. 23(1): 59-71

181. Jaynes, ET., 1982. On the rationale of maximum entropy methods. Proceedings of IEEE 70: 939-952.

182. Jenkins G., Watts D., 1969, Spectral analysis and its applications. Holden-Day series in time series analysis, Holden-Day

183. Jenkinson, A.F., 1955. The frequency distribution of the annual maximum (or minimum) values of meteorological elements. Quarterly Journal of the Royal Meteorological Society 81 (348), 158-171.

184. Jeong, C., Panchang, V.G., 2008. Measurement-based estimates of extreme wave conditions for the Gulf of Mexico, OCEANS 2008, pp. 1-7.

185. Jonathan P, Ewans K., 2013. Statistical modelling of extreme ocean environments for marine design: A review. J Ocean Engineering 62: 91-109.

186. Jonathan, P., Ewans, K. and Randell, D., 2014. Non-stationary conditional extremes of northern North Sea storm characteristics. Environmetrics, 25: 172-188. https://doi.org/10.1002/env.2262

187. Jones, M. C., Marron, J. S. and Sheather, S. J., 1996. A brief survey of bandwidth selection for density estimation. J. Amer. Statist. Assoc. 91 401–407.

188. Kaiser-Weiss AK, Kaspar F, Heene V, Borsche M, Tan DGH, Poli P, et al., 2015. Comparison of regional and global reanalysis near-surface winds with station observations over Germany. Adv Sci Res 2015;12(1):187e98. ISSN 1992-0636, http://www.adv-sci-res.net/12/187/2015/.

189. Kallos, G., Nickovic, S., Papadopoulos, A., Jovic, D., Kakaliagou, O., Misirlis, N., Bou- kas, L., Mimikou, N., Sakellaridis, G., Papageorgiou, J., Anadranistakis, E., and Manousakis, M, 1997. The regional weather forecasting system Skiron: an overview. Proceedings of Symposium on Regional Weather Prediction on Parallel Computer Environments, 15–17 October, Athens, Greece, pp. 109-122, 1997.

190. Kalnay, E., and Coauthors, 1996: The NCEP/NCAR 40-Year Re-analysis Project. Bull. Amer. Meteor. Soc., 77, 437–471.

191. Kalogeri, C., Galanis, G., Spyrou, C., Diamantis, D., Baladima, F., Koukoula, M., Kallos, G., 2017. Assessing the European offshore wind and wave energy resource for combined exploitation. Renew. Energy 101, 1–21. doi: 10.1016/j.renene.2016.08.010

192. Kang, D., Ko, K., Huh, J., 2015. Determination of extreme wind values using the Gumbel distribution. Energy 86, 51-58.

193. Karl T, Knight RW., 1998. Secular trends of precipitation amount, frequency, and intensity in the United States. Bulletin of the American Meteorological Society 79(2): 231–241.

194. Karl TR, Knight RW, Plummer N., 1995. Trends in high-frequency climate variability in the Twentieth Century. Nature 377(6546): 217 – 220.

195. Kasperski, M., 2013. Estimation of the Design Wind Speed, in: Tamura, Y., Kareem, A. (Eds.), Advanced Structural Wind Engineering. Springer Japan, Tokyo, pp. 27-58.

196. Katz RW, Parlange MB, Naveau P., 2002. Statistics of extremes in hydrology. J Adv. Water Resour. 25: 1287–1304.

197. Katz, R. W., 2002. Do weather or climate variables and their impacts have heavy-tailed distributions? 16th Conf. on Probability and Statistics in the Atmospheric Sciences, Orlando, FL, Amer. Meteor. Soc., J3.5. Available online at https://ams.confex.com/ams/annual2002/techprogram/paper_26949.htm.

198. Katz, R.W. and Brown, B.G., 1992. "Extreme events in a changing climate: variability is more important than average", Climate Change, Vol. 21 No. 3, pp. 289-302.

199. Katz, R.W., 2010. Statistics of extremes in climate change. Climatic Change 100 (1), 71-76.

200. Kendall, M., 1976. Rank Correlation Methods, 4th ed., Griffin, London.

201. Kharin, V. V., and F. W. Zwiers, 2005. Estimating extremes in transient climate change simulations. J. Climate, 18, 1156–1173.

202. Kharin, V.V., Zwiers, F.W., 2000. Changes in the extremes in an ensemble of transient climate simulations with a coupled atmosphere-ocean GCM. Journal of Climate 13 (21), 3760-3788.

203. Khintchine, A., 1934. Korrelationstheorie der stationären stochastischen Prozesse. Mathematische Annalen, 109 (1), 604–615

204. Kim S, Shin H, Joo K, Heo J-H., 2012. Development of plotting position for the general extreme value distribution. J of Hydrology 475: 259-269.
205. Kite GW., 1988. Frequency and Risk Analyses in Hydrology. Water Resources Publications, Littleton, Colorado.
206. Kite, G.W., 1977. Frequency and Risk Analyses in Hydrology. Water Resources Publications.
207. Knippertz P, Ulbrich U, Speth P., 2000. Changing cyclone and surface wind speeds over the North Atlantic and Europe in a transient GHG experiment. Clim Res 15:109–120
208. Kočenda, E.- Černý, A., 2007. Elements of Time Series Econometrics: An Applied Approach. Praha : Karolinum Press, 2007. ISBN 978-80-246- 1370-3.
209. Koen Chris, 2006. The Nyquist frequency for irregularly spaced time-series: a calculation formula, Monthly Notices of the Royal Astronomical Society, Volume 371, Issue 3, September, Pages 1390–1394, https://doi.org/10.1111/j.1365-2966.2006.10762.x
210. Konishi, Sadanori and Kitagawa, Genshiro, 2008. Information Criteria and Statistical Modeling, New York, NY: Springer.
211. Kotz S, Nadarajah S., 2000. Extreme Value Distributions: Theory and Applications. Imperial College Press.
212. Koutsoyiannis D. and Montanari A., 2007. Statistical analysis of hydroclimatic time series: Uncertainty and insights, Water Resources Research, 43 (5), W05429, doi:10.1029/2006WR005592.
213. Kreindler, D., Lumsden, CJ, 2006. Effects of the irregular sample and missing data in time series analysis, Nonlinear Dynamics Psychology and Life Sciences, pp. 187-214.
214. Kumar, P., Min, S., Weller, E., Lee, H., & Wang, X. L., 2016. Influence of Climate Variability on Extreme Ocean Surface Wave Heights Assessed from ERA-Interim and ERA-20C, Journal of Climate, 29(11), 4031-4046. Retrieved Feb 1, 2021, from  https://journals.ametsoc.org/view/journals/clim/29/11/jcli-d-15-0580.1.xml
215. Kundzewicz, Z.W. and Robson, A.J., 2004. Change detection in hydrological records - a review of the methodology. Hydrological Sciences Journal - Journal Des Sciences Hydrologiques, 49(1): 7-19.
216. Kunz M, Mohr S, Rauthe M, Lux R, and Kottmeier Ch., 2010. Assessment of extreme wind speeds from Regional Climate Models – Part 1: Estimation of return values and their evaluation. J Nat. Hazards Earth Syst. Sci. 10: 907-922.
217. Kwiatkowski, D., Phillips, P.C.B., Schmidt, P. and Shin, Y., 1992. Testing the null hypothesis of stationarity against the alternative of a unit root. How sure are we that economic time series have a unit root? Journal of Econometrics, 54(1-3): 159-178.
218. Kyselý, J., Picek, J., Beranov́a, R., 2010. Estimating extremes in climate change simulations using thepeaks-over-threshold method with a non-stationary threshold. Global and Planetary Change 72, 55–68
219. Kyselý, J., 2002. Comparison of extremes in GCM-simulated, downscaled and observed central-European temperature series. Climate Research 20 (3), 211-222.
220. Kyselý, J., 2008. A Cautionary Note on the Use of Nonparametric Bootstrap for Estimating Uncertainties in Extreme-Value Models. Journal of Applied Meteorology and Climatology 47 (12), 3236-3251.
221. Landsea, C., C. Anderson, N. Charles, G. Clark, J. Dunion, J. Fernandez-Partagas, P. Hungerford, C. Neumann, and M. Zimmer, 2004. The Atlantic hurricane database re-analysis project: Documentation for the 1851–1910 alterations and additions to the HURDAT database, in Hurricanes and Typhoons: Past, Present and Future, edited by R. J. Murname and K.-B. Liu, pp. 177–221, Columbia Univ. Press, New York.
222. Lang, M., Ouarda, T. B. M. J., and Bobée, B., 1999. Towards operational guidelines for over-threshold modeling, J. Hydrol., 225, 103-117.
223. Larsén, X.G., Mann, J., 2009. Extreme winds from the NCEP/NCAR reanalysis data. Wind Energy 12 (6), 556-573.
224. Larsén, Xiaoli & Mann, Jakob & Rathmann, Ole & Jørgensen, Hans., 2013. Uncertainties of the 50-year wind from short time series using generalized extreme value distribution and generalized Pareto distribution. Wind Energy. 18. 10.1002/we.1683.
225. Lavin, M.F.; Fiedler, P.C.; Amador, J.A.; Ballance, J.T.; Farbor-Lorda, J.; Mestas-Nunez, A.M., 2006. "A review of eastern tropical Pacific oceanography: Summary". Progress in Oceanography. 69 (2006): 391–398. Bibcode:2006PrOce..69..391L. doi:10.1016/j.pocean.2006.03.005.
226. Leadbetter, M. R., Lindgren, G. and Rootźen, H., 1983. Extremes and Related Properties of Random Sequences and Series. New York: Springer-Verlag.
227. Leadbetter, M.R., 1983. Extremes and Local Dependence in Stationary-Sequences. Zeitschrift Fur Wahrscheinlichkeitstheorie Und VerwandteGebiete 65 (2), 291-306.
228. Leadbetter, M.R., Weissman, I., De Haan, L., and Rootźen, H., 1989. On clustering of high levels in statistically stationary series. Proceeding of the 4th Int. Meeting on Statist. Clim. (J. Sansom, ed.) New Zealand Meteorological Service, Wellington,
229. Lieblein, J., 1974: Efficient methods of extreme value methodology. National Bureau of Standards Rep. NBSIR 74-602, 31 pp.

230. Lima, C. H., U. Lall, T. J. Troy, and N. Devineni, 2015. A climate informed model for nonstationary flood risk prediction: Application to negro

231. Lins H.F. and T.A. Cohn, 2011. Stationarity: Wanted Dead or Alive? JAWRA Journal of the American Water Resources, 47(3), 475 - 480, doi = 10.1111/j.1752-1688.2011.00542.x

232. Lomb, N. R., 1976. Least-squares frequency analysis of unequally spaced data, Astrophys. Space Sci., 39, 447–462.

233. Lombardo, FT., 2012. Improved extreme wind speed estimation for wind engineering applications, J. of Wind Engineering and Industrial Aerodynamics, 104–106: 278-284, http://dx.doi.org/10.1016/j.jweia.2012.02.025.

234. Loretan, M. & Philips, P.C.B., 1994. Testing the covariance stationarity of heavy tailed time series: an overview of the theory with applications to several financial datasets, J. R. Statist. Soc. D, 1, 211–248.

235. Madsen H, Rasmussen PF, Rosbjerg D., 1997. Comparison of annual maximum series and partial duration series methods for modeling extreme hydrologic events: 1. At-site modeling. J Water Resour. Res., 33(4):747–758.

236. Makkonen L., 2006. Plotting positions in extreme value analysis. J Appl. Meteor. Climatol. 45: 334–340.

237. Makkonen L., 2008. Problems in the extreme value analysis. J Structural Safety 30(5): 405-419.

238. Manis, P., Bloodworth, A.G., 2017. Climate change and extreme wind effects on transmission towers. Proceedings of the Institution of Civil Engineers: Structures and Buildings 170 (2), 81-97.

239. Mann, H., 1945. Nonparametric tests against trend, Econometrica, 13, 245–259, doi:10.2307/1907187.

240. Marcos, R., González-Reviriego, N., Torralba, V. et al., 2019. Characterization of the near surface wind speed distribution at global scale: ERA-Interim reanalysis and ECMWF seasonal forecasting system 4. Clim Dyn 52, 3307–3319. https://doi.org/10.1007/s00382-018-4338-5

241. MARINA Platform, 2014, EU FP7 Co-ordinated Action Project "marine Renewable Integrated Application Platform-MARINA Platform", https://www.msp-platform.eu/projects/marina-platform

242. Marron, J. S., 1988. Automatic smoothing parameter selection: a survey, Empirical Economics, 13, 187-208.

243. Martins ES, Stedinger JR., 2000. Generalized maximum-likelihood generalized extreme-value quantile estimators for hydrologic data. J Water Resour. Res. 36(3): 737-744.

244. Mathiesen, M., Goda, Y., Hawkes, P.J., Mansard, E., Martín, M.J., Peltier, E., Thompson, E.F., Van Vledder, G., 1994. Recommended practice for extreme wave analysis. J. Hydraul. Res. 32 (6), 803–814.

245. Matulla C, Schöner AWH, von Storch H, Wang XL., 2007. European storminess: late nineteenth century to present. Clim Dyn . doi:10.1007/s00382-007-0333-y

246. Mayo, W., 1993. Spectrum measurements with laser velocimeters in: Adrian, R.J. (Ed.), Selected Papers on Laser Doppler Velocimetry. Society of Photo-Optical Instrumentation Engineers, SPIE Press, pp. 222–235.

247. Mazas, F., Garat, P., Hamm, L., 2014. Questioning MLE for the estimation of environmental extreme distributions. Ocean Engineering 92, 44-54.

248. Meehl, G.A., Karl, T., Easterling, D.R., Changnon, S., Jr., R.P., Changnon, D., Evans, J., Groisman, P.Y., Knutson, T.R., Kunkel, K.E., Mearns, L.O., Parmesan, C., Pulwarty, R., Root, T., Sylves, R.T., Whetton, P., Zwiers, F., 2000. An Introduction to Trends in Extreme Weather and Climate Events: Observations, Socioeconomic Impacts, Terrestrial Ecological Impacts, and Model Projections. Bulletin of the American Meteorological Society 81 (3), 413-416.

249. Mendez, F. J., Menendez, M., Lucenõ, A., and Losada, I. J., 2007. Analyzing monthly extreme sea levels with a time-dependent GEV model. Journal of Atmospheric and Oceanic Technology, 24: 894–911.

250. Middleton JF, Thompson KR., 1986. Return periods of extreme sea levels from short records. Journal of Geophysical Research 91(C10): 11707–11716.

251. Miquel, J., 1984. Guide pratiqued'estimation des probabilites de crue, Eyrolles, Paris.

252. Mo, H.M., Hong, H.P., Fan, F., 2015. Estimating the extreme wind speed for regions in China using surface wind observations and reanalysis data. Journal of Wind Engineering and Industrial Aerodynamics 143, 19-33.

253. Mölter T, Schindler D, Albrecht AT, Kohnle U., 2016. Review on the Projections of Future Storminess over the North Atlantic European Region. Atmosphere; 7(4):60. https://doi.org/10.3390/atmos7040060

254. Monahan, A. H., 2006 a. The Probability Distribution of Sea Surface Wind Speeds. Part I: Theory and Sea Winds Observations, Journal of Climate, 19(4), 497-520. Retrieved Jan 26, 2021, from https://journals.ametsoc.org/view/journals/clim/19/4/jcli3640.1.xml

255. Monahan, A. H., 2006 b. The Probability Distribution of Sea Surface Wind Speeds. Part II: Dataset Intercomparison and Seasonal Variability, Journal of Climate, 19(4), 521-534. Retrieved Jan 27, 2021, from https://journals.ametsoc.org/view/journals/clim/19/4/jcli3641.1.xml

256. Mondal, D., Percival, D.B., 2010. Wavelet variance analysis for gappy time series. Annals of the Institute of Statistical Mathematics 62 (5), 943-966.

257. Morton, I.D, Bowers, J., 1997. Extreme values in a multivariate offshore environments, Applied Ocean Research, Vol 18, pp. 303-317.

258. Morton, I.D., Bowers, J., Mould, G., 1997. Estimating return period wave heights and wind speeds using a seasonal point process model. Coastal Engineering 31 (1-4), 305-326.

259. Muraleedharan, G., Rao, A.D., Kurup, P.G., Unnikrishnan Nair, N., Sinha, M., 2007. Modified Weibull distribution for maximum and significant wave height simulation and prediction. Coast. Eng. 54, 630–638

260. Muraleedharan, G., Sinha, M., Rao, A. D., Nair, N. & Kurup, P. G., 2009. Estimation of wave period statistics using numerical coastal wave model. Natural Hazards, 49(2), 165-186.

261. Nadaraya, E.A., 1964. Some New Estimates for Distribution Functions. Theory of Probability & Its Applications 9 (3), 497-500.

262. Naess, A., 1998. Statistical extrapolation of extreme value data based on the peaks over threshold method. Journal of Offshore Mechanics and Arctic Engineering-Transactions of the Asme 120 (2), 91-96.

263. Naess, A., Clausen, P.H., 2001. Combination of the peaks-over-threshold and bootstrapping methods for extreme value prediction. Structural Safety 23 (4), 315-330.

264. Nandagopalan, S., 1990. Multivariate extremes and estimation of the extremal index Department of Statistics. University of North Carolina at Chapel Hill, NC, USA.

265. Nash JE., 1959. Systematic Determination of Unit Hydrograph Parameters. J of Geophysical Research 64 No.1.

266. Naveau P, Nogaj M, Ammann C, Yiou P, Cooley D, Jomelli V., 2005. Statistical methods for the analysis of climate extremes. J Geoscience 337: 1013-1022.

267. Naveau, P., Huser, R., Ribereau, P., & Hannart, A., 2016. Modeling jointly low, moderate, and heavy rainfall intensities without a threshold selection. Water Resources Research, 52(4), 2753–2769.

268. New M et al., 2000. "Representing twentieth-century space-time climate variability. Part II: development of 1901–96 monthly grids of terrestrial surface climate.". J Clim 13:2217–2238

269. Nicolae Lerma, A., Bulteau, T., Lecacheux, S., Idier, D., 2015. Spatial variability of extreme wave height along the Atlantic and channel French coast. Ocean Engineering 97, 175-185.

270. Nikulin, G., Kjellstrom, E., Hansson, U., Strandberg, G., Ullerstig, A., 2011. Evaluation and future projections of temperature, precipitation and wind extremes over Europe in an ensemble of regional climate simulations. Tellus Series a-Dynamic Meteorology and Oceanography 63 (1), 41-55.

271. Nissen, K.M., Leckebusch, G.C., Pinto, J.G. et al., 2014. Mediterranean cyclones and windstorms in a changing climate. Reg Environ Change 14, 1873–1890. https://doi.org/10.1007/s10113-012-0400-8

272. Nobach, H., 2002. Local time estimation for the slotted correlation function of randomly sampled LDA data. Experiments in Fluids 32 (3), 337-345.

273. Nogaj, M. & Parey, S. & Dacunha-Castelle, D., 2007. Non-stationary extreme models and a climatic application. Nonlinear Processes in Geophysics. 14. 10.5194/npg-14-305-2007.

274. Northrop, P., Jonathan, P., 2011. Threshold modelling of spatially-dependent non-stationary extremes withapplication to hurricane-induced wave heights. Environmetrics 22, 799–809.

275. Northrop, P.J., Coleman, C.L., 2014. Improved threshold diagnostic plots for extreme value analyses. Extremes 17 (2), 289-303.

276. O'Brien, G. L., 1987. 'Extreme values for stationary and Markov sequences', Ann. Probab. 15, 281–291.

277. Ochi, M.K., 1998. Ocean Waves: The Stochastic Approach. Cambridge University Press, Cambridge. https://doi.org/10.1017/CBO9780511529559

278. Oikonomou, C. L. G. and Gradowski, M. and Kalogeri, C. and Sarmento, A. J. N. A., 2020. On defining storm intervals: Extreme wave analysis using extremal index inferencing of the run length parameter. Ocean Engineering, Volume (217), 107988, ISSN 0029-8018

279. Oliver, ECJ, Wotherspoon, SJ, Holbrook NJ., 2014. Estimating extremes from global ocean and climate models: A Bayesian hierarchical model approach. J Progress in Oceanography 122:77-91.

280. Orimolade, A.P., Haver, S., Gudmestad, O.T., 2016. Estimation of extreme significant wave heights and the associated uncertainties: A case study using NORA10 hindcast data for the Barents Sea. Marine Structures 49, 1-17.

281. Palutikof JP, Brabson BB, Lister DH, and Adcock ST., 1999. A review of methods to calculate extreme wind speeds. J Meteorological applications 6:119–132.

282. Panagoulia, D., Economou, P., Caroni, C., 2014. Stationary and nonstationary generalized extreme value modelling of extreme precipitation over a mountainous area under climate change. Environmetrics 25 (1), 29-43.

283. Panchang, V., Jeong, C.K., Demirbilek, Z., 2013. Analyses of extreme wave heights in the gulf of mexico for offshore engineering applications. Journal of Offshore Mechanics and Arctic Engineering 135 (3), 1-15.

284. Panchang, V., Zhao, L., Demirbilek, Z., 1998. Estimation of extreme wave heights using GEOSAT measurements. Ocean Engineering 26 (3), 205-225.

285. Pandey M.D, P.H.A.J.M Van Gelder, J.K Vrijling, 2001. The estimation of extreme quantiles of wind velocity using L-moments in the peaks-over-threshold approach. Structural Safety, Volume 23, Issue 2, Pages 179-192, ISSN 0167-4730, https://doi.org/10.1016/S0167-4730(01)00012-1.

286. Pandey, M. D., P. H. A. J. M. Van Gelder, and J. K. Vrijling, 2003. Bootstrap simulations for evaluating the uncertainty associated with peaks-over-threshold estimates of extreme wind velocity. Environmetrics, 14, 27–43.

287. Papalexiou, S. M., and D. Koutsoyiannis, 2013. Battle of extreme value distributions: A global survey on extreme daily rainfall, Water Resour. Res.,49,187–201,doi:10.1029/2012WR012557.

288. Papoulis, A., 1991. Probability, Random Variables and Stochastic Processes, 3rd edn., McGraw-Hill, New York.

289. Park, B.U. and Marron, J.S., 1990. Comparison of data-driven bandwidth selectors. Journan of American Statistical Association 85, 66-72.

290. Park, Byeong & Turlach, Berwin, 1992. Practical performance of several data driven bandwidth selectors. Computational Statistics. 7. 251-270.

291. Patlakas, P., Galanis, G., Barranger, N., Kallos, G., 2016. Extreme wind events in a complex maritime environment: Ways of quantification. Journal of Wind Engineering and Industrial Aerodynamics 149, 89-101.

292. Pearson K., 1894. Contributions to the Mathematical Theory of Evolution. J Philosophical Transactions of the Royal Society 185:71-110.

293. Perrin, O. & Rootzén, Holger & Taesler, Roger, 2006. A discussion of statistical methods used to estimate extreme wind speeds. Theoretical and Applied Climatology. 85. 203-215. 10.1007/s00704-005-0187-3.

294. Pes, M.P., Pereira, E.B., Marengo, J.A., Martins, F.R., Heinemann, D., Schmidt, M., 2017. Climate trends on the extreme winds in Brazil. Renewable Energy 109, 110-120.

295. Pickands, J. 1975. Statistical inference using extreme order statistics. Annals of Statistics, 3(1), 119-131.

296. Pickands, J., 1971. The two dimensional poisson process and extremal processes. Journal of Applied Probability 8, 745-756.

297. Pinheiro, E. and Ferrari, S., 2015. A comparative review of generalizations of the Gumbel extreme value distribution with an application to wind speed data. Journal of Statistical Computation and Simulation 86: 2241 - 2261.

298. Poli, P., Hersbach, H., Dee, D.P., Berrisford, P., Simmons, A.J., Vitart, F., Laloyaux, P., Tan, D.G.H., Peubey, C., Thépaut, J.-N., Trémolet, Y., Hólm, E.V., Bonavita, M., Isaksen, L., Fisher, M., 2016. ERA-20C: An Atmospheric Reanalysis of the Twentieth Century. Journal of Climate 29 (11), 4083-4097.

299. Poli, P., Hersbach, H., Tan, D., Dee, D., Thépaut, J.-N., Simmons, A.J., Peubey, C., Laloyaux, P., Komori, T., Berrisford, P., Dragani, R., Trémolet, Y., Hólm, E., Bonavita, M., Isaksen, L., Fisher, M., 2013. The data assimilation system and initial performance evaluation of the ECMWF pilot reanalysis of the 20th-century assimilating surface observations only (ERA-20C).

300. Polnikov, V.G., Sannasiraj, S.A., Satish, S., Pogarskii, F.A., Sundar, V., 2017. Estimation of extreme wind speeds and wave heights along the regional waters of India. Ocean Engineering 146, 170-177.

301. Pop, L., Sokol, Z., Hanslian, D., 2016. A new method for estimating maximum wind gust speed with a given return period and a high areal resolution. Journal of Wind Engineering and Industrial Aerodynamics 158, 51-60.

302. Press, W. H., & Rybicki, G. B., 1989. ApJ, 338, 277

303. Press, W. H., Teukolsky, S. A., Vetterling, W. T., & Flannery, B. P., 2007. Numerical Recipes 3rd Edition: The Art of Scientific Computing, 3rd edn. (New York, NY, USA: Cambridge University Press)

304. Press, W. H., Teukolsky, S. A., Vetterling, W. T., and Flannery, B. P., 1992. Numerical recipes in Fortran, Cambridge University Press, Cambridge, USA, 2 edn.

305. Priestley M., 1981. Spectral analysis and time series. No. v. 1 in Probability and mathematical statistics, Academic Press

306. Pryor S C, Barthelmie R J, Clausen N E, Drews M, MacKellar N and Kjellström E., 2012. Analyses of possible changes in intense and extreme wind speeds over northern Europe under climate change scenarios Clim. Dyn. 38 189–208

307. Pryor SC, Barthelmie RJ., 2003. Long-term trends in near-surface flow over Baltic. Int J Climatol 23:271–289

308. Pryor, Sara & Barthelmie, R. & Nikulin, Grigory & Jones, C., 2010. Influence of Regional Climate Model spatial resolution on wind climates. AGU Fall Meeting Abstracts. 117. 10.1029/2011JD016822.

309. Ranneby B., 1984. The maximum spacing method: An estimation method related to the maximum likelihood method. J Scandinavian Journal of Statistics 11:93–112.

310. Razmi, A., Golian, S. & Zahmatkesh, Z. Non-Stationary Frequency Analysis of Extreme Water Level: Application of Annual Maximum Series and Peak-over Threshold Approaches. Water Resour Manage 31, 2065–2083 (2017). https://doi.org/10.1007/s11269-017-1619-4

311. Reed, J.W., 1974. Wind power climatology. Weatherwise 27 (6), 236-242.

312. Reegen P., 2007. SigSpec - I. Frequency- and phase-resolved significance in Fourier space A&A 467 (3) 1353-1371, DOI: https://doi.org/10.1051/0004-6361:20066597

313. Reguero, F.J.M.A.T.R.M.B.G., 2011. A methodology to define extreme wave climate using reanalysis data bases, OCEANS 2011 IEEE, Santander - Spain, pp. 1-10.

314. Rehfeld, K. and Kurths, J., 2014. Similarity estimators for irregular and age-uncertain time series, Clim. Past, 10, 107-122, https://doi.org/10.5194/cp-10-107-2014, 2014.

315. Rehfeld, K., Marwan, N., Heitzig, J., Kurths, J., 2011. Comparison of correlation analysis techniques for irregularly sampled time series. Nonlinear Processes in Geophysics 18 (3), 389-404.

316. Reiss, R.-D. & Thomas, M., 2007. Statistical Analysis of Extreme Values: With Applications to Insurance, Finance, Hydrology and Other Fields, Birkhauser, Boston.

317. Renard, B., X. Sun, and M. Lang, 2013. Bayesian methods for non-stationary extreme value analysis, in Extremes in a Changing Climate, pp. 39–95, Springer, Dordrecht, Netherlands.

318. Rivoal T., 2009. Rational approximations for values of derivatives of the Gamma function, Trans. Amer. Math. Soc. 361, 6115–6149.

319. Roberts, David & Lehar, Joseph & Dreher, John, 1987. Time Series Analysis with Clean - Part One - Derivation of a Spectrum. The Astronomical Journal. 93. 968. 10.1086/114383.

320. Rockel B, Woth K., 2007. Extremes of near-surface wind speed over Europe and their future changes as estimated from an ensemble of RCM simulations. Clim Change 81:267–280

321. Ronold, K.O., Larsen, G.C., 2000. Reliability-based design of wind-turbine rotor blades against failure in ultimate loading. Engineering Structures 22 (6), 565-574.

322. Rosbjerg, D., & Madsen, H., 1992. On the choice of threshold level in partial duration series. In: Østrem, G. (Ed.), Nordic Hydrological Conference, Alta. NHP Rep. 30, Oslo, pp. 604–615.

323. Rudemo, M., 1982. Empirical Choice of Histograms and Kernel Density Estimators. Scandinavian Journal of Statistics, 9, 65-78.

324. Ruf, T., 1999. The Lomb-Scargle Periodogram in Biological Rhythm Research: Analysis of Incomplete and Unequally Spaced Time-Series. Biological Rhythm Research 30: 178–201.

325. Ruggiero, P., P. D. Komar, and J. C. Allan, 2010. Increasing wave heights and extreme value projections: The wave climate of the US Pacific Northwest, Coastal Eng., 57(5), 539–552.

326. Said, S. E. and Dickey, D. A., 1984. Testing for unit roots in autoregressive–moving average models of unknown order. Biometrika, 71, 599–608.

327. Sarkar A, Kumar N, Mitra D., 2014. Extreme Wind Climate Modeling of Some Locations in India for the Specification of the Design Wind Speed of Structures. KSCE Journal of Civil Engineering 18(5):1496-1504.

328. Sartini, L., Mentaschi, L., Besio, G., 2015. Comparing different extreme wave analysis models for wave climate assessment along the Italian coast. Coastal Engineering 100, 37-47.

329. Scargle, J. D., 1981. Studies in astronomical time series analysis. I - Modeling random processes in the time domain. Astroph. J. Supp. 45 1–71

330. Scargle, J.D., 1982. Studies in Astronomical Time Series Analysis II. Statistical Aspects of Spectral Analysis of Unevenly Spaced Data. Astrophysics Journal, 263, 836-853.

331. Scargle, J.D., 1989. Studies in Astronomical Time-Series Analysis .3. Fourier-Transforms, Auto-Correlation Functions, and Cross-Correlation Functions of Unevenly Spaced Data. Astrophysical Journal 343 (2), 874-887.

332. Scarrott, C., MacDonald, A., 2012. A Review of Extreme Value Threshold Estimation and Uncertainty Quantification. Revstat-Statistical Journal 10 (1), 33-60.

333. Schulz, M., Stattegger, K., 1997. SPECTRUM: Spectral analysis of unevenly spaced paleoclimatic time series. Computers & Geosciences 23 (9), 929-945.

334. Schwarz, Gideon E., 1978. "Estimating the dimension of a model", Annals of Statistics, 6 (2): 461–464, doi:10.1214/aos/1176344136

335. Schwarzenberg-Czerny A., 1998. The Distribution of Empirical Periodograms: Lomb-Scargle and PDM Spectra. Monthly Notices of the Royal Astronomical Society, 301(3), 831–840. doi:10.1111/j.1365-8711.1998.02086.x.

336. Schwierz, C., P. Koellner-Heck, E. Mutter, D. N. Bresch, P. Vidale, M. Wild, and C. Schaer, 2010. Modelling European winter wind storm losses in current and future climate, Clim. Change, 101(3–4), 485–514, doi:10.1007/s10584-009-9712-1.

337. Scott DW., 1992. Density estimation: Theory, practice and visualization. The Curse of Dimensionality and Dimension Reduction, pp.195-217, Wiley, New York.

338. Scott, D. W. and Terrell, G. R., 1987. Biased and unbiased cross-validation in density estimation. J. Amer. Statist. Assoc. 82 1131–1146.

339. Serinaldi, F., and C. G. Kilsby, 2014. Rainfall extremes: Toward reconciliation after the battle of distributions, Water Resour. Res., 50, 336–352, doi:10.1002/2013WR014211.

340. Serinaldi, F., Kilsby, C.G., 2015. Stationarity is undead: Uncertainty dominates the distribution of extremes. Advances in Water Resources 77 (Supplement C), 17-36.

341. Shannon CE., 1948. A Mathematical Theory of Communication. J Bell System Technical Journal 27 (3): 379–423.

342. Sheather, S. J. and Jones, M. C., 1991. A reliable data-based bandwidth selection method for kernel density estimation. J. Roy. Statist. Soc. Ser. B 53 683–690.

343. Sheather, S., 2004. Density Estimation. Statistical Science,19(4), 588-597. http://www.jstor.org/stable/4144429

344. Silverman, B., 1986. "Density estimation for statistics and data analysis", Chapman & Hall, London.

345. Simiu, E., Heckert, N.A., 1996. Extreme wind distribution tails: A "peaks over threshold" approach. Journal of Structural Engineering-Asce 122 (5), 539-547.

346. Šimková, T., Picek, J., 2016. A comparison of L-, LQ-, TL-moment and maximum likelihood high quantile estimates of the GPD and GEV distribution. Communications in Statistics - Simulation and Computation, 1-20.

347. Simonoff J. S., 1996. Smoothing Methods in Statistics. Springer, New York.

348. Singh VP., 1998. Entropy-Based Parameter Estimation in Hydrology. Springer Science Business Media Dordrecht.

349. Smith, R. L., 1990. Max-stable processes and spatial extremes. Unpublished manuscript, University of North California

350. Smith, R.L., 1985. Maximum likelihood estimation in a class of nonregular cases. Biometrika 72 (1), 67-90.

351. Smith, R.L., 1986. Extreme value theory based on the r largest annual events. J. Hydrol. 86(1), 27–43

352. Smith, R.L., 1991. Extreme value theory. In Handbook of Applicable Mathematics 7, ed. W. Ledermann. John Wiley, Chichester, 437-472.

353. Smith, R.L., 2003. Statistics of extremes, with applicationsin environment, insurance and finance, edited by B. Finkenstadt and H. Rootzen, Chapman and Hall/CRCPress, London, pp. 1–78.

354. Smith, R.L., Weissman, I., 1994. Estimating the Extremal Index. Journal of the Royal Statistical Society. Series B (Methodological) 56 (3), 515-528.

355. Smith, Richard L., 1989. Extreme Value Analysis of Environmental Time Series: An Application to Trend Detection in Ground-Level Ozone. Statist. Sci. 4, no. 4, 367--377. doi:10.1214/ss/1177012400. https://projecteuclid.org/euclid.ss/1177012400

356. Soares, C.G, Scotto, M.G., 2004. Application of the r largest-order statistics for long-term predictions of significant wave height. Coastal Engineering 51 (5), 387-394.

357. Solomon, S., Qin, D., Manning, M., Chen, Z., Marquis, M., Averyt, K., et al., 2007. Climate Change 2007: The Physical Science Basis. Contributions of Working Group I to the Fourth Assessment Report of the Intergovernmental Panel on Climate Change. Cambridge.

358. Soukissian T., Tsalis C., 2019. Sample size effects to the likelihood of the GEV and GPD distributions and applications in metocean design conditions. (In preparation)

359. Soukissian Takvor, Anastasios Papadopoulos, Panagiotis Skrimizeas, Flora Karathanasi, Panagiotis Axaopoulos, Evripides Avgoustoglou, Hara Kyriakidou, Christos Tsalis, Antigoni Voudouri, Flora Gofa, Petros Katsafados, 2017. Assessment of offshore wind power potential in the Aegean and Ionian Seas based on high-resolution hindcast model results[J]. AIMS Energy, 5(2): 268-289. https://doi.org/10.3934/energy.2017.2.268.

360. Soukissian TH, Papadopoulos A., 2015. Effects of different wind data sources in offshore wind power assessment. Renew Energ 77: 101–114.

361. Soukissian TH, Tsalis Christos, 2018. Effects of parameter estimation method and sample size in metocean design conditions, Journal of Ocean Engineering,

362. Soukissian TH, Kalantzi G., 2006. Extreme value analysis methods used for wave prediction. Proc. of the 16th International Offshore and Polar Engineering Conference 3:10–17.

363. Soukissian, T., Karathanasi, F., Axaopoulos, P., Voukouvalas, E. and Kotroni, V., 2018. Offshore wind climate analysis and variability in the Mediterranean Sea. Int. J. Climatol, 38: 384-402. https://doi.org/10.1002/joc.5182

364. Soukissian, T.H., Kalantzi, G., Karagali, I., 2006. De-clustering of Hs -time series for applying the Peaks-Over-Threshold method, Proceedings of the 16th International Offshore and Polar Engineering Conference, San Francisco, ISOPE, Vol 3, pp 18-25.

365. Soukissian, T.H., Kalantzi, G.D., 2009. A New Method for Applying r-Largest Maxima Model for Design Sea-State Prediction. International Journal of Offshore and Polar Engineering 19 (3), 176-182.

366. Soukissian, T.H., Tsalis, C., 2015. The effect of the generalized extreme value distribution parameter estimation methods in extreme wind speed prediction. Natural Hazards 78 (3), 1777-1809.

367. Soukissian, TH., 1995. "Methods of long-term analysis and prediction of sea wave climate". Ph.D. thesis, Dept. of Naval Architecture & Marine Engineering, National Technical University of Athens (in Greek).

368. Springford A, Eadie G. M. and Thomson D. J., 2020. Improving the Lomb–Scargle Periodogram with the Thomson Multitaper. The Astronomical Journal vol. 159 (5), 205 (12pp) https://doi.org/10.3847/1538-3881/ab7fa1

369. Stefanakos, C.N., Soukissian, T.H., Hatzinaki, M., 2007. Wind and wave extremes in the Eastern Mediterranean Sea, in: Guedes Soares, C., Garbatov, Y., Fonseca, N. (Ed.), 12th International Congress of the International Association of the Mediterranean (IMAM 2007), Varna, Bulgaria. Taylor and Francis Publ., pp. 819–826.

370. Sterl, Andreas & van den Brink, Henk & Haarsma, R. & Stepek, Andrew & Wijnant, Ine & Bakker, Alexander & De Winter, Renske, 2015. Large-scale winds in the southern North Sea region: The wind part of the KNMI'14 climate change scenarios. Environmental Research Letters. 10. 10.1088/1748-9326/10/3/035004.

371. Stoica, P., Li, J. and He, H., 2009. Spectral Analysis of Non-Uniformly Sampled Data: A New Approach Versus the Periodogram, IEEE Transactions on Signal Processing, 57(3):843-858

372. Su, S., Gao, D., Yang, H., Liu, G., Chen, J., Guo, Z., 2017. Spatial Variation in Wind Extremes Under the Context of Climate Change and Its Impact on Safety of Wind Turbines. Gaodianya Jishu/High Voltage Engineering 43 (7), 2378-2385.

373. Sušelj K, Sood A, Heinemann D, 2010. North Sea near-surface windclimate and its relation to the large-scale circulation patterns.TheorApplClimatol 99:403–419

374. Syczewska, E. M., 2010. Empirical power of the Kwiatkowski-Phillips-Schmidt-shin test (No. 45).

375. Tajvidi, N., 2003. Confidence Intervals and Accuracy Estimation for Heavy-Tailed Generalized Pareto Distributions. Extremes 6 (2), 111-123.

376. Tanaka, S. and Takara, K., 2002: A study on threshold selection in POT analysis of extreme floods. IAHS AISH 271, 299–304.

377. Tawn, J.A., 1988. An Extreme-Value Theory Model for Dependent Observations. Journal of Hydrology 101 (1-4), 227-250.

378. Terrell, G. R., 1990. The maximal smoothing principle in density estimation. J. Amer. Statist. Assoc. 85 470–477.

379. Theodoros Katopodis, Diamando Vlachogiannis, Nadia Politi, Nikolaos Gounaris, Stelios Karozis, and Athanasios Sfetsos, 2019. Assessment of climate change impacts on wind resource characteristics and wind energy potential in Greece, Journal of Renewable and Sustainable Energy 11, 066502 https://doi.org/10.1063/1.5118878

380. Torralba V, Doblas-Reyes FJ, Gonzalez-Reviriego N., 2017a. Uncertainty in recent near-surface wind speed trends: a global reanalysis intercomparison. Environ Res Lett 12(11):114,019. https://doi.org/10.1088/1748-9326/aa8a58

381. Torralba, V., Doblas-Reyes, F. J., MacLeod, D., Christel, I., & Davis, M., 2017b. Seasonal Climate Prediction: A New Source of Information for the Management of Wind Energy Resources, Journal of Applied Meteorology and Climatology, 56(5), 1231-1247. Retrieved Jan 27, 2021, from https://journals.ametsoc.org/view/journals/apme/56/5/jamc-d-16-0204.1.xml

382. Towler, E., Rajagopalan, B., Gilleland, E., Summers, R. S., Yates, D., and Katz, R. W, 2010. Modeling hydrologic and water quality extremes in a changing climate: a statistical approach based on extreme value theory, Water Resour. Res., 46, W11504, doi:10.1029/2009WR008876.

383. Tsalis C., Kallos G., 2017. Non-stationary Processes: Application to wind speed design values. Data Science & Environment from 3th-7th of July 2017. TELECOM BRETAGNE - Technopôle Brest-Iroise - CS 83818 - 29238 Brest Cedex 3 - http://conferences.telecom-bretagne.eu/dse2017/

384. Tsalis Christos, Platon Patlakas, Christos Stathopoulos, George Kallos, 2021. Optimizing a new de-clustering approach for relatively small samples of wind speed with an application to offshore design conditions. Ocean Engineering, Volume 228, 108896, ISSN 0029-8018, https://doi.org/10.1016/j.oceaneng.2021.108896.

385. Tsalis Christos, Takvor Soukissian, Platon Patlakas, George Kallos, 2019. A new de-clustering approach in extreme value analysis with an application to wind speed design values. (In preparation)

386. Tsay, R.S., 2002. Analysis of Financial Time Series, Wiley: New York, 472 pages.

387. Tummers, Mark & Passchier, D., 1996. Spectral estimation using a variable window and the slotting technique with local normalization. Measurement Science and Technology. 7. 1541-1546. 10.1088/0957-0233/7/11/001.

388. USWRC, 1976: Guidelines for determining flood flow frequency H. C. Bull.17, Washington DC, United States Water Resources Coun- cil, p. 73.

389. van Belle, G. and Hughes, J.P., 1984. Nonparametric Tests for Trend in Water Quality. Water Resour. Res., 20.

390. Van de Vyver H, Delcloo AW., 2011. Stable estimations for extreme wind speeds. An application to Belgium. J Theor. Appl. Climatol 105:417–429.

391. van Maanen H R E, Nobach H and Benedict L H, 1999. Improved estimator for the slotted autocorrelation function of randomly sampled LDA data Meas. Sci. Technol. 10 L4–7

392. Van Vledder, G., Goda, Y., Hawkes, P., Mansard, E., Martin, M.Y., Mathiesen, M., Peltier, E., Thompson, E., 1993. Case studies of extreme wave analysis: a comparative analysis. In: Proc. Second International Symposium honoring Professor Robert L. Wiegel, WAVES'93, New Orleans, Louisiana, United States, July 25-28, 1993, 978-992.

393. VanderPlas Jacob T., 2018. Understanding the Lomb–Scargle Periodogram. The Astrophysical Journal, 236:16 (28pp), https://doi.org/10.3847/1538-4365/aab766

394. Vanem, E., 2011. Long-term time-dependent stochastic modelling of extreme waves. Stochastic Environmental Research and Risk Assessment 25 (2), 185-209.

395. Vanem, E., 2015. Uncertainties in extreme value modelling of wave data in a climate change perspective. Journal of Ocean Engineering and Marine Energy 1 (4), 339-359.

396. Vanem, E., 2017. A regional extreme value analysis of ocean waves in a changing climate. Ocean Engineering 144, 277-295.

397. Varino, F., Arbogast, P., Joly, B. et al., 2019. Northern Hemisphere extratropical winter cyclones variability over the 20th century derived from ERA-20C reanalysis. Clim Dyn 52, 1027–1048. https://doi.org/10.1007/s00382-018-4176-5.

398. Venables, W. N. and Ripley, B. D., 2002. Modern Applied Statistics with S. Fourth Edition. Springer-Verlag.

399. Villarini, G., Serinaldi, F., Smith, J. A., and Krajewski, W. F. 2009: On the stationarity of annual flood peaks in the continental United States during the 20th century, Water Resour. Res., 45, W08417, doi:10.1029/2008WR007645.

400. Villarini, G., Smith, J.A., and Napolitano, F., 2010. Nonstationary modeling of a long record of rainfall and temperature over Rome. Advances in Water Resources, 33, 1256–1267.

401. Vinoth, J., Young, I.R., 2011. Global estimates of extreme wind speed and wave height. Journal of Climate 24 (6), 1647-1665.

402. Vio, R., Strohmer, T., Wamsteker, W., 2000. On the reconstruction of irregularly sampled time series. Publications of the Astronomical Society of the Pacific 112 (767), 74-90.

403. Viselli, A.M., Forristall, G.Z., Pearce, B.R., Dagher, H.J., 2015. Estimation of extreme wave and wind design parameters for offshore wind turbines in the Gulf of Maine using a POT method. Ocean Engineering 104, 649-658.

404. von Mises, R., 1936. La distribution de la plus grande de n valeurs. [Reprinted in Selected Papers II, American Mathematical Society, Providence R.I., 1954., 271-294].

405. Wada, R., Waseda, T., Jonathan, P., 2016. Extreme value estimation using the likelihood-weighted method. Ocean Engineering 124, 241-251.

406. Wadsworth, J.L., Tawn, J.A., 2012. Likelihood-based procedures for threshold diagnostics and uncertainty in extreme value modelling. Journal of the Royal Statistical Society Series B-Statistical Methodology 74, 543-567.

407. Wallis JR, Matalas NC, Slack JR, 1974. Just a moment! J Water Resources Research 10(2): 211-219.

408. Walshaw, D., 1994. Getting the Most from Your Extreme Wind Data - a Step-by-Step Guide. Journal of Research of the National Institute of Standards and Technology 99 (4), 399-411.

409. Wand, M.P., Jones, M.C., 1994. Kernel Smoothing. Taylor & Francis.

410. Wang QJ., 1996. Direct Sample Estimators of L Moments. J Water Resour. Res. 32(12): 3617–3619.

411. Wang XL, Zwiers FW, Swail V., 2004. North Atlantic Ocean wave climate scenarios for the twenty-first century. J Clim 17:2368–2383.

412. Wang, CH., Holmes, J.D., 2020. Exceedance rate, exceedance probability, and the duality of GEV and GPD for extreme hazard analysis. Nat Hazards 102, 1305–1321. https://doi.org/10.1007/s11069-020-03968-z

413. Wang, J., Qin, S., Jin, S., Wu, J., 2015. Estimation methods review and analysis of offshore extreme wind speeds and wind energy resources. Renewable and Sustainable Energy Reviews 42 (Supplement C), 26-42.

414. Wang, Y., 2017. Optimal threshold selection in the POT method for extreme value prediction of the dynamic responses of a Spar-type floating wind turbine. Ocean Engineering 134, 119-128.

415. Weber, J., Reyers, M., Beck, C. et al., 2019. Wind Power Persistence Characterized by Superstatistics. Sci Rep 9, 19971 (2019). https://doi.org/10.1038/s41598-019-56286-1

416. Wei, K., Arwade, S.R., Myers, A.T., Valamanesh, V., 2016. Directional effects on the reliability of non-axisymmetric support structures for offshore wind turbines under extreme wind and wave loadings. Engineering Structures 106, 68-79.

417. Weissman, I., 1978. Estimationofparametersandquantiles based on the k largest observations. J.Am.Statist.Ass.,73, 812-815

418. Wilks, D., 2011: Statistical Methods in the Atmospheric Sciences, 3rd edn., Academic Press, Oxford,.

419. Wilks, S. S., 1938. The large sample distribution of the likelihood ratio for testing composite hypothesis. Annals of Mathematical Statistics 9, 60–62.

420. Willems, P., 2000. Compound intensity/duration/frequency-relationships of extreme precipitation for two seasons and two storm types, J. Hydrol., 233, 189–205.

421. Wong TST, Li WK., 2006. A note on the estimation of extreme value distributions using maximum product of spacings. IMS Lecture Notes–Monograph Series, Time Series and Related Topics 52: 272–283.

422. Woodroofe, M., 1970. On choosing a delta-sequence. Ann. Math. Statist. 41 1665–1671.

423. Yan, Z., Jones, P.D., 2008. Detecting inhomogeneity in daily climate series using wavelet analysis. Adv. Atmos. Sci. 25, 157–163. https://doi.org/10.1007/s00376-008-0157-7

424. Young IR, Vinoth J, Ziegler S, Babanin AV., 2012. Investigation of trends in extreme value wave height and wind speed. J Geophys. Res 117:1-13.

425. Zachary, S., Feld, G., Ward, G., Wolfram, J., 1998. Multivariate extrapolation in the offshore environment. Applied Ocean Research 20, 273–295.

426. Zappa G, Shaffrey L C, Hodges K I, Samson P G and Stephenson D B, 2013. A multimodel assessment of future projections of North Atlantic and European extratropical cyclones in the CMIP5 climate models J. Clim.265846–62

427. Zecchetto S, Cappa C., 2001. The spatial structure of the Mediterranean Sea winds revealed by ERS-1 scatterometer. Int. J. Remote Sens. 22(1): 45–70. https://doi.org/10.1080/014311601750038848.

428. Zhang, Q., Xu, C.-Y., Zhang, Z., Chen, Y.D., Liu, C.-l., Lin, H., 2008. Spatial and temporal variability of precipitation maxima during 1960–2005 in the Yangtze River basin and possible association with large-scale circulation. Journal of Hydrology 353 (3), 215-227.

429. Zhang, X. F., F. W. Zwiers, and G. Li, 2004b. Monte Carlo experiments on the detection of trends in extreme values. J. Climate, 17, 1945–1952.

430. Zwiers, F.W., Kharin, V.V., 1998. Changes in the extremes of the climate simulated by CCC GCM2 under CO2 doubling. Journal of Climate 11 (9), 2200-2222.

# Publications

## Peer reviewed articles

Takvor H. Soukissian & Christos Tsalis, (2015). The effect of the generalized extreme value distribution parameter estimation methods in extreme wind speed prediction, Journal of the International Society for the Prevention and Mitigation of Natural Hazards, https://doi.org/10.1007/s11069-015-1800-0.

Takvor Soukissian, Anastasios Papadopoulos, Panagiotis Skrimizeas, Flora Karathanasi, Panagiotis Axaopoulos, Evripides Avgoustoglou, Hara Kyriakidou, Christos Tsalis, Antigoni Voudouri, Flora Gofa, Petros Katsafados, (2017). Assessment of offshore wind power potential in the Aegean and Ionian Seas based on high-resolution hindcast model results[J]. AIMS Energy, 5(2): 268-289. https://doi.org/10.3934/energy.2017.2.268.

Takvor H. Soukissian & Christos Tsalis, (2018). Effects of parameter estimation method and sample size in metocean design conditions, Journal of Ocean Engineering, https://doi.org/10.1016/j.oceaneng.2018.09.017

Christos Tsalis, Platon Patlakas, Christos Stathopoulos, George Kallos, (2021). Optimizing a new de-clustering approach for relatively small samples of wind speed with an application to offshore design conditions. Ocean Engineering, Volume 228, 108896, ISSN 0029-8018, https://doi.org/10.1016/j.oceaneng.2021.108896

Patlakas P, Stathopoulos C, Tsalis C, Kallos G, (2020). Wind and wave extremes associated with tropical-like cyclones in the Mediterranean basin. Int J Climatol.; 1–22. https://doi.org/10.1002/joc.6795

Stathopoulos, C.; Patlakas, P.; Tsalis, C.; Kallos, G., (2020). The Role of Sea Surface Temperature Forcing in the Life-Cycle of Mediterranean Cyclones. Remote Sens., 12, 825, https://doi.org/10.3390/rs12050825

## Conferences with proceedings

Tsalis C., Kallos G., 2017. Non-stationary Processes: Application to wind speed design values. Data Science & Environment from 3th-7th of July 2017. TELECOM BRETAGNE - Technopôle Brest-Iroise - CS 83818 - 29238 Brest Cedex 3 - http://conferences.telecom-bretagne.eu/dse2017/

## Conference presentations and workshops

11th international conference on Extreme Value Analysis, at Faculty of Science, Univeristy of Zagreb, Croatia, 1-5 July 2019, https://web.math.pmf.unizg.hr/eva2019/application/files/6415/6163/8771/AllSpeakersEVA2019.pdf.

Data Science & Environment from 3th-7th of July 2017. TELECOM BRETAGNE - Technopôle Brest-Iroise - CS 83818 - 29238 Brest Cedex 3 - http://conferences.telecom-bretagne.eu/dse2017/

## Scholarship

NSRF (National Strategic Reference Framework), title of research project "Modelling Extreme Environmental Values using Weather Forecast Models and Stochastic Processes", 2017 (MIS 5007050). rc@elke.uoa.gr